# Development of High Throughput Screening Platforms for Biotechnology

A thesis submitted to the University of Manchester for the degree of Doctor of Philosophy in the Faculty of Science and Engineering

**2021**

**Emily E. Kempa**

**Department of Chemistry**

# Table of contents

**Word count: 59558**

# List of Figures

# List of Tables

## Abbreviations

| Abbreviation | Full Name |
|---|---|
| AGC | Automatic Gain Control |
| AMI | Acoustic Mist Ionisation |
| APIs | Active Pharmaceutical Ingredients |
| BBSRC | Biology and Biotechnology Research Council |
| BSA | Bovine Serum Albumin |
| CAD | Computer Aided Design |
| CASE | Collaborative Awards in Science and Engineering |
| CE | Collision energy |
| CFE | Cell Free Extract |
| CID | Collision Induced Association |
| cm | centimetres |
| CMN | Centre for Mesoscience and Nanofabrication |
| DDI | Drug-Drug Interactions |
| DESI | Desorption Electrospray Ionisation |
| DiBT | Direct Biotransformation |
| DMSO | Dimethyl Sulphoxide |
| DNA | Deoxyribose Nucleic Acid |
| DTIMS | Drift Tube Ion Mobility Mass Spectrometry |
| DTP | Doctoral Training Program |
| EIC | Extracted Ion Chromatogram |
| EPSRC | Engineering and Physical Sciences Research Council |
| ESI | Electrospray Ionisation |
| ETD | Electron Transfer Dissociation |
| F | Phenylalanine |
| FF (Chapter 2) | Flow Focusing (microfluidic channel geometry) |
| FF (Chapter 5) | Diphenylalanine (dipeptide) |
| FTIR | Fourier Transform Infra-Red |
| FT-MS | Fourier Transform Mass Spectrometry |
| GalKs | Galactokinases |
| GAL-P | Galactose Phosphate |
| HDI | High Definition Imaging |
| HF | Hydrofluoric Acid |
| HPLC | High Performance Liquid Chromatography |
| hrs | Hours |
| HTS | High Throughput Screening |
| HV | High Voltage |
| Hz | Hertz ($s^{-1}$) |
| $IC_{50}$ | Half-maximal inhibitory concentration |

| | |
|---|---|
| ICP | Inductively Coupled Plasma |
| ID | Inner Diameter |
| IM | Ion Mobility |
| IMAC | Immobilized metal-ion affinity chromatography |
| IM-MS | Ion Mobility Mass Spectrometry |
| INT | iodonitrotetrazolium or 2-(4-iodophenyl)-3-(4-nitrophenyl)-5-phenyl-2H-tetrazolium |
| IREDs | Imine Reductase |
| kDa | kilo Dalton |
| $K_M$ | Michaelis Constant |
| $KP_i$ | Inorganic Potassium Phaophate |
| kV | kilovolts |
| LASER | Light Amplification by Stimulated Emission of Radiation |
| LB | Lysogeny Broth |
| LC | Liquid Chromatography |
| L-DOPA | l-3,4-dihydroxyphenylalanine |
| LDTD | LASER Diode Thermal Desorption |
| LESA | Liquid Extraction Surface Analysis |
| LOC | Lab-on-a-Chip |
| LTD | Limited |
| M | Molar |
| m/z | mass to charge ratio |
| MALDI-MS | Matrix Assisted LASER Desorption Ionisation |
| MAMS | Micro Arrays for Mass Spectrometry |
| MeOH | Methanol |
| mg | milligram |
| MHz | megahertz |
| MIB | Manchester Institute of Biotechnology |
| min | minute |
| MIO | methylidene-imidazolone |
| mL | millilitres |
| mm | millimetres |
| mM | millimolar |
| MS | Mass Spectrometry |
| ms | milliseconds |
| MS/MS | Tandem Mass Spectrometry |
| MSI | Mass Spectrometry Imaging |
| NADPH | Nicotinamide adenine dinucleotide phosphate (reduced form) |
| NahKs | N-acetylhexamine kinases |

| | |
|---|---|
| nanoPOTS | Nanodroplet Processing in One pot for Trace Samples |
| nESI | Nano-Electrospray Ionisation |
| nL | nanolitres |
| NMR | Nuclear Magnetic Resonance |
| OD | Outer Diameter |
| PAL | Phenyl Ammonium Lyase |
| PCR | Polymer Chain Reaction |
| PDB | Protein Data Bank |
| PDMS | Polydimethyl Siloxane |
| PEB | Post Exposure Bake |
| pg | picograms |
| pL | picolitres |
| PLA | Polylactic acid |
| QIT | Quadrupole Ion Trap (Mass Spectrometer) |
| Q-TOF | Quadrupole Time-of-Flight (Mass Spectrometer) |
| RBT | Degenerate codon bases (**R** = A, G, **B** = C, G, T, **T** = T) |
| RF | Radio Frequency |
| ROI | Region of Interest |
| rpm | Revolutions per minute |
| s | seconds |
| s/well | seconds per well |
| SAWN | Surface Acoustic Wave Nebulisation |
| SIMS | Secondary Ion Mass Spectrometry |
| SOC | Super Optimal broth with Catabolites repression |
| SPE | Solid Phase Extraction |
| TcPAM | Phenylalanine aminomutase from Taxus chinensis |
| TIC | Total Ion Chromatogram |
| TLC | Thin Layer Chromatography |
| TMA | Tissue Microarray |
| TOF | Time-of-Flight |
| TWIMS | Travelling wave ion mobility spectrometry |
| µg | microgram |
| uHTS | Ultra-High Throughput Screening |
| µL/hr | microliters per hour |
| µm | micrometres |
| UV | Ultraviolet |
| UVB | Ultraviolet B |
| V | Volts |
| xC-MS | (any) Chromatography Coupled Mass Spectrometry |

## Abstract

High throughput screening can be transformative in the discovery of new pharmaceutical products, improving enzyme variants and for cell differentiation. Methods that can screen upwards of $10^4$ samples per day are mostly reliant on inherent or incorporated fluorescent labels as the detectable species, which can restrict analyte scope. Label-free analytical platforms based on mass spectrometry (MS) measurements provide an alternative route, however, the throughput of current commercially available platforms is limited by their sample infusion robotics. The ability to screen reaction mixtures in their crude form is desirable, as sample purification methods for biological systems are often lengthy to limit contamination and improve the sensitivity of the mass spectrometry method employed. This thesis focuses on the use and development of two mass spectrometry-based sample introduction methods namely desorption electrospray ionisation (DESI)-MS and microfluidics and applies these to the study of model analytes and enzymatic reactions.

In Chapter 2 I show how DESI-MS can be applied to directly monitor biotransformations, termed DiBT-MS. This screening methodology is successfully applied to industrially relevant biocatalysts and the application of the workflow to a directed evolution experiment allowed for the activity enhancement of a phenylalanine ammonia lyase (PAL) enzyme towards electron-rich cinnamic acid derivatives. The output from this approach provides mass-selected heat-maps of the product(s) in a format analogous to 96-well plates and is semi-quantitative when compared with NMR and HPLC. DiBT-MS screening of these samples permitted throughputs equivalent to ~40 seconds per sample.

Commercial droplet microfluidics coupled MS platforms are still in their infancy, and in Chapter 3 I show how we have designed and interfaced microfluidic chips to four different commercially available mass spectrometers showing how the fluidics and chips can be adapted to different electrospray ionisation (ESI) ion sources. Hardware and software developments allow throughputs of 33 samples per second to be reached on an ion mobility mass spectrometer, with particular emphasis put upon establishing a platform suited to biotechnology workflows. The advantages and disadvantages of the different ion sources and mass spectrometers are explored, and the designs allowing MS coupling presented. Looking forward, the application of the methods and means described here will be significant to the development of successful commercial droplet microfluidics-MS apparatus and the Final Chapter (4) describes recent work wherein droplet reinjection is demonstrated, which will further the applications of coupling MS with uHTS microfluidics.

## Declaration

No portion of the work referred to in the thesis has been submitted in support of an application for another degree or qualification at this or any other university or other institute of learning.

## Copyright Statement

*One raindrop raises the sea.*

## Acknowledgements

First and foremost I would like to thank my supervisor, Prof. Perdita Barran, for the opportunity to work within her research group on such an exciting project. Her guidance throughout the time that we have worked together has always been second-to-none and she has supported me greatly both in my research and going forward into my future career.

With much gratitude, I must also thank my industrial sponsors Sphere Fluidics Ltd. Both Clive and Xin have not only answered (many!) emails, their expertise and guidance have been critical to the success of this thesis. Many thanks also go to CEO Frank for supporting me in my next step, and I am looking forward to continuing working alongside SF again in the immediate future. Much of the work described in this thesis would also not be possible without assistance from Waters Corp., and particular thanks go to Emrys, Keith and Steve for their inputs along the way.

Fellow members of PBRG, MIB and the SYNBIOCHEM centre have provided me with much-needed support during my time spent researching. Namely, these are Ellie 1, Ashley, Chris N, Jakub, Rosie, Lukasz, Alina, Ellie 2, Aidan, Florian, Jack, Dale, Emma, Charlotte, Caitlin, Alexey, Jo, Chris G, Lennart, Ruth, Drupad, Depanjan, Kamila, Danielle, Kat, Cunyu, Andy, Ros, Kath, Alex, and many others that I have inevitably forgotten. A big thank you also goes to Bruno and Reynard who were *instrumental* not only in keeping the lab ticking over but providing me with experimental suggestions and sanity checks along the way. Many thanks also go to the Turner-Flitsch group, notably Fabio, James G and James M, for their excellent sample preparation and putting up with me while working on the DESI project.

I have been very lucky to visit and work in several other institutes during my PhD, and much of the work would not have been possible without guidance from those at the CMN and NGI. Particular thanks go to Alex Lincoln and Ernie Hill for my clean room training, and fellow PhD students for their tips and tricks!

Although cut short due to COVID-19, my time at FELIX (Radboud University, The Netherlands) would not have come about without hospitality from Prof. Anouk Rijs and others (Thank you – Anouk, Sjors, Sander, Iuilia and Lisa, for making me feel so welcome!). In addition, many thanks go to the Belder group (University of Leipzig, Germany) for allowing me to visit their laboratory in November 2018 and for providing support on email along the way.

I must thank my mermaids, Rachelle, Olivia and the rest of the "soft-side-Bodybarre-crew" as well as our fab instructors Penny, Kaz and Flo. They have provided weekly laughs and motivated me through the much-needed respite that is the world of aerial artistry!

Last (but not least), I would like to thank my family and partner for all of their support during my PhD, particularly my mum, dad, Matthew and Kieran. Both in-person and at the end of the phone, they not only lent their ears to me venting my frustrations about the science but also offered encouragement, love and guidance when needed. Many thanks also go to Kieran for doing numerous bowls of washing up, cuddles with Stitchy and supplying me with copious amounts of iced tea, cake and biscuits.

## Preface

As will be described in the introduction to this thesis (Chapter 1), several technologies both commercial and developmental are available for the high throughput mass spectrometry (MS) analysis of biological samples. The focus in this thesis is the advancement of two of these technologies, desorption electrospray mass spectrometry (DESI-MS) and droplet microfluidics coupled-MS, for the screening of efficient biocatalysts and directed evolution studies. Located subsequent to results Chapters 2, 3 and 4, is an appendix detailing additional methodology used throughout the project. These methods are presented as 'step-by-step' guides to the procedures followed, with the intention of them remaining in the laboratory as teaching tools for future researchers.

DESI-MS for biocatalysis has been explored previously by the Barran group, however, expansion of the DiBT protocol towards high throughput screening had not been explicitly demonstrated. Working in collaboration with the Turner and Flitsch biocatalysis groups, Chapter 2 aims to apply DiBT MS screening to a range of biotransformations in differing mediums, including purified enzyme reactions, lysates and whole-cell material. The approach taken to high throughput screening focuses upon the application of well-plate layouts. In addition to the experimental work performed to increase the throughput of samples by DESI-MS, the methodology is also applied to a directed evolution workflow to identify mutants with enhanced activity towards electron-rich cinnamic acid derivatives relevant to lignocellulosic biomass degradation. The addition of ion mobility to the workflow is also explored, with particular benefits highlighted for products similar in mass to the $^{13}C$ isotopes of the starting materials.

Although droplet microfluidics has been previously coupled with MS by several groups, a commercial interface is yet to become available. In Chapters 3 and 4, chip-MS interfacing is explored using a range of commercial mass spectrometers to identify ease of coupling, the maximum achievable throughput and applicability to different sample types. Chapter 3 focuses upon using chip designs that facilitate immediate infusion of droplets after their generation. Particular emphasis is put upon increasing the detectable frequency of droplet infusion using the available MS hardware and software. This will be key to the success and desirability of the technology for high throughput screening applications.

Chapter 4 explores a potential workflow for high throughput screening utilising droplet-reinjection methodologies, allowing for droplets to be stored, incubated or even manipulated before MS analysis. Unfortunately, the extension of the generation workflow described in Chapter 3 to droplet reinjection-MS is not trivial, with the coalescence of droplet populations a newly arising challenge. Chapter 4, not only highlights these difficulties but trials solutions to overcome droplet coalescence when coupled to electrospray ionisation mass spectrometry.

# 1

# Introduction

## 1.1 Declaration

The main body of this chapter has been reproduced from a published review article which I wrote:

E. E. Kempa, K. A. Hollywood (KAH), C. A. Smith (CAS) and P. E. Barran (PEB), "High throughput screening of complex biological samples with mass spectrometry – from bulk measurements to single cell analysis", *Analyst*, 2019, **144**, 872-891.

For this first author publication, I drafted and edited the manuscript with additional edits provided by KAH, CAS and PEB. The article has been reproduced here in an unchanged format except for minor adjustments to incorporate the text and figures into this thesis. It is noted that since this reviews publication in 2018, there have been advances in the field which are not covered in this thesis chapter. Instead these advances are described in the introductions to results Chapters 2, 3, and 4.

# High throughput screening of complex biological samples with mass spectrometry – from bulk measurements to single cell analysis.

Emily E. Kempa,[a] Katherine A. Hollywood,[b] Clive A. Smith[c] and Perdita E. Barran[a,b]

[a] Michael Barber Centre for Collaborative Mass Spectrometry, Manchester Institute of Biotechnology, The University of Manchester, Manchester, M1 7DN, UK.

[b] Manchester Centre for Synthetic Biology of Fine and Speciality Chemicals (SYNBIOCHEM), Manchester Institute of Biotechnology, The University of Manchester, Manchester M1 7DN, UK

[c] Sphere Fluidics Limited, The Jonas-Webb Building, Babraham Research Campus, Babraham, Cambridge, CB22 3AT, UK

Publication Date (Web): 10th December 2018

## 1.2 Abstract

High throughput screening (HTS) of molecular analytes is in high demand from and implemented in many areas of chemistry, medicine and industrial biotechnology including the discovery of biomarkers and the development of new chemical entities. Despite its prevalence, technical challenges remain in many of the new application areas of HTS which require rapid results from complex mixtures, for example in screening biotransformations; targeted metabolomics; and in locating drugs and/or metabolites in biological matrices. Common to all of these are lengthy and costly sample preparation stages, involving recovery from cell cultures, extractions followed by low throughput LC-MS/MS methods or specific fluorescence measurements. In the latter, the target molecules need to be inherently fluorescent or to include a fluorescent label or tag which can adversely influence a cellular system. Direct infusion mass spectrometry coupled with robotic sample infusion is a viable contender for information-rich HTS with sub-second analysis times, and recent developments in ambient ionisation have heralded a new era where screening can be performed on crude cell lysates or even from live cells. Besides commercially available technologies such as RapidFire, Acoustic Mist Ionisation, and the TriVersa ChipMate there are promising new developments from academic groups. Novel applications using desorption electrospray ionisation, microfluidics, rapid LC-separation and 'one cell' direct infusion methods offer much potential for increasing throughput from 'messy' complex samples and for significantly reducing the amount of material that needs to be analysed. Here we review recent advances in HTS coupled with MS with an emphasis on methods that reduce or remove all sample preparation and will facilitate single cell screening approaches.

## 1.3 High throughput screening (HTS) and ultra-high throughput screening (uHTS)

High throughput screening (HTS) and ultra-high throughput screening (uHTS) techniques are described as methods able to analyse ten to one hundred thousand samples per day. [1–6] The opportunity to screen at this speed is in high demand from the pharmaceutical and biotechnological industries as well as for disease and health monitoring, to develop new drug leads and to develop high-value chemicals. [5,7,8] Accompanying such an aspiration to screen complex mixtures ever more rapidly are regulatory requirements, which necessitate more sustainable processes, and require reproducible methods. Industrial biotechnology aims to use bacterial cells or other small organisms to produce compounds of interest in a manner that produces less waste and consumes less energy than the equivalent synthetic chemistry route. This is an aspect of synthetic biology, where new biological components such as enzymes and genetic circuits are reprogramed into bacterial cells to alter cellular behaviour or properties [9,10] in order to manufacture specified products such as biofuels and biomaterials. [11–13] Synthetic biology can be used to produce new compounds *via* a process known as directed evolution where genetic sequences are randomly altered to improve the efficiency of a given cellular process, [10,13] with a concomitant requirement for the analysis of up to and over 100 000 cellular variations for a given target. [13–15]

Traditionally, the starting components for a screen are provided in 96, 384 or even 1536-well plate formats [16,17] for their ease of flexibility between plate handling robotics [4,5] and multiple analytical techniques; particularly fluorescent or colourimetric well plate readers [18–20] and chromatography and mass spectrometry injection systems. [21,22] Fluorescent well plate screening is widely utilised, [6,23] notably in the analysis of drug interactions to produce dose-response curves. [18,24–27] These systems often offer the highest throughput, with a fluorescent well plate reader achieving below 1 s per sample, [28] and additionally do not require great amounts of data analysis to determine 'hit' rates, allowing for a simple positive or negative response for each well in the plate. However, these assays rely on the presence of an

active chromophore within the system of interest, or to be coupled to secondary chemical reactions [29] or fluorescent tags as an indirect readout of activity. Both cases can suffer from interference and require high system suitability for successful and accurate assays to take place.

Decreasing the reliance on fluorescent and colourimetric assays for monitoring chemical flux in cells increases the number of detectable species that define the process, or indeed are the target applicable to many areas including disease screening and synthetic biology. Mass Spectrometry (MS) is heavily utilised in these fields [30–33] due to its ability to detect a characteristic mass to charge ratio ($m/z$) of analytes in the sample, providing the analyte can form a gas phase ion or ions. [34] The range of platforms available for MS and the diversity of ionisation sources mean that different samples are amenable to MS analysis. For many analyses, the most common approach is to include a separation step prior to MS – most notably gas or liquid chromatography. [34] Most of the apparatus for these systems utilise autosamplers to increase the throughput; however, the separation of a complex biological sample, for example, plasma or liquid bacterial extracts, can take in excess of 30 minutes per sample – i.e. not ideal for studies which require analysis of greater than 500 samples. As a consequence, there has been considerable effort to remove lengthy chromatographic separations with many optimised state of the art methods now utilising run times of 1 to 5 minutes. Omitting the chromatography step all together and infusing the sample directly into the mass spectrometer is also now a common approach allowing higher throughput analysis.

Commercialised instruments that are coupled to mass spectrometers for direct infusion discussed herein include the TriVersa NanoMate, LESA and the Agilent RapidFire, with the applications, advantages and disadvantages discussed for each within the relevant sections. Instruments yet to be brought to the market, such as microfluidics and Labcyte Echo coupled MS (or Acoustic Mist Ionisation MS) systems, are also detailed as well as MS imaging technologies which have shown the potential to be adapted for HTS applications. Figure 1.1 summarises the throughput and the smallest amount of sample required for the aforementioned techniques. The

latter half of this review will concentrate on MS technologies utilised in the realm of single cell analysis, with particular focus on their current throughput and the potential for this to be advanced. It is noted that many of these single cell MS technologies are yet to come to the market and have been developed by academic groups; hence, an assessment of the future marrying of HTS, commercialised instrumentation and single cell analysis will be made, alongside recommendations regarding the technological improvements needed to achieve such a goal.

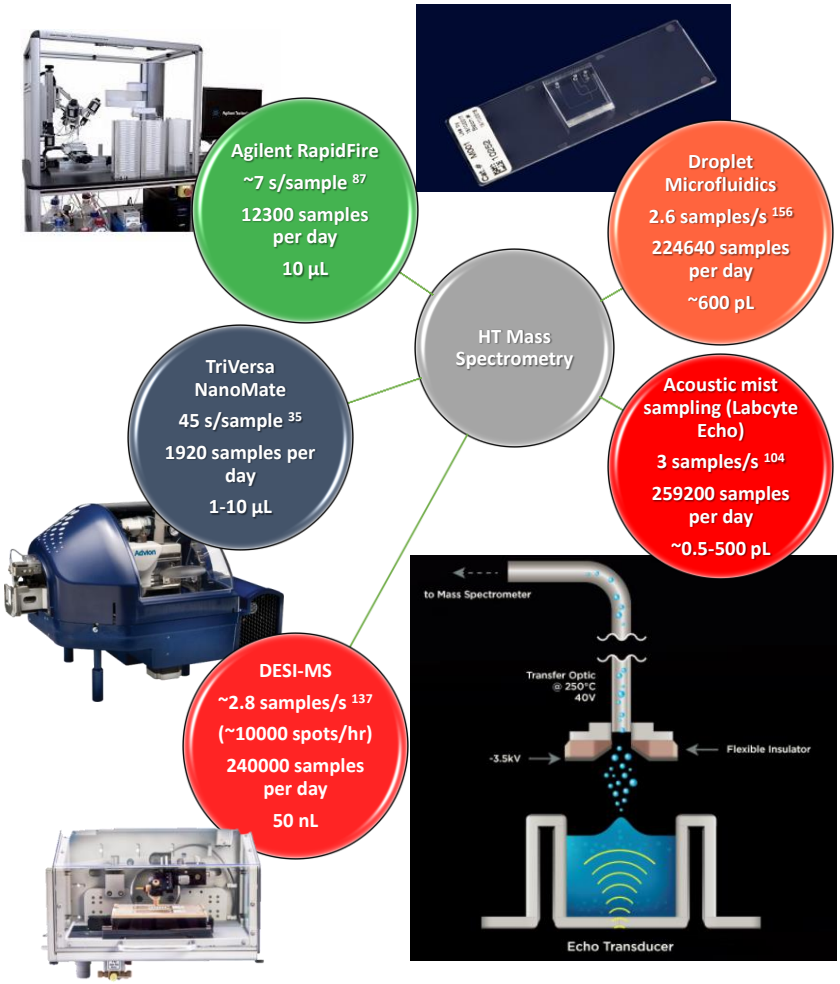


*Figure 1.1: Selected commercialised mass spectrometry HTS instrumentation discussed here depicted from low to ultra-high sample throughput. The reported rate of sample analysis for each has been converted into the number of samples possible to analyse per 24 hour period (day) should the instrumentation be performed continuously at this level. The minimum sample volume has also been quoted for each technique. All schematics and photography of the instrumentation summarised have been taken from the websites of the respective manufacturers (https://www.agilent.com/en/ products/mass-spectrometry/rapidfire-high-throughput-ms-systems/rapidfire-365, https://advion.com/products/triversa-nanomate/, http://www. sphere fluidics.com/product-category/microfluidic-biochips/, https://prosolia.com/products/desi-2d/, https://www.labcyte.com/echo-technology/ acoustic-mass-spec).*

## 1.4 TriVersa NanoMate and LESA

### 1.4.1 NanoMate

The TriVersa NanoMate (Advion, Ithaca, NY) is a fully automated nanoelectrospray (nESI) sample introduction method for the mass spectrometry analysis of multiple samples, including those directly obtained from microtiter plates. [35–38] This front end system consists of a liquid handling robot coupled with a silicon microchip containing an array of up to 400 nanoelectrospray nozzles to deliver the sample to the mass spectrometer inlet *via* a pipette tip into which the sample has been aspirated from a conventional well plate. [35,36] Each nozzle and pipette is used only once to minimise sample carryover between experiments and, as with conventional nESI, only requires small sample volumes (1–10 μL). [35,36,39,40] Upon delivery of the sample from the pipette tip, nitrogen gas and a spray voltage are applied to the nozzle to generate a nESI plume directed towards the MS inlet (see Figure 1.2). [35,40] MS data acquisition can then take place for a pre-set time for each sample, a parameter which can be shortened to increase sample throughput or lengthened to improve data quality (increased number of data points per sample). [35] Van Pelt *et al*. reported that MS data acquisition of 5 seconds, and a NanoMate cycle time of 40 seconds, allowed for a 1 μL sample to be analysed every 45 seconds. [35] This equates to just under 2000 samples in 24 hours, positioning the NanoMate at the lower end of a scale of samples per time unit (Figure 1.1). Early inceptions of this instrument struggled with analysis in negative ionisation mode, and this problem has not been entirely surmounted. In addition, the advantages gained by reducing carryover provided by using single use nozzles and chip orifices mean that each analysis is costly. Chip orifices do clog and some solvents can strip the conductive coating from the sampling chip. Despite these disadvantages, the NanoMate is versatile and has been interfaced with numerous different mass spectrometers across multiple vendors. [39,41–43] The low flow rates and lower applied voltage of nESI bring increased sensitivity, milder ionisation conditions allowing non-covalent complexes to be examined [38,40] and lower sample volumes in comparison with electrospray ionisation (ESI) mass spectrometry, as well as no carryover. [36,38] The lack of an LC separation stage can lead to ion suppression of some analytes and oxidation of certain compounds due to the conductive pipette tips

utilised to apply the nESI voltage to the solution. [35] Due to the one time use of the chip and electrospray nozzles, sustained procurement of consumables is needed for this apparatus to run continuously in a high throughput manner. This may become unsustainable for laboratories in comparison with LC-MS approaches or even direct infusion from an autosampler. The TriVersa NanoMate has also been used to facilitate LESA (Liquid Extraction Surface Analysis) approaches (discussed in Section 1.4.2), which have enabled ganglioside [38] and ceramide lipidomic analysis, [42] top down[40] and bottom up proteomics [37] as well as selected [39] and multi-reaction monitoring. [37]

Omitting LC separation can remove in excess of 30 minutes of run time per sample, leading to greatly increased throughput; however, the lack of separation can lead to ion suppression during the electrospray process due to both co-elution and matrix effects, which may affect the accuracy of quantitative results. Van Pelt *et al*. undertook a study in 2003 where they compared a fully automated NanoMate approach with an LC-MS/MS method for the analysis of Caco-2 cell samples. Here the LC method consisted of a gradient elution time of 5 minutes per sample, whereas the NanoMate method achieved sufficient sample data in 1 minute and 45 seconds per sample, an increase in throughput of almost 2.9 times. However, it is important to note that for the NanoMate analysis an additional off-line desalting step was required, but again this can be undertaken through the use of C18 ZipTips and a fully automated liquid handling robot to minimise loss of throughput. In this case, two different internal standards were analysed within the sample sets and the results were in good agreement, leading to the conclusion that the NanoMate method was robust and holds great potential as a high throughput alternative to current LC-MS/MS methods. [35] More than 15 years since its launch, the NanoMate continues to be a useful method for HTS in many laboratories. [44,45]

Gangliosides are complex glycosphingolipids composed of a ceramide lipid unit and an oligosaccharide chain. These species are prominent within the cells of the human nervous system and are known to play key roles in cell signalling processes and are often the focus of research into biomarkers of brain diseases including cancer.

[38,46] In the past (and still to this day), chromatographic methods (both LC and TLC) were key to the characterisation of these species due to the need to separate complex mixtures prior to mass spectrometry analysis; [38,43,46,47] however, many groups have now begun to omit this chromatography step due to lack of sensitivity and instead adopt the high throughput capabilities of a NanoMate MS/MS workflow. Zamfir and Serb *et al*. have demonstrated their ability to identify different gangliosides in both healthy and tumorous nervous system tissues by mass assignments obtained using a NanoMate workflow. [43,46,47] In 2011, mass spectra were acquired under identical conditions at a rate of 1 minute per sample, with the healthy tissues found to contain a larger variety of singly, doubly and triply charged ganglioside structures in comparison with diseased samples, which were instead found to contain only singly charged moieties with shorter oligosaccharide chain lengths and reduced sialic acid content. [46] The rapid characterisation of such structures has potential for biomarker discovery and enables the identification of biological pathways which can eventually lead to the development of a therapeutic intervention. Park *et al*. also adopted tandem MS analysis for metabolomics and biomarker identification, in which the MS profiles of ceramide species were studied in mouse skin following UVB irradiation. [42]

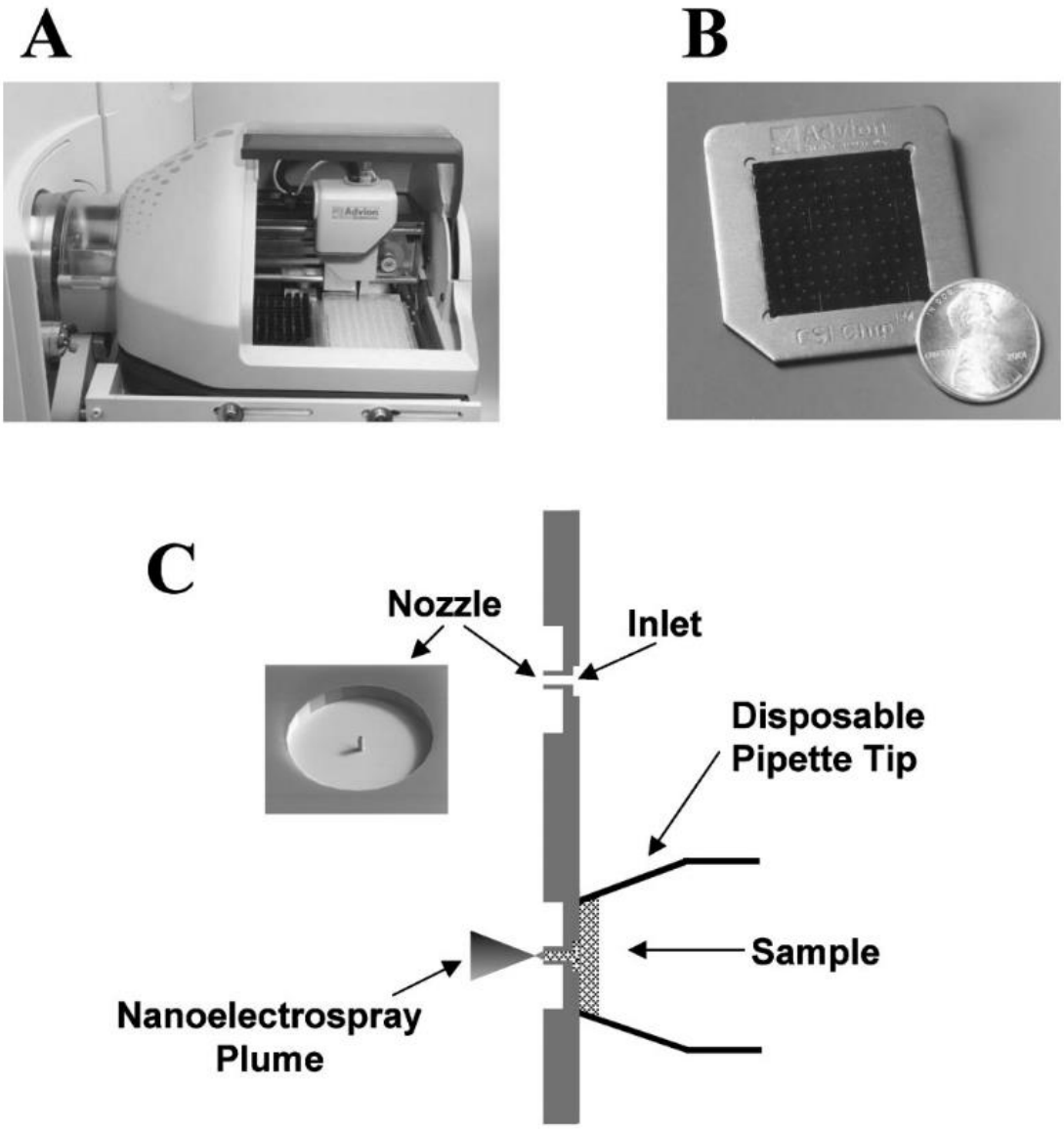


*Figure 1.2: A) Photograph of the TriVersa NanoMate mounted on a mass spectrometer. B) Photography of the NanoMate nESI chip containing 10 nozzles with a US quarter dollar for scale (24.3 mm). C) A schematic illustration of the Avidon TriVersa NanoMate action, in which the sample containing a pipette tip is pressed onto the nESI chip, where a voltage is applied to generate an electrospray plume. Reproduced with permission from Van Pelt et al., Rapid Commun. Mass Spectrom., 2003, 17, 1576.* [35]

Flangea *et al*. developed high throughput top-down sequencing with samples infused by a NanoMate employing ETD (electron transfer dissociation) and CID (collision induced dissociation) using a high-capacity ion trap MS. [40] Top-down analysis of intact proteins allows analysis of protein complexes and non-covalent interactions, and quantification of post-translational modifications and can result in higher sequence coverage in comparison with bottom-up methods. [48] Flangea *et al*.

achieved 80% sequence coverage for the 16+ charge state of apomyoglobin (16.95 kDa) using a NanoMate and performed ETD with high reproducibility during only 30 seconds of fragmentation time within the mass spectrometer. [40] Hence, this information rich, high throughput approach gives hope that larger proteins may be sequenced this way, along with detailed studies of their post-translational modifications.

### 1.4.2 Liquid extraction surface analysis (LESA)

Liquid extraction surface analysis (LESA) is an analyte extraction technique first described by van Berkel and co-workers and was commercialised by Advion, allowing surfaces to be subjected to automated sampling and MS analysis through its coupling with ambient ionisation (nESI chips). [37,49–51] The LESA extraction procedure utilises the conductive pipette tips mentioned above, in which a solvent is aspirated from a trough or well and deposited onto the surface for a defined period of time (Figure 1.3). During this time the pipette tip remains in contact with the liquid spot as the solvent extracts analytes from the surface into the droplet, before being re-aspirated and inserted into the inlet side of the nESI chip. [49–53] At this stage, a voltage is applied to the chip along with nitrogen gas pressure to directly electrospray the extracted analytes from the solvent droplet. This extraction procedure can then continue, under the control of the on-board camera, [52,54] or pre-programmed XYZ positions across the sample to achieve high throughput analysis of different sections of the solid surface. Surfaces that have been successfully analysed in this way include bloodspots previously dropped onto paper, [37,52] biological tissue sections, [51,55,56] agar plates [50,53] or even the surface of a fruit or vegetable. [54] As with conventional NanoMate, the nozzles and pipettes are single use, thus minimizing carryover between each sample, and adding to its advantages is its ability to minimise sample preparation steps such as extraction prior to analysis. However, as mentioned above, the single use of nature of these chips does result in increased consumable costs for the laboratory, a downfall which is exacerbated by the increased susceptibility of LESA procedures to nozzle blocking from surface particulates.

The LESA-NanoMate coupled to an LTQ-OrbitrapXL MS (Thermo Fisher Scientific, Bremen, Germany) has been used to monitor antibiotic product formation directly from bacterial colonies on an agar plate. [53] Optimisation of solvent composition and procedure minimised the extraction of media components from the agar. Additionally, only small modifications to the Petri dish were required to accommodate the NanoMate platform size. [53] This application to whole colony screening (and similar approaches involving other ambient ionisation methods; see later in this review [57]) has great potential for synthetic biology applications to rapidly identify and quantify products from genomic variants. [58] In 2014, Randall and co-workers took a similar approach to the direct analysis of *E. coli* strains using LESA to observe a range of intact proteins, confirming that this approach to analysis is feasible for a range of bacterial strains and compound classes. This method is still at an early stage, and more work must be done to facilitate the transmission and analysis of lower abundance proteins. The authors show that the appearance of some proteins and subsequent top-down analysis can help to determine the health of a given colony, which may have future use in analysing contaminated surfaces. [50]

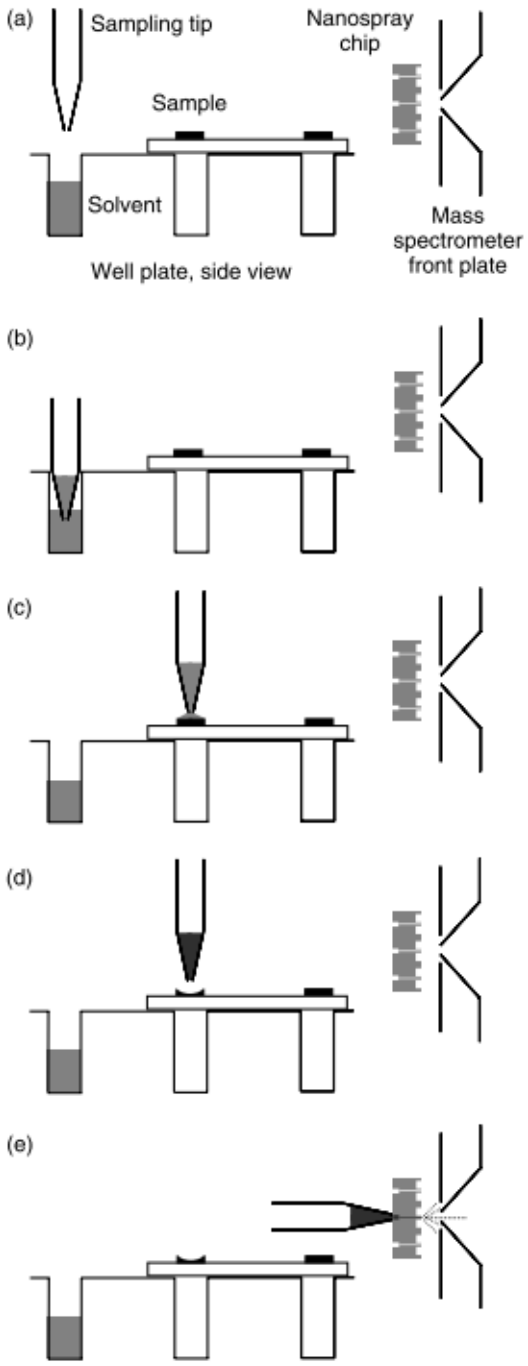


*Figure 1.3: Illustration detailing the individual steps undertaken during LESA surface analysis. A) A clean conductive pipette tip is taken up by the robotic arm. B) Extraction solvent is aspirated from a well. C) Extraction solvent is deposited onto the sample position. D) Extraction solvent and dissolved sample analytes are re-aspirated into the tip. E) The pipette tip is pressed onto the nESI chip for MS analysis. Image reproduced with permission from Kertesz et al., J. Mass Spectrom., 2010, 45, 255 .*[51]

## 1.5 The use of solid phase extraction coupled to mass spectrometry

Solid phase extraction (SPE) is a sample preparation technique first introduced in the 1970s, which selectively isolates compounds of interest from a liquid sample through the use of a cartridge or syringe packed with a porous solid phase chosen for the retention of the analyte class in question. [59–61] The sample is loaded onto a stationary phase through manual pipetting or an automated injection system. Washing the stationary phase with varying solvent compositions removes the sample matrix (as illustrated in Figure 1.4 [62]) which may interfere with downstream processing, for example in MS analysis. [61] Post clean-up, the sample is then re-eluted for further processing or analysis before re-equilibration of the porous phase to remove any strongly retained species. [59] Cartridges can be disposable or reusable, situated online, coupled with chromatography, or offline within the workflow. [61] SPE has been and is still a fundamental sample preparation technique applied in many areas including food science, [63,64] pesticide analysis, [65,66] drug discovery and evaluation, [67–69] forensics [70] and bioanalysis. [71–73] In the past, higher throughput sample preparation has also been achieved by employing automated SPE approaches such as the Zymark Rapid Trace which can perform extractions of up to ten samples in tandem. [74]

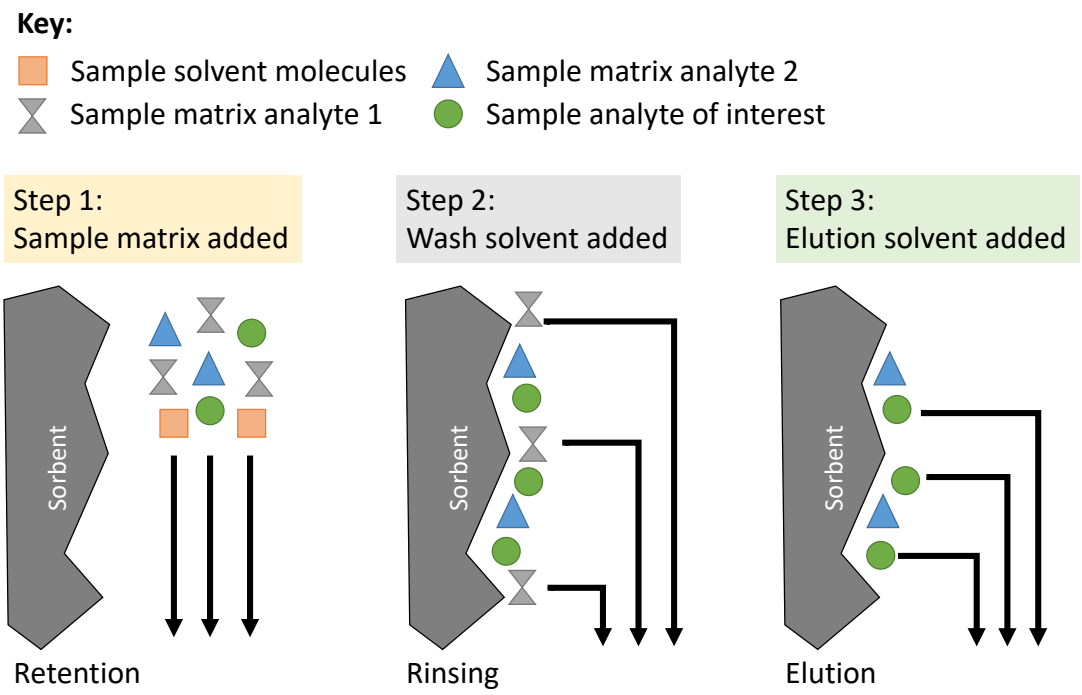


*Figure 1.4: Diagrammatic representation of a solid phase extraction procedure (SPE) highlighting the retention of the sample analytes to the sorbant (step 1), rinsing of the sorbent to remove and discard unwanted analytes (step 2), and elution steps to remove and collect the molecules of interest (step 3). Redrawn and adapted with permission from Solid-Phase Extraction: Principles, Techniques and Applications.* [62]

### 1.5.1 Agilent RapidFire

The Agilent RapidFire is a front-end sample introduction system for mass spectrometry, which is based on a solid phase extraction procedure in the place of a LC column to achieve salt removal and sample clean-up prior to analysis. [75–77] This online preparation system can deliver a cycle time as small as seven seconds per sample. [77–79] The procedure first involves sample aspiration (or 'sipping') from a well plate, before adsorption (or 'loading') of the sample onto a removable SPE cartridge of a user defined stationary phase. A washing step then removes buffer salts and other non-retained analytes from the cartridge for a set period of time, before a solvent of differing composition is then used to co-elute the remaining sample components of interest from the cartridge and into the mass spectrometer inlet for analysis. The cartridge is then re-equilibrated to the clean-up method starting conditions before injection of the next sample. [80–84] Each wash cycle, sipping time (i.e. sample volume loaded onto the cartridge), elution time and MS acquisition time

contributes to the total sample analysis time. Timings need optimisation for differing sample types, and similarly, both wash and elution solvent compositions and the cartridge stationary phase will also need to be considered, with each cartridge capable of enduring in excess of 3000 injections before decline. [75,79,81] The instrument also incorporates a robot such that up to 63 well plates (96 or 384 wells) can be handled at a time. [85,86] The whole system facilitates the analysis of a maximum of 24192 samples before plate intervention, and if the minimum reported cycle time of ~7 seconds per sample is possible, [87] 12 300 samples can be screened in one 24 hour period. This quoted time of 7 s is rarely achieved, and ~30 s are more commonly presented.

Similar to other 'chromatography-free' approaches, ion suppression and matrix effects during the analysis of complex samples can be problematic due to the lack of a separation step and, equally, insufficient washing of the SPE cartridge leads to carryover between samples. [88,89] In comparison with LC-MS, the time taken to analyse a blank sample by the RapidFire system is negligible; hence the addition of blank runs at suitable intervals to check for carryover need not significantly hinder the throughput of the method. [75] Elution and re-equilibration steps during analysis must also be optimised to minimise carryover from the SPE cartridge and retain high throughput. For complex samples, some clean-up prior to analysis is common, the fluidic lines can start to clog and the sensitivity of the ionisation is therefore reduced. Despite these disadvantages, the Agilent RapidFire is a robust platform which is ubiquitously employed for HTS in the pharmaceutical industry. Noteworthy applications undertaken by the RapidFire system include lead molecule identification, [90] removal of false positive results from prior fluorescence assays, [77] and analysis of blood, [91] plasma, [79] honey, [92] and in particular, P450 binding interactions. [76,93]

Lim *et al*. and Wu *et al*. have demonstrated the use of the Agilent RapidFire system in place of fluorescence and/or LC-MS/MS approaches to quantitatively probe reactions between P450 enzymes and drug candidates. [76,93] Drug-drug interaction (DDI) between existing and new drug candidates has become a major concern when

considering a new drug for use, and cytochrome P450 enzymes have been used as exemplar systems to develop new targeting approaches due to previous false positives. [76,94] So far, recombinant P450 enzymes have been used in fluorescence based assays with up to 1536-well plates to increase throughput, although these may not best represent endogenous interactions. Alternatively, LC-MS monitoring of reaction products between enzymes and substrates has been used to quantitatively probe drug-drug interactions; however, the lengthy nature of the LC separation step required hampers this approach as a high throughput technique. [76] SPE approaches permit the extraction of the desired components within a matter of seconds rather than minutes. Both of these studies [76,93] utilised liquid handling robots to prepare multiple concentrations of each substrate with various P450 enzymes within standard well plates, and dose-response curves of each substrate allowed for the determination of the binding constants and inhibition concentrations, $K_M$ and $IC_{50}$, between enzyme and drug. Both SPE-MS/MS methods employed a cycle time of 9 s per well, and in each case they compared RapidFire results to those generated using an LC-MS method. Wu *et al*. concluded that the SPE-MS/MS approach might be used to initially screen drug libraries and determine lead compounds, which would then in turn have their inhibition levels confirmed by LC-MS/MS. [76] Lim *et al*. found that the SPE-MS/MS method for probing their P450 systems gave a 15-fold increase in throughput in comparison with the traditional LC-MS/MS approach, and the method was both sensitive and reproducible. [93]

To improve the throughput further and to obtain rates similar to those of fluorescence assays, Leveridge *et al*. developed a strategy in which sets of 4 samples were pooled (or 'multiplexed') during well plate preparation prior to RapidFire analysis. [90] Approaches such as these do necessitate more complex data analysis and more intelligent compound management, for example, the requirement to combine compounds which will not react with one another; however, this can be a small price to pay for a 4-fold decrease in analysis time in comparison with the conventional method of 1 sample per well. Given the acquisition speed of many modern mass spectrometers, multi-reaction monitoring is still possible and has, for example, been employed for the analysis of peptides. Using two RapidFire instruments and 4-fold

sample multiplexing, it has been stated that up to 280 000 compounds could be screened in 1 week. [90] Potentially more samples could be incubated within a single well to increase throughput further; however, this would be sample dependent and require optimisation.

## 1.6 Acoustic droplet mass spectrometry

### 1.6.1 Labcyte Echo liquid handling technology

Acoustic droplet ejection technology is a promising recently developed alternative to traditional tip-based liquid handling robotics, and with the commercialisation of the Labcyte Echo, this has allowed for the decrease in sample preparation time, in particular aiding in the generation of well plate assays for subsequent high throughput screening methods. [95–97] The focusing of sound waves through the use of transducers allows nanolitre volumes of liquids to be transferred from one reservoir to another without the need for a manual or automated pipette. In the case of the Labcyte Echo, 2.5 nL droplets are moved from a source plate into a destination plate well that is suspended upside down to achieve a desired transfer volume. [98] To avoid samples 'falling out' of the well, the volumes transferred are optimised to ensure that surface tension overcomes gravity. [99,100] This 'tipless' approach not only removes the risk of carryover between samples but additionally allows for increased accuracy and precision during dispensing due to the removal of forces such as surface tension and viscosity between the liquid sample and a disposable tip. [99–101] The removal of tip-based transfers is also advantageous for the avoidance of shear force upon cell cultures which can, in turn, cause damage and affect cellular viability. [100] As with traditional automated liquid handling approaches, here operational speeds are increased and the miniaturizations of sample volumes also benefit the throughput of subsequent screening approaches. [101] Once prepared, the destination well plate can then proceed to optical analysis such as fluorescence or even to prepare plates for automated injection for direct infusion mass spectrometry analysis (Figure 1.5).

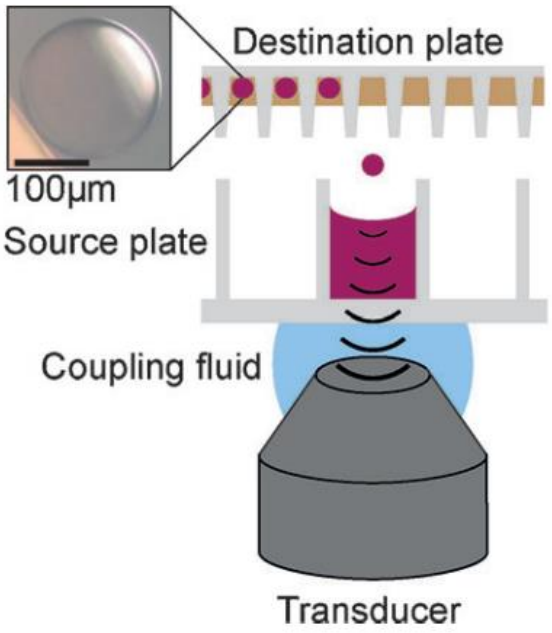


*Figure 1.5: Schematic diagram of the Labcyte Echo highlighting the destination and source plate. The acoustic transducer causes ejection of a droplet from the reservoir and is captured within an empty well held upside down above the source plate. Adapted with permission from Seidel et al., Angew. Chem., Int. Ed., 2010, 53, 7948–7951.* [98]

### 1.6.2 Acoustic mist ionisation mass spectrometry

The use of acoustic technologies to aid throughput within mass spectrometry sample preparation has been possible for over 10 years, most notably during the deposition of MALDI matrices directly onto sample plates. [102,103] More recently, manipulation of liquids by acoustic waves or pulses has allowed the transfer of samples from well plates or other reservoirs directly into the mass spectrometer. This has been achieved both directly by Sinclair *et al*. [104] *via* an adaptation of the Echo liquid handling system termed Acoustic Mist Ionisation (AMI) and through the coupling of SAWN (surface acoustic wave nebulisation) to mass spectrometers, [105] examples of each will be described below.

A novel advancement in acoustic droplet ejection which holds great promise in dramatically improving the rates of HTS was demonstrated in 2016 by Sinclair *et al*. as part of a collaboration between AstraZeneca (Macclesfield, UK), Waters Corporation (Wilmslow, UK), and Labcyte Inc. (Sunnyvale, CA, USA). [104] In this method, ultrasonic pulses eject a mist of femtolitre volume droplets from well plates

directly into the mass spectrometer inlet *via* a heated transfer tube (see Figure 1.6). The fine droplets become charged during this process, due to a voltage gradient applied between the well plate and the sampling orifice, desolvation of these ultralow volume droplets and subsequent transfer to the mass spectrometer is rapid. An xyz stage accommodating a 384-well plate has automated the sample analysis with cited analysis times of 250 ms per well, meaning that an entire 384-well plate can be analysed in less than two minutes. This throughput of approximately three samples per second means that this technology surpasses, in terms of frequency of each sample delivery, any commercially available mass spectrometry introduction technique. Since its initial conception, this technology has subsequently been acquired by Danaher and is currently marketed by Sciex in combination with the Open Port Inlet. The reduction of the droplet diameter from the acoustic wave device may drastically improve ionisation efficiency as has been shown in nESI tips by Williams and co-workers, [106,107] however, during acoustic dispensing to the MS, no ESI Taylor cone is observed and more comparative experiments are needed to determine the efficiency of this ionisation method with conventional ESI and nESI approaches. As with all direct ionisation MS approaches this platform omits chromatographic separation of complex mixtures with commensurate ion suppression and matrix effects; however, it is noted that the addition of ion mobility separation again has the potential to add another dimension to structure identification should it be incorporated into the current assembly. [104]

Although not directly coupled with mass spectrometry and similar to MALDI plate depositions, an approach of Haarhoff *et al*. utilises acoustic transfers for the deposition of assay mixtures including drug–enzyme inhibition studies from traditional well plates on to a 384 LazWell plate for laser diode thermal desorption (LDTD) MS/MS analysis. [28] Using a Labcyte Echo 550, the transfer of 100 nL portions of material for 384 wells can be undertaken in three minutes and with a LDTD-MS/MS analysis time of ~2 s per sample, the incorporation of this sample deposition technique has greatly improved the throughput in comparison with manual spotting of 1–2 microliter samples onto LazWell plates. It is also noted that the minimised sample volume effectively eliminates associated sample drying time, something that

also needs to be taken into consideration during manual deposition of larger amounts. $IC_{50}$ and dose-response curves for the assays undertaken were compared and yielded good agreement with the results obtained from RapidFire assay analysis; however, since the analysis time for RapidFire averaged ~10 s per well, the Echo coupled LDTD approach offered greater throughput and miniaturised volumes. The lack of any SPE cartridge and mobile phase in LDTD also removes the possibility of sample carryover between wells. [28]

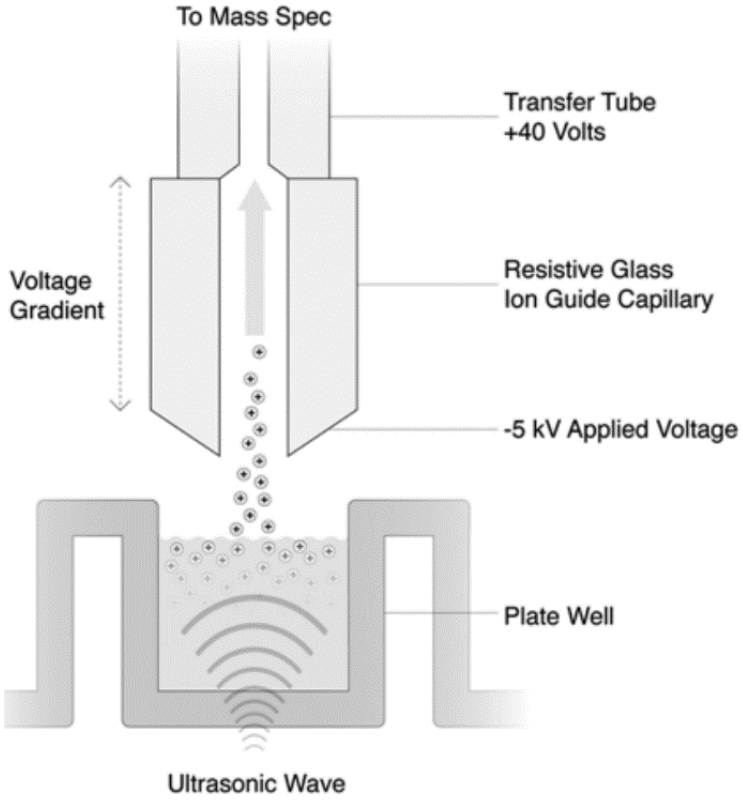


*Figure 1.6: Schematic diagram of the acoustic misting process undertaken from a well plate during the coupling of a Labcyte Echo with a MS. As the ejected droplets enter the ion guide capillary they become charged due to the application of a voltage before undergoing the desolvation process within the source. Adapted with permission from Sinclair et al., J. Lab. Autom., 2016, 21, 19–26.* [104]

## 1.7 Desorption Ionisation Mass spectrometry for HTS

Desorption ionisation MS refers to a number of techniques often utilised in mass spectrometry imaging experiments (or MSI) to build a 2D (and sometimes 3D) map of the location of chemical species within a sample, and is of particular use for solid samples and surface analysis. [108] The major techniques include desorption electrospray ionisation (DESI), matrix assisted laser desorption ionisation (MALDI) and secondary ionisation mass spectrometry (SIMS) each of which has its own advantages and disadvantages. [109,110] These desorption ionisation approaches each offer different spatial resolutions, with DESI reaching ~40 μm, [51,111] MALDI ~5 μm [112–114] and SIMS ~100 nm. [115] SIMS in this case offers the greatest potential for application in single cell analysis; however, as the throughput and sensitivity of this technique are limited it will not be discussed here.

### 1.7.1 MALDI-MS

Matrix assisted laser desorption ionisation (or MALDI-MS) is an approach in which a laser is used alongside a chemical charge donor (or 'matrix') to promote ionisation and transfer of non-volatile analytes into the gas phase for subsequent mass analysis. [116] This technique is deemed as 'soft' ionisation and is often used for labile molecules and is particularly useful in biochemistry for the analysis of peptides, proteins, lipids and metabolites without fragmentation of the molecules of interest. [116,117] Although MALDI-MS has been utilised in imaging applications such as the profiling of tissue sections, [118–120] the instrumentation also lends itself well to the microarray format (sometimes referred to as MAMS – microarrays for mass spectrometry) which is often utilised to increase sample throughput. [121,122] These arrays often take a similar format and size to a multi-well plate and are mounted on a translatable stage in order for each sample to be 'struck' or irradiated by the laser in turn. Additionally, to increase throughput further prior to analysis, automated or spray based matrix deposition can be employed, for example, the use of an acoustic multi-spotter. [123]

MAMS coupled with MALDI allowed for high throughput monitoring of cocaine in hair samples. [121] This procedure utilises a custom made MAMS slide which

can contain 600 hydrophilic spots, with each MALDI target plate able to hold 3 of these custom made slides (i.e. 1800 spots per target plate). Besides the fabrication of the target plate, an aliquoting procedure *via* a metal slider was developed to generate 60 replicate deposits of a sample from a reservoir also incorporated into the MAMS slide design. The same sliding technique facilitated reproducible spotting of the matrix onto all of the sample spots, with one pass of the slider device. Samples in the reservoir consist of a 'solvent-based' liquid extraction from hair samples followed by MALDI-TOF-MS analysis involving continuous sample plate stage motion.

Microarray formats can also be of use for tissue and organ section analysis as the grid like application generates defined co-ordinates for systematic sampling across a surface. [124, 125] This is particularly useful when the tissue sections are large in area, and for screening multiple sections. Arraying the matrix allows the analysis time to be reduced as the instrumentation can be targeted to quickly raster across a larger area, but this limits sample collection to predefined spots. The advantage of this is that the entirety of the tissue section is not destroyed or perturbed by the sample preparation procedure, or by the impact of the laser beam, allowing the sample to be revisited for further analysis including histology if required. Groseclose *et al*. employed tissue microarrays and MALDI microarray formats in a high throughput proteomic study. Each tissue biopsy was analysed in a grid formation following automated spotting of trypsin solution and matrix upon the tissue (i.e. the entirety of the tissue section was not coated with trypsin or matrix solution). [125] Only the grid coordinates which contained the trypsin digest/matrix spots were then subjected to MALDI-MS analysis (Figure 1.7). The proteolytic peptide mass spectra acquired along with histology staining produced a training set then applied in the identification of cancerous and non-cancerous regions. Although this approach holds promise with regard to the throughput and the breadth of the ensuing data produced, the authors caution that more robust data analysis tools and larger sample sets of differing types would be required before translation into the clinic. [125]

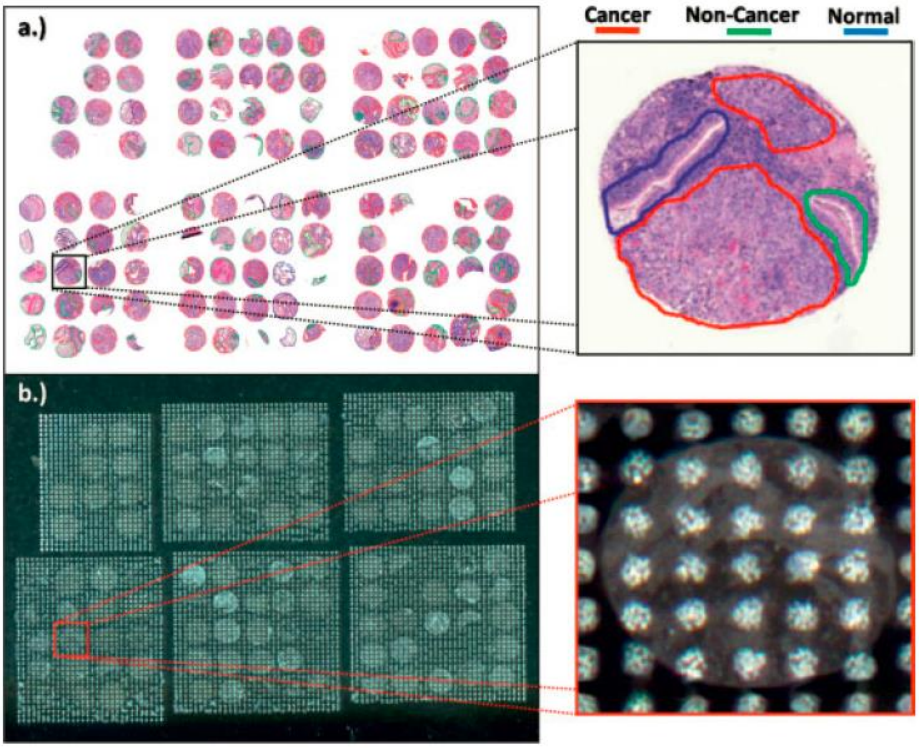


*Figure 1.7: Example of mass spectrometry imaging utilising tissue microarrays. The TMA used in this study contained various types of biopsies including squamous cell carcinoma, adenocarcinoma, and bronchioloalveolar carcinoma as well as non-cancer tissue from matched individuals. a) Cylindrical tissue biopsies are first taken from individual tumours with cancerous and normal cell regions indicated by the inset. b) Trypsin and matrix are spotted in selected positions across the array with the inset demonstrating on average 6 × 6 sample spots available per tissue microarray. Adapted with permission from Groseclose et al.* [125]

### 1.7.2 DESI-MS

Desorption electrospray ionisation (DESI) mass spectrometry is a relatively new technique in comparison with MALDI, and was first described in 2004 by Z. Takáts and R. G. Cooks. [126] Utilising a solvent stream, gas flow and applied voltage, an electrospray plume is generated and directed at the surface of interest under ambient conditions. As the charged droplets impact the surface, sample analytes are dissolved within the electrospray stream, and secondary droplets transferred towards the mass spectrometry interface, into which desolvation occurs and the charges within the droplet come to reside upon the analyte, as seen in conventional ESI mechanisms. [127–130] An xyz stage mounted below the DESI spray facilitates imaging analysis to be conducted at varying speeds and resolution as desired by the user. Since its inception DESI-MS has been applied to many sample types, namely

tissue sections, [131,132] bacterial and fungi analysis [57,133,134] and even for foodstuffs; [135,136] however, for the purpose of this review two high throughput applications (direct bacterial colony analysis [57] and reaction substrate screening [137]) will be briefly discussed.

A compatible xyz stage (such as the one manufactured by Prosolia, Inc.) facilitates screening in microarray format to be undertaken with DESI, as demonstrated by Wleklinski *et al*., who performed reaction screening upon DESI plates containing 6144 (50 nL) sample spots. Under the speeds and spot densities analysed, sample throughput approached ~10 000 spots per hour, a throughput that rivals many other techniques. [137] Reaction screening undertaken allowed the assessment of product formation from a number of different substrates tested within an n-alkylation reaction, and also the effect of different bases on a Suzuki cross-coupling reaction, both of which have important applications within medicinal chemistry. Each reaction was first prepared within 384-well plates before transfer to the DESI plate with both of these steps performed by a liquid handling robot. [137]

Yan and co-workers have used DESI to analyse bacterial colonies in order to determine the production of particular biotransformation products – terming it DiBT-MS (Direct BioTransformation-Mass Spectrometry). [57] This was achieved by culturing bacterial colonies upon agar plates containing a nylon membrane support, which allowed intact colonies to be subjected to a range of different reaction conditions and substrates and subsequently analysed using DESI (see Figure 1.8). Not only does DiBT-MS permit different reaction conditions to be screened, but also post sampling, colonies of interest can be recovered and subjected to subsequent DNA analysis to identify the mutations which may be of interest. [57] This approach has promise for industrial biotechnology and synthetic biology as the number of different genetic variations of interest often surpasses the throughput of currently available label-free technologies. Yan *et al*. show that DiBT-MS can quantify the substrate–product conversion rates and also perform some semi-quantitative limit of detection analysis; however, absolute quantification (readily achieved by LCMS) remains a challenge. Limit of detection levels are required to be quoted in units of area, which does not

translate well to colonies spread unevenly upon the membrane. Additionally, colonies are variable and behave differently with different substrates, which indicates that reaction conversion rates will be challenging to evaluate.

As the above examples show, methods based on DESI-MS hold much promise in the area of HTS, and it is noted that this technology has recently become available as a standard 'inclusive instrument package' *via* Waters Corp. (Wilmslow, UK), which may herald an increased uptake. Wleklinski *et al*. and Yan *et al*. have both demonstrated the potential of DESI-MS for HTS, but in our experience, such experiments still require significant time to optimise. In particular, the sprayer position relative to the sample stage requires 'tuning' for each membrane for optimum results, indicating the need for specialised sample stages. Another obstacle that must be overcome in future applications of MS imaging techniques to HTS is that of the software that controls the scan rate across surfaces. For biomedical imaging applications, the DESI sprayer will be controlled by software to carefully (and slowly) raster across the surface, whereas for HTS a randomised data directed search which may sacrifice resolution for speed would be more appropriate.

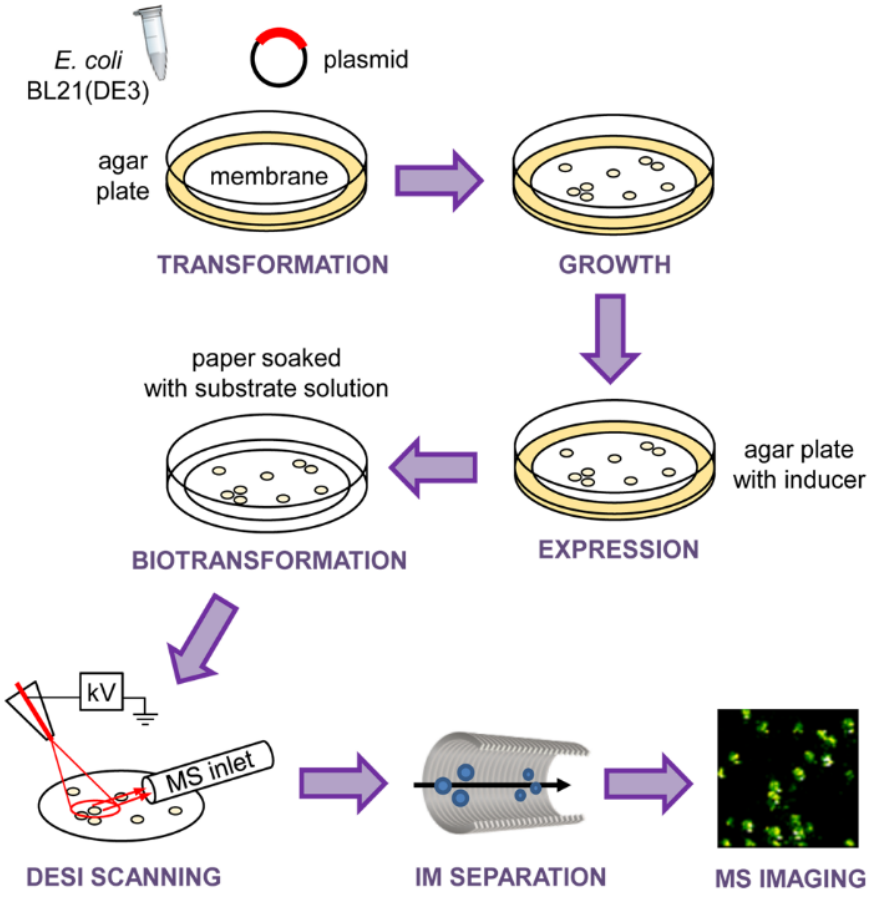


*Figure 1.8: Workflow utilised for the direct monitoring of biotransformations within live bacterial colonies by DESI-IM-MS. E. coli cells containing the plasmid of interest are first spread onto agar plates containing a nylon membrane support, on which the cells actively grow and are transferred between agar plates containing a protein inducer. After growth the membranes are removed and placed upon filter paper soaked in the reaction substrate. The membrane containing colonies are then analysed by DESI-IM-MS. Adapted with permission from Yan et al., J. Am. Chem. Soc., 2017, 139, 1408–1411.* [57]

## 1.8 Microfluidics coupled with mass spectrometry

### 1.8.1 Microfluidics overview

The transition towards lab-on-a-chip devices from traditional glass and plasticware has already brought significant benefits to the analysis of chemical and biological samples. Integration of robotic methods for chemical synthesis or robotic handling systems for cell-based chemical assays followed by high throughput analytical screening into one device which incorporates only small fluid volumes will have substantial advantages. [138] Microfluidics is central to lab-on-a-chip approaches and allows compartmentalised picolitre to nanolitre volumes of liquid to be manipulated for experiments and assays equivalent to those undertaken in microtitre

well plates. [139–141] Such small volumes mean reduced reagent cost and consumption, as well as decreased labour requirements. Emerging technologies allow several analytical processes to be incorporated within the same chip-based device, including reagent mixing, reaction termination and analysis. [142] Many analytical techniques involve preparation steps that result in sample losses, and whilst working with ultra-small volumes can be challenging for the human analyst, microfluidics lab-on-a-chip approaches can bridge these gaps through full automation of sample processing and analysis without losses. [143]

The most common microfluidic approaches can be categorised into two subdivisions, digital microfluidics and droplet microfluidics. Digital microfluidics manipulates a liquid into sub-microliter volumes using an array of electrodes which alter the interfacial tension between the liquid and the surface; [141,144] whereas droplet microfluidics utilises the flow of two immiscible liquid phases and pre-formulated channels to form droplets of the required dimensions with high mono-dispersity. [145,146] This review will largely consider the applications and technologies of the latter approach due to its higher throughput capabilities, [23] and more specifically it will focus on the coupling of droplet microfluidics with electrospray ionisation mass spectrometry.

### 1.8.2 Microfluidics coupled with electrospray ionisation (ESI) mass spectrometry

The coupling of MS to microfluidics has attracted increasing attention in recent years, due to its ability to offer a sensitive, label-free detection technique for both on and off chip analysis. [146,147] ESI and MALDI have been the most commonly exploited ionisation techniques and have been utilised in many applications such as protein identification, [148] metabolomics-based studies of *E. coli* [149] and *in situ* reaction monitoring.[150] ESI and closely related coupling techniques are discussed below, with MALDI-based microfluidic techniques discussed elsewhere in the literature. [147,150,151]

The most common approach to on-line microfluidics to mass spectrometry coupling is ESI, in particular *via* nanoflow (nESI), due to its ability to generate a stable spray of the dissolved analyte into the mass spectrometer inlet with flow rates in the

range of microliters per hour. [152] Other advantages of nESI over conventional electrospray configurations include increased sensitivity, higher ionisation efficiency and the application of lower electrospray voltages at the emitter tip due to the decreased tip aperture. [153] To couple microfluidic chips to a mass spectrometer, different approaches have been used including spraying directly from the edge of a chip, [152,154] the addition of an electrospray tip to the channel outlet post chip fabrication (external emitter), [155] and the integration of a sprayer tip in the initial chip design and fabrication stages (integrated emitter). [144,153,156] Successful chip–MS coupling utilising an integrated emitter and borosilicate microfluidic chip has been demonstrated by Belder *et al*. [156] with several applications, including on-chip organocatalysis, [157] and micro-freeflow electrophoresis separation. [158] Although fabrication of chips assembled from glass often requires intricate micromilling or HF wet etching, [159] the integration of emitters within these chips avoids many of the disadvantages associated with external emitters, especially in their assembly. [156] As a number of other materials become amenable to integrated emitter fabrication, [160,161] this may become the favoured method of chip based MS coupling to ensure reliable use. However, one such example yielding promise for high throughput applications, in which an external emitter (in the form of an inserted gold coated ESI capillary) has been utilised for droplet MS analysis, has been described by Smith *et al*. [162] This allowed for highly sensitive (sub-femtomole) label-free identification of individual droplets filled with proteins ranging from 12 kDa to 148 kDa in molecular weight. In these experiments, a high voltage in the range of 2.5–3.6 kV was applied to the gold coated silica capillary (50 μm ID) *via* a copper wire, with a MS scan rate optimised to the flow rate of droplets travelling towards the emitter. Single scans allowed each protein to be identified by accurate mass analysis, although it was reported that there were small amounts of surfactant and protein cross-contamination in some scans, possibly due to incomplete spraying of the previous droplet as the next droplet reaches the emitter. There is said to be no indication that droplet fusion or protein cross-talk occurs during the droplet mixing or re-injection stage, and this re-injection occurs at a rate of up to 2.6 droplets per second. [162] This setup has the potential to be improved further through chip design, and will likely become applicable for whole

cell analysis, as the droplets would have the ability to be utilised as discrete bioreactors (Figure 1.9).

In the external ESI coupling approach of Smith *et al*. described above, [162] the continuous oil phase (along with the pico-droplet) enters the mass spectrometer inlet freely, as the oil does not substantially interfere with the mass spectrum obtained for each protein. Perfluorous components (both oil and surfactant) available for droplet microfluidic flows are now specifically designed to minimise positive mode ESI interferences. However, in instances where interference does become a problem, it may be necessary to transfer or extract the droplet or encapsulated components into an alternative continuous phase. [143,163] Additionally, since publication in 2013, a similar droplet–MS coupling approach of Belder and co-workers utilised Teflon tubing inserted below the electrospray emitter as an 'oil drain', less so due to oil interference, but instead to ensure a stable electrospray process. [164–166] Although this oil drain fulfils its purpose to reduce the interference, it introduces some added complexity during fabrication. Another approach to oil removal has been demonstrated by Kelly *et al*., where a purposely designed chip allowed for contact between adjacent oil and aqueous streams through cylindrical baffles spaced approximately 3 μm apart. Differences in interfacial tension between the two adjacent liquids prevented bulk mixing; however, as the aqueous droplet or plug (generated prior to this junction) enters the baffle region, rapid coalescence of the droplet into the aqueous stream occurs through the gaps between the baffles. The droplet then travels with the aqueous stream to the ESI emitter, and the oil stream is diverted to waste. [143] Differences in the length of the carrier channel from the coalescence junction to the MS inlet were also investigated to identify the extent of droplet dilution prior to the MS analysis, as minimal analyte dilution, particularly in sample-limited analysis, is desired. Shorter distances resulted in superior analyte MS signal with less dilution and band broadening, whereas larger distances were found to be better suited to analyte separations such as those that transpire in capillary electrophoresis. [143]

With its low sample volumes allowing for miniaturised assays, microfluidics does indeed seem to be a viable approach for future generations of HTS, particularly in the realm of single cell analysis (see later sections). A number of downfalls, however, can be identified – namely in device manufacture and testing. Often, multiple iterations of device designs and fabrication approaches are required before a final (or even usable) chip is acquired. Fabrication requires specialist equipment, training and materials, and often for the smallest of design features (sub-100 μm) a low dust environment such as a class 1000 or better laboratory is recommended, something that increases the cost of undertaking projects such as these exponentially. Repeated usage of devices can also cause difficulties as once a microfluidic channel has become blocked the device is often rendered unusable, requiring repeated fabrication of the same design. Often the microfluidics industry and research groups do not explicitly showcase these failures within their published work, often leading others to believe that chip–MS coupling is easily achievable with their current mass spectrometer. Hence, such an undertaking should be approached with caution, as often a number of analysts will be required to work on such a project at any one given time if results are required promptly.

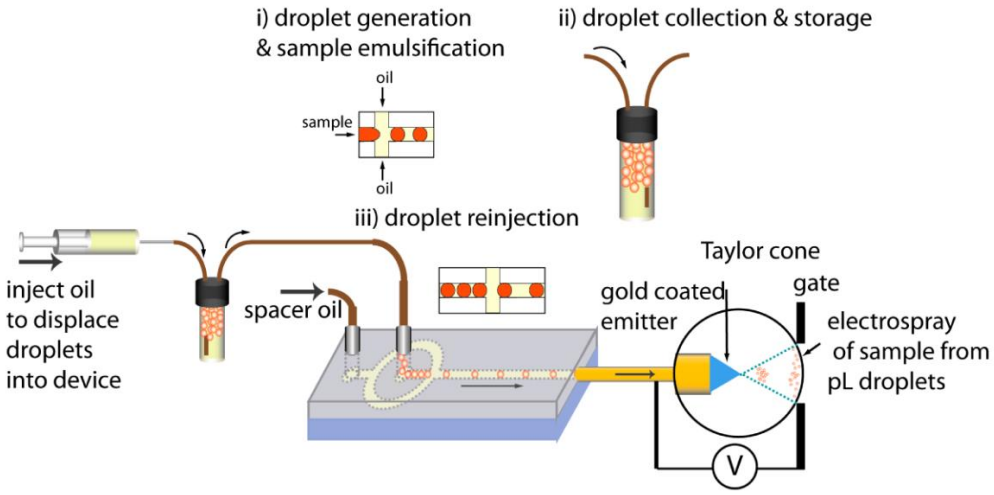


*Figure 1.9: Integration of a microfluidic chip with ESI-MS for the analysis of ~500 pL droplet filled with proteins. (i) Droplets of the sample of interest are generated; (ii) these droplets are collected and then stored overnight; (iii) droplets are re-injected into the mass spectrometer chip with the aid of a spacing oil. Droplets flow through the chip towards a gold coated electrospray emitter, at the end of which a voltage is applied to generate an electrospray of the droplet and the surrounding spacing oil. Adapted with permission from Smith et al., Anal. Chem., 2013, 85, 3812–3816.* [162]

## 1.9 Towards single cell mass spectrometry analysis in systems biology

The analysis of heterogeneity between cells of the same phenotype can allow for a greater understanding of biological systems, in particular, the study of intracellular processes, and how these infer differentiation of healthy and disease states and cause certain remedial resistances in both mammalian and bacterial cells. [167–170] One such advantage of studying these processes is to facilitate earlier diagnosis of disease and to aid therapeutic intervention. Current and established techniques in single cell analysis are focused on microscopic and cytometric-based methods coupled with fluorescence; [167,171] however, these approaches limit the applicability of the cell types and molecules to be analysed. If the sample of interest is not inherently fluorescent, then the analyst must incorporate a fluorescent marker either chemically or genetically. [172] Other competing detection technologies for single cell analysis include FTIR (Fourier-transform infrared spectroscopy), [173] Raman spectroscopy, [174,175] and mass spectrometry, [176–178] each with its advantages and disadvantages. Mass spectrometry single cell analysis is often coupled with other techniques and to date, most approaches are not reliable or sensitive enough for high throughput application. As mentioned previously, secondary ion mass spectrometry (SIMS) can map the spatial distribution of small molecular biomarkers in cells, [179–182] for example, metabolites [183] and lipids, [184] but SIMS remains time consuming, and the instrumentation currently available is not able to perform high throughput analysis.

The following sections consider mass spectrometry approaches for the analysis of 'a few to single cells' within the context of systems biology. It is noted that single cell analysis is the ultimate goal for the determination of heterogeneity between cells, with the analysis of 'a few' cells concurrently unable to distinguish between individuals. Despite this, the movement towards 'a few' cells from those methods previously employing entire colonies or tissues, illustrates the advancement in sensitivity of analytical technologies. Thus, single cell isolation strategies then become the major barrier to determining such heterogeneity.

### 1.9.1 Proteomics from a few to single cells

One such example of combining a number of differing techniques for single cell mass spectrometry analysis was presented by Mellors *et al*. in 2010, in which an automated microfluidic device was integrated with capillary electrophoresis and ESI-MS. [185] Their microchip was able to incorporate a number of operations including cell delivery, cell lysis, separation of lysed products *via* capillary electrophoresis and ionisation for ESI-MS analysis, all with a throughput of 5 s per single cell. Using fluorescence imagery, single cells were visualised passing through the microchip to the mass spectrometer and were found to have random spacing between cells. This was also visualised in the corresponding total ion chromatogram in which it was believed that the majority of peaks were due to single cells passing through the microchip and the mass spectra for the haemoglobin $\alpha$ and $\beta$ units within these cells could be obtained for that event. [185] This work provides great promise for the coupling of microfluidics with MS for high throughput single cell analysis of overexpressed proteins and metabolites within cells. Refinement is needed, however, as only one hour of good performance was attained before buildup of lysed cellular components occurred, and flushing steps were required to restore the performance. [185] As the manufacture of these microfluidic devices becomes more routine (something that will require additional development investment from industry and research groups), it is likely that such issues will become less of an occurrence.

Although not explicitly a single cell analysis, an approach termed nanoPOTS (nanodroplet processing in one pot for trace samples) detailed by Zhu *et al*. shows great potential wherein sufficient data are obtained for whole proteome analysis to be performed on very few cells (~10 to ~140 cells). [186] This chip based system coupled with a robotic platform capable of dispensing picolitre volumes allows for proteomic sample preparation, including reduction, alkylation, and digestion, before peptide collection within a capillary, which can be stored prior to analysis by ultra-sensitive LC-MS. This chip-based approach also facilitates cell counting *via* microscopic imaging, and the miniaturised volumes (<200 nL) and surface area seen by the sample reduces protein and peptide losses during preparation. Using this method the authors were able to identify ~1500 to ~3000 proteins within ~10–140 cells

respectively, a coverage that has only previously been achieved from cultures containing several thousands of cells. [186] The liquid handling system used here has been estimated to dispense 350 droplets in less than 30 minutes, offering the possibility for scaling up towards high throughput analysis although this would necessitate a redesign of the chip to accommodate a larger number of droplets. This workflow does, however, include a number of incubation steps (1 of which is overnight) to achieve efficient digestion for bottom-up proteomic analysis, and although these do limit the throughput prior to analysis, this research may pave the way for similar chip systems that could be coupled with top-down proteomics, to reduce sample pre-processing and increase sample throughput (Figure 1.10).

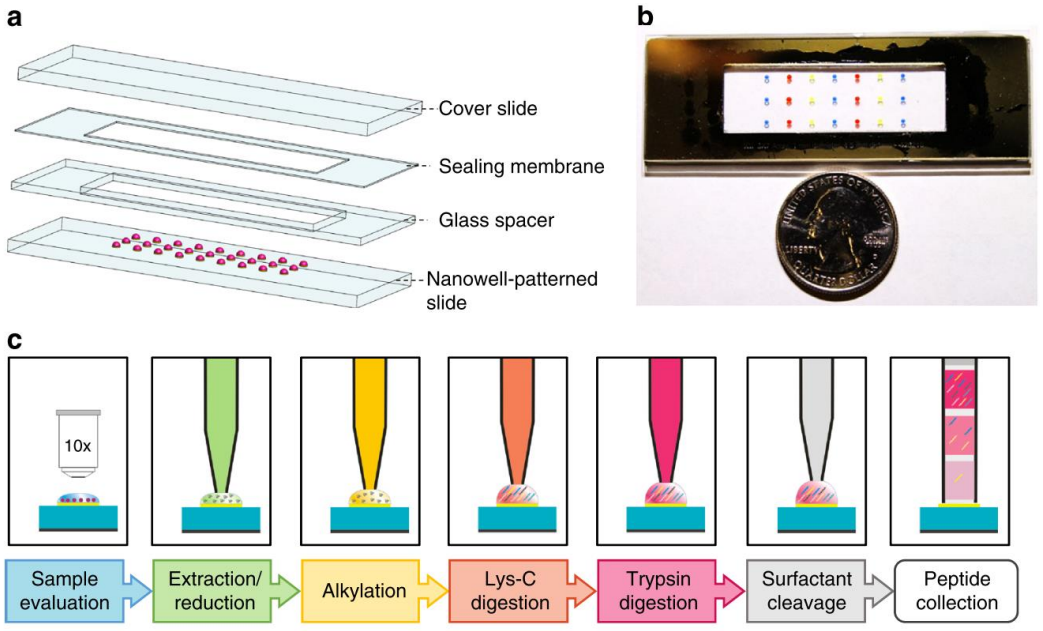


*Figure 1.10: A) Expansion of the components of the nanoPOTS chip. B) Relative size of the nanoPOTS chip in comparison with a US quarter dollar. C) Schematic diagram detailing the procedure employed during nanoPOTS sample preparation including analysis of the number of cells present within the well, reduction of proteins, alkylation of free cysteine residues, 2 protein digestion steps, surfactant cleavage and collection of the resulting peptides within a capillary. Reproduced with permission from Zhu et al., Nat. Commun., 2018, 9, 1–10.* [186]

### 1.9.2 Metabolomics from few to a single cells

A relatively new approach in single cell capture is the use of fluid force microscopy coupled with MALDI-MS for the metabolomics analysis of single cells. This method has recently been published by Guillaume-Gentil *et al.*, where HeLa cells are selected underneath a microscope, and the fluid force microscopy probe is

positioned above the cell to allow for in situ collection of the cytoplasm (1–3 pL). The probe was then retracted and the extract deposited on to the MALDI target plate and MALDI matrix applied. [187] This again utilises the MALDI microarray format employed within many single cell analyses and allowed for the retrieval of up to 20 metabolite types with minimal perturbation of the cell within its cultured environment. The cells remained viable after collection allowing for other analysis types to be subsequently performed, and it is also noted that this approach could allow time course experiments upon the same single cell to be carried out, [187] with the authors demonstrating $^{13}$C-glucose feeding experiments in which labelled carbon atoms were detected within the cell metabolites. However, the extraction and deposition times of each sample take ~3 and ~4 minutes respectively, and there are a number of manual steps such as finding the cells under the microscope and depositing the MALDI extract which all add to the total analysis time per single cell. Again some refinement is needed to increase throughput before this promising approach could become routine for single cell analysis (Figure 1.11).

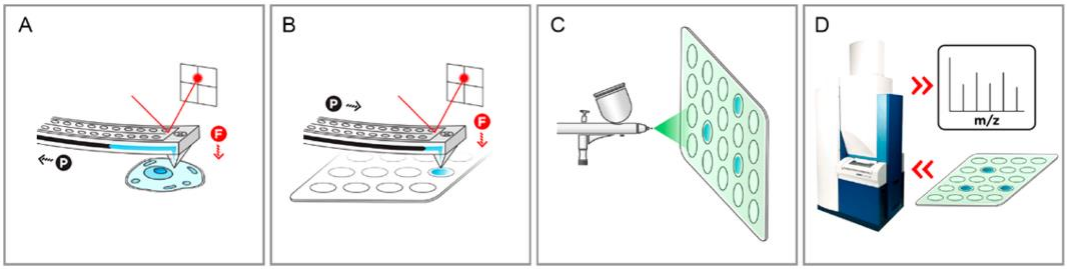


*Figure 1.11: Fluid force microscopy coupled with MALDI-MS workflow for single cell metabolomics analysis. A) The fluid force microscopy probe is positioned above a single cell and the cytoplasm extracted. B) The extracted cytoplasm is deposited onto a MALDI plate. C) the MALDI plate is coated in a MALDI matric solution. D) MALDI-MS analysis of deposited samples. Reproduced with permission from Gillaume-Gentil et al., Anal. Chem., 2017, 89, 5017–5023.* [187]

### 1.9.3 Lipidomics from a few to single cells

A microfluidics coupled MS approach reported by Xie *et al*. has applied MALDI imaging to the analysis of phospholipids from single cells. Using a micro-well format, cells were efficiently captured within a well-organised grid and MALDI matrix deposited upon the cell positions. This micro-well based device was fabricated using standard photolithography and soft lithography techniques, and cell capture

was optimised by altering both the well diameters and cell suspension concentrations, resulting in >90% of the wells being filled with 1–4 lung cancer cells. The resultant capture efficiency, defined as wells from which phospholipids could be identified *via* MALDI-MS, was ~25%, although it is noted that the single cell phospholipid concentration was not sufficient for tandem MS analysis and hence lipid extracts from a denser cell population were utilised to perform more in depth structural identification. [190] Ultimately, this suggests that for MALDI, and possibly other single cell MS approaches, sensitivity is a limiting factor that will need to be addressed before the field can progress in other aspects such as throughput. MALDI analysis time for the microarray is not explicitly stated within the work; however, the high density of cells able to adhere to the device (10 000 wells per $cm^2$) is a step forward for uncomplicated single cell isolation techniques. In a number of other publications single cell analysis has been performed using MALDI-MS although not all are high throughput. [191–194]

An alternative method for generating single cell microarrays has been described by Ellis *et al*., in which inkjet printing is used to obtain high spatial control of cells to assist in the subsequent analysis of lipids by LESA-MS. [195] Inkjet technology (or bioprinting) allows cell suspensions to be deposited onto glass slides in a 10 by 10 grid, resulting in single cell deposition according to a Poisson distribution. In this case, approximately 37% of the wells contained single cells. The spots were dried and microscopy image analysis was used to determine positions upon the slide which correctly contained a single cell. LESA-MS sampled these positions in a similar manner to the procedure depicted in Figure 1.3. Using this technology the authors acquired 8.3 minutes of MS (and MS/MS) data per spot containing 1–5 cells, which is at the lower end of the desired throughput scale; however, it is noted that this approach yields good reproducibility even at the single cell level as well as sufficient sensitivity for a number of different cell types investigated. Comparisons of spots containing up to 100 cells with those of single occupancy found a number of lipids to be present in both positions with similar abundances, and the resulting lipid fingerprints allowed for cell identification between different cell types by multivariate analysis. It was noted that there was little heterogeneity between the

single cells analysed, which may have been a consequence of the controlled nature in which the cells were cultured. [195] The use of microarrays allows for accountability of a sample position within a grid similar to that of microtitre well plates, a system that is favoured by many analysts.

Nanomanipulation of cells is another technique that has been successfully coupled with differing types of MS for the analysis of lipids by Verbeck and co-authors. [196–200] This has been achieved through the use of a nanomanipulator workstation (DCG Systems Inc., Fremont, CA, USA) which utilises either quartz rods, micropipettes or nESI capillary emitters [197] to extract single cells or even organelles from a culture dish or tissue. This procedure has been termed 'One-Cell' analysis, and as the cell or organelle of interest has been located under a microscope prior to analysis, its spatial information relative to the tissue (which in some applications is cancerous) is retained. [197] Additionally, nearby cells and structures also remain viable for future analysis due to the ambient nature of the technique. In regard to MS coupling, the two ionisation techniques here are nESI and MALDI. For nESI the material of interest is collected directly into a metal coated emitter tip and transferred to the MS source for direct ionisation and analysis of the extracted components. This has been achieved for lipidomic determinations within cancerous and normal breast tissues, in which lipid droplets were extracted from the inside of single adipocytes, and the triglyceride and fatty acid contents probed by MS and MS/MS experiments. [197] Coupling nanomanipulation with MALDI-MS for adipocyte analysis follows a similar approach; however, instead of the extraction emitter transferring directly to nESI, the emitter is positioned on a glass slide and the extracted components ejected. Matrix deposition on the ejected components then takes place using a second emitter system. In the presence of an appropriate matrix, triacylglyceride species were determined *via* MALDI ionisation and accurate mass measurements. [200] In regard to throughput, this extraction procedure is lengthy (<30 min) in comparison with some of the other techniques discussed in this review; however, for single cell lipidomic analysis this time frame is relatively short in comparison with traditional chromatographic separations and purification steps, [200] and does include the additional spatial information of cellular location within a tissue section. Coupling to

MALDI within an array and other hardware improvements may have the potential to advance this technique in the future.

## 1.10 Conclusions and outlook

To conclude, recent developments in the coupling of automated and chip based sample inlet systems to mass spectrometers are enabling the analysis of >10000 samples in a 24 hour time period at increased sensitivity. Ambient ionisation, SPE methods and MSI techniques have facilitated the analysis of material from untreated biofluids, tissues, organs and intact live cells, substantially lowering the time required to prepare samples prior to the acquisition of useful MS data. Whilst many of the techniques described herein are commercially available, still, more are emerging from the adaptation of technologies by academic groups often in close collaboration with industry. Challenges surrounding contamination, ion suppression, carryover and device fouling due to excessive cellular components can limit the sensitivity of these techniques, although ion mobility has gone some way to alleviate the first two of these. Future microfluidics developments will address the latter two. Many HTS-MS approaches are aimed towards targeted analysis where yes/no answers are required and ultrahigh sensitivity is not the ultimate aim, but it must be noted that many methods described such as 'nanoPOTS' and the 'Echo–MS' have indicated impressive sensitivity along with substantially reduced amounts of starting material. This increased sensitivity at higher throughput from decreasing amounts of sample (truly 'less is more') indicates an increased efficiency of ESI when there is less to analyse, and is also attributed to many developments in the transmission and detection of ions in modern mass spectrometers.

## 1.11 Acknowledgements

This review was supported by the BBSRC through the award of a DTP studentship to EK (BB/M011208/1) and by the funding from our SYNBIOCHEM centre (BB/M017702/1), and we acknowledge the entire SYNBIOCHEM team for their on-going contributions in support of our work in microfluidics and intact cell mass spectrometry. Sphere Fluidics Ltd has also supported this work in the form of a BBSRC CASE award to EK.

## 1.12 References


1 J. Inglese, R. L. Johnson, A. Simeonov, M. Xia, W. Zheng, C. P. Austin and D. S. Auld, *Nat. Chem. Biol.*, 2007, **3**, 466–479.

2 R. P. Hertzberg and A. J. Pope, *Curr. Opin. Chem. Biol.*, 2000, **4**, 445–451.

3 M. de Raad, C. R. Fischer and T. R. Northen, *Curr. Opin. Chem. Biol.*, 2016, **30**, 7–13.

4 J. W. Armstrong, *Am. Biotechnol. Lab.*, 1999, **17**, 26–28.

5 S. A. Sundberg, *Curr. Opin. Biotechnol.*, 2000, **11**, 47–53.

6 P. Szymański, M. Markowicz and E. Mikiciuk-Olasik, *Int. J. Mol. Sci.*, 2012, **13**, 427–452.

7 A. A. Hajare, S. S. Salunkhe, S. S. Mali, S. S. Gorde, S. J. Nadaf and S. A. Pishawikar, *Am. J. Pharmtech Res.*, 2014, **4**, 112–129.

8 J. P. Hughes, S. S. Rees, S. B. Kalindjian and K. L. Philpott, *Br. J. Pharmacol.*, 2011, **162**, 1239–1249.

9 D. E. Cameron, C. J. Bashor and J. J. Collins, *Nat. Rev. Microbiol.*, 2014, **12**, 381–390.

10 P. C. Gach, K. Iwai, P. Kim, N. J. Hillson and A. K. Singh, *Lab Chip*, 2017, **17**, 3388–3400.

11 D. F. Savage, J. Way and P. A. Silver, *ACS Chem. Biol.*, 2008, **3**, 13–16.

12 A. S. Khalil and J. J. Collins, Nat. Rev. Genet. , 2010, 11, 367–379.

13 J. J. Agresti, E. Antipov, A. R. Abate, K. Ahn, A. C. Rowat, J.-C. Baret, M. Marquez, A. M. Klibanov, A. D. Griffiths and D. A. Weitz, *Proc. Natl. Acad. Sci.*, 2010, **107**, 6550–6550.

14 M. T. Reetz, D. Kahakeaw and R. Lohmer, *ChemBioChem*, 2008, **9**, 1797–1804.

15 F. H. Arnold, *Acc. Chem. Res.*, 1998, **31**, 125–131.

16 P. Jacques, M. Béchet, M. Bigan, D. Caly, G. Chataigné, F. Coutte, C. Flahaut, E. Heuson, V. Leclère, D. Lecouturier, V. Phalip, R. Ravallec, P. Dhulster and R. Froidevaux, *Bioprocess Biosyst. Eng.*, 2017, **40**, 161–180.

17 S. Bershtein and D. S. Tawfik, *Curr. Opin. Chem. Biol.*, 2008, **12**, 151–158.

18 Y.-C. Tung, A. Y. Hsiao, S. G. Allen, Y. Torisawa, M. Ho and S. Takayama, *Analyst*, 2011, **136**, 473–478.

19 E. E. Swartzman, S. J. Miraglia, J. Mellentin-Michelotti, L. Evangelista and P. M. Yuan, *Anal. Biochem.*, 1999, **271**, 143–151.

20 P. Hodder, R. Mull, J. Cassaday, K. Berry and B. Strulovici, *J. Biomol. Screen.*, 2004, **9**, 417–426.

21 M. Yadav, P. Contractor, V. Upadhyay, A. Gupta, S. Guttikar, P. Singhal, S. Goswami and P. S. Shrivastav, *J. Chromatogr. B Anal. Technol. Biomed. Life Sci.*, 2008, **872**, 167–171.

22 S. X. Peng, T. M. Branch and S. L. King, *Anal. Chem.*, 2001, **73**, 708–714.

23 D. Hümmer, F. Kurth, N. Naredi-Rainer and P. S. Dittrich, *Lab Chip*, 2015, **16**, 447–458.

24 O. V Trubetskoy, J. R. Gibson and B. D. Marks, *J. Biomol. Screen.*, 2005, **10**, 56–66.

25 M. Smilkstein, N. Sriwilaijaroen, J. X. Kelly, P. Wilairat and M. Riscoe, *Antimicrob. Agents Chemother.*, 2004, **48**, 1803–1806.

26 M. Wodnicka, R. D. Guarino, J. J. Hemperly, M. R. Timmins, D. Stitt and J. B. Pitner, *J. Biomol. Screen.*, 2000, **5**, 141–152.

27 S. M. Rodems, B. D. Hamman, C. Lin, J. Zhao, S. Shah, D. Heidary, L. Makings, J. H. Stack and B. A. Pollok, *Assay Drug Dev. Technol.*, 2002, **1**, 9–19.

28 Z. Haarhoff, A. Wagner, P. Picard, D. M. Drexler, T. Zvyaga and W. Shou, *J. Biomol. Screen.*, 2016, **21**, 165–175.

29 L. Wu and X. Qu, *Chem. Soc. Rev.*, 2015, **44**, 2963–2997.

30 M. R. Wenk, *Nat. Rev. Drug Discov.*, 2005, **4**, 594–610.

31 R. Aebersold and M. Mann, *Nature*, 2003, **422**, 198–207.

32 K. Dettmer, P. A. Aronov and B. D. Hammock, *Mass Spectrom. Rev.*, 2007, **26**, 51–78.

33 M. T. Henke and N. L. Kelleher, *Nat. Prod. Rep.*, 2016, **33**, 942–950.

34 E. de Hoffmann and V. Stroobant, *Mass Spectrometry: Principles and Applications*, John Wiley & Sons, Chichester, 3rd edn., 2007.

35 C. K. Van Pelt, S. Zhang, E. Fung, I. Chu, T. Liu, C. Li, W. a Korfmacher and J. Henion, *Rapid Commun. Mass Spectrom.*, 2003, **17**, 1573–1578.

36 C. Flangea, C. Mosoarca, C. Cozma, M. Galusca, M. Przybylski and A. D. Zamfir, *Electrophoresis*, 2013, **34**, 1572–1580.

37 N. J. Martin, J. Bunch and H. J. Cooper, *J. Am. Soc. Mass Spectrom.*, 2013, **24**, 1242–1249.

38 R. Almeida, C. Mosoarca, M. Chirita, V. Udrescu, N. Dinca, Ž. Vukelić, M. Allen and A. D. Zamfir, *Anal. Biochem.*, 2008, **378**, 43–52.

39 K. Geddes, G. Adamson, N. Dube, S. Crathern and R. C. King, *Rapid Commun. Mass Spectrom.*, 2009, **23**, 1303–1312.

40 C. Flangea, C. Schiopu, F. Capitan, C. Mosoarca, M. Manea, E. Sisu and A. D. Zamfir, *Cent. Eur. J. Chem.*, 2012, **11**, 25–34.

41 A. D. Zamfir, N. Lion, Z. Vukelic, L. Bindila, J. Rossier, H. H. Girault and J. Peter-Katalinic, *Lab Chip*, 2005, **5**, 298–307.

42 H. M. Park, J. H. Shin, J. K. Kim, S. J. Lee, G. S. Hwang, K. H. Liu and C. H. Lee, *Metabolomics*, 2014, **10**, 663–676.

43 A. Serb, C. Schiopu, C. Flangea, Z. Vukelić, E. Sisu, L. Zagrean and A. D. Zamfir, *Eur. J. Mass Spectrom.*, 2009, **15**, 541–553.

44 C. Y. Chen, B. L. Lam and S. K. Bhattacharya, *Mol. Vis.*, 2014, **20**, 1605–1611.

45 H. Ye, J. Hill, A. C. Gucinski, M. T. Boyne and L. F. Buhse, *AAPS J.*, 2015, **17**, 405–415.

46 A. D. Zamfir, A. Serb, Ž. Vukelić, C. Flangea, C. Schiopu, D. Fabris, S. Kalanj-Bognar, F. Capitan and E. Sisu, *J. Am. Soc. Mass Spectrom.*, 2011, **22**, 2145–2159.

47 A. F. Serb, E. Sisu, Ž. Vukelić and A. D. Zamfir, *J. Mass Spectrom.*, 2012, **47**, 1561–1570.

48 T. K. Toby, L. Fornelli and N. L. Kelleher, *Annu. Rev. Anal. Chem.*, 2016, **9**, 499–519.

49 M. Bailey, E. C. Randall, C. Costa, T. Salter, A. . Race, M. de Puit, M. Koeberg, M. Baumert and J. Bunch, *Anal. Methods*, 2016, **8**, 3373–3382.

50 E. C. Randall, J. Bunch and H. J. Cooper, *Anal. Chem.*, 2014, **86**, 10504–10510.

51 V. Kertesz and G. J. Van Berkel, *J. Mass Spectrom.*, 2010, **45**, 252–260.

52 R. L. Griffiths, A. Dexter, A. J. Creese and H. J. Cooper, *Analyst*, 2015, **140**, 6879–6885.

53 M. Kai, I. González, O. Genilloud, S. B. Singh and A. Svatoš, *Rapid Commun. Mass Spectrom.*, 2012, **26**, 2477–2482.

54 D. Eikel and J. Henion, *Rapid Commun. Mass Spectrom.*, 2011, **25**, 2345–2354.

55 W. B. Parson, S. L. Koeniger, R. W. Johnson, J. Erickson, Y. Tian, C. Stedman, A. Schwartz, E. Tarcsa, R. Cole and G. J. Van Berkel, *J. Mass Spectrom.*, 2012, **47**, 1420–1428.

56 M. Wisztorski, A. Desmons, J. Quanico, B. Fatou, J. P. Gimeno, J. Franck, M. Salzet and I. Fournier, *Proteomics*, 2016, **16**, 1622–1632.

57 C. Yan, F. Parmeggiani, E. A. Jones, E. Claude, S. A. Hussain, N. J. Turner, S. L. Flitsch and P. E. Barran, *J. Am. Chem. Soc.*, 2017, **139**, 1408–1411.

58 P. Carbonell, A. J. Jervis, C. J. Robinson, C. Yan, M. Dunstan, N. Swainston, M. Vinaixa, K. A. Hollywood, A. Currin, N. J. W. Rattray, S. Taylor, R. Spiess, R. Sung, A. R. Williams, D. Fellows, N. J. Stanford, P. Mulherin, R. Le Feuvre, P. Barran, R. Goodacre, N. J. Turner, C. Goble, G. G. Chen, D. B. Kell, J. Micklefield, R. Breitling, E. Takano, J.-L. Faulon and N. S. Scrutton, *Commun. Biol.*, 2018, **1**, 66.

59 C. F. Poole, A. D. Gunatilleka and R. Sethuraman, *J. Chromatogr. A*, 2000, **885**, 17–39.

60 M. J. Telepchak, *Forensic Sci. Med.*, 2004, **122**, 41–53.

61 M.-C. Hennio, *J. Chromatogr. A*, 1999, **856**, 3–54.

62 N. J. K. Simpson and J. M. Wells, Martha, in *Solid-Phase Extraction: Principles, Techniques, and Applications*, Marcel Dekker Inc., New York, 2000, pp. 1–2.

63 A. Becalski, B. P. Y. Lau, D. Lewis, S. W. Seaman, S. Hayward, M. Sahagian, M. Ramesh and Y. Leclerc, *J. Agric. Food Chem.*, 2004, **52**, 3801–3806.

64 A. Molinelli, R. Weiss and B. Mizaikoff, *J. Agric. Food Chem.*, 2002, **50**, 1804–1808.

65 D. Štajnbaher and L. Zupančič-Kralj, *J. Chromatogr. A*, 2003, **1015**, 185–198.

66 M. J. M. Wells and J. L. Michael, *Anal. Chem.*, 1987, **59**, 1739–1742.

67 R. J. Lewis, R. D. Johnson, M. K. Angier and R. M. Ritter, *J. Chromatogr. B Anal. Technol. Biomed. Life Sci.*, 2004, **806**, 141–150.

68 E. Kim, J. Lee, S. Choi, M. Lim and H. Chung, *Forensic Sci. Int.*, 2008, **174**, 197–202.

69 R. J. Lewis, R. D. Johnson and R. A. Hattrup, *J. Chromatogr. B Anal. Technol. Biomed. Life Sci.*, 2005, **822**, 137–145.

70 H. Choi, S. Baeck, M. Jang, S. Lee, H. Choi and H. Chung, *Forensic Sci. Int.*, 2012, **215**, 81–87.

71 Z. Kuklenyik, J. A. Reich, J. S. Tully, L. L. Needham and A. M. Calafat, *Environ. Sci. Technol.*, 2004, **38**, 3698–3704.

72 F. Lachâtre, P. Marquet, S. Ragot, J. M. Gaulier, P. Cardot and J. L. Dupuy, *J. Chromatogr. B Biomed. Sci. Appl.*, 2000, **738**, 281–291.

73 P. M. Kabra, J. H. Wall and P. Dimson, *Clin. Chem.*, 1987, **33**, 2272–2274.

74 D. T. Rossi and N. Zhang, *J. Chromatogr. A*, 2000, **885**, 97–113.

75 P. J. Jannetto and L. J. Langman, *Clin. Biochem.*, 2016, **49**, 1032–1034.

76 X. Wu, J. Wang, L. Tan, J. Bui, E. Gjerstad, K. McMillan and W. Zhang, *J. Biomol. Screen.*, 2012, **17**, 761–772.

77 G. C. Adam, J. Meng, J. M. Rizzo, A. Amoss, J. W. Lusen, A. Patel, D. Riley, R. Hunt, P. Zuck, E. N. Johnson, V. N. Uebele and J. D. Hermes, *J. Biomol. Screen.*, 2014, **20**, 212–222.

78 C. Haslam, J. Hellicar, A. Dunn, A. Fuetterer, N. Hardy, P. Marshall, R. Paape, M. Pemberton, A. Resemannand and M. Leveridge, *J. Biomol. Screen.*, 2016, **21**, 176–186.

79 I. Vrobel, H. Janeckova, E. Faber, K. Bouchalova, K. Micova, D. Friedecky and

T. Adam, *Ther. Drug Monit.*, 2016, **38**, 516–524.

80 H. Lu, L. Kopcho, K. Ghosh, M. Witmer, M. Parker, S. Gupta, M. Paul, P. Krishnamurthy, B. Laksmaiah, D. Xie, J. Tredup, L. Zhang and L. M. Abell, *Anal. Biochem.*, 2016, **501**, 56–65.

81 D. Grote-Koska, S. Czajkowski and K. Brand, *Ther. Drug Monit.*, 2015, **37**, 400–404.

82 M. Takamiya, M. Sakurai, F. Teranishi, T. Ikeda, T. Kamiyama and A. Asai, *Biochem. Biophys. Res. Commun.*, 2016, **480**, 721–726.

83 L. J. Gordon, M. Allen, P. Artursson, M. M. Hann, B. J. Leavens, A. Mateus, S. Readshaw, K. Valko, G. J. Wayne and A. West, *J. Biomol. Screen.*, 2016, **21**, 156–164.

84 A. H. Luippold, T. Arnhold, W. Jörg and R. D. Süssmuth, *Int. J. Mass Spectrom.*, 2010, **296**, 1–9.

85 J. R. Neifeld, L. E. Regester, J. M. Holler, S. P. Vorce, J. Magluilo, G. Ramos and T. Z. Bosy, *J. Anal. Toxicol.*, 2016, **40**, 379–387.

86 Agilent Technologies, *Agilent G9530A RapidFire 365 High-throughput Mass Spectrometry System User Guide*, 2014.

87 M. Razavi, L. E. Frick, W. A. Lamarr, M. E. Pope, C. A. Miller, L. N. Anderson and T. W. Pearson, *J. Proteome Res.*, 2012, **11**, 5642–5649.

88 A. Amaral, C. Saran, J. Amin and P. Hatsis, *J. Biomol. Screen.*, 2016, **21**, 620 – 625.

89 D. Danso, P. J. Jannetto, R. Enger and L. J. Langman, Ther. Drug Monit., 2015, 37, 319–324.

90 M. Leveridge, R. Buxton, A. Argyrou, P. Francis, B. Leavens, A. West, M. Rees, P. Hardwicke, A. Bridges, S. Ratcliffe and C. W. Chung, *J. Biomol. Screen.*, 2014, **19**, 278–286.

91 M. K. Highkin, M. P. Yates, O. V. Nemirovskiy, W. A. Lamarr, G. E. Munie, J. W. Rains, J. L. Masferrer and M. M. Nagiec, *J. Biomol. Screen.*, 2011, **16**, 272–277.

92 B. T. Veach, T. K. Mudalige and P. Rye, *Anal. Chem.*, 2017, **89**, 3256–3260.

93 K. B. Lim, C. C. Ozbal and D. B. Kassel, *J. Biomol. Screen.*, 2010, **15**, 447–52.

94 C. K. Imamura, K. Furihata, S. Okamoto and Y. Tanigawara, *J. Clin. Pharmacol.*, 2016, **56**, 408–413.

95 A. Zimmerlin, M. Trunzer and B. Faller, *Drug Metab. Dispos.*, 2011, **39**, 1039–1046.

96 Q. K. Huynh, S. J. Wise, K. a Koch, L. a Castonguay, B. G. Reid, E. E. Pagratis, D. Koditek, C. B. Glascock, K. R. Pitts, B. a Turner, X. Liu, M. Hung, B. Han

and N. Pagratis, *J. Biomol. Screen.*, 2011, **16**, 724–33.

97 C.-W. Shu, C. Madiraju, D. Zhai, K. Welsh, P. Diaz, E. Sergienko, R. Sano and J. C. Reed, *J. Biomol. Screen.*, 2011, **16**, 174–182.

98 S. A. I. Seidel, N. A. Markwardt, S. A. Lanzmich and D. Braun, *Angew. Chemie - Int. Ed.*, 2014, **53**, 7948–7951.

99 R. J. Grant, K. Roberts, C. Pointon, C. Hodgson, L. Womersley, D. C. Jones and E. Tang, *J. Biomol. Screen.*, 2009, **14**, 452–459.

100 M. A. Liebert and R. Ellson, *Assay Drug Dev. Technol.*, 2005, 3, 607–612.

101 P. Kanigowska, Y. Shen, Y. Zheng, S. Rosser and Y. Cai, *J. Lab. Autom.*, 2016, **21**, 49–56.

102 H. Aerni, D. S. Cornett and R. M. Caprioli, Anal. Chem., 2006, 78, 827–834.

103 J. Chin, E. Wood, G. S. Peters and D. M. Drexler, *J. Lab. Autom.*, 2016, **21**, 204–207.

104 I. Sinclair, R. Stearns, S. Pringle, J. Wingfield, S. Datwani, E. Hall, L. Ghislain, L. Majlof and M. Bachman, *J. Lab. Autom.*, 2016, **21**, 19–26.

105 S. H. Yoon, T. Liang, T. Schneider, B. L. Oyler, C. E. Chandler, R. K. Ernst, G. S. Yen, Y. Huang, E. Nilsson and D. R. Goodlett, *Rapid Commun. Mass Spectrom.*, 2016, **30**, 2555–2560.

106 A. C. Susa, Z. Xia and E. R. Williams, *Anal. Chem.*, 2017, **89**, 3116–3122.

107 D. N. Mortensen and E. R. Williams, *Anal. Chem.*, 2014, **86**, 9315–9321.

108 C. Wu, A. L. Dill and L. S. Eberlin, *Mass Spectrom. Rev.*, 2013, **32**, 218–243.

109 E. R. Amstalden van Hove, D. F. Smith and R. M. A. Heeren, *J. Chromatogr. A*, 2010, **1217**, 3946–3954.

110 M. Setou, Ed., *Imaging Mass Spectromety*, Springer Japan, Tokyo, 2nd edn., 2010.

111 D. I. Campbell, C. R. Ferreira, L. S. Eberlin and R. G. Cooks, *Anal. Bioanal. Chem.*, 2012, **404**, 389–398.

112 A. D. Feenstra, M. E. Dueñas and Y. J. Lee, *J. Am. Soc. Mass Spectrom.*, 2017, **28**, 434–442.

113 A. Römpp and B. Spengler, *Histochem. Cell Biol.*, 2013, **139**, 759–783.

114 D. R. Bhandari, Q. Wang, W. Friedt, B. Spengler, S. Gottwald and A. Römpp, *Analyst*, 2015, **140**, 7696–7709.

115 M. Kubicek, G. Holzlechner, A. K. Opitz, S. Larisegger, H. Hutter and J. Fleig, *Appl. Surf. Sci.*, 2014, **289**, 407–416.

116 F. Hillenkamp and J. Peter-Katalinic, *MALDI MS: A Practical Guide to Instrumentation, Methods and Applications*, Wiley Blackwell, Weinheim, 2nd

Editio., 2013.

117 N. Singhal, M. Kumar, P. K. Kanaujia and J. S. Virdi, *Front. Microbiol.*, 2015, **6**, 1–16.

118 R. M. Caprioli, T. B. Farmer and J. Gile, *Anal. Chem.*, 1997, **69**, 4751–4760.

119 T. C. Rohner, D. Staab and M. Stoeckli, *Mech. Ageing Dev.*, 2005, **126**, 177–185.

120 L. H. Cazares, D. A. Troyer, B. Wang, R. R. Drake and O. John Semmes, *Anal. Bioanal. Chem.*, 2011, **401**, 17–27.

121 A. Kernalléguen, R. Steinhoff, S. Bachler, P. S. Dittrich, F. Saint-Marcoux, S. El Bakhi, F. Vorspan, G. Léonetti, D. Lafitte, A. L. Pélissier-Alicot and R. Zenobi, *Anal. Chem.*, 2018, **90**, 2302–2309.

122 A. Svatoš, *Anal. Chem.*, 2011, **83**, 5037–5044.

123 H. R. Aerni, D. S. Cornett and R. M. Caprioli, *Anal. Chem.*, 2006, **78**, 827–834.

124 J. Kononen, L. Bubendorf, A. Kallioniemi, M. Bärlund, P. Schraml, S. Leighton, J. Torhorst, M. J. Mihatsch, G. Sauter and O. P. Kallioniemi, *Nat. Med.*, 1998, **4**, 844–847.

125 M. R. Groseclose, P. P. Massion, P. Chaurand and R. M. Caprioli, *Proteomics*, 2008, **8**, 3715–3724.

126 Z. Takáts, J. M. Wiseman, B. Gologan and R. G. Cooks, *Science (80-. ).*, 2004, **306**, 471–473.

127 Z. Takáts, J. M. Wiseman and R. G. Cooks, *J. Mass Spectrom.*, 2005, **40**, 1261–1275.

128 A. Venter, M. Nefliu and R. Graham Cooks, *Trends Anal. Chem.*, 2008, **27**, 284–290.

129 Z. Takáts, J. M. Wiseman, B. Gologan and R. G. Cooks, *Anal. Chem.*, 2004, **76**, 4050–4058.

130 C. Wu, A. L. Dill, L. S. Eberlin, R. G. Cooks and D. R. Ifa, *Mass Spectrom. Rev.*, 2013, **32**, 218–243.

131 J. M. Wiseman, D. R. Ifa, Y. Zhu, C. B. Kissinger, N. E. Manicke, P. T. Kissinger and R. G. Cooks, *Proc. Natl. Acad. Sci. U. S. A.*, 2008, **105**, 18120–18125.

132 J. Tillner, V. Wu, E. A. Jones, S. D. Pringle, T. Karancsi, A. Dannhorn, K. Veselkov, J. S. McKenzie and Z. Takats, *J. Am. Soc. Mass Spectrom.*, 2017, **28**, 2090–2098.

133 A. Tata, C. J. Perez, M. O. Ore, D. Lostun, A. Passas, S. Morin and D. R. Ifa, *RSC Adv.*, 2015, **5**, 75458–75464.

134 C. F. F. Angolini, P. H. Vendramini, F. D. S. Araújo, W. L. Araújo, R. Augusti, M. N. Eberlin and L. G. De Oliveira, *Anal. Chem.*, 2015, **87**, 6925–6930.

135 J. F. Garcia-Reyes, A. U. Jackson, A. Molina-Diaz and R. G. Cooks, *Anal. Chem.*, 2009, **81**, 820–829.

136 S. Gerbig, G. Stern, H. E. Brunn, R. A. Düring, B. Spengler and S. Schulz, *Anal. Bioanal. Chem.*, 2017, **409**, 2107–2117.

137 M. Wleklinski, B. P. Loren, C. R. Ferreira, Z. Jaman, L. Avramova, T. J. P. Sobreira, D. H. Thompson and R. G. Cooks, *Chem. Sci.*, 2018, **9**, 1647–1653.

138 H. A. Stone, A. D. Stroock and A. Ajdari, *Annu. Rev. Fluid Mech.*, 2004, **36**, 381–411.

139 L. Mazutis, J. Gilbert, L. Ung, D. A. Weitz, A. D. Griffiths and J. A. Heyman, *Nat. Protoc.*, 2013, **8**, 870–891.

140 A. K. Price and B. M. Paegel, *Anal. Chem.*, 2016, **88**, 339–353.

141 W. L. Chou, P. Y. Lee, C. L. Yang, W. Y. Huang and Y. S. Lin, *Micromachines*, 2015, **6**, 1249–1271.

142 L. Mazutis, J.-C. Baret, P. Treacy, Y. Skhiri, A. F. Araghi, M. Ryckelynck, V. Taly and A. D. Griffiths, *Lab Chip*, 2009, **9**, 2902–2908.

143 R. T. Kelly, J. S. Page, I. Marginean, K. Tang and R. D. Smith, *Angew. Chemie Int. Ed.*, 2009, **48**, 6832–6835.

144 K. Choi, A. H. C. Ng, R. Fobel and A. R. Wheeler, *Annu. Rev. Anal. Chem.*, 2012, **5**, 413–440.

145 A. Zinchenko, S. R. A. Devenish, B. Kintses, P. Y. Colin, M. Fischlechner and F. Hollfelder, *Anal. Chem.*, 2014, **86**, 2526–2533.

146 Y. Zhu and Q. Fang, *Anal. Chim. Acta*, 2013, **787**, 24–35.

147 D. Gao, H. Liu, Y. Jiang and J.-M. Lin, *Lab Chip*, 2013, **13**, 3309–3322.

148 J. Ji, L. Nie, L. Qiao, Y. Li, L. Guo, B. Liu, P. Yang and H. H. Girault, *Lab Chip*, 2012, **12**, 2625–2629.

149 J. Heinemann, B. Noon, M. J. Mohigmi, A. Mazurie, D. L. Dickensheets and B. Bothner, *J. Am. Soc. Mass Spectrom.*, 2014, **25**, 1755–1762.

150 M. Brivio, R. H. Fokkens, W. Verboom, D. N. Reinhoudt, N. R. Tas, M. Goedbloed and A. Van Den Berg, *Anal. Chem.*, 2002, **74**, 3972–3976.

151 S. K. Küster, M. Pabst, K. Jefimovs, R. Zenobi and P. S. Dittrich, *Anal. Chem.*, 2014, **86**, 4848–4855.

152 Q. Xue, F. Foret, Y. M. Dunayevskiy, P. M. Zavracky, N. E. McGruer and B. L. Karger, *Anal. Chem.*, 1997, **69**, 426–430.

153 K. Sander and E. Verpoorte, *Lab Chip*, 2007, **7**, 1394–1412.

154 R. S. Ramsey and J. M. Ramsey, *Anal. Chem.*, 1997, **69**, 1174–1178.

155 N. H. Bings, C. Wang, C. D. Skinner, C. L. Colyer, P. Thibault and D. J.

Harrison, *Anal. Chem.*, 1999, **71**, 3292–3296.

156 P. Hoffmann, U. Häusig, P. Schulze and D. Belder, *Angew. Chemie - Int. Ed.*, 2007, **46**, 4913–4916.

157 S. Fritzsche, S. Ohla, P. Glaser, D. S. Giera, M. Sickert, C. Schneider and D. Belder, *Angew. Chemie - Int. Ed.*, 2011, **50**, 9467–9470.

158 C. Benz, M. Boomhoff, J. Appun, C. Schneider and D. Belder, *Angew. Chemie - Int. Ed.*, 2015, **54**, 2766–2770.

159 K. Ren, J. Zhou and H. Wu, *Acc. Chem. Res.*, 2013, **46**, 2396–2406.

160 E. Mery, F. Ricoul, N. Sarrut, O. Constantin, G. Delapierre, J. Garin and F. Vinet, *Sensors Actuators, B Chem.*, 2008, **134**, 438–446.

161 A. V. Forzano, V. Becirovic, R. S. Martin and J. L. Edwards, *Anal. Methods*, 2016, **8**, 5152–5157.

162 C. A. Smith, X. Li, T. H. Mize, T. D. Sharpe, E. I. Graziani, C. Abell and W. T. S. Huck, *Anal. Chem.*, 2013, **85**, 3812–3816.

163 S. Mashaghi, A. Abbaspourrad, D. A. Weitz and A. M. van Oijen, *Trends Anal. Chem.*, 2016, **82**, 118–125.

164 L. Mahler, K. Wink, R. J. Beulig, K. Scherlach, M. Tovar, E. Zang, K. Martin, C. Hertweck, D. Belder and M. Roth, *Sci. Rep.*, 2018, **8**, 13087.

165 K. Wink, L. Mahler, J. R. Beulig, S. K. Piendl, M. Roth and D. Belder, *Anal. Bioanal. Chem.*, 2018, 410, 7679-7687.

166 R. J. Beulig, R. Warias, J. J. Heiland, S. Ohla, K. Zeitler and D. Belder, *Lab Chip*, 2017, **17**, 1996–2002.

167 T. W. Murphy, Q. Zhang, L. B. Naler, S. Ma and C. Lu, *Analyst*, 2018, **143**, 60–80.

168 W. M. Weaver, P. Tseng, A. Kunze, M. Masaeli, A. J. Chung, J. S. Dudani, H. Kittur, R. P. Kulkarni and D. Di Carlo, *Curr. Opin. Biotechnol.*, 2014, **25**, 114–123.

169 B. L. Khoo, P. K. Chaudhuri, N. Ramalingam, D. S. W. Tan, C. T. Lim and M. E. Warkiani, *Int. J. Cancer*, 2016, **139**, 243–255.

170 F. Lyu, M. Pan, S. Patil, J. H. Wang, A. C. Matin, J. R. Andrews and S. K. Y. Tang, *Sensors Actuators, B Chem.*, 2018, **270**, 396–404.

171 K. Galler, K. Bräutigam, C. Große, J. Popp and U. Neugebauer, *Analyst*, 2014, **139**, 1237–1273.

172 R. Trouillon, M. K. Passarelli, J. Wang, M. E. Kurczy and A. G. Ewing, *Anal. Chem.*, 2013, **85**, 522–542.

173 J. Doherty, G. Cinque and P. Gardner, *Appl. Spectrosc. Rev.*, 2017, **52**, 560–587.

174 R. Smith, K. L. Wright and L. Ashton, *Analyst*, 2016, **141**, 3590–3600.

175 M. Li, J. Xu, M. Romero-Gonzalez, S. A. Banwart and W. E. Huang, *Curr. Opin. Biotechnol.*, 2012, **23**, 56–63.

176 L. Zhang and A. Vertes, *Angew. Chemie Int. Ed.*, 2018, **57**, 4466–4477.

177 T. J. Comi, T. D. Do, S. S. Rubakhin and J. V. Sweedler, *J. Am. Chem. Soc.*, 2017, **139**, 3920–3929.

178 T. Masujima, *Anal. Sci.*, 2009, **25**, 953–960.

179 T. L. Colliver, C. L. Brummel, M. L. Pacholski, F. D. Swanek, A. G. Ewing and N. Winograd, *Anal. Chem.*, 1997, **69**, 2225–2231.

180 J. S. Fletcher, N. P. Lockyer, S. Vaidyanathan and J. C. Vickerman, *Anal. Chem.*, 2007, **79**, 2199–2206.

181 S. Parry and N. Winograd, *Anal. Chem.*, 2005, **77**, 7950–7957.

182 P. Sjövall, J. Lausmaa, H. Nygren, L. Carlsson and P. Malmberg, *Anal. Chem.*, 2003, **75**, 3429–3434.

183 N. Musat, R. Foster, T. Vagner, B. Adam and M. M. M. Kuypers, *FEMS Microbiol. Rev.*, 2012, **36**, 486–511.

184 H. W. Li, X. Hua and Y. T. Long, *Chinese J. Anal. Chem.*, 2018, **46**, 61–66.

185 J. S. Mellors, K. Jorabchi, L. M. Smith and J. M. Ramsey, *Anal. Chem.*, 2010, **82**, 967–973.

186 Y. Zhu, P. D. Piehowski, R. Zhao, J. Chen, Y. Shen, R. J. Moore, A. K. Shukla, V. A. Petyuk, M. Campbell-Thompson, C. E. Mathews, R. D. Smith, W. J. Qian and R. T. Kelly, *Nat. Commun.*, 2018, **9**, 1–10.

187 O. Guillaume-Gentil, T. Rey, P. Kiefer, A. J. Ibáñez, R. Steinhoff, R. Brönnimann, L. Dorwling-Carter, T. Zambelli, R. Zenobi and J. A. Vorholt, *Anal. Chem.*, 2017, **89**, 5017–5023.

188 S. Meyer, A. López-Serrano, H. Mitze, N. Jakubowski and T. Schwerdtle, *Metallomics*, 2018, **10**, 73–76.

189 L. Mueller, H. Traub, N. Jakubowski, D. Drescher, V. I. Baranov and J. Kneipp, *Anal. Bioanal. Chem.*, 2014, **406**, 6963–6977.

190 W. Xie, D. Gao, F. Jin, Y. Jiang and H. Liu, *Anal. Chem.*, 2015, **87**, 7052–7059.

191 Y. Schober, S. Guenther, B. Spengler and A. Römpp, *Anal. Chem.*, 2012, **84**, 6293–6297.

192 M. E. Dueñas, J. J. Essner and Y. J. Lee, *Sci. Rep.*, 2017, **7**, 1–10.

193 A. Amantonico, P. L. Urban, S. R. Fagerer, R. M. Balabin and R. Zenobi, *Anal. Chem.*, 2010, **82**, 7394–7400.

194 A. J. Ibanez, S. R. Fagerer, A. M. Schmidt, P. L. Urban, K. Jefimovs, P. Geiger,

R. Dechant, M. Heinemann and R. Zenobi, *Proc. Natl. Acad. Sci.*, 2013, **110**, 8790–8794.

195 S. R. Ellis, C. J. Ferris, K. J. Gilmore, T. W. Mitchell, S. J. Blanksby and M. In Het Panhuis, *Anal. Chem.*, 2012, **84**, 9679–9683.

196 M. Phelps, J. Hamilton and G. F. Verbeck, Rev. Sci. Instrum., 2014, 85, 124101.

197 J. S. Hamilton and G. F. Verbeck, *J. Anal. Oncol.*, 2016, **5**, 47–54.

198 J. S. Hamilton, R. Aguilar, R. A. Petros and G. F. Verbeck, *J. Am. Soc. Mass Spectrom.*, 2017, **28**, 918–928.

199 P. J. Horn, N. R. Ledbetter, C. N. James, W. D. Hoffman, C. R. Case, G. F. Verbeck and K. D. Chapman, *J. Biol. Chem.*, 2011, **286**, 3298–3306.

200 M. S. Phelps, D. Sturtevant, K. D. Chapman and G. F. Verbeck, *J. Am. Soc. Mass Spectrom.*, 2016, **27**, 187–193.

# 2

# Rapid screening of Diverse Biotransformations for enzyme evolution

## 2.1 Declaration

This chapter has been reproduced from an article that I wrote in collaboration with James L. Galman. This article currently features as a pre-print, whilst it is in review at a peer-reviewed journal:

Emily E. Kempa, James L. Galman (JLG), Fabio Parmeggiani (FP), James R. Marshall (JRM), Julien Malassis (JM), Clement Q. Fontenelle (CQF), Jean-Baptiste Vendeville (J-BV), Bruno Linclau (BL), Simon J. Charnock (SJC), Sabine L. Flitsch (SLF), Nicholas J. Turner (NJT) and Perdita E. Barran (PEB), "Rapid screening of Diverse Biotransformations for enzyme evolution.", *ChemRxiv. Preprint*, 2020, https://doi.org/10.26434/chemrxiv.13203986.v1

For this first author publication, I was responsible for developing the DiBT-MS workflow, running samples, data analysis and collation of the project data and figures. Along with JLG, I drafted and edited the initial manuscript and figures. JLG and FP prepared evolution libraries, enzyme preparations, biotransformations and performed additional analytics for the Kinase and PAL samples. JRM prepared the metagenomic plates (under the supervision of SJC and Prozomix Ltd) and performed biotransformations and additional analytics for the IRED samples. JM, CQF, J-BV, and BL provided fluorinated sugars for kinase reactions. Supervision, experimental directions and manuscript editing were provided by NJT, SLF and PEB. The article has been reproduced here in an unchanged format except for minor adjustments to incorporate the text and figures into this thesis, and the referencing style updated to be akin to the other chapters of this thesis.

# Rapid screening of Diverse Biotransformations for enzyme evolution

Emily E. Kempa, [1, 5] James L. Galman, [1,5] Fabio Parmeggiani, [2] James R. Marshall, [1] Julien Malassis, [3] Clement Q. Fontenelle, [3] Jean-Baptiste Vendeville, [3] Bruno Linclau, [3] Simon J. Charnock, [4] Sabine L. Flitsch, [1] Nicholas J. Turner [1] and Perdita E. Barran. [1]

[1] School of Chemistry, University of Manchester, Manchester Institute of Biotechnology, 131 Princess Street, Manchester, M1 7DN, United Kingdom.

[2] Department of Chemistry, Materials and Chemical Engineering "G. Natta", Politecnico di Milano, Via Mancinelli 7, 20131, Milano, Italy.

[3] School of Chemistry, University of Southampton, Highfield, SO17 1BJ, Southampton, United Kingdom.

[4] Prozomix Ltd., Building 4, West End Ind. Estate, Haltwhistle, Northumberland, NE49 9HA, United Kingdom.

[5] These authors contributed equally: Emily E. Kempa, James L. Galman.

Publication Date (Web): 16th November 2020

https://doi.org/10.26434/chemrxiv.13203986.v1

## 2.2 Abstract

The lack of label-free high throughput screening technologies presents a major bottleneck in the identification of active and selective biocatalysts, with the number of variants often exceeding the capacity of traditional analytical platforms to assess their activity in a practical timescale. Here we show the application of direct infusion mass spectrometry (DiBT-MS) screening to a variety of enzymes, in different formats, achieving sample throughputs equivalent to ~40 seconds per sample. The heat-map output allows rapid selection of active enzymes within 96-well plates facilitating identification of industrially relevant biocatalysts. This DiBT-MS screening workflow has been applied to the directed evolution of a phenylalanine ammonia lyase (PAL), enhancing its activity towards electron-rich cinnamic acid derivatives which are relevant to lignocellulosic biomass degradation. Additional benefits of the screening platform include the discovery of biocatalysts (kinases, imine reductases) with novel activities and the incorporation of ion mobility technology for the identification of product hits with increased confidence.

## 2.3 Introduction

Biocatalysis provides an alternative and increasingly attractive sustainable pathway for the production of high-value chemical building blocks and intermediates. However, the application of biocatalysts in chemical synthesis is limited when using naturally occurring enzymes because of narrow substrate tolerance, low activity and poor operational stability. During the past 10 years, advances in protein engineering and directed evolution have demonstrated that many of these important parameters can be altered to position many more biocatalysts for preparative organic synthesis. Despite the increasing use of directed evolution for improving biocatalyst performance, a major bottleneck remains in the laborious processes required for screening libraries of variant enzymes to identify candidates with improved properties. [1] The majority of in vitro techniques that are available for analysing enzyme libraries deploy chromatographic methods which provide high-quality data regarding chemical identity but are not suitable for libraries in excess of $10^4$ enzyme variants.

Applying desorption electrospray ionisation (DESI) MS to crude reaction mixtures permits the analysis of products *in situ*, [2] (Figure 2.1) which has significant benefits for monitoring biocatalytic reactions compared to more traditional xC-MS methods. This approach shortens the analysis time and removes the need for much of the solvent. Further, the ability to correlate the spatial positions of spotted reactions and colonies with products provides a visual reference on the identified enzyme 'hits', followed by DNA extraction/PCR amplification to determine the sequence. [3] Coupling this DiBT-MS high throughput screening method, which provides semi-quantitative chemical information, to a protein engineering strategy accelerates the evolution of enzymes as demonstrated here.

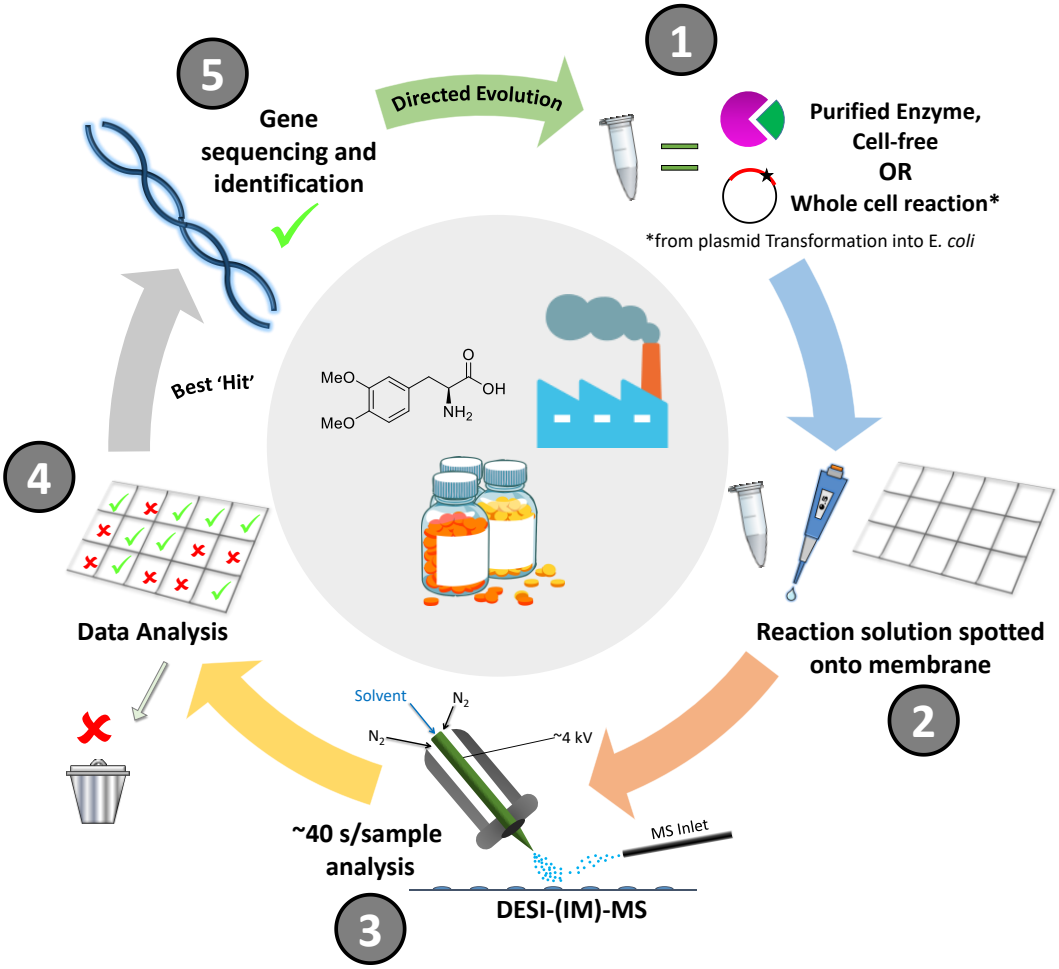


*Figure 2.1: Overview of the DiBT-MS workflow for screening biocatalytic reactions and identifying improved enzyme variants. Initially the reactions (whole cell or purified enzyme) are performed within Eppendorf tubes or 96/384-well plates (1) before spotting (0.5 µL) of the quenched reaction on to a nylon membrane grid (see photograph, Figure 2.6) prepared for DiBT-MS analysis (2). The membrane containing dried spotted reactions is subjected to DiBT-MS analysis where necessary with ion mobility (IM) separation (3) and the resulting mass and mobility resolved heat maps assessed for wells with highest product detection (4). The solution remaining in the corresponding 96/384-well plate or Eppendorf tube can then be extracted for DNA sequencing to identify the mutations responsible for improved activity (5).*

## 2.4 Results

### 2.4.1 Kinase Screening (Purified Enzymes)

Selective phosphorylation of monosaccharides, mediated by anomeric sugar kinases, is an important reaction to access natural and modified glycans. Anomeric kinases (galactokinases, GalKs, [4] and N-acetylhexosamine kinases, NahKs [5]) are efficient enzymes for the conversion of their natural substrates but tolerate only limited modifications to the structure of the sugar although homologues can often

display a considerably different substrate spectrum. [6,7] These kinases therefore present attractive targets for rapid screening of various substrate/enzyme combinations to identify successful phosphorylation reactions.

A panel of 11 different wild-type kinases (5 GalKs and 6 NahKs) were tested against 15 variously substituted deoxyfluorinated monosaccharides (**1a-o**, Figure 2.7), in order to compare our DiBT-MS screening protocol against a previously reported $^{19}$F-NMR method to determine reaction conversions. [8] The output from this screen (Figure 2.2a) is an *m*/*z* selected heat map of the location of the product ion of interest. Each reaction mixture is deposited in a grid format (Figure 2.6) which provides mass resolved heatmaps allowing easy visual identification of enzyme-substrate pairs with high activity (brightest coloured pixels). Due to the isomeric nature of some of the substrates tested in this screen, extracting mass spectral data for a single *m*/*z* value (M-1) (**2a-2h**, 261.1 Da) is sufficient to view results from 88 reactions (yellow pixels). Alternatively, if substrates (and consequently products) are different in mass (**1i-1o**, Table 2.2), multiple *m*/*z* values may be selected and the resulting heat maps can be overlaid to generate a single, easy to interpret, image (red, green and blue pixels). When we compared DiBT-MS heatmaps with the results of quantitative $^{19}$F-NMR analysis (Table 2.3), we found a semi-quantitative correspondence between the two methods (Supplementary information Figure 2.8 and 2.9, with the calculated reaction conversions (%) indicated below the corresponding DiBT-MS spot).

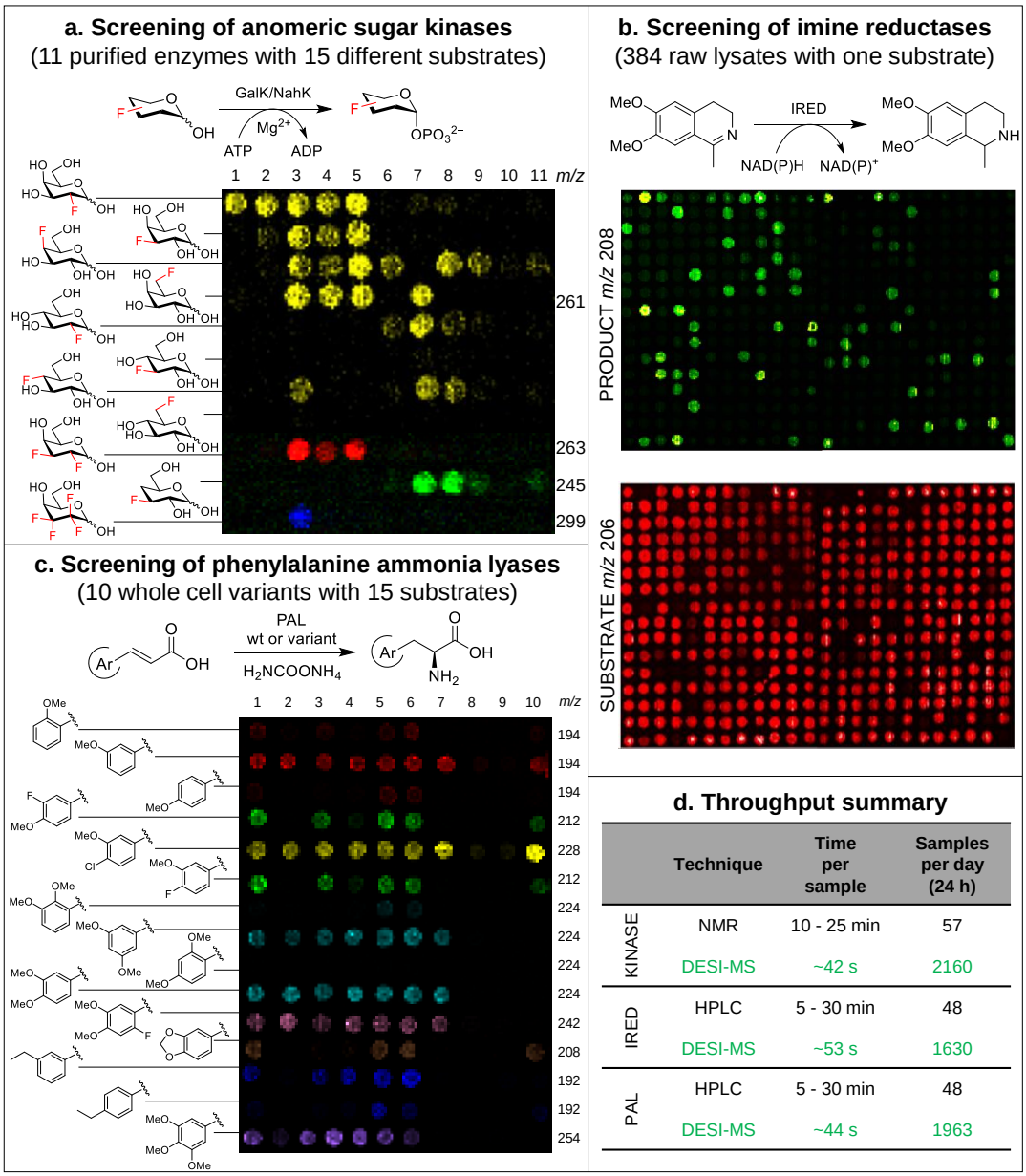


**d. Throughput summary**

| | Technique | Time per sample | Samples per day (24 h) |
|---|---|---|---|
| KINASE | NMR | 10 - 25 min | 57 |
| | DESI-MS | ~42 s | 2160 |
| IRED | HPLC | 5 - 30 min | 48 |
| | DESI-MS | ~53 s | 1630 |
| PAL | HPLC | 5 - 30 min | 48 |
| | DESI-MS | ~44 s | 1963 |

*Figure 2.2: Representative results of DiBT-MS screening of diverse biotransformations. a) DiBT-MS heat map obtained upon screening 11 purified kinase enzymes with 11 monosaccharide substrates. In total 15 substrates were screened, with the full results including reaction conversions as determined by $^{19}$F-NMR given in Figure 2.8 and 2.9. b) Resulting heat maps for imine reductase (IRED) reactions performed in a 384-well metagenomic plate. The heat maps indicate areas in which starting material (red) and product (green) are present on the membrane with each m/z value detected simultaneously. c) DiBT-MS heat map results for PAL whole cell reaction screening. 10 enzyme variants were screened against 15 cinnamic acid substrates for conversion to the corresponding phenylalanine derivative. Reaction conversions obtained by HPLC-(UV) analysis for each of these reactions are given in Figure 2.17. d) Table to show the increase in throughput achieved for three specific reaction types when employing DiBT-MS as the primary screening technique in comparison to alternative techniques, wherein the longer time denotes discovery and the shorter time indicates an optimised assay.*

### 2.4.2 Screening of Metagenomic Imine Reductases (IREDs)

Among the toolbox of enzymes available for the generation of chiral amines, NADPH-dependent imine reductases (IREDs) have emerged as practical and versatile biocatalysts for both asymmetric imine reduction and reductive amination.[9–11] Access to these biocatalysts has recently been enhanced by exploring metagenomic sequence space to construct the largest panel of IREDs available to date.[12]

A panel of 384 IREDs were screened for the reduction of 6,7-dimethoxy-1-methyl-1,2,3,4-dihydroisoquinoline **3** (Figure 2.11). Formation of the product **4** was observed in *m*/*z* selected heat maps where both substrate and product ions are shown (Figure 2.2b and 2.13, see methods for dimensions and grid preparation). The reverse reaction, i.e. oxidation of **4** to **3**, was also assessed using our recently developed colorimetric screen [12] with high correlation to the DiBT-MS method (Supplementary information Figure 2.12). Following DiBT-MS and colorimetric screening, five enzymes were selected for analytical biotransformations in the reductive direction (see Table 2.4). All enzymes showed excellent conversions (>99%) and excellent enantioselectivities (>99%) where metagenomic IREDs afforded both (S)- and (R)-**4**.[13]

#### 2.4.2.1 Incorporation of Ion Mobility

Within IRED DiBT-MS screening (Figure 2.2b and 2.13) the second $^{13}C$ isotope *m*/*z* of the substrate (major ion *m*/*z* 206.1) is *m*/*z* coincident with the major product ion observed (*m*/*z* 208.1). Since this IRED imine to amine biotransformation results in a product only two mass units higher than the substrate, a low-intensity positive hit was identified in every well plate position 'beneath' the genuine biotransformation result. To remove these false positives, travelling wave ion mobility (TWIMS) [14,15] was employed to 'filter' the $^{13}C$ isotope from the product ion. Results from such a DiBT-IM-MS screen are presented in Figure 2.3c, in which 5 wells of an IRED reaction cultured within a metagenomic plate were analysed by this method. Removal is possible as the major product ion (amine) and the substrate (imine) present with differing drift times (Figure 2.14). The heat map data obtained

without ion mobility separation are shown alongside one another in Figure 2.3c to illustrate the removal of the underlying false positive. The decision to analyse with or without ion mobility separation should consider the compound dynamic range of each mode prior to sample analysis, as the additional separation step may result in some loss of sensitivity.

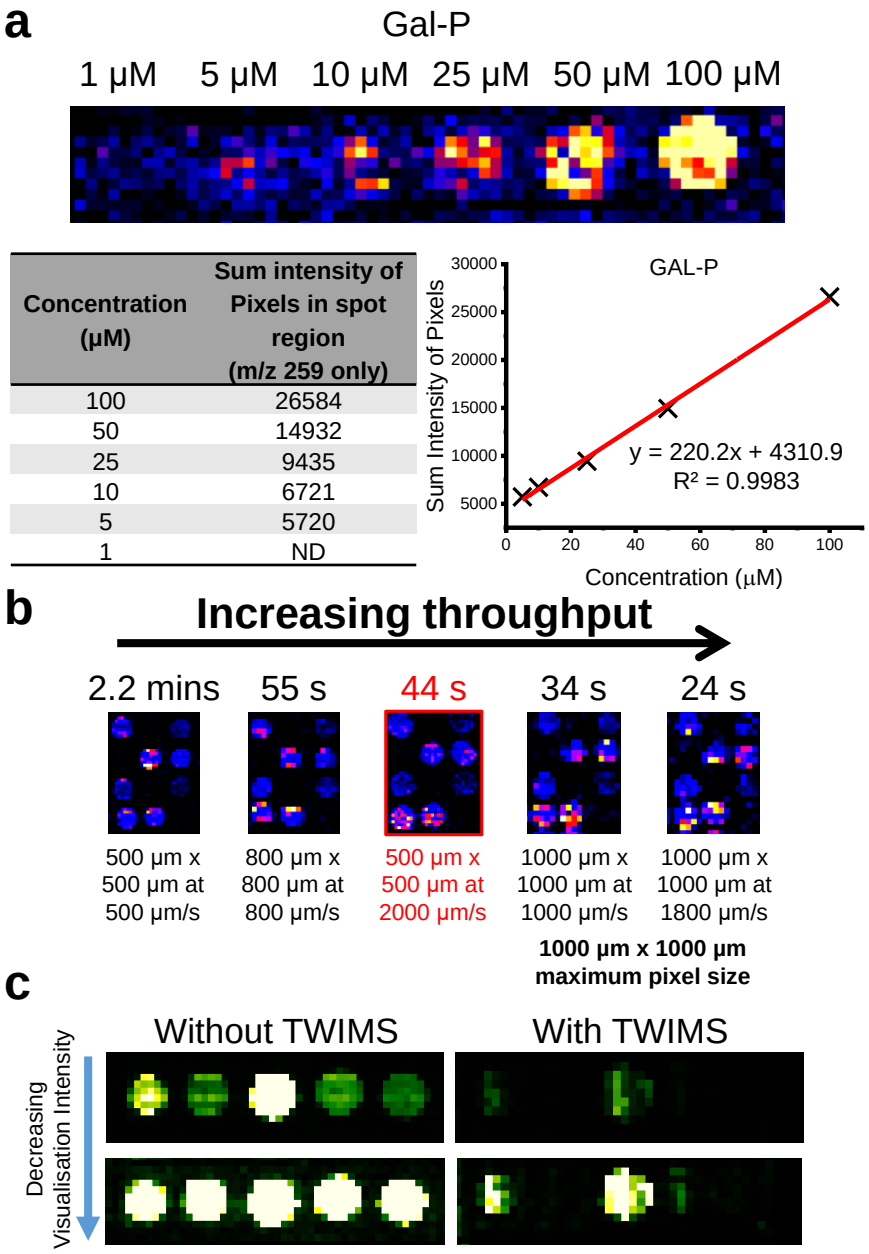


*Figure 2.3: a) Mass resolved heat map indicating the limit of detection of six different concentrations of galactose-1-phosphate using a pixel size of 500 µm x 500 µm and a rate of 2000 µm/s. The intensity of each pixel within each concentration spot has been summed and plotted versus the concentration of that spot. The graph shows good linearity between the concentration of each spot and the summed pixel intensity. b) DiBT-MS analysis of 12 kinase biotransformations at varying pixels sizes and stage speeds. The resulting throughput per sample has been noted. A 44 s/sample throughput has been highlighted as being the optimal conditions for high throughput screening without compromising data quality. c) Heat maps obtained when analysing IRED reactions in 5 different wells of a metagenomic plate both with (right) and without (left) travelling wave ion mobility (TWIMS) enabled within the SYNAPT mass spectrometer. Two visualisations of each heat map are given to show IM filtering of the substrates second $^{13}C$ isotope ion from the major product ion within the heat maps.*

### 2.4.3 PAL Screening

Phenylalanine ammonia lyases (PALs) catalyse the enantioselective addition of ammonia to cinnamic acids to yield L-phenyl alanine derivatives. Currently, the available suite of PALs are limited to substrates with multiple electron-donating substituents on the phenyl ring of both amino acid and acrylic acid substrates. [16,17] As such, we sought to use DiBT-MS to identify PALs able to accept electron-rich derived cinnamic acid derivatives (Figure 2.15 and Table 2.5) that are present in lignocellulosic biomass degradation (e.g., p-coumaric, ferulic, sinapic acid). The derived phenylalanine derivatives are key building blocks for biologically active molecules and active pharmaceutical ingredients (APIs) such as the anti-Parkinson drug L-DOPA. [18]

Initially, the activities of a panel of wild-type PALs were compared by HPLC (Table 2.1, full data set in Table 2.6), including enzymes from published sources and metagenomic origin, against a broad panel of methoxy-substituted arylacrylic acids **5a**-**5u** (Supplementary dataset S1 available upon request). PbPAL from Planctomyces brasiliensis [19] and metagenomic AL-11 (accession number: MW026687) accepted substrates **5a**-**5k** similarly; however, AL-11 showed much greater substrate conversions to the amino acid products **6a**, **6d**, **6f**, **6g**, **6h**, **6k**). It is worth noting that AL-11 revealed low activity with an electron-donating group solely at the para position (**5c**, **5j**) compared to PbPAL.

Moreover, AL-11 exhibited remarkable activity with di- or trimethoxycinnamic acids (**5o**-**q**, **5s**), which are generally inactive in the known PAL sequence space. [20] It is reasonable to suppose that the low activity is not only due to the presence of electron-donating groups but a complex network of stereoelectronic effects which mean the substituents are more weakly bound in the enzyme active site.

*Table 2.1: AL-catalysed hydroamination of various electron-rich substituted cinnamic acids. [a]Determined on non-chiral reverse phase HPLC. [b]Determined by reverse-phase chiral HPLC.*

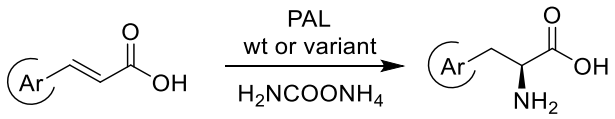


| No. | EDG | PbPAL [a] | AL-11 [b] |
|---|---|---|---|
| **5a** | 2-MeO | 27 | 68 |
| **5b** | 3-MeO | 92 | 61 |
| **5c** | 4-MeO | 8 | 5 |
| **5d** | 3-MeO-4-F | 79 | 91 |
| **5e** | 3-MeO-4-Cl | 91 | 59 |
| **5f** | 3-F-4-MeO | 40 | 81 |
| **5g** | 3-Cl-4-MeO | 38 | 87 |
| **5h** | 2-Et | 48 | 91 |
| **5i** | 3-Et | 30 | 76 |
| **5j** | 4-Et | 48 | 5 |
| **5k** | 2,3-($OCH_2O$) | 92 | 98 |
| **5l** | 3,4-($OCH_2O$) | 3 | 11 |
| **5m** | 2,3-$(MeO)_2$ | <1 | 5 |
| **5n** | 2,4-$(MeO)_2$ | <1 | <1 |
| **5o** | 3,4-$(MeO)_2$ | <1 | 92 |
| **5p** | 3,4-$(MeO)_2$-6-F | <1 | 96 |
| **5q** | 3,5-$(MeO)_2$ | <1 | 98 |
| **5r** | 2,4,6-$(MeO)_3$ | <1 | <1 |
| **5s** | 3,4,5-$(MeO)_3$ | <1 | 97 |
| **5t** | 2,3,4-$(MeO)_3$ | <1 | 4 |
| **5u** | 2,4,5-$(MeO)_3$ | <1 | 73 |

Although the hydroamination reaction does not proceed with naturally occurring lignin monomers such as ferulic acid, to our surprise, excellent conversion (92%) and perfect enantioselectivity (>99%) ee could be achieved with the alkylated 3,4-dimethoxycinnamic acid **5o** as a substrate, to generate L-veratrylglycine (a key building block for a variety of biological building blocks to L-DOPA and anti-cancer agents [21]). Closer inspection of the sequence alignments revealed slight active-site deviation from previously identified 'selectivity residues' such as the otherwise conserved amino acid residue L90 in PbPAL which corresponds to A80 in AL-11. This

variation was predicted to allow accommodation of the large m-MeO substituents in the active site of AL-11. Similar evidence was discovered that introducing a leucine to alanine point mutation in a related phenylalanine aminomutase enzyme from Taxus canadensis (TcPAM) which increased the activity of m-Me compounds. [22]

To improve the activity of the PAL enzymes with o-MeO substituents (**5m, 5r, 5s**), which gave an overall conversion of <5%, we performed a blast sequence alignment of AL-11 against previously reported PAL homologues and found highly conserved active site residues surrounding the electrophilic MIO catalytic ring moiety. An energy-minimised homology model was constructed from Anabaena variabilis AvPAL [17,23] (PDB:5LTM) with a 3,4-dimethoxycinnamic acid **5o** ligand docked in the hydrophobic enzyme active site (Figure 2.4 and 2.16).

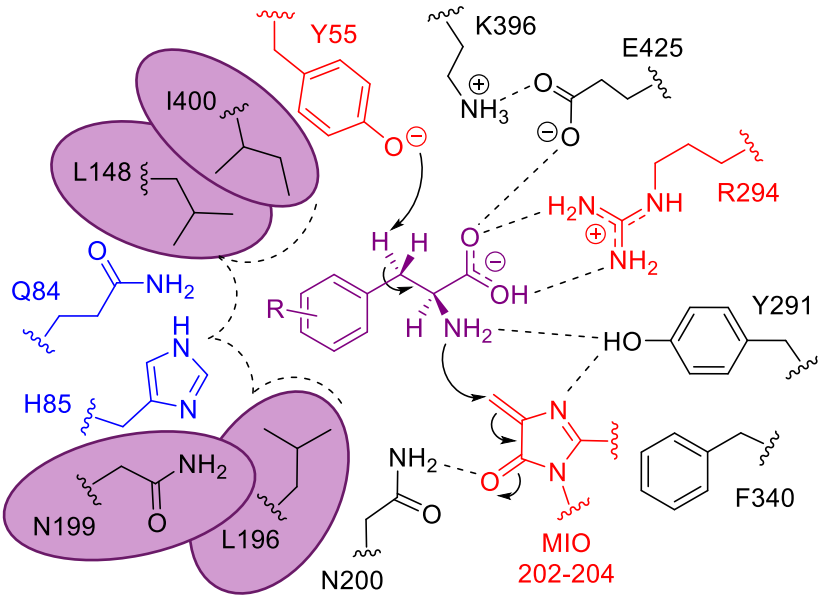


*Figure 2.4: A homology-based active site model of AL-11 enzyme highlighting the amino acid residues conferring selectivity and reactivity from the structure of AvPAL (PDB: 5LTM) [17] with selectivity residues highlighted (blue). The post-translationally modified 3,5-dihyro-5-methylene-4H-imidazol-4-one (MIO) ring and the neighbouring polar side chains are shown (black). Residues circled (purple) were selected for reduced degenerate codon library (RBT) creation.*

The first engineering approach involved the point mutation of the large polar amino acid residue Q84 to smaller hydrophobic groups, which widens the substrate cavity in close proximity to the p- substituents that gave rise to variants such as Q84A, Q84I, and Q84V. The second approach attempted to mimic the activities of the related

aromatic ammonia lyase family members [24,25] PALs/TALs/HALs that are known to contain large hydrophobic groups (Q84F, Q84Y) or a positively charged side chain (Q84H). Of the variants tested under the same condition as WT using the selected test substrate **5m**, the variant Q84V had greater than 7-fold conversion (37%) to the unnatural amino acid product. Other point mutations were tested on the amino acid residue H85, which proved to be overall detrimental to product conversions, even abolishing WT activity with all substrates screened (Figure 2.17).

In addition to the Q84V variant and to limit the screening efforts we created combinatorial libraries targeting neighbouring active site residues N199, L196, L148 and I400 surrounding the cinnamic acid aromatic moiety using a degenerate codon set RBT (coding for the 6 amino acids T, S, I, G, A, V). Double mutation libraries were designed and gave rise to a total number of 36 possible amino acid combinations; this required screening approximately 106 clones to achieve 95% coverage. [26]

DiBT-MS screening of Library A (L148RBT/L196RBT) (Figure 2.5a) gave few hits and revealed the crucial importance of conserving the L148 amino acid. In accordance with a previous report using PcPAL a large decrease in product conversion was shown in o-MeO substituents with the complementary conserved L206 amino acid residue mutated to valine. [16] By contrast, the mutational changes within the L196RBT library gave rise to conversions up to 62% and 70% from variants L196A and L196T respectively.

The screening of Library B (N199RBT/I400RBT) (Figure 2.5a) detected hits where point mutations were present at the conserved amino acid residue N199. Activity was determined with mutated variants to the smaller hydrophobic side chain residues (G, V, I, T) but the N199V mutation was the most prevalent and noticeable in the DiBT-MS screening. Interestingly, other homologues in the aromatic ammonia lyase family exhibit this corresponding valine amino acid residue. [24, 27] In the same manner, variants of the highly conserved I400 residue were not detected presumably due to the critical structural role of this residue in enzyme active site.

After identifying amino acid hotspots from our two previous mutagenic libraries we sought to recombine L196RBT and N199RBT to create Library C (Figure

2.5a) containing the best possible combinations. Most hits were detected in Library C with predominantly featured L196T mutation in combination with mutated residue N199I, N199G or N199V which gave >95% conversion of **5m** to the corresponding product (Figure 2.5b). In addition, we further explored trisubstituted cinnamic acids **5t**-**5u** containing the di-substitution motif of **5m** against our selected 'hits' and found variants that gave >99% conversion to the corresponding L-phenylalanine derivatives (Figure 2.18).

To demonstrate the practical applicability of these enzymes, we performed preparative scale biotransformations with the best variants for 7 of the most challenging substrates considered in the panel (**5m**,**o**,**p**,**q**,**s**,**t**,**u**). The corresponding amino acid products were isolated in pure form by adsorption on ion-exchange resin in good isolated yields (68-90%) and >97% ee (Supplementary dataset S2 available upon request).

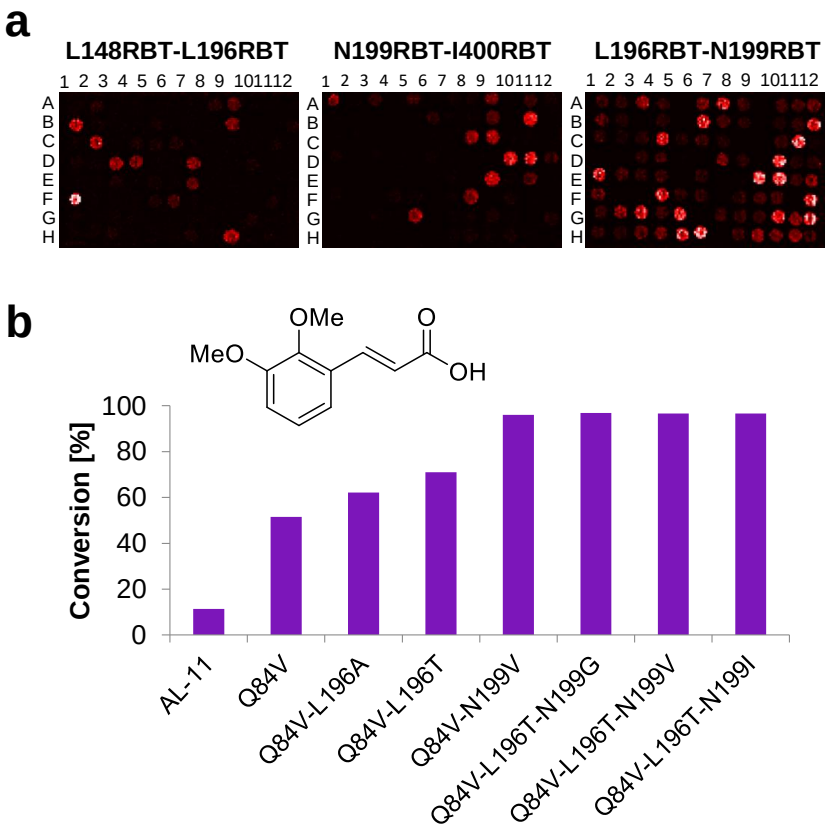


*Figure 2.5: a) DiBT-MS screening results for Library A (L148RBT/L196RBT), library B (N199RBT/I400RBT) and library C (N196RBT/N1999RBT) in a 96-well plate format as indicated. b) Analytical scale biotransformations using **5m** as a substrate with AL-11 and variants identified during DiBT-MS screening.*

## 2.5 Discussion and Outlook

DiBT-MS screening is highly effective across different enzyme classes (kinases, imine reductases, phenylalanine ammonia lyases) presented in different formats (purified enzymes, cell-free lysates and whole-cell reactions) with a screening frequency of 42-50 s per sample. This versatility suggests that the method will be readily adaptable to many more reaction families, as long as the products are detectable as ions. The heat map view of the screen enables facile identification of reactions yielding increased amounts of product, and successful variant enzymes can easily be identified by plasmid sequencing from the corresponding reaction well plate. DiBT-MS can be used quantitatively, with sensitivity down to 5 μM, and good linearity of response over 1.5 orders of magnitude. These limits are determined by the stage raster speed and pixel size, and higher throughput will decrease analyte sensitivity. The linearity afforded from summing pixel signal intensities across a sample deposition region gave a high $R^2$ value of 0.9983 (obtained across a range from 5 μM to 100 μM), with saturation occurring for this compound above ~1 mM (Figure 2.3a and 2.10).

Although full quantification by DESI-MS has not been performed for the majority of the compounds within this work, the capability for semi-quantitative measurement is certainly apparent when visually comparing heat map intensities with reaction conversion data (%) obtained from alternative analytical techniques ($^{19}$F-NMR and HPLC-(UV)). Full reaction conversion data sets for both the Kinase and PAL reactions can be found in Supplementary Figures 2.8, 2.9 and 2.17 respectively. In each case, a brighter spot corresponds with higher reaction conversion allowing mutants with increased activity to be identified for each substrate. The method can detect products with as low as 9% conversion for kinase purified enzyme reactions and down to 3% for the PAL whole-cell reactions. The fastest throughput afforded by this method corresponds to a less than ~50 s per sample without compromising data quality (Figure 2.3b), more than 30 times faster than an equivalent NMR screen and with much lower solvent consumption.

The inclusion of ion mobility within this workflow (Figure 2.3c) increases identification confidence with an additional 'drift time' feature, characteristic of the product ion. This is of high utility in reduction reactions in which the mass shift between starting material and product differs by an increase in 2 *m*/*z* units. The drift time is also diagnostic and can separate isomeric and isobaric ions, for example to determine the products of a regioselective reaction. [28]

## 2.6 Conclusion

The DiBT-MS screening platform offers a facile and rapid method for screening biocatalysts generated *via* directed evolution and protein engineering strategies. It provides product identification in a mobility separated readout of activity, in a heat map format which enables quantitative analysis from crude reaction mixtures. The screen is performed without the need for additional purification, solvent extraction or chemical derivatization for product quantification. In particular, this method facilitates screening for in vitro activity under harsh reaction conditions, such as the PAL-catalysed ammonia addition which requires 4 M ammonia carbamate to thermodynamically drive the hydroamination reaction to the desired products.

## 2.7 Methods

### 2.7.1 Materials

Commercially available reagents were used without further purification. Aldehydes, malonic acid, piperidine and all other reagents were purchased from Sigma Aldrich (St Louis, MO, USA) AlfaAesar or Fisher Scientific. Restriction enzymes, T4 polynucleotide kinase, T4 DNA ligase, Q5® High-fidelity DNA polymerase, and broad protein marker (2-212 kDa) were purchased from New England Biolabs (Ipswich, MA, USA). Escherichia coli DH5$\alpha$ and BL21 (DE3) cells were purchased from New England Biolabs (Ipswich, MA, USA). Expression vector pET-28b was purchased from Novagen (Darmstadt, Germany) and was used for gene expression. LB Broth Base including trace elements was supplied by Formedium (Norfolk, UK). Synthesised oligonucleotides were purchased from Eurofins Genomics (Ebersberg, Germany).

### 2.7.2 General Methods

$^{1}H$ and $^{13}C$ NMR spectra were recorded on a Bruker Avance 400 spectrometer (400.1 MHz) without additional internal standard. Chemical shifts are reported as δ in parts per million (ppm) and are calibrated against the residual solvent signal.

Reverse-phase HPLC was performed on an Agilent 1200 Series LC system equipped with a G1379A degasser, a G1312A binary pump, a G1329 autosampler unit, a G1316A temperature-controlled column compartment and a G1315B diode array detector.

### 2.7.3 Analysis Surface Preparation

Nylon membranes (Roche, 82 mm diameter) were cut to size, allowing for a 25 $mm^2$ area per sample. Cut membranes were fixed to a glass slide with double-sided tape ensuring a flat surface, and sample areas (5 mm x 5 mm) were marked with a scalpel in a grid formation (Figure 2.6). Excess tape was removed from around the membrane.

### 2.7.4 Kinase biotransformations and $^{19}F$ NMR analysis

Reactions were carried out in Tris buffer (50 μL, 100 mM, pH 8.0) at 37 °C for 24 h. The mixture contained monosaccharide (8 mM), ATP (10 mM), $MgCl_2$ (5 mM) and GalK or NahK (6 μg, final kinase conc. 0.12 mg $mL^{-1}$). The presence of the sugar-1-phosphate product was determined by HRMS and the conversion was determined quantitatively by $^{19}F$ NMR, according to the following method. Samples (50 μL) were diluted with MeOH/$H_2O$ (1:1, 450 μL) and centrifuged (10 000 x g, 5 min) to remove any insoluble matter. The solution was transferred to a 5 mm NMR tube, with either a sealed glass capillary tube containing $D_2O$ for locking and referencing. $^{19}F$ NMR spectra were recorded at 25°C on a Bruker Avance 500 MHz spectrometer (operating at 470 MHz) equipped with a QCI-F cryoprobe. Conversions were determined by taking the relative integration of the corresponding resonances of the starting material and product, which were typically baseline-separated.[8]

For DiBT screening, reactions were first diluted with MeOH/$H_2O$ (1:1, 300-450 μL). 0.5 μL of each solution was transferred onto a pre-prepared nylon membrane grid mounted on a glass slide as detailed above and allowed to air dry before analysis.

### 2.7.5 Whole-cell biotransformations (PALs)

Wild type AL-11 and variants were transformed into *E. coli* BL21 (*DE3*) for yielding *E. coli* BL21 (*DE3*) pET28b-AL-11. A single colony was selected and grown in a 3 mL overnight starter culture supplemented with 50 μg $mL^{-1}$ kanamycin at 37°C at 200 rpm. The freshly-prepared starter culture was used to inoculate 500 mL of LB-based autoinduction media containing 50 μg $mL^{-1}$ kanamycin in 2 L baffled flasks at a rotary shaking rate of 200 rpm at 18°C for 72 h. The cells were harvested by centrifugation (4°C, 3,250 x g, 20 min). The cells were resuspended with $KP_i$ buffer (100 mM, pH 8.0) and harvested again by centrifugation (4°C, 3250 x g, 20 min). The cell pellet was subsequently aliquoted and stored at -20°C.

The whole-cell biotransformation was conducted by resuspending 50 mg $L^{-1}$ of cell paste in an appropriate volume of ammonium carbamate solution (4 M, pH ~9.9, unadjusted) supplemented with the relevant arylacrylic acid **5a-5u** at the required concentration (5 mM for screening, 10-20 mM for preparative applications). All biotransformations were performed at 30 °C with agitation of 250 rpm. After a 24 h incubation period, the samples were centrifuged (5 min, 13 000 rpm) to remove cell debris. The crude supernatant was then dissolved in 50% MeOH (v/v), and 500 μL was transferred to a 0.45 mm filter vial for analysis by HPLC with the remaining solution reserved for analysis.

Conversion values for the PAL reactions of arylacrylic acids **5a-5u** were determined by HPLC on a non-chiral reverse-phase Zorbax C-18 Extend column (50 mm x 4.6 mm x 3.5 μm, Agilent), flow rate 1.0 mL $min^{-1}$, temperature 40 °C, detection wavelength 210 nm. Mobile phase: aq $NH_4OH$ 0.1 M pH 10.0/MeOH, 9:1. For DESI-MS analysis 0.5 μL of each solution was transferred onto a pre-prepared nylon membrane grid mounted on a glass slide as detailed above and allowed to air dry before analysis.

Enantiomeric excess (ee) values for the isolated PAL reaction products were determined by HPLC on a chiral reverse-phase Crownpak CR(+)column (150 mm x 4 mm x 3.5 μm, Daicel), flow rate 1.0 mL $min^{-1}$, temperature 40 °C, detection wavelength 210 nm. Mobile phase: aq $HClO_4$ 1.14% w/v / MeOH, 85:15.

Preparative scale PAL reactions were performed as described above for analytical scale reactions, with an increased substrate concentration (10-20 mM) and addition of DMSO (5% v/v) as a cosolvent. Products were isolated by adsorption on ion exchange Dowex® 50WX8 resin and elution with ammonium hydroxide solution (as described previously [19]).

### 2.7.6 Screening of metagenomic IREDs

A 384-well 0.5 mg CFE plate was acclimatised to room temperature. Each well was then re-suspended to 10 mg $mL^{-1}$ to in 0.1 M Tris-HCl pH 8.0. To a 384-well deep-well plate (Corning), the following solution was dispensed: 10 mM 6,7-dimethoxy-1-methyl-3,4-dihydroisoquinoline, 50 mM glucose, 0.5 mM $NADP^+$, 0.5 mg $mL^{-1}$ GDH (CDX-901), 4 mg $mL^{-1}$ IRED lysate, made up to a total reaction volume of 50 μL in 0.1 M Tris-HCl pH 8.0. The plate was then sealed at centrifuged (1000 rpm, 1 min). The 384-deep well plate was then incubated at 30 °C for 24 h at 1000 rpm. The reaction was then quenched with the addition of 50:50 MeOH/$H_2O$ and centrifuged (1000 rpm, 1 min) before DiBT-MS screening. 0.5 μL from each well was transferred onto a pre-prepared nylon membrane grid mounted on a glass slide as detailed above and allowed to air dry before DiBT-MS analysis.

#### 2.7.6.1 Singular IRED biotransformations

Stock solutions of the IREDs were prepared (pIR-2, -9, -170, -204, and -364) by weighing out crude lyophilised cell-free extract and rehydrated to a concentration of 10 mg/mL in 0.1 M TRIS-HCl buffer pH 8.0. Biotransformations were performed on a 500 μL scale. The reaction mixture contained 10 mM imine 3, 50 mM D-glucose, 0.5 mM NADP+, 0.5 mg/mL GDH (Codexis-901), 4 mg/mL IRED lysate or 1 mg/mL AspRedAm (IMAC grade purified), reaction volume was made up to 500 μL in 0.1 M TRIS-HCl buffer pH 8.0. Reactions were incubated at 30 °C for 24 hours. Reactions were quenched by the addition of 50 μL 10 M NaOH and extracted twice with 750 μL

of tert-butyl methyl ester. The organic fractions were combined and dried by MgSO4 and analysed by chiral-HPLC. 13

#### 2.7.6.2 384-well IRED colorimetric screen

A mastermix reagent was made up to 25 mL, containing 0.125 mg $mL^{-1}$ INT and 10 mM amine substrate in Tris-HCl (0.1 M) adjusted to pH 9.0. 50 μL of the mastermix was aliquoted to each well of the plate. The plate was then spun down (1,000 rpm, 1 min) and red membrane removed. The plate was incubated (in the dark) at 30 °C for 24 h. An absorbance reading at $\lambda$=490 nm was taken at 0 h, 1 h, 4 h and 24 h. Expected false positives in wells B02, D08, F12, H21, I02, I07, K16, O01, O08 and P17 were unaccounted for. The same procedure was followed for the 384 IREDy-to-go blank plate, except no amine was added to the mastermix.

### 2.7.7 Instrumentation

All DiBT-MS experiments were performed on a SYNAPT™ G2 Si mass spectrometer (Waters Corporation, Manchester, UK) coupled with a DESI 2D Omni Spray Ion Source (Prosolia, Indianapolis, IN, USA).

#### 2.7.7.1 DESI Source

DESI solvent comprised of a methanol-water mixture (49:1) at a flow rate of 2.5 μL $min^{-1}$. Nitrogen gas flow (3 bar) and a capillary voltage of 3.5 kV or 4.0 kV (+ve/-ve respectively) was used to generate an electrospray plume towards the surface of interest. The DESI sprayer position was then adjusted to ensure optimum signal intensity was achieved from a solution of the product dried on a nylon membrane. The sampling area was defined by HD Imaging software V1.4 (Waters Corporation, Manchester, UK) with pixel size and stage speed defined as per the throughput of the experiment. (Figure 2.3b)

#### 2.7.7.2 Mass Spectrometer

The mass spectrometer was operated using MassLynx v4.2 (Waters Corporation, Manchester, UK) in negative mode, with a source cone voltage of 58 V, and a source temperature of 150 °C. The trap and transfer cell voltages were set at 4 V and 2 V respectively. All mass spectrometry data was processed (0.2 Da window,

20000 resolution, top 10 000 peaks) and heat maps analysed using HD Imaging software.

### 2.7.8 Code Availability

DNA sequence information for AL-11 has been deposited with GenBank accession no. MW026687.

### 2.7.9 Acknowledgements

The authors would like to acknowledge several research staff within the Manchester Institute of Biotechnology for their assistance and useful suggestions whilst undertaking this work: Joanne Porter, Nicholas J. Weise, Cunyu Yan, Chris J. Gray, Neil Dixon and Lukasz G. Migas. Particular thanks go to Emrys Jones of Waters Corporation for technical assistance with the DESI-MS instrumentation. We would also like to thank James Finnigan of Prozomix Ltd. for deposition of the AL-11 sequence in the GenBank. This work would not have been possible without funding made available from the Biotechnology and Biological Sciences Research Council (BBSRC), (BB/M011208/1, BBSRC-FAPESP grant BB/P01738X/1, IBCarb BB/L013762/1, BB/M027791/1, BB/M02903411, BB/M029034/1 BB/M028836/1) and the European Research Council (ERC), (788231-ProgrES-ERC-2017-ADG).

## 2.8 References


1 A. Aharoni, A. D. Griffiths and D. S. Tawfik, *Curr. Opin. Chem. Biol.*, 2005, **9**, 210–216.

2 Z. Takáts, J. M. Wiseman, B. Gologan and R. G. Cooks, *Science (80-. ).*, 2004, **306**, 471–473.

3 C. Yan, F. Parmeggiani, E. A. Jones, E. Claude, S. A. Hussain, N. J. Turner, S. L. Flitsch and P. E. Barran, *J. Am. Chem. Soc.*, 2017, **139**, 1408–1411.

4 M. McAuley, H. Kristiansson, M. Huang, A. L. Pey and D. J. Timson, *Biochem. Soc. Trans.*, 2016, **44**, 116–122.

5 Y. Li, H. Yu, Y. Chen, K. Lau, L. Cai, H. Cao, V. K. Tiwari, J. Qu, V. Thon, P. G. Wang and X. Chen, *Molecules*, 2011, **16**, 6396–6407.

6 J. Yang, X. Fu, Q. Jia, J. Shen, J. B. Biggins, J. Jiang, J. Zhao, J. J. Schmidt, P. G. Wang and J. S. Thorson, *Org. Lett.*, 2003, **5**, 2223–2226.

7 M. Chen, L. L. Chen, Y. Zou, M. Xue, M. Liang, L. Jin, W. Y. Guan, J. Shen, W. Wang, L. Wang, J. Liu and P. G. Wang, *Carbohydr. Res.*, 2011, **346**, 2421–2425.

8 T. Keenan, F. Parmeggiani, J. Malassis, C. Q. Fontenelle, J.-B. Vendeville, W. Offen, P. Both, K. Huang, A. Marchesi, A. Heyam, C. Young, S. J. Charnock, G. J. Davies, B. Linclau, S. L. Flitsch and M. A. Fascione, *Cell Chem. Biol.*, 2020, **27**, 1199-1206.

9 T. W. Thorpe, S. P. France, S. Hussain, J. R. Marshall, W. Zawodny, J. Mangas-Sanchez, S. L. Montgomery, R. M. Howard, D. S. B. Daniels, R. Kumar, F. Parmeggiani and N. J. Turner, *J. Am. Chem. Soc.*, 2019 , **141**, 19208-19213.

10 G. Grogan, *Curr. Opin. Chem. Biol.*, 2018, **43**, 15–22.

11 G. J. Ford, N. Kress, A. P. Mattey, L. J. Hepworth, C. R. Baldwin, J. R. Marshall, L. S. Seibt, M. Huang, W. R. Birmingham, N. J. Turner and S. L. Flitsch, *Chem. Commun.*, 2020, **56**, 7949-7952.

12 J. Marshall, P. Yao, S. Montgomery, J. Finnigan, T. Thorpe, R. Palmer, J. Mangas-Sanchez, R. Duncan, R. Heath, K. Graham, D. Cook, S. Charnock and N. Turner, *Nat. Chem.*, 2021, **13**, 140-148.

13 G. A. Aleku, S. P. France, H. Man, J. Mangas-Sanchez, S. L. Montgomery, M.

Sharma, F. Leipold, S. Hussain, G. Grogan and N. J. Turner, *Nat. Chem.*, 2017, **9**, 961–969.

14 S. D. Pringle, K. Giles, J. L. Wildgoose, J. P. Williams, S. E. Slade, K. Thalassinos, R. H. Bateman, M. T. Bowers and J. H. Scrivens, *Int. J. Mass Spectrom.*, 2007, **261**, 1–12.

15 C. Yan, J. W. Schmidberger, F. Parmeggiani, S. A. Hussain, N. J. Turner, S. L. Flitsch and P. Barran, *Analyst*, 2016, **141**, 2351–2355.

16 E. Z. A. Nagy, S. D. Tork, P. A. Lang, A. Filip, F. D. Irimie, L. Poppe, M. I. Toşa, C. J. Schofield, J. Brem, C. Paizs and L. C. Bencze, *ACS Catal.*, 2019, **9**, 8825–8834.

17 N. J. Weise, S. T. Ahmed, F. Parmeggiani, J. L. Galman, M. S. Dunstan, S. J. Charnock, D. Leys and N. J. Turner, *Sci. Rep.*, 2017, **7**, 13691.

18 K. Min, K. Park, D. H. Park and Y. J. Yoo, *Appl. Microbiol. Biotechnol.*, 2015, **99**, 575–584.

19 S. T. Ahmed, F. Parmeggiani, N. J. Weise, S. L. Flitsch and N. J. Turner, *ACS Catal.*, 2018, **8**, 3129–3132.

20 F. Parmeggiani, N. J. Weise, S. T. Ahmed and N. J. Turner, *Chem. Rev.*, 2018, **118**, 73–118.

21 T. Li and X. Li, *Green Chem.*, 2014, **16**, 4241–4256.

22 L. Feng, U. Wanninayake, S. Strom, J. Geiger and K. D. Walker, *Biochemistry*, 2011, **50**, 2919–2930.

23 S. L. Lovelock and N. J. Turner, *Bioorganic Med. Chem.*, 2014, **22**, 5555–5557.

24 G. V. Louie, M. E. Bowman, M. C. C. Moffitt, T. J. Baiga, B. S. S. Moore and J. P. Noel, *Chem. Biol.*, 2006, **13**, 1327–1338.

25 S. Bartsch and U. T. Bornscheuer, *Angew. Chemie - Int. Ed.*, 2009, **48**, 3362–3365.

26 M. T. Reetz and J. D. Carballeira, *Nat. Protoc.*, 2007, **2**, 891–903.

27 S. Bartsch and U. T. Bornscheuer, *Protein Eng. Des. Sel.*, 2010, **23**, 929–933.

28 E. Sinclair, K. A. Hollywood, C. Yan, R. Blankley, R. Breitling and P. Barran, *Analyst*, 2018, **143**, 4783–4788.

## 2.9 Supporting Information

### 2.9.1 DiBT Method Development

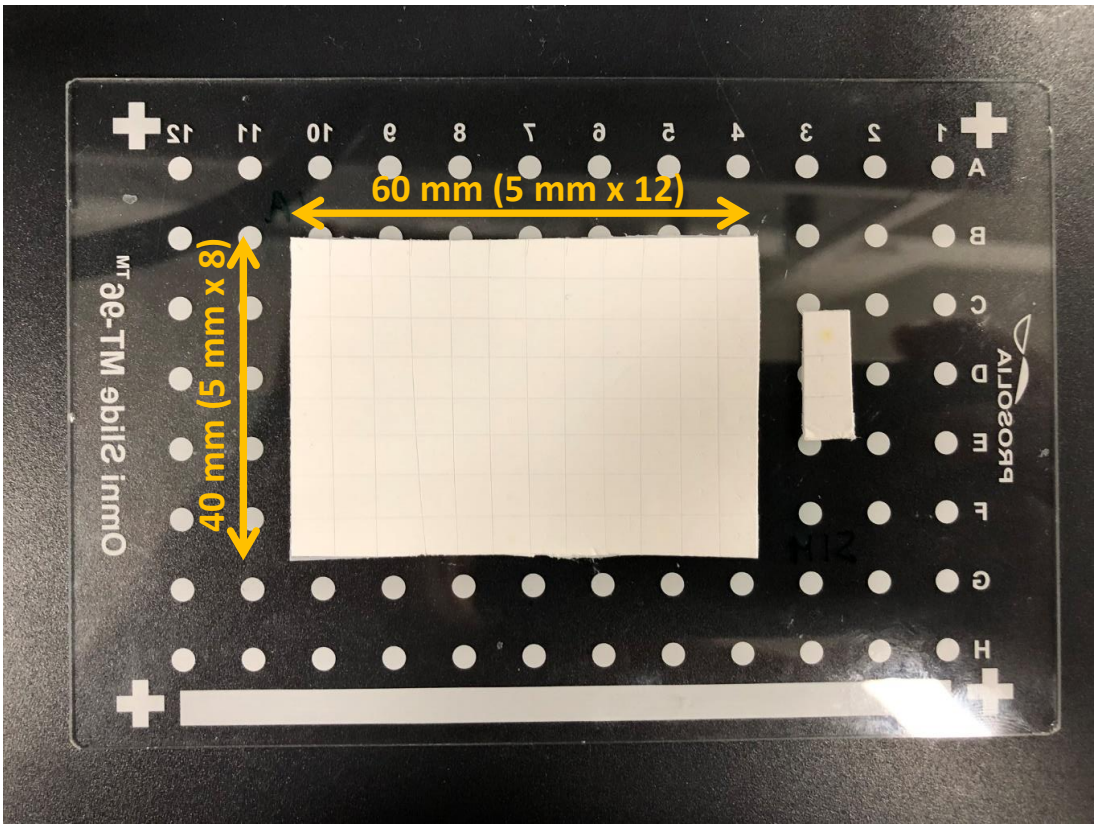


*Figure 2.6: Photograph of a DESI membrane 96-well plate, prepared on a PROSOLIA 96-well Teflon glass slide. The underside of the slide (i.e. non-Teflon coated side) has been used to adhere the membrane that was pre-cut to size (40 mm x 60 mm) with double sided tape. Once adhered, an 8 by 12 grid was etched into the membrane using a scalpel to produce 96 segments of ~25 mm² each into to which samples were to be deposited.*

### 2.9.2 Kinases

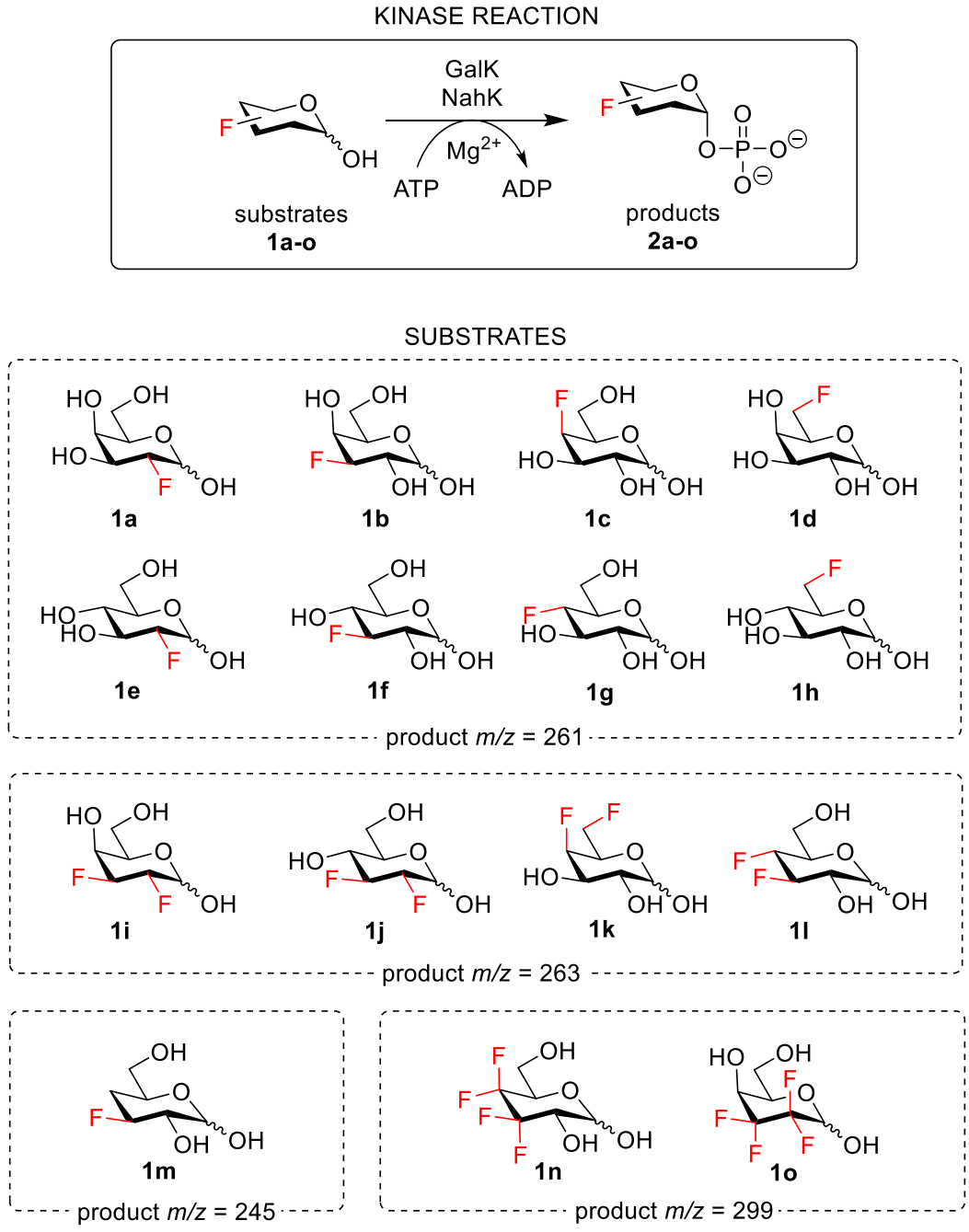


*Figure 2.7: Kinase reaction scheme and structures of fluorinated monosaccharide substrates used during biotransformation screening experiments.*

*Table 2.2: Chemical formula and exact masses of fluorinated substrates and products from kinase reactions.*

| Substrates | | | Products | | |
|---|---|---|---|---|---|
| **Subs.** | **Chemical formula** | **Exact mass** | **Prod.** | **Chemical formula** | **Exact mass** |
| **1a (Gal2F)** | $C_6H_{11}FO_5$ | 182.058 | **2a** | $C_6H_{12}FO_8P$ | 262.025 |
| **1b (Gal3F)** | $C_6H_{11}FO_5$ | 182.058 | **2b** | $C_6H_{12}FO_8P$ | 262.025 |
| **1c (Gal4F)** | $C_6H_{11}FO_5$ | 182.058 | **2c** | $C_6H_{12}FO_8P$ | 262.025 |
| **1d (Gal6F)** | $C_6H_{11}FO_5$ | 182.058 | **2d** | $C_6H_{12}FO_8P$ | 262.025 |
| **1e (Glc2F)** | $C_6H_{11}FO_5$ | 182.058 | **2e** | $C_6H_{12}FO_8P$ | 262.025 |
| **1f (Glc3F)** | $C_6H_{11}FO_5$ | 182.058 | **2f** | $C_6H_{12}FO_8P$ | 262.025 |
| **1g (Glc4F)** | $C_6H_{11}FO_5$ | 182.058 | **2g** | $C_6H_{12}FO_8P$ | 262.025 |
| **1h (Glc6F)** | $C_6H_{11}FO_5$ | 182.058 | **2h** | $C_6H_{12}FO_8P$ | 262.025 |
| **1i (Gal23F$_2$)** | $C_6H_{10}F_2O_4$ | 184.055 | **2k** | $C_6H_{11}F_2O_7P$ | 264.021 |
| **1j (Glc23F$_2$)** | $C_6H_{10}F_2O_4$ | 184.055 | **2l** | $C_6H_{11}F_2O_7P$ | 264.021 |
| **1k (Gal46F$_2$)** | $C_6H_{10}F_2O_4$ | 184.055 | **2m** | $C_6H_{11}F_2O_7P$ | 264.021 |
| **1l (Glc34F$_2$)** | $C_6H_{10}F_2O_4$ | 184.055 | **2n** | $C_6H_{11}F_2O_7P$ | 264.021 |
| **1m (Gal3F4D)** | $C_6H_{11}FO_4$ | 166.064 | **2i** | $C_6H_{12}FO_7P$ | 246.030 |
| **1n (Gal3344F$_4$)** | $C_6H_8F_4O_4$ | 220.036 | **2o** | $C_6H_9F_4O_7P$ | 300.002 |
| **1o (Gal2233F$_4$)** | $C_6H_8F_4O_4$ | 220.036 | **2p** | $C_6H_9F_4O_7P$ | 300.002 |

*Table 2.3: NMR conversion tables (%) for kinase reaction from range of substrates and enzymes (from ref.[S1])*

| | **Kinase** | | | | | | | | | | |
|---|---|---|---|---|---|---|---|---|---|---|---|
| | **1** | **2** | **3** | **4** | **5** | **6** | **7** | **8** | **9** | **10** | **11** |
| **1a** | >95 | >95 | >95 | >95 | >95 | <5 | 25 | 20 | <5 | 0 | 5 |
| **1b** | <5 | <5 | >95 | 83 | 74 | 0 | 0 | 0 | 0 | 0 | 0 |
| **1c** | <5 | <5 | >95 | 72 | 91 | 29 | 7 | >95 | 49 | 11 | 27 |
| **1d** | <5 | <5 | >95 | 74 | 67 | 0 | 0 | 0 | 0 | 0 | 0 |
| **1e** | 0 | 0 | 0 | 0 | 0 | 26 | 64 | 30 | 0 | 0 | 7 |
| **1f** | 0 | 0 | 0 | 0 | 0 | 0 | 0 | 0 | 0 | 0 | 0 |
| **1g** | 0 | 0 | 0 | 0 | 0 | <5 | 23 | 37 | <5 | 0 | <5 |
| **1h** | 0 | 0 | 0 | 0 | 0 | 0 | 0 | 0 | 0 | 0 | 0 |
| **1j** | 0 | <5 | >95 | 43 | 45 | 0 | 0 | 0 | 0 | 0 | 0 |
| **1m** | 0 | 0 | 0 | 0 | 0 | <5 | 11 | 21 | <5 | 0 | <5 |
| **1o** | 0 | 0 | 12 | 0 | 0 | 0 | 0 | 0 | 0 | 0 | 0 |

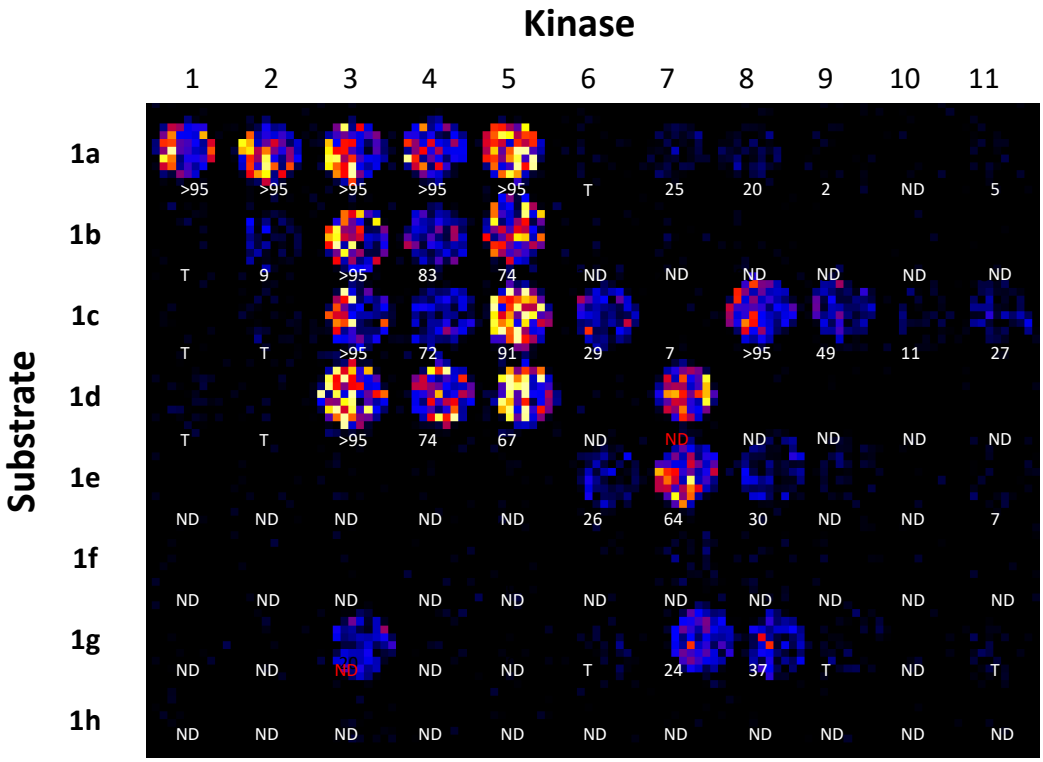


*Figure 2.8: Kinase plate 1 – 88 reaction screening (8 substrates x 11 enzymes) DESI-MS heat map of m/z 261. Substrates consisted of 8 isomeric mono-fluorinated monosaccharides and hence the product produced all present at the same m/z value (261). Pixels were defined as 500 µm x 500 µm and analysed at a stage speed of 2000 µm/s. Total analysis time for these 88 samples was 61 minutes, equivalent to 42 s/sample. Reaction conversion data obtained from $^{19}$F-NMR analysis has been overlain (white text) below the location of the corresponding reaction spot for comparison. *Note: two inconsistencies between the NMR and DiBT-MS data sets have been identified and indicated in red text below the corresponding reaction spot. These inconsistencies have been attributed to human errors when preparing a large number of samples for the 2 data sets by hand.*

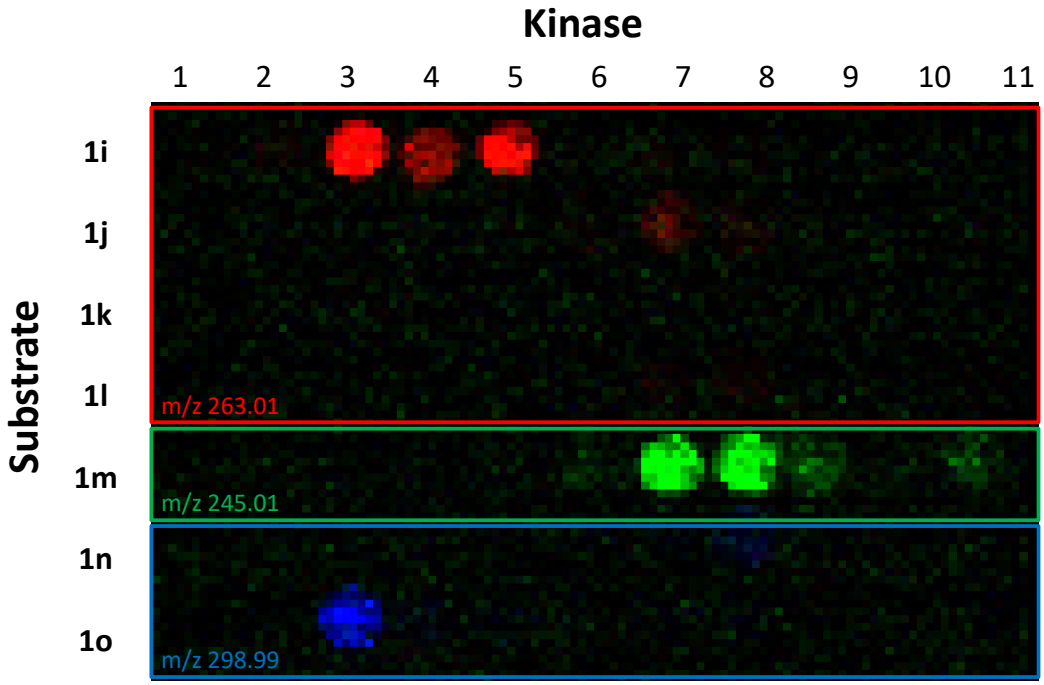


*Figure 2.9: Kinase plate 2 – 77 reaction screening (7 substrates x 11 enzymes) heat maps (overlain m/z). Substrates consisted of a mixture of di-fluorinated, mono-deoxy-mono-fluorinated and tetra-fluorinated monosaccharides. Substrates are grouped via their expected product m/z, as indicated by the red, green and blue highlighted boxes. All m/z values are monitored simultaneously, and hence separate analyses of this plate for each substrate mass was not required. Pixels were defined as 500 µm x 500 µm and analysed at a stage speed of 500 µm/s. Total analysis time for these 77 samples was 174 minutes, equivalent to 2.26 minutes/sample.*

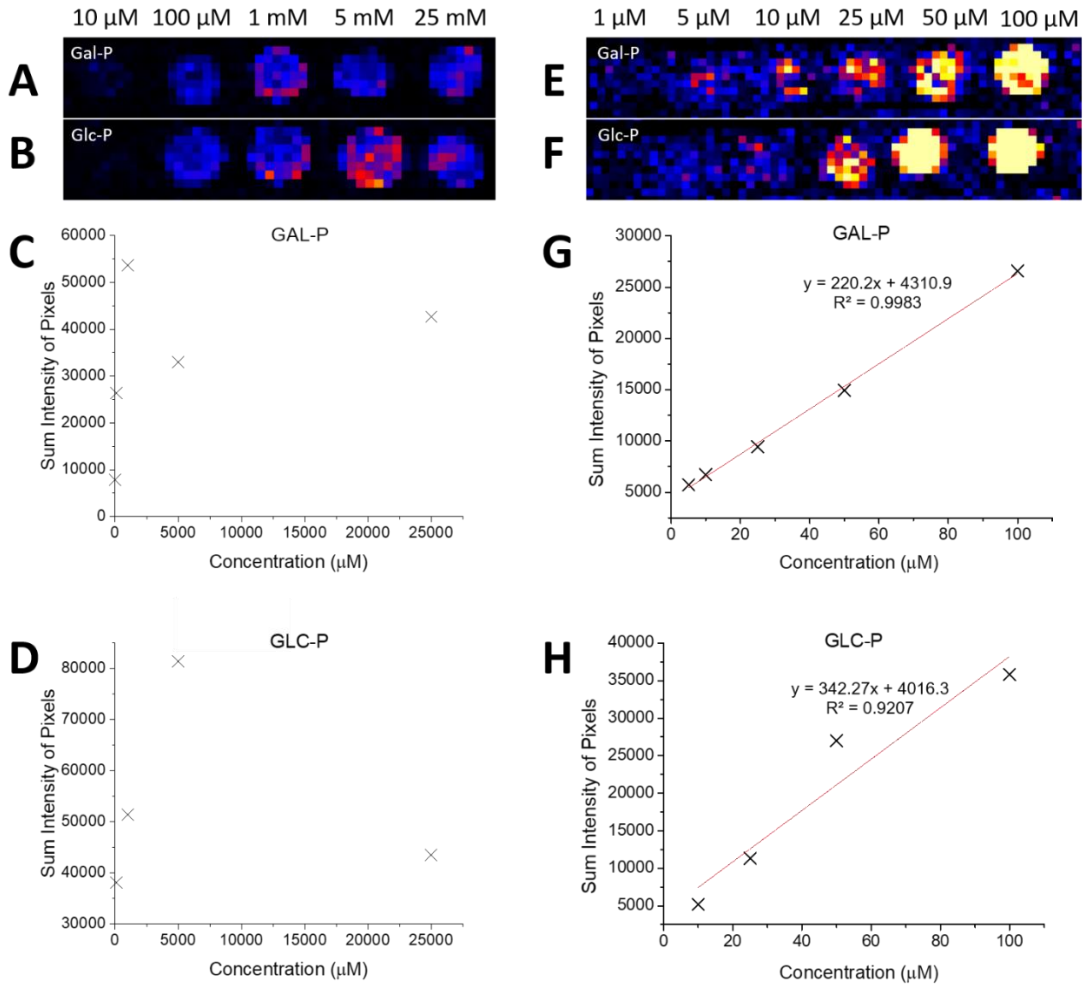


*Figure 2.10: Linearity analysis of galactose-1-phosphate and glucose-1-phosphate over 2 concentration ranges, 10 µM – 25 mM and 1 µM – 100 µM. Analysis of DESI-MS heat maps A and B yielded linearity graphs C and D respectively with both illustrating poor linearity for both product compounds over a large concentration range (10 µM - 25 mM). Heat maps E and F correspond to DESI-MS analysis over a smaller range of lower concentration standard solutions for each product with analysis yielding improved linearity over the range 10 µM – 100 µM as is observed in graphs G and H.*

### 2.9.3 IREDs

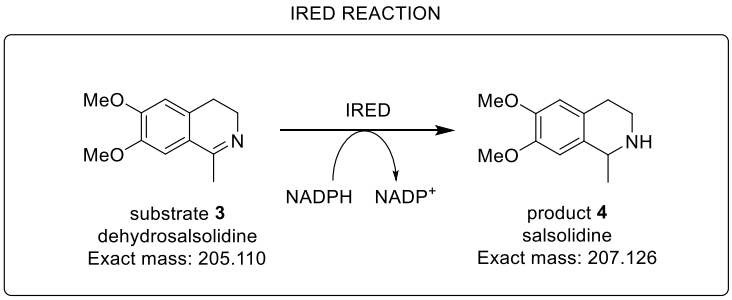


*Figure 2.11: IRED reaction schematic including structures of the substrate screened (dehydrosalsolidine) and product detected (salsolidine).*

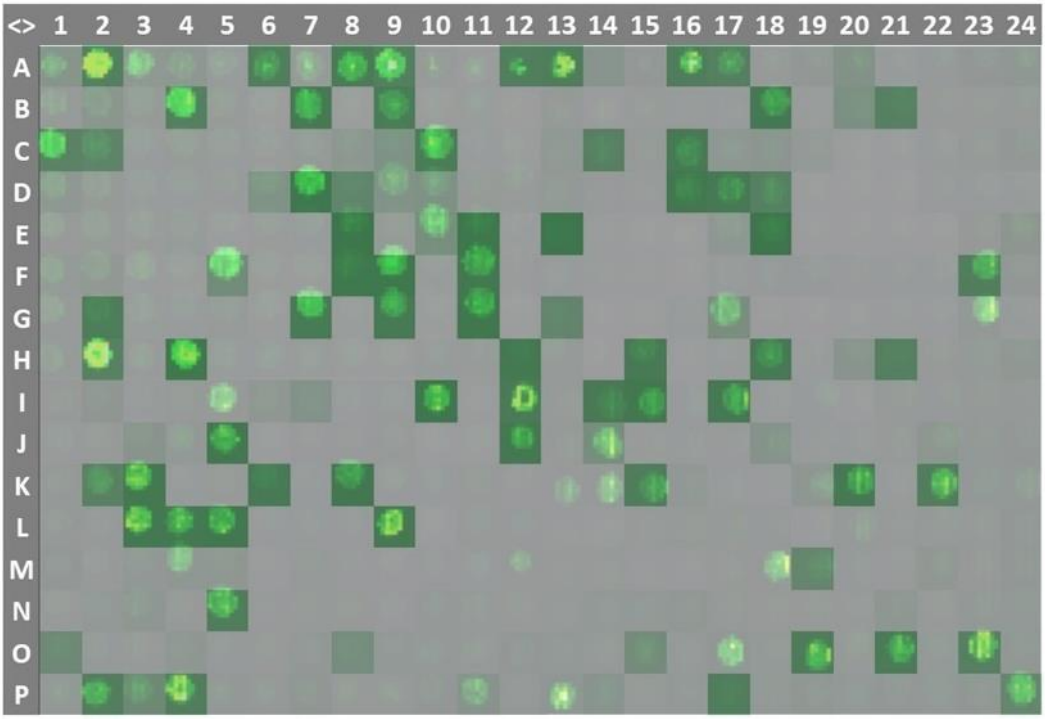


*Figure 2.12: Overlay of IRED colorimetric screening results with IRED DESI-MS screening for the oxidation of* **4** *to* **3**. *Colorimetric results are denoted as the transparent squares, with the darker green colouring indicating a higher response obtained during the colorimetric screen. Circular regions indicate locations on the 384-well plate in which DESI-MS screening detected presence of the product ion (m/z 208), with the brighter circular spots indicating a higher response detected.*

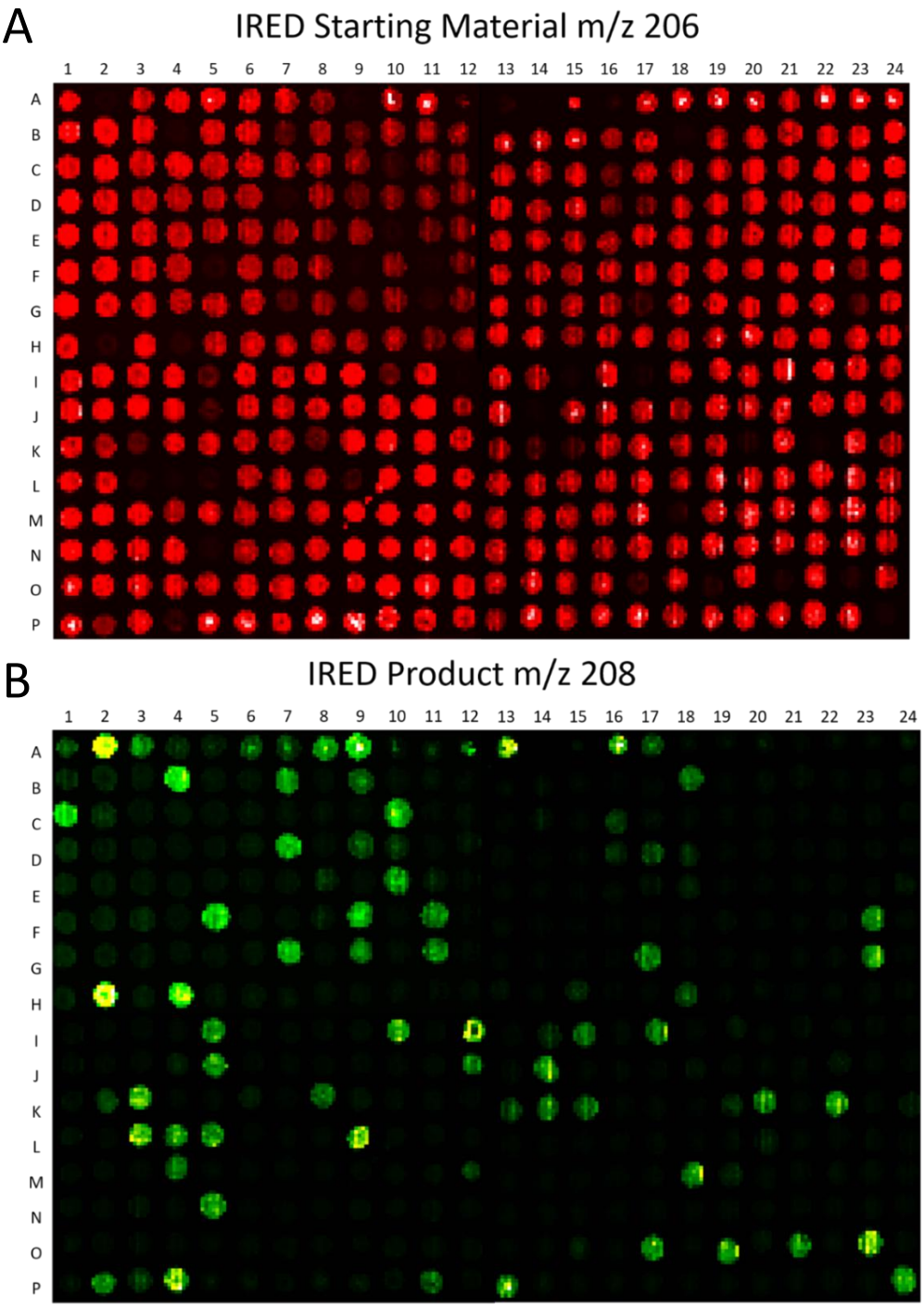


*Figure 2.13: 384-well plate DESI-MS heat maps of IRED starting material (**3**, m/z 206, (A), red) and product (**4**, m/z 208, (B), green). Both m/z values were monitored simultaneously. DESI-MS pixel sizes were set to 500 µm x 500 µm and analysed using a stage speed of 1500 µm/s. The total DESI-MS analysis time was equivalent to a throughput of 52 s/sample.*

*Table 2.4: Results of Singular IRED Biotransformations for the reduction of **3** to **4** as determined by HPLC. (HPLC method as per ref [S2]).*

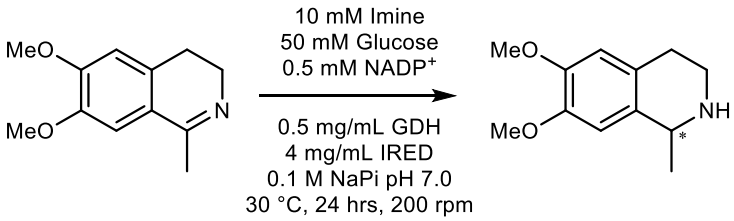


**3** **4**

| IRED No. | % conversion | % ee |
|---|---|---|
| **2** | >99% | >99%$^{R}$ |
| **9** | >99% | >99%$^{R}$ |
| **170** | >99% | >99%$^{S}$ |
| **196** | >99% | >99%$^{S}$ |
| **364** | >99% | >99%$^{S}$ |
| ***Asp*RedAm (control)** | >99% | >99%$^{R}$ |

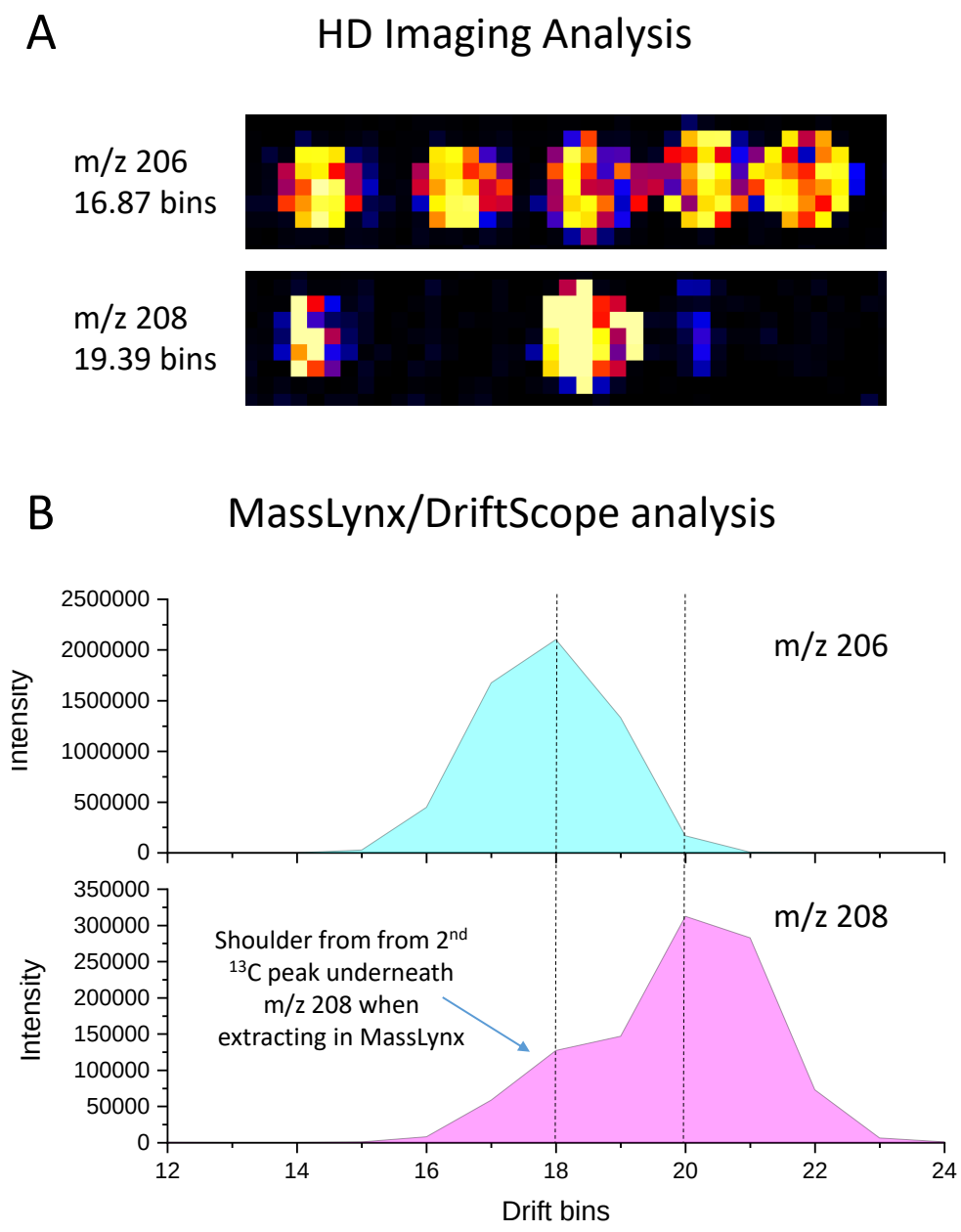


*Figure 2.14: Additional IRED ion mobility data analysis, illustrating that the starting material and product can not only be separated on their m/z but also TWIMS drift time. This separates the product from the 2nd $^{13}C$ isotope of the starting material, removing false positive results. A) HD Imaging analysis of five wells of the IRED metagenomic plate showing the differing drift times, m/z values and heat maps between product and starting material. B) MassLynx analysis with the ion mobility drift profiles of each m/z value.*

### 2.9.4 PALs

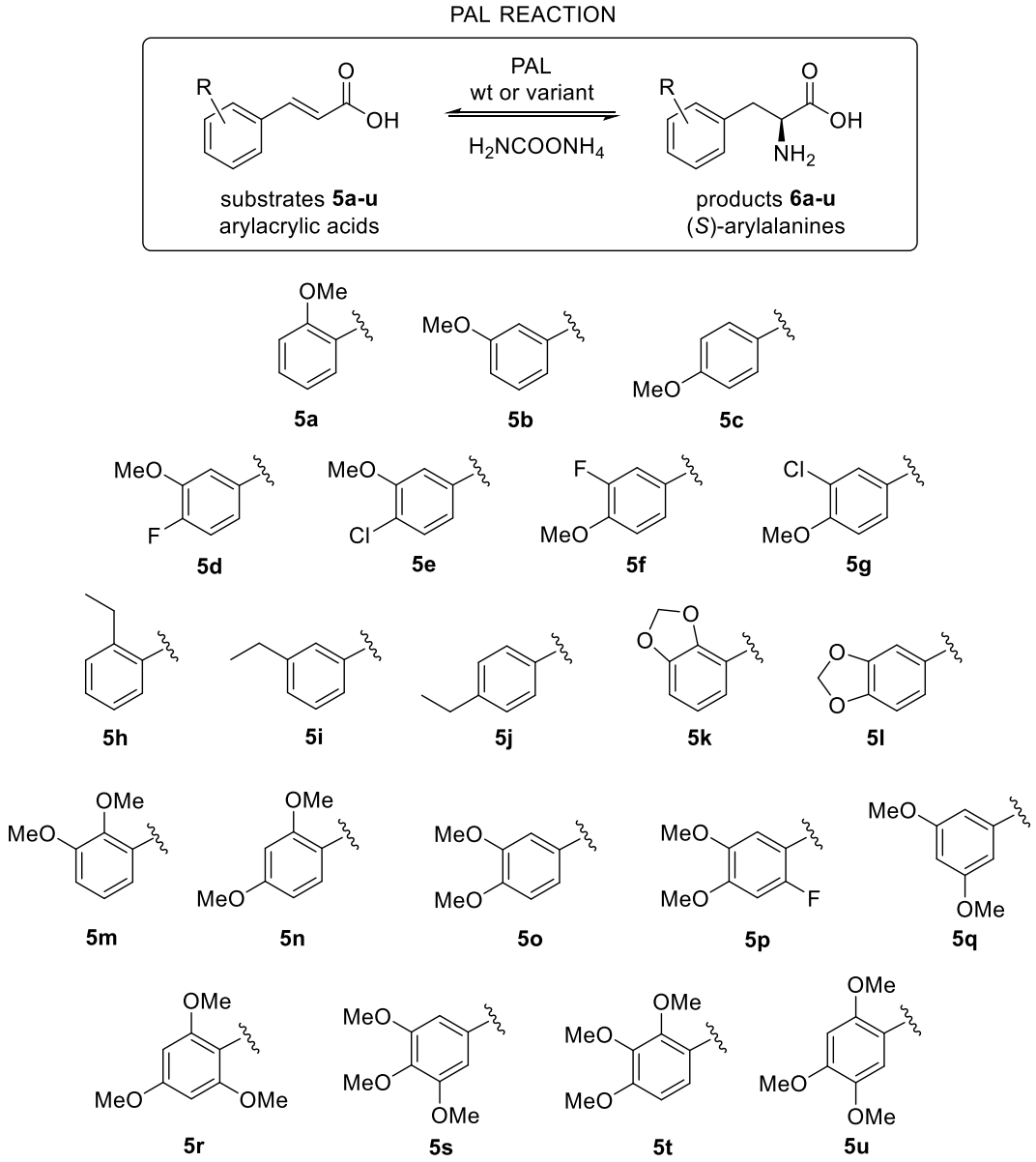


*Figure 2.15: PAL reaction scheme and structures of substituted cinnamic acid substrates used in PAL whole cell reactions.*

*Table 2.5: Chemical formula and exact masses of cinnamic acid substrates and phenylalanine derived products used for PAL biotransformation screening.*

| Substrate | Substituents | Chemical formula | Exact mass | Product | Chemical formula | Exact mass |
|---|---|---|---|---|---|---|
| **5a** | 2-MeO | $C_{10}H_{10}O_3$ | 178.063 | **6a** | $C_{10}H_{13}NO_3$ | 195.090 |
| **5b** | 3-MeO | $C_{10}H_{10}O_3$ | 178.063 | **6b** | $C_{10}H_{13}NO_3$ | 195.090 |
| **5c** | 4-MeO | $C_{10}H_{10}O_3$ | 178.063 | **6c** | $C_{10}H_{13}NO_3$ | 195.090 |
| **5d** | 3-MeO-4-F | $C_{10}H_9O_3F$ | 196.054 | **6d** | $C_{10}H_{12}NO_3F$ | 213.080 |
| **5e** | 3-MeO-4-Cl | $C_{10}H_9O_3Cl$ | 212.024 | **6e** | $C_{10}H_{12}NO_3Cl$ | 229.051 |
| **5f** | 3-F-4-MeO | $C_{10}H_9O_3F$ | 196.054 | **6f** | $C_{10}H_{12}NO_3F$ | 213.080 |
| **5g** | 3-Cl-4-MeO | $C_{10}H_9O_3Cl$ | 212.024 | **6g** | $C_{10}H_{12}NO_3Cl$ | 229.051 |
| **5h** | 2-Et | $C_{11}H_{12}O_2$ | 176.084 | **6h** | $C_{11}H_{15}NO_2$ | 193.110 |
| **5i** | 3-Et | $C_{11}H_{12}O_2$ | 176.084 | **6i** | $C_{11}H_{15}NO_2$ | 193.110 |
| **5j** | 4-Et | $C_{11}H_{12}O_2$ | 176.084 | **6j** | $C_{11}H_{15}NO_2$ | 193.110 |
| **5k** | 2,3-($OCH_2O$) | $C_{10}H_8O_4$ | 192.042 | **6k** | $C_{10}H_{11}NO_4$ | 209.069 |
| **5l** | 3,4-($OCH_2O$) | $C_{10}H_8O_4$ | 192.042 | **6l** | $C_{10}H_{11}NO_4$ | 209.069 |
| **5m** | 2,3-$(MeO)_2$ | $C_{11}H_{12}O_4$ | 208.074 | **6m** | $C_{11}H_{15}NO_4$ | 225.100 |
| **5n** | 2,4-$(MeO)_2$ | $C_{11}H_{12}O_4$ | 208.074 | **6n** | $C_{11}H_{15}NO_4$ | 225.100 |
| **5o** | 3,4-$(MeO)_2$ | $C_{11}H_{12}O_4$ | 208.074 | **6o** | $C_{11}H_{15}NO_4$ | 225.100 |
| **5p** | 3,4-$(MeO)_2$-6-F | $C_{11}H_{11}O_4F$ | 226.064 | **6p** | $C_{11}H_{14}NO_4F$ | 243.091 |
| **5q** | 3,5-$(MeO)_2$ | $C_{11}H_{12}O_4$ | 208.074 | **6q** | $C_{11}H_{15}NO_4$ | 225.100 |
| **5r** | 2,4,6-$(MeO)_3$ | $C_{12}H_{14}O_5$ | 238.084 | **6r** | $C_{12}H_{17}NO_5$ | 255.111 |
| **5s** | 3,4,5-$(MeO)_3$ | $C_{12}H_{14}O_5$ | 238.084 | **6s** | $C_{12}H_{17}NO_5$ | 255.111 |
| **5t** | 2,3,4-$(MeO)_3$ | $C_{12}H_{14}O_5$ | 238.084 | **6t** | $C_{12}H_{17}NO_5$ | 255.111 |
| **5u** | 2,4,5-$(MeO)_3$ | $C_{12}H_{14}O_5$ | 238.084 | **6u** | $C_{12}H_{17}NO_5$ | 255.111 |

*Table 2.6: The conversions of a panel wild type ammonia lyases analysed by LC-MS. Not detected = n.d. Not tested = NT.*

| Subs. | EDG | RgPAL | AvPAL | PbPAL | DdPAL | RsTAL | AL-11 |
|---|---|---|---|---|---|---|---|
| **5a** | 2-MeO | 15 | 2 | 27 | 10 | <1 | 68 |
| **5b** | 3-MeO | 35 | 21 | 92 | 45 | 59 | 61 |
| **5c** | 4-MeO | <1 | <1 | 8 | <1 | 2 | 5 |
| **5d** | 3-MeO-4-F | 19 | 3 | 79 | 53 | n.d. | 91 |
| **5e** | 3-MeO-4-Cl | 5 | 13 | 91 | 80 | 2 | 59 |
| **5f** | 3-F-4-MeO | <1 | <1 | 40 | <1 | 22 | 81 |
| **5g** | 3-Cl-4-MeO | 2 | 2 | 38 | 2 | 26 | 87 |
| **5h** | 2-Et | 84 | 18 | 48 | 28 | n.d. | 91 |
| **5i** | 3-Et | 78 | <1 | 30 | <1 | 8 | 76 |
| **5j** | 4-Et | <1 | <1 | 48 | <1 | 3 | 5 |
| **5k** | 2,3-($OCH_2O$) | 96 | 87 | 92 | 90 | n.d. | 98 |
| **5l** | 3,4-($OCH_2O$) | <1 | <1 | 3 | <1 | 2 | 11 |
| **5m** | 2,3-$(MeO)_2$ | <1 | <1 | <1 | <1 | 14 | 5 |
| **5n** | 2,4-$(MeO)_2$ | <1 | <1 | <1 | <1 | <1 | <1 |
| **5o** | 3,4-$(MeO)_2$ | <1 | <1 | <1 | <1 | <1 | 92 |
| **5p** | 3,4-$(MeO)_2$-6-F | <1 | <1 | <1 | <1 | 6 | 96 |
| **5q** | 3,5-$(MeO)_2$ | <1 | <1 | <1 | <1 | 26 | 98 |
| **5r** | 2,4,6-$(MeO)_3$ | <1 | <1 | <1 | <1 | <1 | <1 |
| **5s** | 3,4,5-$(MeO)_3$ | <1 | <1 | <1 | <1 | n.d. | 97 |
| **5t** | 2,3,4-$(MeO)_3$ | NT | NT | NT | NT | <1 | 4 |
| **5u** | 2,4,5-$(MeO)_3$ | NT | NT | NT | NT | <1 | 73 |

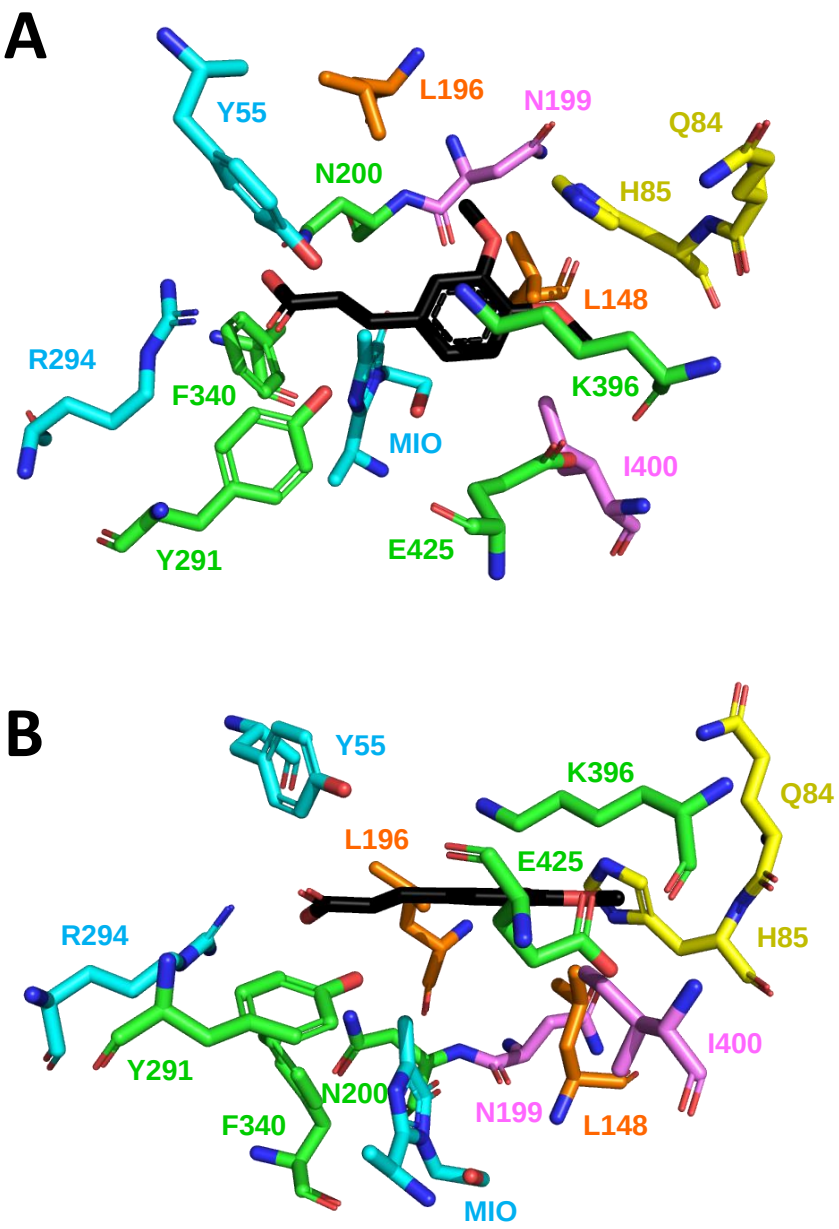


*Figure 2.16: Homology model of the active site of AL-11 enzyme with ligand* ***5o*** *docked. Mechanism-related residues are shown in cyan, selectivity residues are shown in yellow, library A residues in orange, library B residues in pink, other residues in close contact in green, substrate in black. (A) Top view. (B) Side view.*

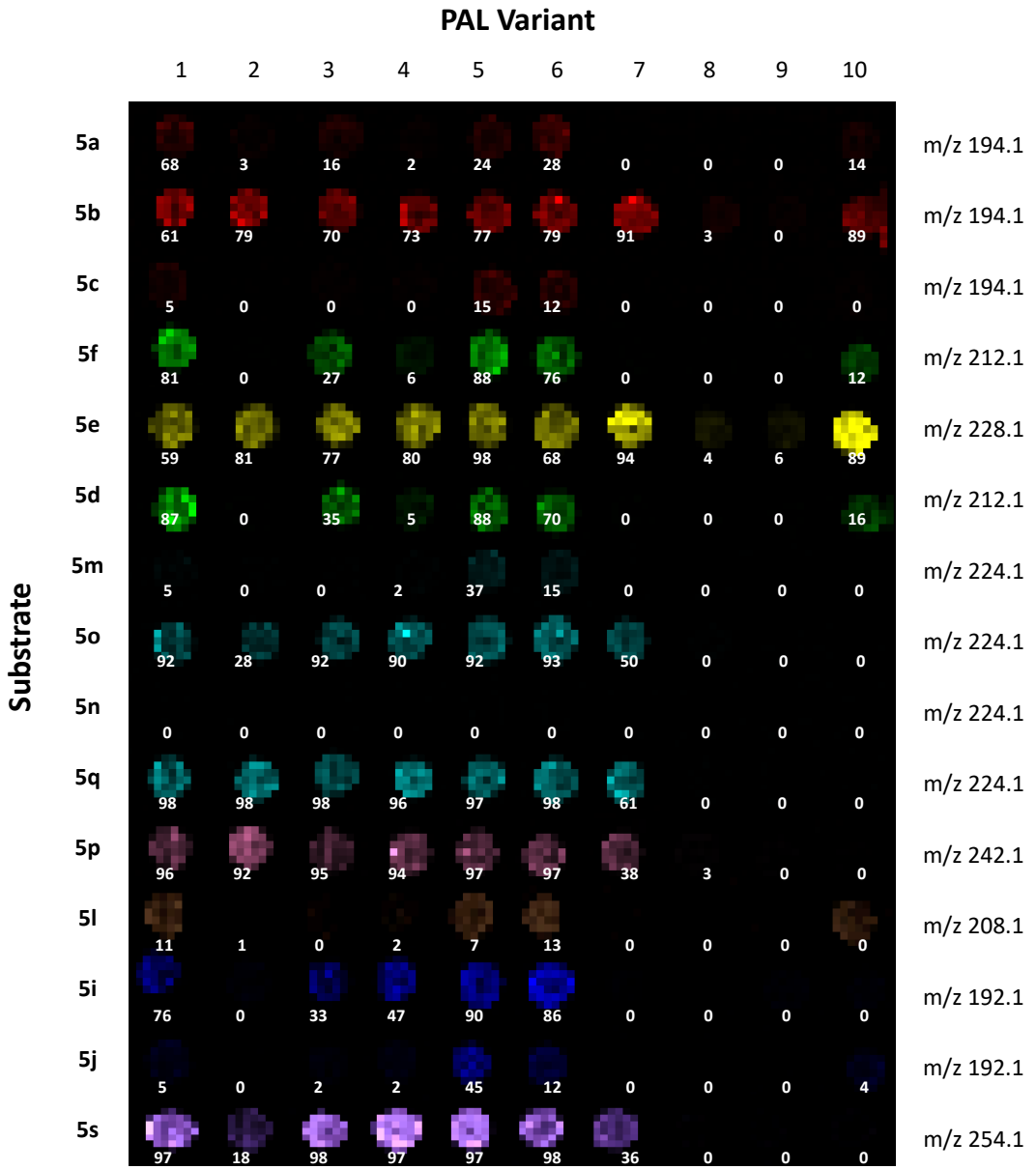


*Figure 2.17: DESI-MS heat map of screening results from PAL whole cell reactions (10 mutants x 15 substrates). The m/z heat maps for each product ion have been assigned differing colours and then collated to obtain a final image indicating locations of product yielding reactions. Reaction conversion data (%) obtained by HPLC-(UV) analysis or each reaction mixture has been overlain (white text) with each reaction location for comparison with DESI-MS results. DESI-MS pixel sizes were set to 500 µm x 500 µm and analysed using a stage speed of 1500 µm/s. This is equivalent to a throughout of 44 s/sample. Variants: 1 = wt (Q84-H85); 2 = Q84F, 3 = Q84H, 4 = Q84I; 5: Q84V; 6: Q84A; 7: Q84Y; 8: Q84Y-H85I; 9: Q84I-H85V; 10: Q84A-H85V.*

#### 2.9.4.1 Site-directed mutagenesis for generating AL-11 single and double mutant libraries

Site-directed mutagenesis libraries were introduced into the AL-11 gene cloned in the pET28b expression vector. Synthetic oligonucleotide primers were purchased from MWG Eurofins (Table 2.6) and designed to contain the desired mutations annealed to the plasmid DNA. Site directed mutagenesis procedure involved amplifying the template DNA using an inverse PCR technique with Q5® High-fidelity 2X DNA polymerase master mix from New England Biolabs (Ipswich, MA, USA). The following PCR protocol was used: 1 min denaturation at 98 °C and then 30 cycles of 30 s denaturation at 98 °C, 30 s annealing at 58 °C and 2 min 30 s elongation at 72 °C with a 5 min final extension time at 72 °C. The amplicons were treated with a Dpn1 digest for 1h at 37 °C and subsequently purified. The purified amplicons (180ng) were placed in a one-pot phosphorylation and ligation reaction mixture with T4 polynucleotide kinase (10 U) and T4 ligase (20 U) in the presence of ligase buffer containing ATP and left to incubate at room temperature for 1h. The variants were transformed in *E. coli* DH5$\alpha$ cells and plated onto kanamycin agar plates (50 μg/mL) and left to incubate overnight at 37 °C. Colonies were picked and grown in LB media and the plasmids were subsequently isolated and sequenced to confirm desired mutations underlined. Libraries L148RBT/N196RBT and N199RBT/I400RBT were created using the quikchange protocol. Inverse PCR was used to create library L196RBT/N199RBT and was phosphorylated and ligated and transformed in DH5$\alpha$ cells as above.

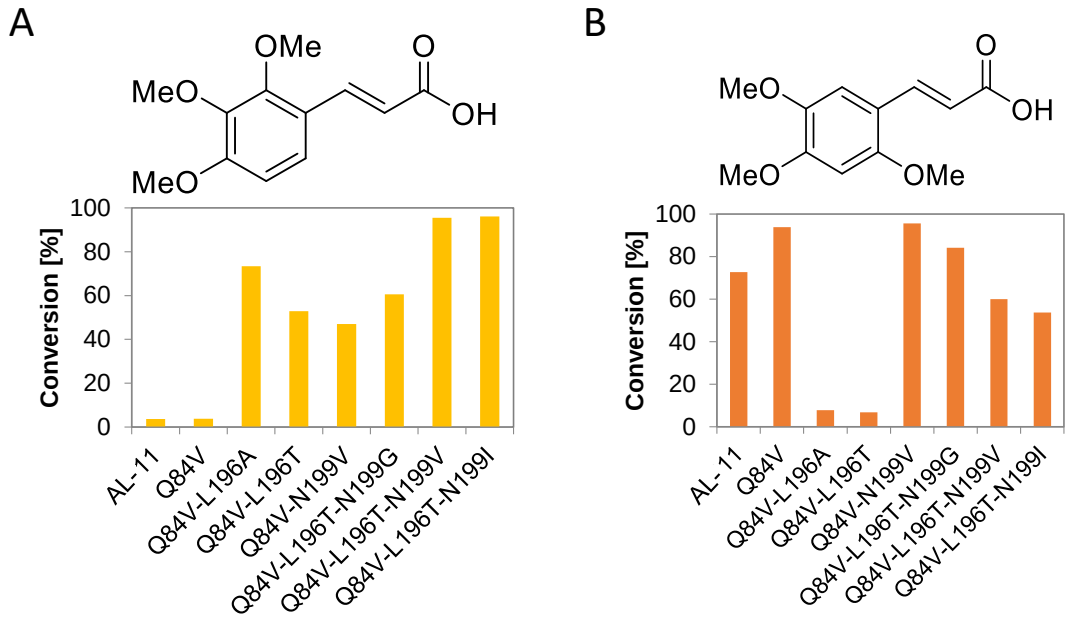


*Figure 2.18: Conversion values (LC-MS) of additional analytical scale hydroamination reactions with AL-11 and newly identified mutants with trisubsituted cinnamic acid substrates. A) Substrate 5t. B) Substrate 5u.*

### 2.9.5 Supporting Information References


[S1] T. Keenan, F. Parmeggiani, J. Malassis, C. Q. Fontenelle, J.-B. Vendeville, W. Offen, P. Both, K. Huang, A. Marchesi, A. Heyam, C. Young, S. J. Charnock, G. J. Davies, B. Linclau, S. L. Flitsch and M. A. Fascione, *Cell Chem. Biol.*, 2020, **27**, 1199-1206.

[S2] G. A. Aleku, S. P. France, H. Man, J. Mangas-Sanchez, S. L. Montgomery, M. Sharma, F. Leipold, S. Hussain, G. Grogan and N. J. Turner, *Nat. Chem.*, 2017, **9**, 961–969.

# 3

# Coupling droplet microfluidics with mass spectrometry for ultra-high-throughput analysis of complex mixtures up to and above 30Hz

## 3.1 Declaration

This chapter has been reproduced from a published article which I wrote:

Emily E. Kempa, Clive A. Smith (CAS), Xin Li (XL), Bruno Bellina (BB), Keith Richardson (KR), Steven Pringle (SP), James L. Galman (JLG), Nicholas J. Turner (NJT) and Perdita E. Barran (PEB), "Coupling droplet microfluidics with mass spectrometry for ultra-high throughput analysis of complex mixtures up to and above 30Hz.", *Analytical Chemistry*, 2020, **92**, 18, 12605-12612.

For this first author publication, I performed the method development, chip fabrication and the majority of experimental procedures. CAS, XL, BB, KR and SP provided technical assistance. Biotransformations were performed by JG under the supervision of NJT. I drafted and edited the manuscript with edits provided by PEB. The article has been reproduced here in an unchanged format except for minor adjustments to incorporate the text and figures into this thesis. Additionally, the referencing style has been altered to be cohesive with the other chapters in this thesis.

# Coupling droplet microfluidics with mass spectrometry for ultra-high throughput analysis of complex mixtures up to and above 30Hz.

Emily E. Kempa,[†] Clive A. Smith,[‡] Xin Li,[‡] Bruno Bellina,[†] Keith Richardson,[¶] Steven Pringle,[¶] James L. Galman,[§] Nicholas J. Turner[§] and Perdita E. Barran.[†]

[†] Michael Barber Centre for Collaborative Mass Spectrometry, Manchester Institute of Biotechnology, Manchester, M1 7DN, UK

[‡] Sphere Fluidics Limited, McClintock Building, Suite 7, Granta Park, Great Abington, Cambridge, CB21 6GP, UK

[¶] Waters Corporation, Stamford Avenue, Altrincham Road, Wilmslow, SK9 4AX, UK

[§] Manchester Institute of Biotechnology, Manchester, M1 7DN, UK

Publication Date (Web): 30th July 2020

https://doi.org/10.1021/acs.analchem.0c02632

## 3.2 Abstract

High and ultra-high throughput label-free sample analysis is required by many applications, extending from environmental monitoring to drug discovery and industrial biotechnology. HTS methods predominantly are based on a targeted workflow, which can limit their scope. Mass spectrometry readily provides chemical identity and abundance for complex mixtures and here, we use microdroplet generation microfluidics to supply picolitre aliquots for analysis at rates up to and including 33 Hz. This is demonstrated for small molecules, peptides and proteins up to 66 kDa on three commercially available mass spectrometers from salty solutions to mimic cellular environments. Designs for chip-based interfaces that permit this coupling are presented and the merits and challenges of these interfaces are discussed. On an Orbitrap platform droplet infusion rates of 6 Hz are used for the analysis of cytochrome c, on a DTIMS Q-TOF similar rates were obtained and on a TWIMS Q-TOF utilizing IM-MS software rates up to 33 Hz are demonstrated. The potential of this approach is demonstrated with proof of concept experiments on crude mixtures including egg white, unpurified recombinant protein and a biotransformation supernatant.

## 3.3 Introduction

High throughput screening (HTS) and ultra-high throughput screening (uHTS) methodologies aim to analyse tens to hundreds of thousands of samples per day. [1–5] In both industry and academia, the use of micro-titer plate formats has become ubiquitous for sample handling and HTS. This format is used across many different analytical platforms such as fluorescent readers [6] and liquid chromatography injection systems. [7,8] Label-free detection strategies are often coupled to microtiter plates *via* robotics and measure intrinsic physical properties of the sample in contrast to as those based upon ligated chromophores (fluorescent or colour metric) or radioisotopes. [9,10] Workflows which fulfil both 'label-free' and high throughput prerequisites are highly sought after by coupling the highest throughput analytical instrumentation currently available with robotics.

In recent years developments in microfluidics have shown that it is possible to reproducibly manipulate volumes of liquids within channels measuring less than 1 mm in diameter. [11–13] Droplet microfluidics, in particular, involves the transport and study of compartmentalised 'bursts' of analyte formed by the transport of two immiscible phases, with droplet generation often occurring 'on-chip'. [14–18] Microfluidic devices, or chips, are often fabricated from glass, polymers or silicon, [15,19] with in-built channels that facilitate the movement of droplets through the device towards the analytical technique in operation. Previously, droplet microfluidic chips have been successfully coupled to a wide range of analytical instrumentation, including fluorescence [20] and optical detection, [21] mass spectrometry, [22,23] Raman spectroscopy [24] and NMR, [25] with each droplet considered as an individual sample or reaction vessel. Combining these techniques with microfluidics supplied analyte at speeds up to 10 000 droplets per second [26] would facilitate high throughput screening in an alternative arrangement to microtiter plate formats.

Mass spectrometry (MS) is a highly sensitive, analytical technique widely employed to qualitatively and quantitatively probe the composition of a sample. Acquisition speed is analyser dependent and this is determined by physics, electronics, software and manufacturer, to some extent by the operator, the mass and charge upon ions in question, and the mass resolution required. The coupling of automated sample introduction with mass spectrometry is not new, [27,28] although as higher throughput analysis is required analysers and acquisition modes have become faster and faster. Time of flight (TOF) mass spectrometers inherently have the highest acquisition speeds, without compromising resolution [29] and are most obviously suited to HTS applications.

Coupling of HTS microfluidics to mass spectrometers is commonly achieved through the incorporation of a liquid outlet similar to that of an electrospray (ESI) or nano-electrospray (nESI) emitter into a chip, allowing for direct infusion of the analytes into the ion source. [30–32] Droplet microfluidics directly coupled with MS has been hindered by the need to extract or divert the analyte-containing phase (commonly aqueous) from the separative phase (commonly hydrophobic) prior to

MS infusion. [33–35] Separative phases can contaminate MS instrumentation, and dual-phase fluidics can lead to Taylor cone instability and inadequate electrospray ionisation. A number of reports in which a dual-phase system has exploited the alternating aqueous and oil phases exiting the microfluidic device for droplet detection have been highlighted. Smith et al., [23] Wink et al. [22] and Steyer et al. [36] all directly infuse both oil and aqueous streams directly into MS instrumentation through varying different emitter types and display MS detection of individual droplets. Recently, high throughput micro-droplet infusion with MS detection for HTS, with a throughput of up to 10 Hz has been reported by Steyer et al. in 2019; we note that this was implemented in selected ion monitoring mode [36], with commensurate sensitivity gains, compared with measuring a full mass spectrum.

The majority of literature entries only report the adaption of microdroplet microfluidics with one ESI MS platform; however, here we illustrate flexibility through chip-MS coupling to instruments from three different vendors. We demonstrate how MS droplet screening can be extended to rates over 30 microdroplets per second using fast scanning acquisition IM-Q-TOF instrumentation. We envision such a platform could be utilised in biotechnology to detect reaction products along with the modified enzyme. This would have particular relevance to directed evolution studies if mass spectrometry could directly inform on the nature of successful mutation(s) in the evolved enzyme, and prevent a subsequent PCR step.

## 3.4 Methods and Materials

All standards (L-Tyrosine, leucine enkephalin, bovine ubiquitin, equine cytochrome c, and bovine serum albumin (BSA)) were purchased along with ammonium acetate from Sigma Aldrich (Dorset, UK). Leucine enkephalin was dissolved in deionised water (obtained from a Milli-Q Advantage ultrapure water filtration system, Merck Millipore, Darmstadt, Germany) containing 0.1% Formic acid (Fisher Scientific, Loughborough, UK) to produce a ~1.3 mM solution of the peptide. Other standard materials (proteins and small molecules) were dissolved in a solution of 100 mM ammonium acetate in deionised water to produce ~100 μM solutions of each standard respectively (unless stated otherwise). Preparation of egg

white solution required separation of egg white from the yolk prior to dilution in 1 M ammonium acetate solution (1:5 v/v) before vortexing for ~30 seconds. [37] Whole cell biotransformations were performed upon addition of a substituted cinnamic acid species (5 mM) to the Phenylalanine Ammonium Lysate (PAL) cell paste suspended within a 4 M solution of ammonium carbonate and incubated at 30 °C, 250 rpm for 24 hrs. For analysis, the resulting solution was centrifuged (5 min, 13 000 rpm) to remove insoluble cellular material and the supernatant diluted to 800 mM ammonium carbonate with 100 mM ammonium acetate solution. In every case, the separative oil phase consisted of Pico-Surf™ 1 (Sphere Fluidics Ltd., Cambridge, UK) diluted to 1% in Novec™ 7500 Engineered Fluid (3M, Maplewood, MN, USA).

## 3.5 Chip Design and Fabrication

All microfluidic chips used in this work were fabricated from polydimethylsiloxane (PDMS, Dow Chemical Company, MI, USA) using established photolithography and soft lithography techniques as described in the literature. [13,38] A detailed procedure can be found in the supporting information to this paper. Stainless steel capillaries (Vita Needle Company, Needham, MA, US) of varying lengths with an internal diameter of 76 μm were incorporated into the fluidic outlet channel of the final PDMS devices and secured using ELASTOSIL E43 silicon sealant (Wacker Chemie AG, München, Germany) as described by Wink et. al. [22]

## 3.6 Coupling to ESI sources and establishing droplet flow

Infusion to each mass spectrometer was achieved through the coupling of a designed chip to the respective vendor's nESI source (Figure 3.1). Exact coupling methods differ as described and all experiments were undertaken in positive ionisation mode. The oil and aqueous connections required to generate droplets with the microfluidic chip consisted of 1.09 mm outer diameter tubing (0.38 mm ID, Smiths Medical Inc., Minneapolis, MI, USA) between the punched chip inlets and the syringe pump (neMESYS low-pressure syringe pump, CETONI GmbH, Korbußen, Germany) in each case. As droplets are generated with a diameter larger than that of the internal diameter of the stainless steel emitter, droplets and the segmented oil phase reach the outlet of the emitter as 'plugs' of that phase, and as such do not lose their inter-droplet

spacing as they enter the mass spectrometer. Prior to infusion into the mass spectrometer, the frequency of the generated droplets and their diameter were determined *via* optical analysis. This was achieved through the use of the Picodroplet Single Cell Encapsulation System instrumentation (Sphere Fluidics Ltd., Cambridge, UK). Observed frequencies are dependent on the device dimensions and the flow rates utilised during infusion, and consistency of droplet frequency for a given flow rate can be used to validate the manufacturing process. Chip designs of varying channel dimensions were used in this study to generate droplets at differing frequencies and dimensions. Note that the chips used are interchangeable between instruments with the design chosen in each case due to device availability only.

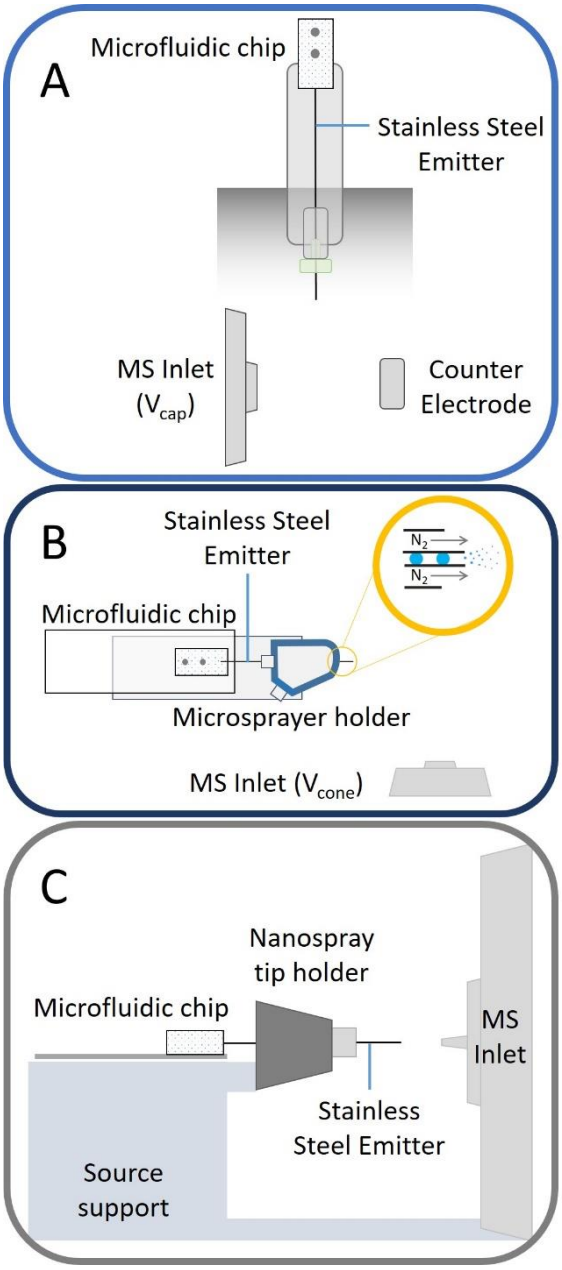


*Figure 3.1: A) Schematic (side view) of the adaptation of a vertically mounted Agilent Nanospray ESI source to incorporate a microfluidic chip. The emitter is grounded and held ~ 0.3 cm from a counter electrode held at ~1.75 kV. The entire assembly is enclosed from the lab. B) Schematic representation (top view) of the microfluidic chip interfaced to a Waters z-spray source by adapting a micro-spray assembly (source support not shown). A close up (yellow ringed inset) indicates coaxial gas flow around the stainless steel emitter. The emitter is held at ~2.8 kV and positioned 0.5 cm from the conical counter electrode which is the entrance to the mass spectrometer held at Vcone (~54V). C) Schematic (side view) of the droplet microfluidic chip interfaced with the Thermo Fisher Q Exactive nESI source, in which the stainless steel emitter is inserted in the place of the nanospray tip and held in place with a conductive screw. The distance between the emitter and the entrance to the MS is 0.5 cm. These schematics are not to scale. Photographic representations indicating scale and dimensions of the microfluidic chip within all 3 instrumental configurations can be found in the supporting information SI figures 3.8, 3.9 and 3.11.*

Infusion of the oil and aqueous phases allowed droplet generation with the droplet emulsion exiting the outlet of the stainless steel emitter able to be observed by eye. Upon application of the electrospray voltage fluid reaching the outlet of the emitter can be seen to enter the MS inlet in the form of an electrospray plume (see Figure 3.8 F for an example of this). As microdroplets enter the mass spectrometer individually, increases in the mass spectrometry signal are observed in the total ion and extracted ion chromatograms. If the instrumental acquisition speed is sufficient, each droplet is observed as a peak in the chromatogram, with peaks arising at the rate of droplet generation.

## 3.7 DTIMS Q-TOF Coupling

Interfacing the droplet microfluidic chip with an Agilent 6560 IM-Q-TOF (Agilent Technologies, Santa Clara, CA, USA) required incorporation of a stainless steel emitter of approximately 12 cm in length into the device. The chip was carefully removed from a supporting glass slide and the stainless steel emitter threaded through a metal union, conductive ferrule and a finger tight screw, before being placed in the nESI source probe as indicated in the photograph in Figure 3.8 B. The outer casing of the nESI probe was replaced and the probe inserted vertically into the source (Figure 3.1 A). The position of the stainless steel capillary emitter between the MS inlet and the counter electrode can be observed *via* the internal camera.

Figure 3.2 shows droplet infusion from a solution of leucine enkephalin occurring at ~ 5 Hz (optical analysis data not shown), with a commensurate frequency for mass spectrometry detection as determined by the total ion chromatogram (TIC Figure 3.2 A). Akin to chromatography, a mass spectrum can then be extracted for an individual droplet, Figure 3.2 B shows the mass spectrum of leucine enkephalin acquired from a single droplet. The Agilent Q-TOF acquisition range is restricted to ±50 mass units from the parent ion mass of intact leucine enkephalin (*m*/*z* 556.27), to facilitate enhanced sensitivity for targeted detection of the species of interest. To detect each droplet produced at 5 Hz, the Q-TOF scan speed was set to 35 scans/s in the acquisition software giving ~7 scans per droplet TIC. This scan rate is sufficient to delineate the analyte signal from each droplet and the maximum permitted scan

rate (50 scans/s) provides a little more resolution between droplets. For higher droplet infusion frequencies (10 Hz and above), the resolution is compromised, and a faster acquisition system would be needed to capture all of the mass spectrometry information from each droplet.

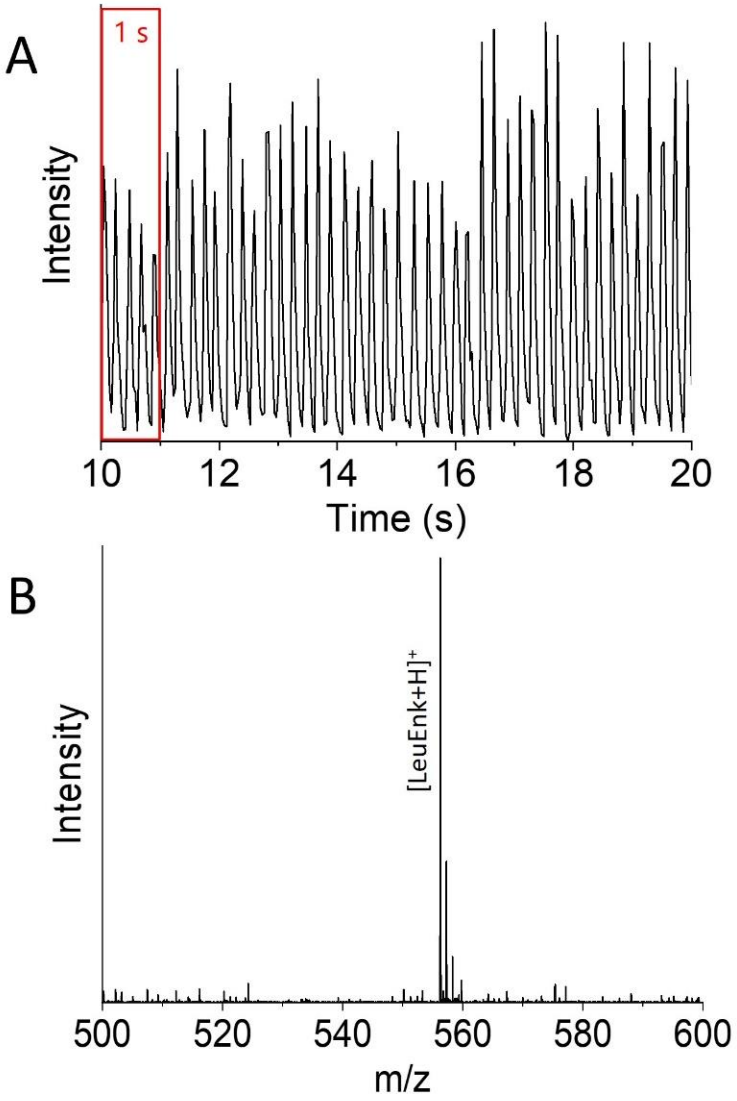


*Figure 3.2: Total Ion Chromatogram (TIC) acquired during infusion of droplets (~2.1 nL) containing leucine enkephalin (LeuEnk, ~1.3 mM solution) at an infusion rate of approximately 5 droplets per second (Hz). Each individual peak indicates one droplet reaching the Agilent 6560 IM-Q-TOF detector. Mass Spectrum (m/z range 500-600) acquired from one droplet containing LeuEnk, ([LeuEnk+H]+ = 556.27 Da).*

## 3.8 TWIMS Q-TOF Coupling

The microfluidic chip was mounted on a Waters nESI source with micro-sprayer for infusion into a Waters SYNAPT G2Si Q-TOF (Waters Corp., Milford, MA, USA) (Figure 3.1 B). Due to the dimensions of the micro-sprayer device, a shorter stainless steel emitter (approximately 6 cm) was incorporated into the droplet generation device, which also reduces the back pressure on the droplets. Upon insertion of the stainless steel emitter to the micro-sprayer assembly, the emitter was fastened in place by tightening the supporting screw, and the glass slide secured to the base of the micro-sprayer using Blu Tack (Figure 3.1 B). A ~ 1 mm protrusion of the stainless steel emitter from the micro-sprayer outlet was found to be optimal for stable electrospray.

Mounting of the micro-sprayer-chip construct on to the Waters nESI source XYZ stage (Figure 3.1 B and 3.9 B) allowed the emitter to be optimally positioned perpendicular to the source inlet cone. As droplets are generated and reach the end of the stainless steel emitter, the electrospray voltage (~2.8 kV) applied directly to the emitter allows for the generation of an electrospray plume. This is assisted by a coaxial flow of nitrogen (1.5 Bar) (Figure 3.1 B insert). As for data obtained from the Agilent 6560 IM-Q-TOF instrument (Figure 3.2 A), droplet peaks in the TIC are observed at a frequency close to that of droplet generation. A TIC obtained from this instrument is indicated in Figure 3.10 B, with droplet generation occurring at a rate of approximately 9 Hz. The acquisition speed utilised during this experiment was equal to 0.016 s, with an interscan delay of 0.010 s, corresponding to ~38 scans/s. This is the maximum permitted speed for MS data acquisition on this platform. Figure 3.10 C shows the extracted mass spectrum obtained from 1 of these droplet TICs, indicating that under these conditions, as for nESI from an equivalent concentration of aqueous ammonium acetate the major charge ions observed for this protein are $[M+6H]^{6+}$ and $[M+5H]^{5+}$. (Ubiquitin intact mass ~8.6 kDa).

### 3.8.1 Sensitivity analysis using TWIMS Q-TOF

Sample concentrations of the solutions analysed in Figures 3.2, 3.10 and 3.12 are all in excess of 100 μM. When expressing detection limits for such a dual-phase

system not only must the solution concentration be considered but also the droplet size. For example, the droplets infused at 9 Hz during the experiment described above had approximate volumes of 0.8 nL and an ubiquitin concentration of 100 μM (Figure 3.10) which equates to detection of ~700 pg of protein per droplet. Lowering the concentration to 5 μM corresponds to ~150 pg of protein per droplet (Figure 3.13), albeit the lower infusion rates and slightly differing chip dimensions give droplets 3.6 nL in volume. We envisage that detection limits for solutions below 5 μM are possible with both MS and microfluidic chip optimisation, but caution that absolute limits will be droplet size, instrument and analyte specific.

## 3.9 Orbitrap Coupling

Interfacing the microfluidic chip with the Thermo Fisher Scientific Q Exactive (Waltham, MA, USA) nESI source followed a similar approach to that for the Waters instrument above. The chip, mounted upon a glass slide, incorporated a ~6 cm stainless steel emitter, which was inserted through the rear of the nano-source tip holder and secured in place using a stainless steel nut, (Figure 3.1 C). The emitter position can be adjusted using the XYZ stage. In this arrangement, the electrospray voltage (~2.4 kV) is applied continuously to the chip emitter as droplets are being generated and subsequently infused.

A similar result to that of the previous instruments discussed is observed (e.g. Figure 3.2 A), with microdroplets appearing as discrete peaks in the EIC as they are infused (an example EIC from this instrumentation can be found in Figure 3.12 B). The irregularity in droplet frequency and intensity is attributed to a mismatch between the acquisition frequency and the droplet infusion rate, whereby the acquisition of data (comprising both AGC and trap fill time) occurs at intervals which do not exactly coincide with the presence of a droplet. In order to obtain the maximum scan rate of this instrument, a decrease in the instrumental resolution is required, whereupon an instrumental scan rate of 30.3 Hz is attainable. For microdroplet infusion in the range of 6 Hz (as seen in Figure 3.12 B) such an acquisition rate is achievable, however, the lack of resolving power means that for massive ions, the isotopic resolution is lost. This is demonstrated here for the ~12.2

kDa protein cytochrome c (inset, Figure 3.12 C). This is a feature of FT-MS and if isotopic resolution is required, coupling orbitrap instruments in their current inceptions to such high throughput sample delivery will be limited to small molecule and more targeted detection.

## 3.10 Expansion of Sample Scope

Our goal is to infuse microdroplets that contain crude reaction mixtures, and use HTS to monitor biocatalytic processes both at the product and modified enzyme level. To work towards this we chose to examine dilute egg white (Figure 3.3). As with purified samples, a total ion chromatogram is obtained with each peak arising corresponding to the infusion of 1 droplet (Figure 3.3 A). Ovalbumin, a major protein (~44 kDa) found within egg white is clearly present in the corresponding mass spectra (Figure 3.3 B) which also has the form of a natively folded protein, possessing a narrow charge state distribution. A similar TIC is observed when infusing a crude lysate of a recombinant nanobody (Figure 3.16) and also the 66 kDa protein BSA (Bovine serum albumin, Figure 3.15) infused from a native MS solution.

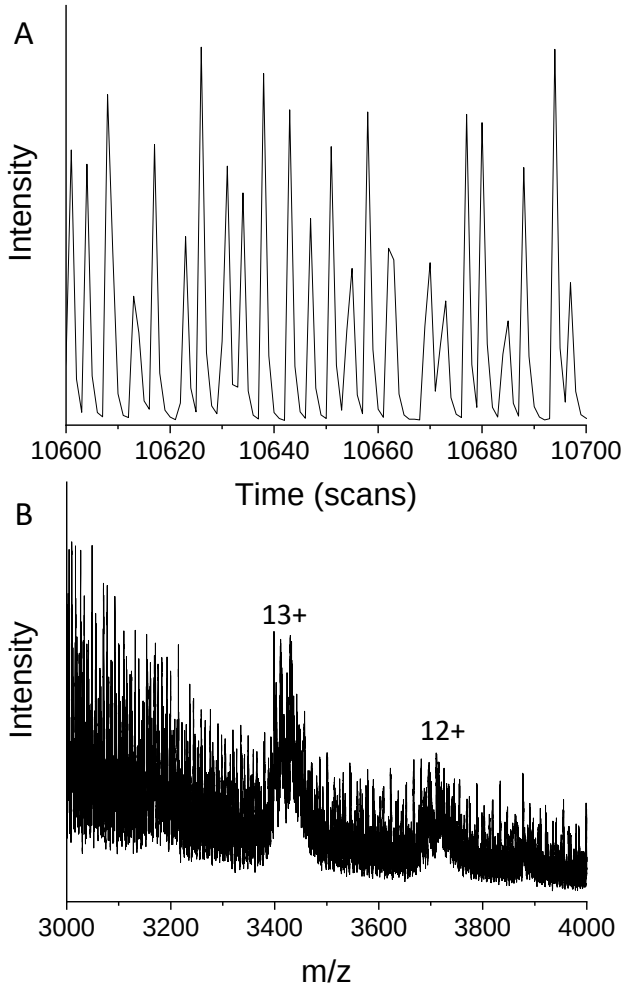


*Figure 3.3: Data for the infusion of droplets containing egg white in aqueous ammonium acetate solution (1 M) obtained using TWIMS Q-TOF instrumentation. A) Total ion chromatogram of infused egg white droplets, 100 scans equivalent to ~ 2.6 s are shown (MS total cycle time = 0.026 s/scan). B) Mass spectrum (unmodified) obtained for the infusion of egg white droplets upon combining ~8 minutes of acquisition. Ovalbumin protein (44 kDa) from egg white has been identified in the spectrum with the major charge states of ovalbumin monomer (12+ and 13+) indicated.*

Detection of small molecules within a biotransformation supernatant at 800 mM ammonium carbonate is demonstrated in Figure 3.4. A TIC trace and EIC traces for both the reaction starting material and product (Figure 3.4 A) are obtained following the infusion of the reaction mixture, with 1 droplet MS data obtainable (Figure 3.4 B). It is noted that the TIC traces obtained for these high-salt solutions (Figures 3.3 and 3.4) can differ from those for standard solutions (Figure 3.2, 3.10, 3.12, and 3.14) by way of their peak-to-peak (i.e. droplet-to-droplet) repeatability. The

crude mixtures show more variation in droplet peak area, and the frequency of the incoming droplets is not as consistent as its standard solution counterparts. We anticipate these differences are attributable to the higher viscosities of these solutions, thus altering the generation frequency of droplets within the chip at the flow-focusing junction. Additionally, the increased salt concentrations are a likely cause of electrospray instabilities at the emitter outlet in droplet mode (although this is not seen in direct infusion). Despite this, full mass spectra are obtained from single droplets and the broad scope of such assignments demonstrates the platforms label-free capabilities.

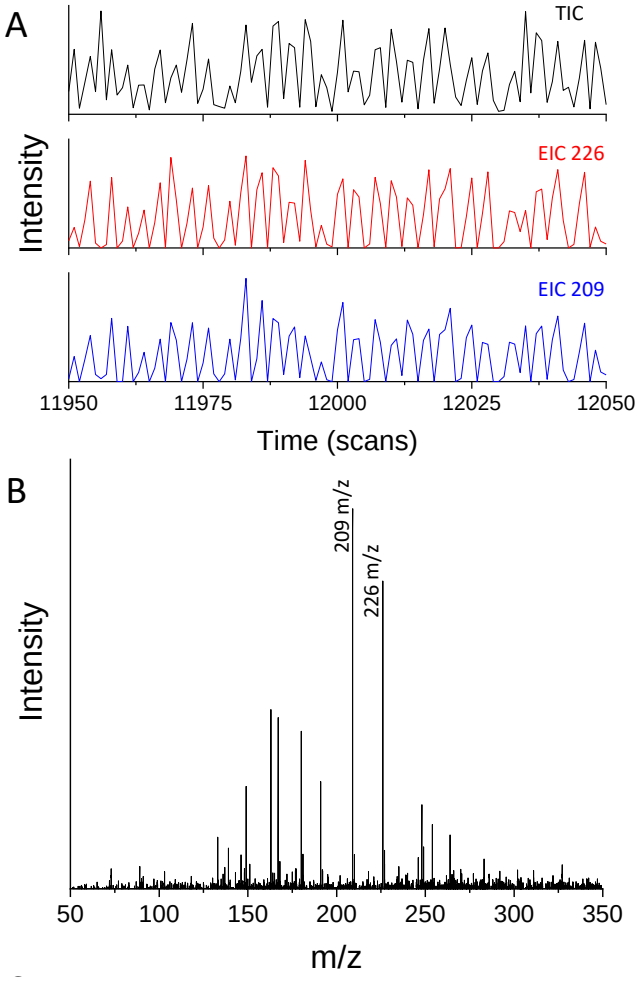


*Figure 3.4: Data for the infusion of droplets containing Phenylalanine Ammonium Lyase (PAL) biotransformation supernatant in aqueous ammonium acetate solution (100 mM) obtained using TWIMS Q-TOF instrumentation. A) Total and extracted on chromatograms obtained from infused supernatant droplets. 100 scans equivalent to ~ 2.6 s are shown (MS total cycle time = 0.026 s/scan). B) Mass spectrum obtained from 1 supernatant droplet indicating detection of the biotransformation starting material (m/z 209) and product (m/z 226).*

All experimental work described here exploits detection of a full *m*/*z* scan range opposed to a selected ion approach taken by Steyer et al. [36] Utilisation of a full scan also prevails over alternative detection methodologies such as fluorescence due to its ability to detect and distinguish multiple analytes simultaneously. Selected ion mode of course has a role to play and here we have shown that we can *m*/*z* select individual charge states of protein ions, which would be the first step toward a top down sequencing strategy to identify mutations in a given enzyme (Figure 3.18).

## 3.11 Fast Scanning Acquisition – TWIMS Q-TOF

To increase the throughput achieved upon the Waters SYNAPT G2Si instrument, a faster scanning acquisition mode was implemented as a variant of the SONAR acquisition mode developed by Waters for rapid data-independent acquisition. [39] In this mode, the instrument is essentially operating in a standard MS mode, but additional spectra are accumulated using the SYNAPT's ion mobility acquisition architecture. In this way, one acquisition cycle comprises 200 sequentially acquired 'spectral bins' obtained in the same time as one original MS scan. This allows a potential increase from ~38.5 spectra/s to 7,700 spectra/s, however, for the purpose of these 'proof of concept' experiments, the acquisition cycle time was fixed at 1 s therefore; the acquisition rate was equivalent to 200 spectra/s, representing an approximately five-fold increase in sampling points.

The interface utilised between chip and mass spectrometer was akin to that presented in Figure 3.1 B, with identical channel dimensions employed. Initially, the microdroplet infusion rate generated from a solution of ubiquitin (~60 μM) reached 11 Hz prior to the activation of the fast scanning acquisition mode to confirm droplet detection at the upmost Q-TOF scan rate, with detection at this rate observed in Figure 3.5 A. However, the limited number of points gathered per droplet peak results in trilateral peak shapes and does not allow for a further increase in droplet infusion. Activating the fast scanning acquisition and applying a scan time of 1 s, allows droplets to be visualised in the drift time real-time display (not shown) as individual peaks similar to that seen within the total ion chromatogram. This real-time display also allowed for further tuning of the instrumentation to improve the

stability of infusion and droplet peak shape. Direct visualisation of the data acquired in this mode was possible *via* DriftScope (version 2.8, Waters Corp., Milford, MA, USA). However, for convenience and compatibility with existing software, a script was written and used to unpack the mobility file structure into a continuous 'chromatogram-like' output prior to data analysis (Figure 3.5 B and C). This total ion chromatogram can be extracted to obtain a mass spectrum for each individual droplet with MassLynx (version 4.2, SCN893, Waters Corp., Milford, MA, USA). Comparing Figure 3.5 A with 3.5 B, each chromatogram has been obtained with a droplet infusion frequency of ~11 Hz, and Figure 3.5 B has an increased number of mass spectra across each peak. Droplet peaks are therefore sampled at a higher frequency more accurately representing the underlying peak shape. Increasing the acquisition frequency (i.e. scan rate) allows for a further increase in droplet infusion rate. This is illustrated in Figure 3.5 C where now the rate is increased to 33 Hz. Further increases in throughput may be possible through the optimisation of device design, specifically, the channel and stainless steel emitter dimensions. The microdroplet throughput reported here demonstrates a greater than 10-fold improvement on the detected infusion rate reported by Smith et al. in 2013 for microdroplet reinjection (2.6 Hz). [24] Operation at an infusion rate of 33 Hz would facilitate the analysis of over 2.8 million samples in one 24-hour period. Label-free MS sample throughputs at these speeds would revolutionise screening approaches in areas which rely on indirect measurements or those which require additional labelling procedures due to the MS ability to distinguish compounds by molecular weight. More specifically, applications within synthetic biology and biotechnology have the potential to benefit most from the fusion of high throughput droplet microfluidics with MS; screening for both improved genetic variations and reaction conditions often require considerable time and resources. In addition, the high flexibility of microfluidic chip design and the ability to encapsulate cells within droplets also complements the evaluation and miniaturisation of synthetic biology assays.

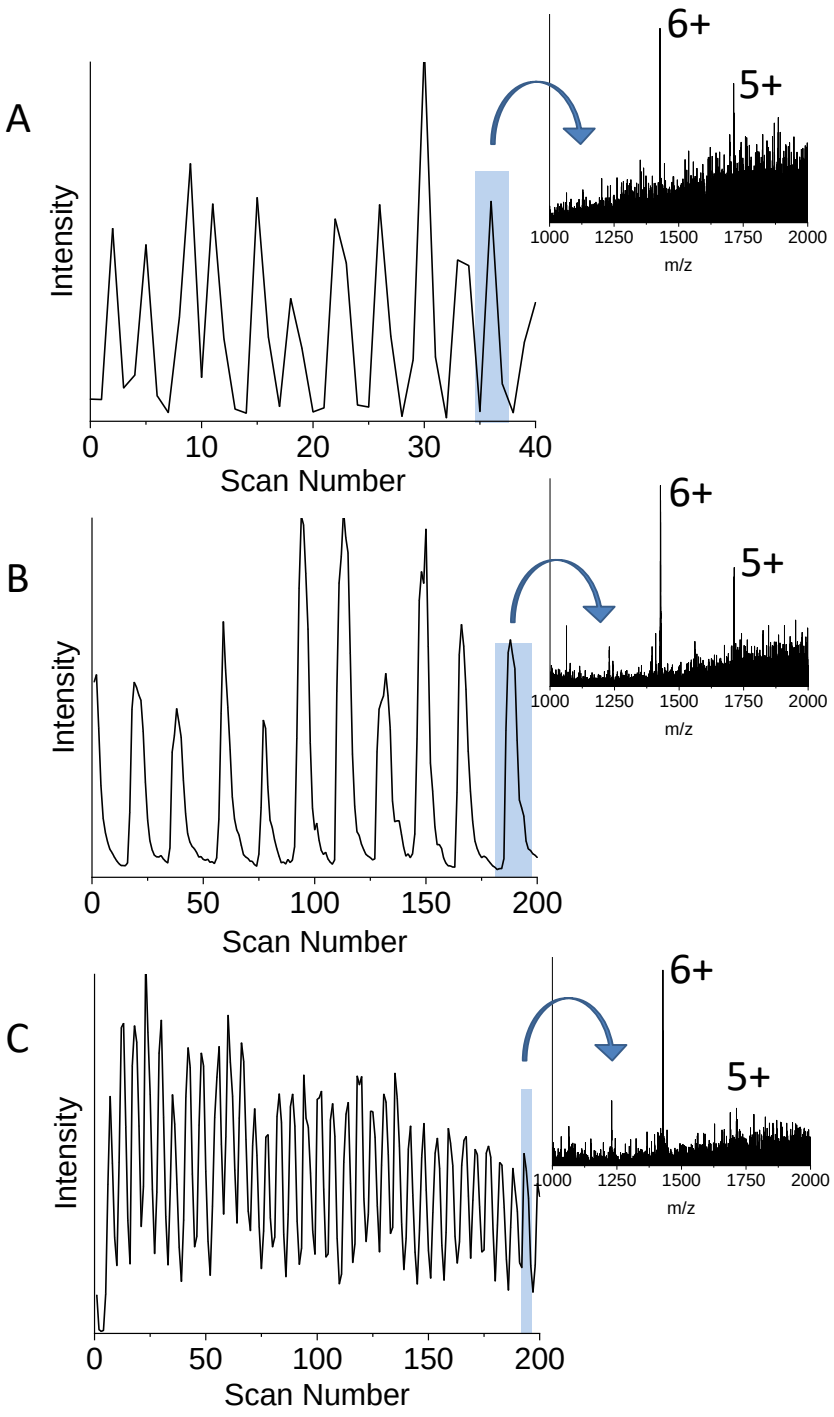


*Figure 3.5: Data acquired using droplets of 60 μM ubiquitin and different acquisition modes on the SYNAPT at varying microdroplet infusion rates. Each mode is accompanied by a mass spectrum extracted from one droplet. A) TIC obtained from a microdroplet infusion rate of 11 Hz acquired in standard MS mode with a scan time of 0.016 s, (1s, ~40 scans shown). B) TIC obtained at the same infusion rate but acquired using the fast-scanning acquisition mode (1 s, 200 scans shown). C) TIC obtained using the fast-scanning mode, but at an increased infusion rate of 33 Hz (1 s, 200 scans shown).*

## 3.12 Instrument Comparison

Each instrument platform has advantages and disadvantages in terms of the ease with which the chip-based inlet can be incorporated into the mass spectrometer (Table 3.1). We found that the Waters nESI source readily coupled to our chip-based inlet. The emitter can be simply inserted through the micro-sprayer, with the bulk of the chip remaining on the XYZ stage platform, allowing for both easy access to the fluidic inlets and convenient alteration of the XYZ stage location. The Thermo nESI source utilises a similar facile insertion of the emitter however, there is no extended platform for the device to be mounted upon. A temporary support was installed (Figure 3.11) to address this issue, a more robust solution would allow xyz adjustment. The most cumbersome of the three arrangements, during both assembly and use, was the Agilent Nanospray source due to the encapsulation of the chip and emitter inside the nESI probe. Insertion of the probe into the source region without due care risked emitter damage and positioning it in an optimal location between the source inlet and the counter electrode was non-trivial due to the nature of the stage controls. Future modifications would seek to locate the infusion pumps proximal to a modified probe to optimise access to the fluidic connections.

*Table 3.1: Table summarising the user accessible MS acquisition scan speeds, advantages and disadvantages of the three instrumental configurations assessed in this article when coupled with droplet microfluidics. * User accessible MS acquisition scan speed, droplet frequency and size detected when SONAR technology is employed. ‡ The droplet sizes and frequencies stated correspond to the conditions described in this article.*

| **Instrument Type** | **DTIMS Q-TOF** | **TWIMS Q-TOF** | **Orbitrap (FT-MS)** |
|---|---|---|---|
| Instrument model | Agilent 6560 IM-Q-TOF | Waters SYNAPT G2Si | Thermo Fisher Q Exactive |
| Fastest scan speed | 50 scans/s | 38 scans/s, 7700 scans/s* | 30 scans/s |
| Coupling ease | Difficult | Easy | Easy |
| Advantages | Grounded emitter<br>Fastest user accessible scan/s | Easy coupling<br>SONAR technology addition | Easy coupling |
| Disadvantages | Stage controls not intuitive<br>Interscan delay not variable<br>Mounted chip not visible during usage | Voltage applied to emitter<br>Interscan delay<br>ESI source accessibility | Voltage applied to emitter<br>Interscan delay not visible<br>Isotopic resolution lost when increasing scan speed |
| Droplet frequency detected ‡ | 5 Hz | 11 Hz, 33 Hz* | 6 Hz |
| Droplet Size ‡ | 2.1 nL | 0.8 nL, 1.4 nL* | 0.8 nL |

Despite the challenges involved in mounting a chip-based inlet into the Agilent source, the ESI configuration wherein the capillary/emitter is grounded wrt a source held at lower potential was advantageous to droplet stability. The droplets remained intact and were not prone to coalescence. Application of a positive potential to the emitter, as implemented in the Waters SYNAPT and Thermo Scientific Q Exactive ESI sources, is acceptable for microdroplet generation, however, we had greater difficulties in a droplet reinjection workflow (such as that described by Smith et al). [23] Application of a voltage to a pre-generated solution of droplets was found to cause coalescence of the collected droplets.

When considering high-speed acquisition, the Agilent 6560 has the highest user accessible rate for data collection (50 scans/s); the Waters SYNAPT is similar (~38 scans/s). The requirement to include some form of delay in which data is not recorded, between each acquisition block may cause droplet information to be missed when infusing at such high rates. The Q Exactive FT-MS offers the lowest acquisition speed of the three instruments, and a decrease in mass resolution accompanies operation at the highest acquisition rate ~30 scans/s. This may curtail uHTS utilization on FT-MS instruments, although the Q Exactive performs well at infusion rates of 1 Hz or lower, which will be adequate for many applications. TOF instrumentation offers increased MS acquisition speeds with the potential to exploit the intrinsically high TOF pusher rate, governed by the acceleration voltage and the longest time of flight of a given ion. Currently, the restrictions on this acquisition rate are a consequence of a combination of hardware, system band-width and operating system speed, including manufacturers' software, and practical data file size constraints. Whilst collecting each TOF spectrum individually is conceptually possible without compromising mass resolving power, one must also consider the effect on the resulting in-spectra dynamic range.

## 3.13 Conclusions and Outlook

We have demonstrated the coupling of microdroplet microfluidics with mass spectrometry on three instruments platforms from different MS vendors. The microfluidic device with the incorporated emitter is readily interfaced with commercially available nESI sources without extensive modifications allowing for an infusion of microdroplets up to a rate of 9 Hz. Discrete droplets are easily visualised within the total and extracted ion chromatograms from which mass spectra for each individual droplet can be obtained. Upon assessment of the three instruments, we have found the Waters nESI source to be marginally the most accessible, due to the ease at which the device could be integrated into the micro-sprayer adaption, although all sources required some modification and more would be required for optimal permanent use. Application of the voltage directly to the ESI emitter is adequate for infusion but causes droplet coalescence when working with pre-defined droplets (i.e. droplet reinjection). We are currently working on further modifications to the chips and the sources to prevent this.

All three mass spectrometers utilised in this study were capable of detecting droplets infused at a rate of 5 Hz and above. The Agilent 6560 IM-Q-TOF harnesses the highest speed of 50 scans/s in its commercial configuration, however with additional fast scanning acquisition software available for Waters instruments, detection of increased droplet infusion and has been demonstrated here up to and over a rate of 30 Hz. We believe this can be improved upon further through alteration of the microfluidic channel dimensions and emitter specifications and envision infusion at a rate of 100 Hz achievable in the future. We have demonstrated the ability to infuse droplets of complex salty samples containing small molecules, peptides and proteins, since we aim to develop biotechnological application for uHTS, but we envisage a broader class of molecules and accompanying scientific challenges that could benefit from such rapid information rich analysis.

## 3.14 Acknowledgment

The authors would like to acknowledge the support of Waters Corporation (Manchester, UK) for use of their fast scanning acquisition software and Sphere Fluidics Ltd (Cambridge, UK) for their expertise in droplet microfluidic chip design and fabrication. We would also like to acknowledge the Centre for Mesoscience and Nanofabrication (Manchester, UK), for the use of their cleanroom facilities and equipment. In addition, we thank Francesco Bramonti and Aidan P. France for supplying the egg white sample. Funding for this work has been provided through a BBSRC DTP CASE studentship to EK (BB/M011208/1) and includes sponsorship from Sphere Fluidics Ltd. Additionally, we are grateful for funding from BBSRC for the SYNBIOCHEM Centre (BB/M017702/1) and EPSRC in awards EP/S005226/1, EP/T019328/1 which further support this work.

## 3.15 References


1 L. M. Mayr and D. Bojanic, *Curr. Opin. Pharmacol.*, 2009, **9**, 580–588.

2 J. Inglese, R. L. Johnson, A. Simeonov, M. Xia, W. Zheng, C. P. Austin and D. S. Auld, *Nat. Chem. Biol.*, 2007, **3**, 466–479.

3 P. Szymański, M. Markowicz and E. Mikiciuk-Olasik, *Int. J. Mol. Sci.*, 2012, **13**, 427–452.

4 M. de Raad, C. R. Fischer and T. R. Northen, *Curr. Opin. Chem. Biol.*, 2016, **30**, 7–13.

5 R. P. Hertzberg and A. J. Pope, *Curr. Opin. Chem. Biol.*, 2000, **4**, 445–451.

6 P. Hodder, R. Mull, J. Cassaday, K. Berry and B. Strulovici, *J. Biomol. Screen.*, 2004, **9**, 417–426.

7 M. Yadav, P. Contractor, V. Upadhyay, A. Gupta, S. Guttikar, P. Singhal, S. Goswami and P. S. Shrivastav, *J. Chromatogr. B*, 2008, **872**, 167–171.

8 S. X. Peng, T. M. Branch and S. L. King, *Anal. Chem.*, 2001, **73**, 708–714.

9 U. Bilitewski, *Anal. Chim. Acta*, 2006, **568**, 232–247.

10 A. Syahir, K. Usui, K. Tomizaki, K. Kajikawa and H. Mihara, *Microarrays*, 2015, **4**, 228–244.

11 G. M. Whitesides, *Nature*, 2006, **442**, 368–373.

12 H. A. Stone, A. D. Stroock and A. Ajdari, *Annu. Rev. Fluid Mech.*, 2004, **36**, 381–411.

13 J. C. McDonald and G. M. Whitesides, *Acc. Chem. Res.*, 2002, **35**, 491–499.

14 M. T. Guo, A. Rotem, J. A. Heyman and D. A. Weitz, *Lab Chip*, 2012, **12**, 2146–2155.

15 S. Y. Teh, R. Lin, L. H. Hung and A. P. Lee, *Lab Chip*, 2008, **8**, 198–220.

16 V. B. Varma, A. Ray, Z. M. Wang, Z. P. Wang and R. V. Ramanujan, *Sci. Rep.*, 2016, **6**, 1–12.

17 P.-Y. Colin, B. Kintses, F. Gielen, C. M. Miton, G. Fischer, M. F. Mohamed, M. Hyvönen, D. P. Morgavi, D. B. Janssen and F. Hollfelder, *Nat. Commun.*, 2015, **6**, 10008.

18 A. Zinchenko, S. R. A. Devenish, B. Kintses, P. Y. Colin, M. Fischlechner and F. Hollfelder, *Anal. Chem.*, 2014, **86**, 2526–2533.

19 R. Seemann, M. Brinkmann, T. Pfohl, B. Jin, Y. W. Kim, Y. Lee, T. P. Lagus and J. F. Edd, .

20 M. He, J. S. Edgar, G. D. M. Jeffries, R. M. Lorenz, J. P. Shelby and D. T. Chiu, *Anal. Chem.*, 2005, **77**, 1539–1544.

21 S. L. Anna, N. Bontoux and H. A. Stone, *Appl. Phys. Lett.*, 2003, **82**, 364–366.

22 K. Wink, L. Mahler, J. R. Beulig, S. K. Piendl, M. Roth and D. Belder, *Anal. Bioanal. Chem.*, 2018, **410**, 7679-7687.

23 C. A. Smith, X. Li, T. H. Mize, T. D. Sharpe, E. I. Graziani, C. Abell and W. T. S. Huck, *Anal. Chem.*, 2013, **85**, 3812–3816.

24 M. P. Cecchini, J. Hong, C. Lim, J. Choo, T. Albrecht, A. J. DeMello and J. B. Edel, *Anal. Chem.*, 2011, **83**, 3076–3081.

25 Y. Lin, S. Schiavo, J. Orjala, P. Vouros and R. Kautz, *Anal. Chem.*, 2008, **80**, 8045–8054.

26 V. R. Yelleswarapu, H.-H. Jeong, S. Yadavali and D. Issadore, *Lab Chip*, 2017, **17**, 1083–1094.

27 L.-A. Appelqvist and K.-A. Melin, *Lipids*, 1967, **2**, 351–352.

28 Z. Pento, *Clin. Chem.*, 1985, **31**, 439–441.

29 A. G. Marshall and C. L. Hendrickson, *Annu. Rev. Anal. Chem.*, 2008, **1**, 579–599.

30 J. Kameoka, R. Orth, B. Ilic, D. Czaplewski, T. Wachs and H. G. Craighead, *Anal. Chem.*, 2002, **74**, 5897–5901.

31 P. Hoffmann, U. Häusig, P. Schulze and D. Belder, *Angew. Chemie - Int. Ed.*, 2007, **46**, 4913–4916.

32 J. Lee, S. A. Soper and K. K. Murray, *J. Mass Spectrom.*, 2009, **44**, 579–593.

33 L. M. Fidalgo, G. Whyte, B. T. Ruotolo, J. L. P. Benesch, F. Stengel, C. Abell, C. V. Robinson and W. T. S. Huck, *Angew. Chemie - Int. Ed.*, 2009, **48**, 3665–3668.

34 L. M. Fidalgo, G. Whyte, D. Bratton, C. F. Kaminski, C. Abell and W. T. S.

Huck, *Angew. Chemie - Int. Ed.*, 2008, **47**, 2042–2045.

35 R. T. Kelly, J. S. Page, I. Marginean, K. Tang and R. D. Smith, *Angew. Chemie Int. Ed.*, 2009, **48**, 6832–6835.

36 D. J. Steyer and R. T. Kennedy, *Anal. Chem.*, 2019, **91**, 6645–6651.

37 A. P. France, F. Bramonti, J. Ujma, J. W. Bye, K. M. Carroll, B. Bellina, R. A. Curtis and P. E. Barran, The Application of Native Mass Spectrometry to Analyse Proteins Directly from Food, *Manuscript in Preparation*, 2020.

38 S. Tang and G. Whitesides, in *Optofluidics: Fundamentals, Devices, and Applications*, 2010, pp. 7–32.

39 I. Sinclair, M. Bachman, D. Addison, M. Rohman, D. C. Murray, G. Davies, E. Mouchet, M. E. Tonge, R. G. Stearns, L. Ghislain, S. S. Datwani, L. Majlof, E. Hall, G. R. Jones, E. Hoyes, J. Olechno, R. N. Ellson, P. E. Barran, S. D. Pringle, M. R. Morris and J. Wingfield, *Anal. Chem.*, 2019, **91**, 3790–3794.

## 3.16 Supporting Information

### 3.16.1 Device Fabrication

Microfluidic chip designs were drawn using DraftSight software (Dassault Systèmes, Vélizy-Villacoublay, France) before being converted to a film photomask (Micro Lithography Services Ltd, Essex, UK). Device masters were produced by spinning SU-8 2025 epoxy negative photoresist (MicroChem, MA, USA) to a depth of 70 μm upon a silicon wafer. The resulting wafer was baked prior to exposure of the SU-8 2025 using an MJB-4 mask aligner (SUSS MicroTec SE, Garching, Germany), and subsequently, a post-exposure bake was also performed. Designs were developed through the submersion of the exposed wafer in MICRODEPOSIT ™EC solvent (Dow Chemical Company, MI, USA), rinsed, dried and baked again to cement the SU-8 design on to the wafer. The master was placed in a petri dish and a mixture of Sylgard 184 silicone elastomer (10:1, base: curing agent, Dow Chemical Company, MI, USA) added to the dish to the required device thickness. The elastomer was then degassed in a vacuum desiccator, and baked overnight at 70 °C. Removal of the elastomer from the silicon-SU-8 master was performed using a scalpel to expose the design face, and fluidic connections were added using a 1.00 mm biopsy punch (Kai Medical, Solingen, Germany). Microfluidic chip MS designs consist of both a bottom and a top piece, each containing differing design features. The non-feature containing faces of the bottom piece of each design, along with a glass microscope slide, were exposed to oxygen plasma (Harrick Plasma, NY, USA), and the plasma exposed surfaces bound together. A further round of oxygen plasma activation was then performed upon the feature containing surfaces of both the bottom and the top piece of the PDMS device before these two pieces were bound together employing methanol (~10 μL) as a lubricant to ensure the design on each surface were aligned with one another. The device was then baked overnight at 110 °C, prior to insertion of the stainless steel capillary (OD 176 μm, ID 76 μm, Vita Needle Company, Needham, MA, US). Insertion of the capillary was performed under a microscope, ensuring the capillary came into contact with the end of the pre-designed channel, and ELASTOSIL E43 silicone sealant (Wacker Chemie AG, München, Germany) added to the PDMS-capillary interface and allowed to solidify.

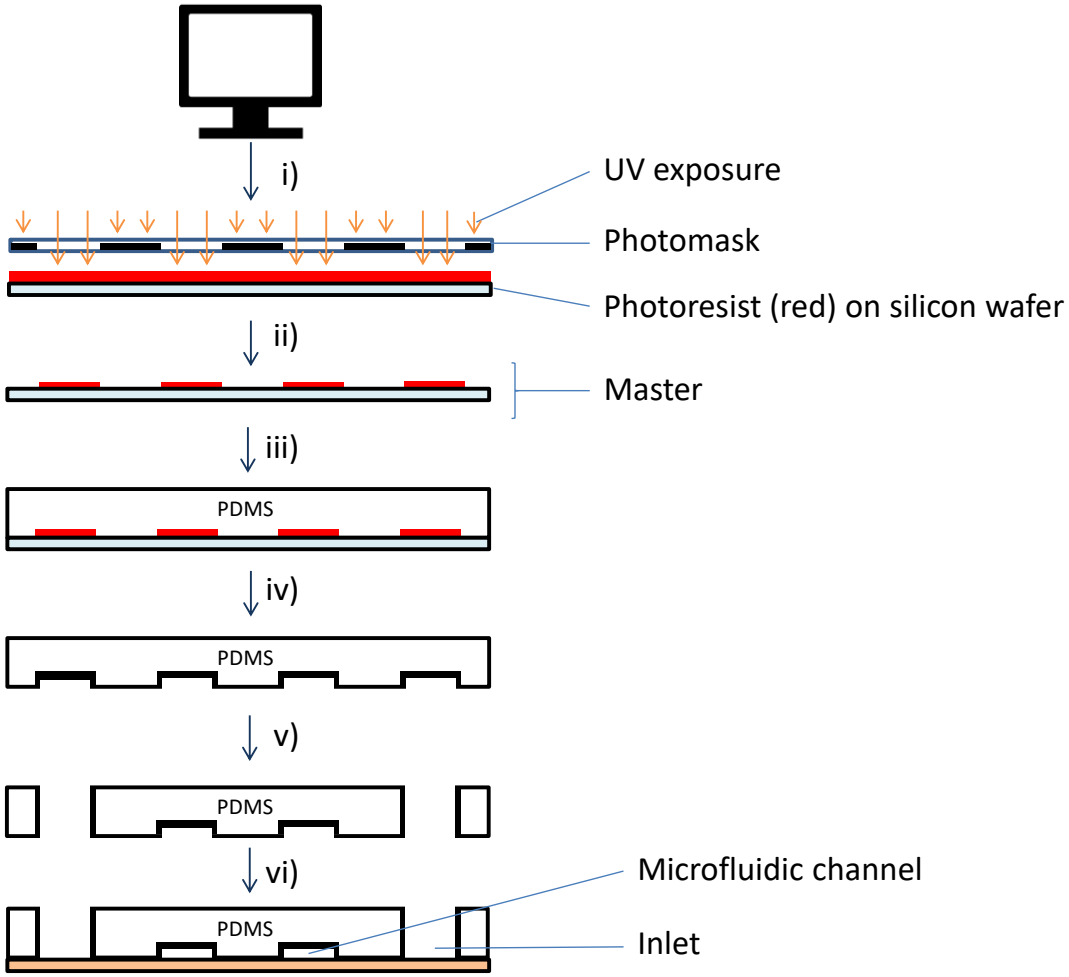


*Figure 3.6: Soft lithography schematic illustrating the steps involved to fabricate a microfluidic chip. i) CAD production of a photomask. ii) Generation of the master by photolithography. iii) Addition of liquid PDMS and curing agent into master. iv) Removal of PDMS from the master. v) Introduction of ports by punching. vi) Binding of PDMS to a glass slide (orange) to create channels.*

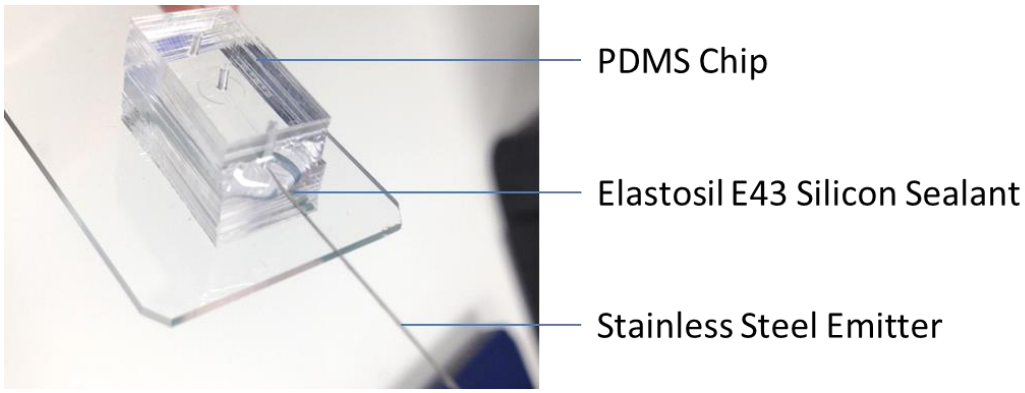


*Figure 3.7: Photograph of the microfluidic-MS chip, indicating the location of ELASTOSIL E43 sealant around the stainless steel emitter.*

### 3.16.2 Instrument Coupling

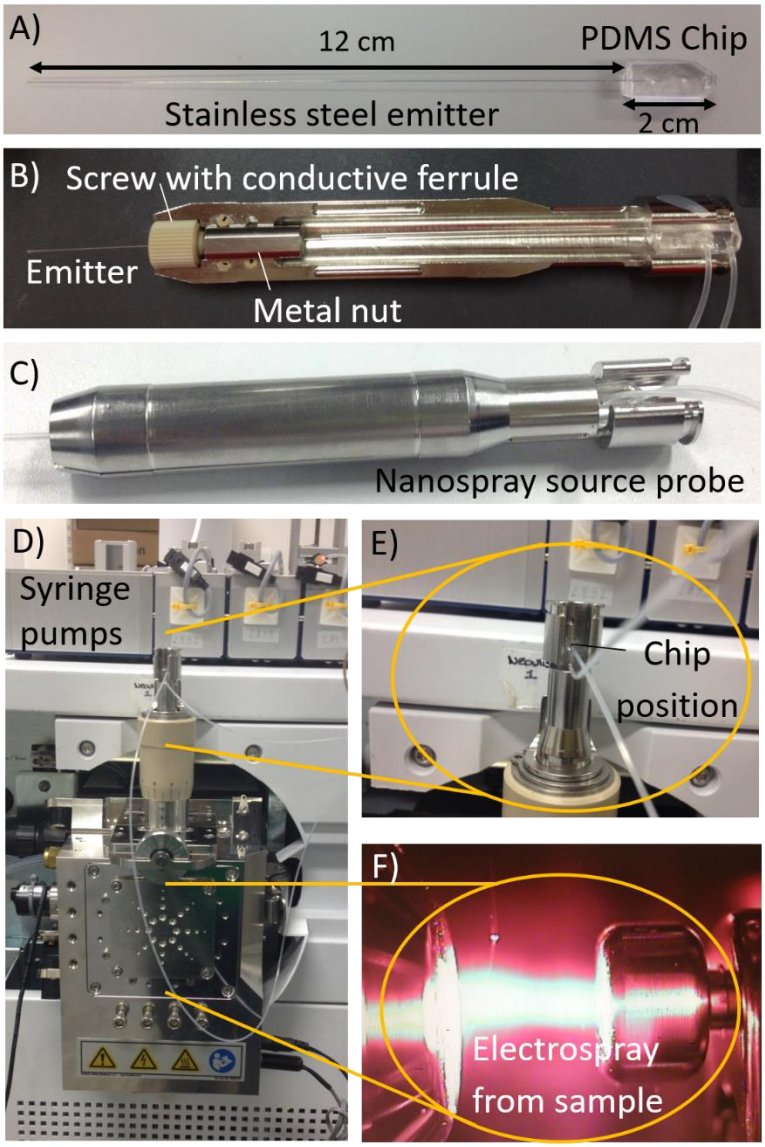


*Figure 3.8: Photographs of Agilent 6560 IM Q-TOF Chip-MS coupling. A) Generation-MS droplet microfluidic chip cut to holder size. B) The bottom section of the nanospray ion source holder indicating chip positioning and added grounding components. C) Enclosed nanoelectrospray source holder ready for insertion into the source. D) Photograph of the Agilent 6560 nanospray ion source indicating chip position and syringe pumps. E) Close up photograph of the droplet microfluidic chip sitting vertically within the holder that inserts into the nanospray ion source. F) Internal camera image of the inside of the nanospray ion source indicating the emitter position between the MS inlet and counter electrode.*

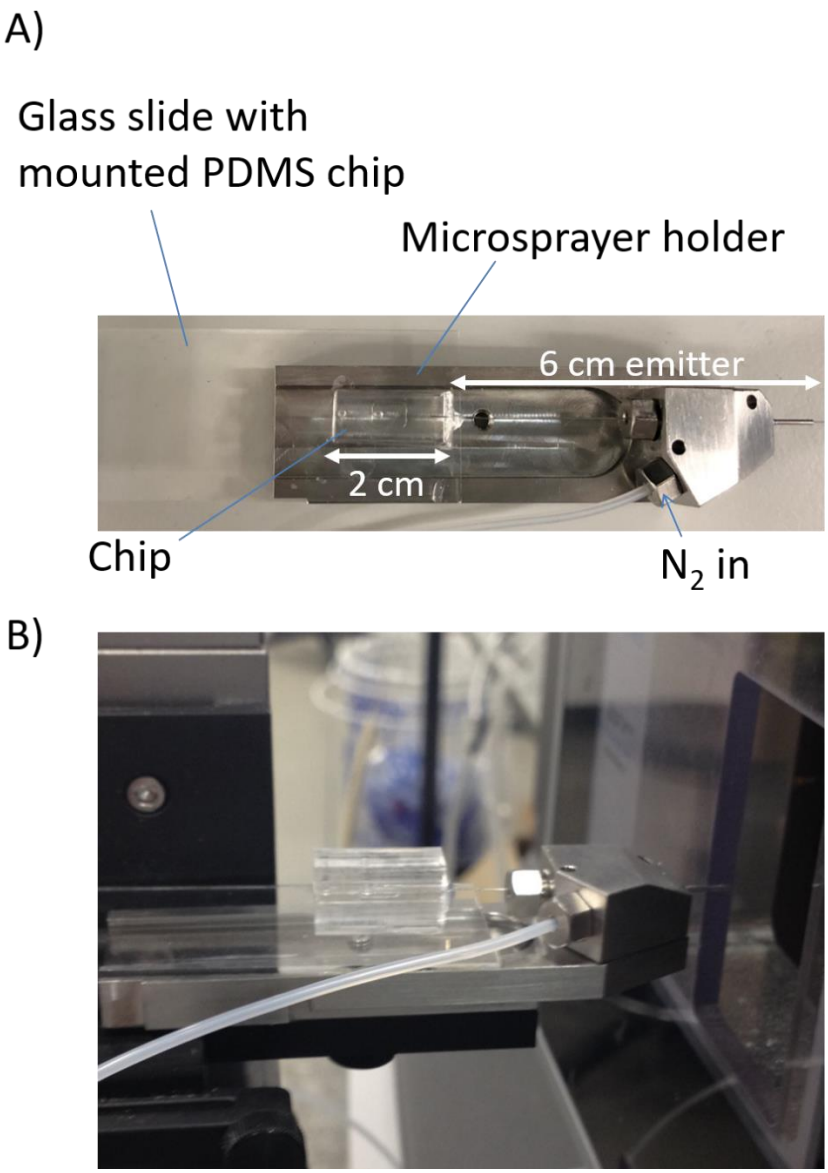


*Figure 3.9: Photographs of Waters Synapt G2Si Chip-MS coupling. A) Photographic representation of the microfluidic chip incorporated into the microsprayer device. B) Side on view of the microsprayer adaption when interfaced with the droplet microfluidic chip and mounted on to the nanoelectrospray source.*

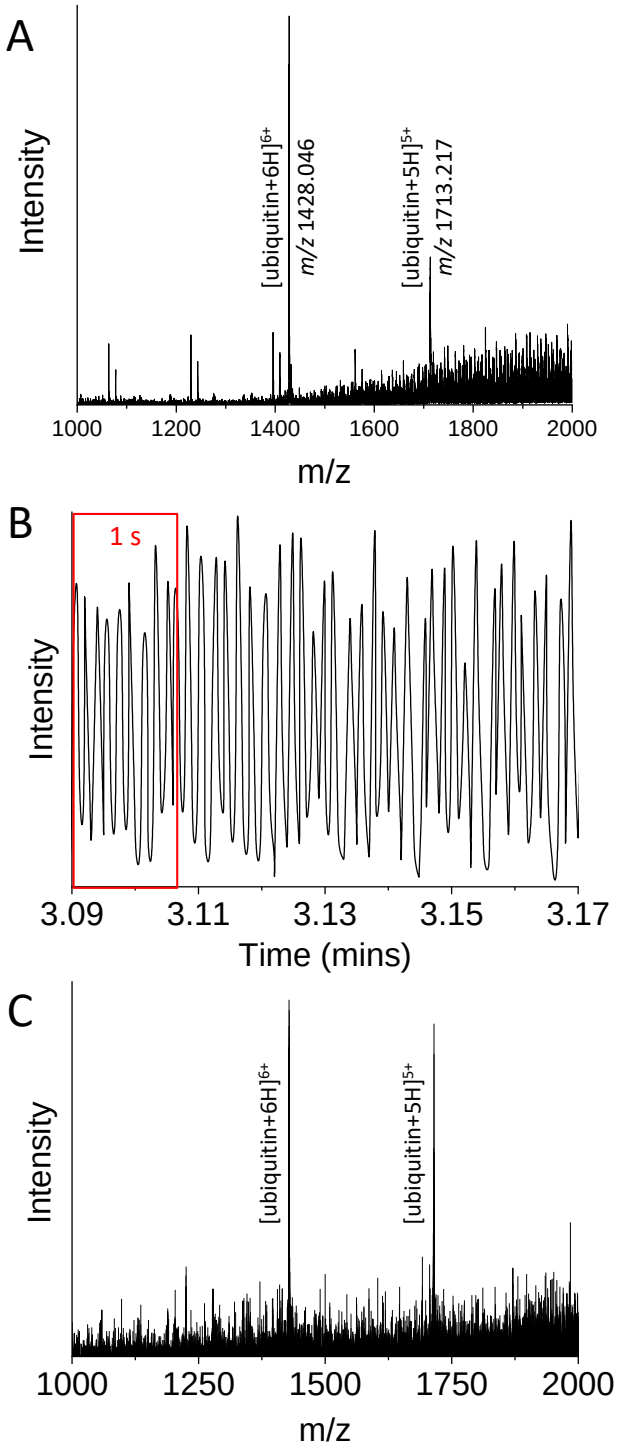


*Figure 3.10: A) nESI mass spectrum of ubiquitin acquired using an SYNAPT G2-Si Q ToF mass spectrometer. A 60 μM solution of ubiquitin dissolved in 100 mM ammonium acetate solution was sprayed from a microfluidic chip. B) Total Ion Chromatogram (TIC) acquired during infusion of droplets (~0.8 nL) containing ubiquitin (~100 μM solution) at an infusion rate of approximately 9 droplets per second (Hz). Each individual peak indicates one droplet reaching the SYNAPT G2Si detector. C) Mass spectrum extracted from 1 droplet peak containing ubiquitin, indicating the two major charge states observed under these conditions (1714.59 m/z, 5+ and 1428.43 m/z, 6+).*

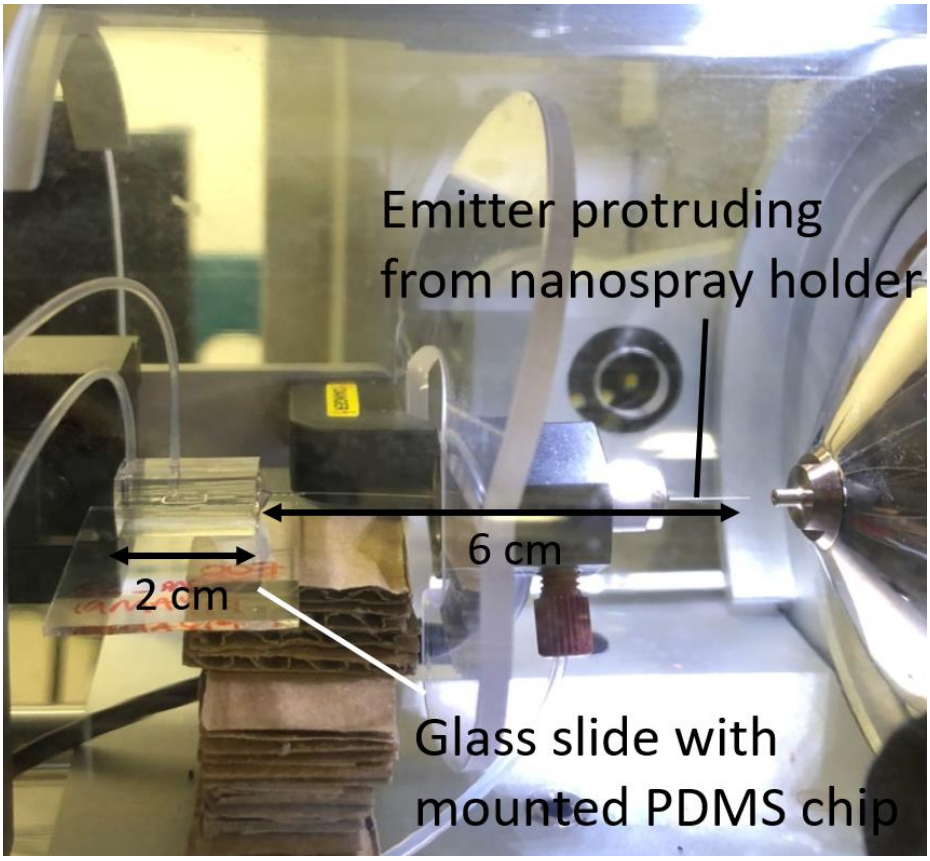


*Figure 3.11: Photograph of a Thermo Fisher Q Exactive Chip-MS coupling, indicating the microfluidic chip position and incorporated emitter.*

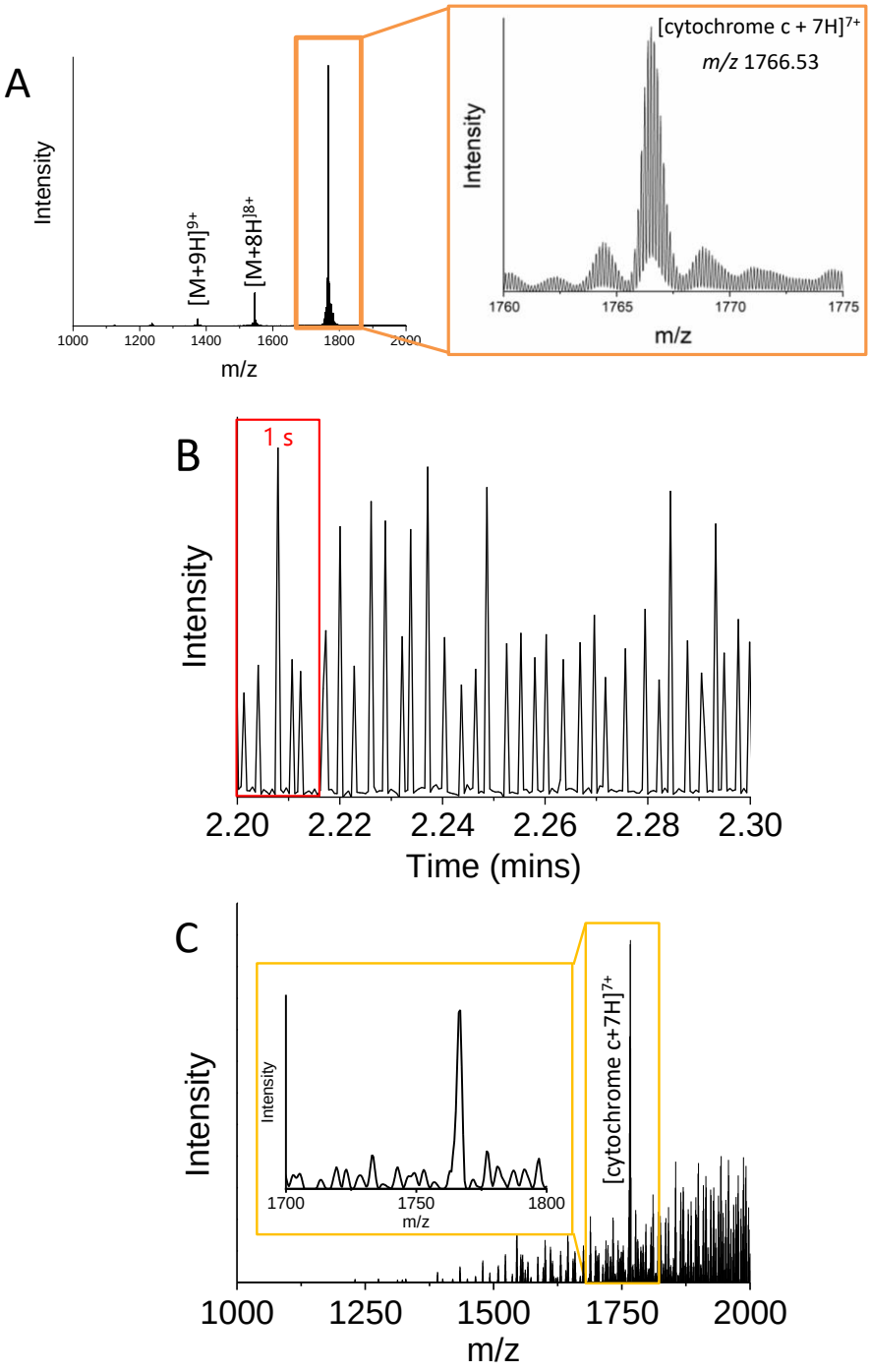


*Figure 3.12: A) nESI mass spectrum of cytochrome c acquired using an Q Exactive FT-MS. A 100 µM solution of ubiquitin dissolved in 100 mM ammonium acetate solution was sprayed from a microfluidic chip using a flow rate of 100 µL/hr and ~2.4 kV capillary voltage. B) Extracted Ion Chromatogram (EIC) acquired during infusion of droplets (~0.8 nL) containing cytochrome c (~100 µM solution) at an infusion rate of approximately 6 droplets per second (Hz). Each individual peak indicates one droplet reaching the Thermo Scientific Q Exactive detector. C) Mass Spectrum (m/z range 1000-2000) acquired from one droplet containing cytochrome c, indicating the most prominent charge state (1766.60 m/z, 7+) in this m/z range. The spectrum inset illustrates the lack of isotopic resolution achieved for the 7+ charge state in comparison to that seen in A.*

### 3.16.3 Sensitivity Analysis

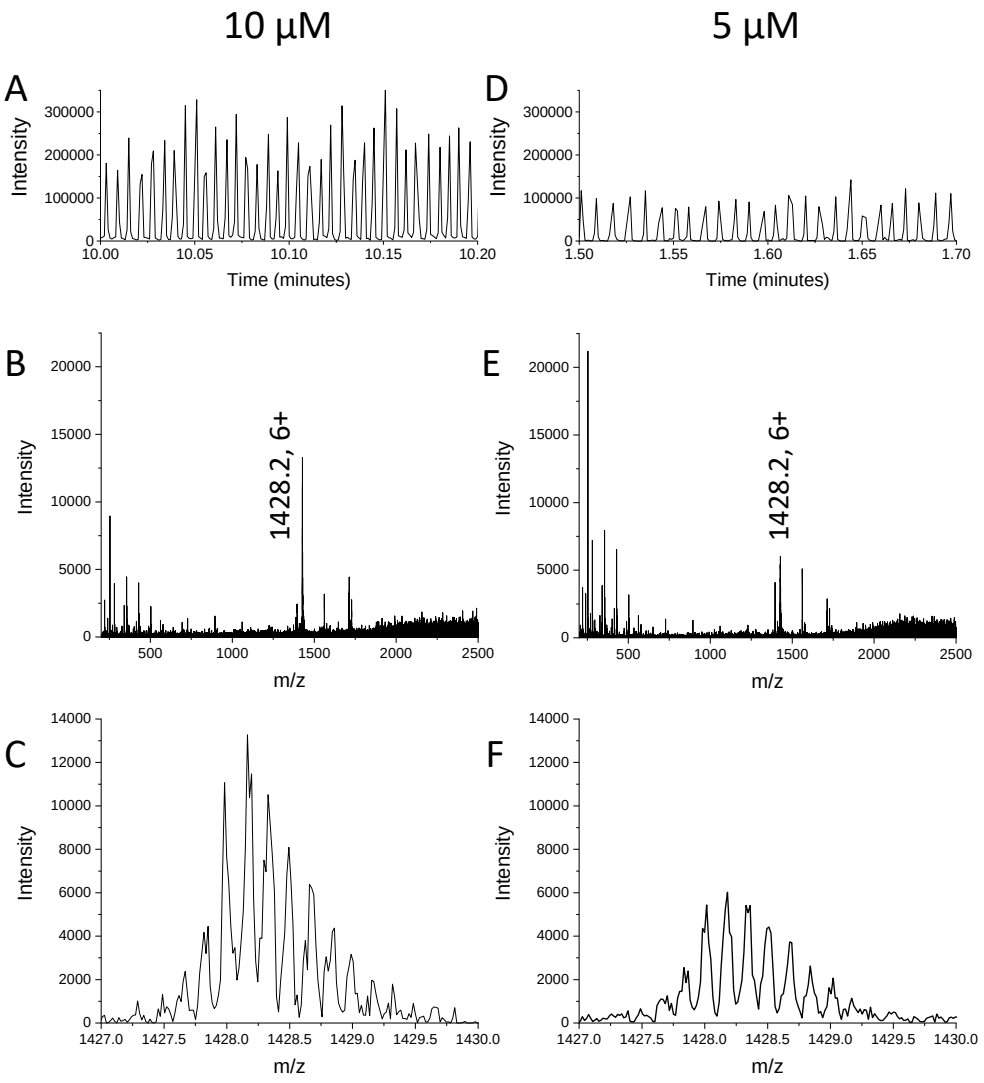


*Figure 3.13: A) Extracted ion chromatogram (m/z 1428) of infused droplets containing 10 µM ubiquitin dissolved in 100 mM ammonium acetate solution. B) Mass spectrum obtained from 1 droplet containing 10 µM ubiquitin solution. C) MS expansion of m/z 1428 ion obtained from 1 droplet containing 10 µM ubiquitin solution. D) Extracted ion chromatogram (m/z 1428) of infused droplets containing 5 µM ubiquitin dissolved in 100 mM ammonium acetate solution. E) Mass spectrum obtained from 1 droplet containing 5 µM ubiquitin solution. F) MS expansion of m/z 1428 ion obtained from 1 droplet containing 5 µM ubiquitin solution.*

### 3.16.4 Expansion of sample scope

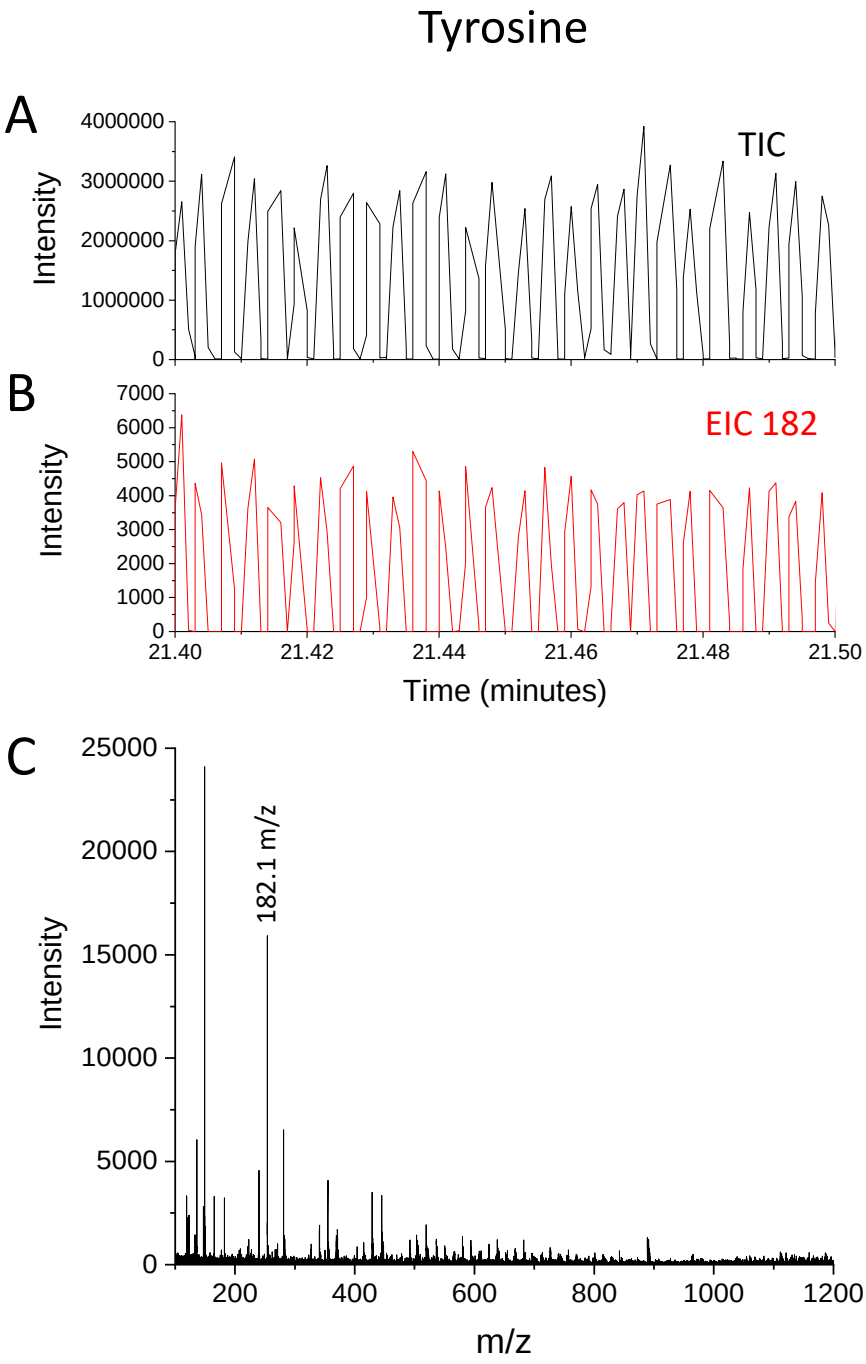


*Figure 3.14: Additional droplet-MS infusion data for the infusion of droplets containing 100 μM L-Tyrosine in aqueous solution containing 0.1% formic acid. Droplet infusion frequency = ~4.5 Hz. A) Total Ion Chromatogram (TIC) of infused Tyrosine droplets. B) Extracted ion chromatogram (EIC) (m/z 182.1) of infused Tyrosine droplets. C) Mass spectrum obtained from 1 droplet peak indicating the major tyrosine analyte ion observed, m/z 182.1, [L-Tyrosine+H]⁺.*

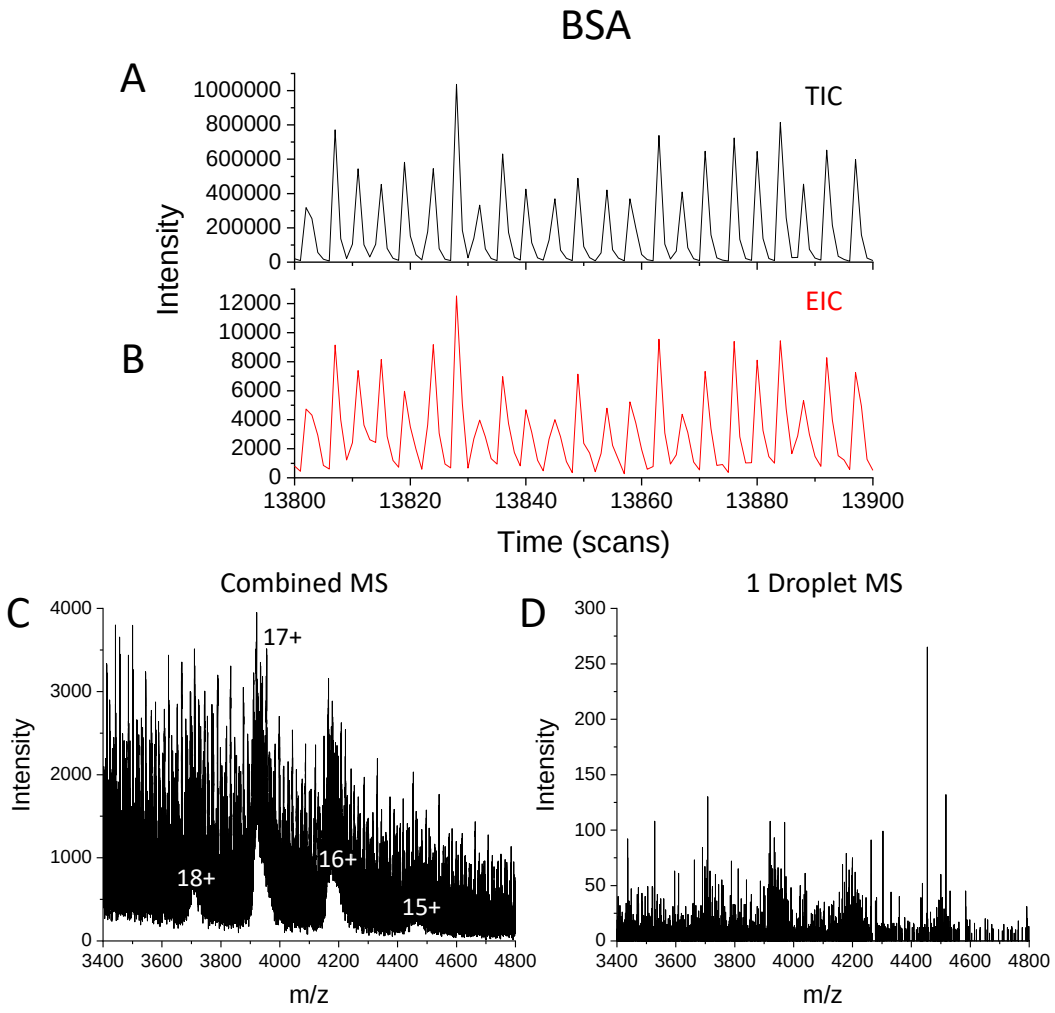


*Figure 3.15: Additional droplet-MS infusion data for the infusion of droplets containing 140 μM Bovine Serum Albumin (BSA, 66 kDa) in aqueous solution containing 100 mM ammonium acetate. For chromatograms, 100 scans (~2.6 s) are shown, with the scan time set to 0.016 s and inter san delay to 0.01 s (total cycle time = 2.6 s). Droplet infusion frequency = ~9 Hz. A) Total Ion Chromatogram (TIC) of infused BSA droplets. B) Extracted ion chromatogram (EIC) (m/z range = 3900-4000) of infused BSA droplets. C) Mass spectrum obtained from combining spectra obtained over ~1 minutes of droplet infusion. The major BSA charge states observed (15+ → 18+) are indicated. D) Mass spectrum obtained from 1 BSA droplet peak.*

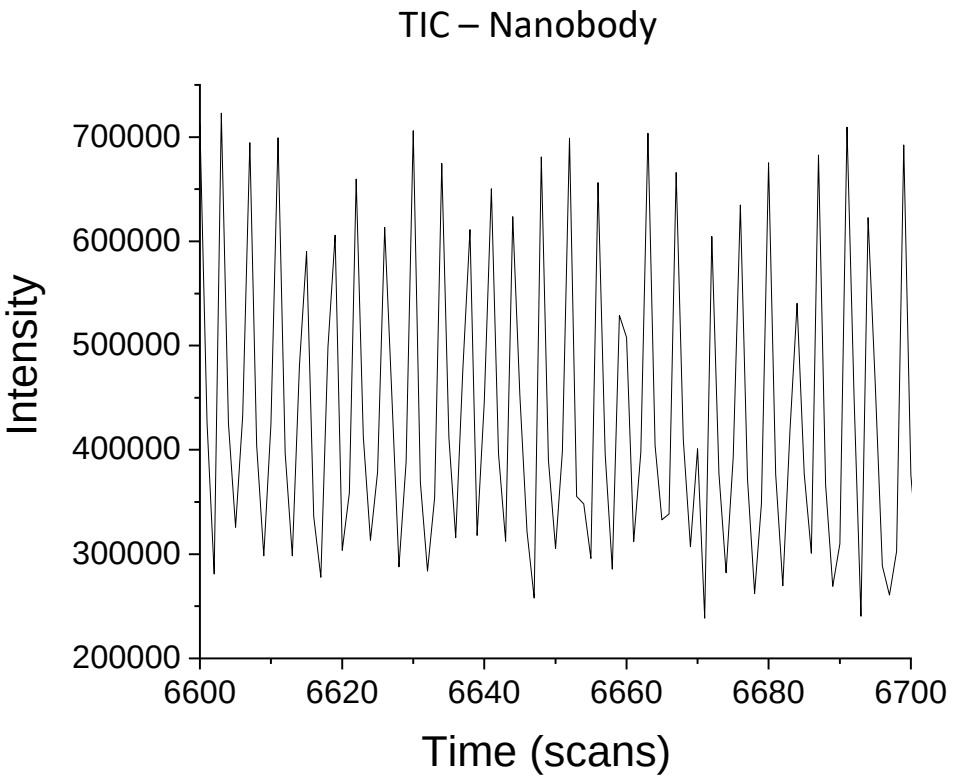


*Figure 3.16: Total ion chromatogram obtained upon the infusion of droplets containing nanobody protein dissolved in a 1 M ammonium acetate solution. 100 scans equivalent to ~ 2.6 s are shown (MS total cycle time = 0.026 s/scan). Droplet infusion frequency = ~ 9 Hz. Droplet size = ~0.8 nL.*

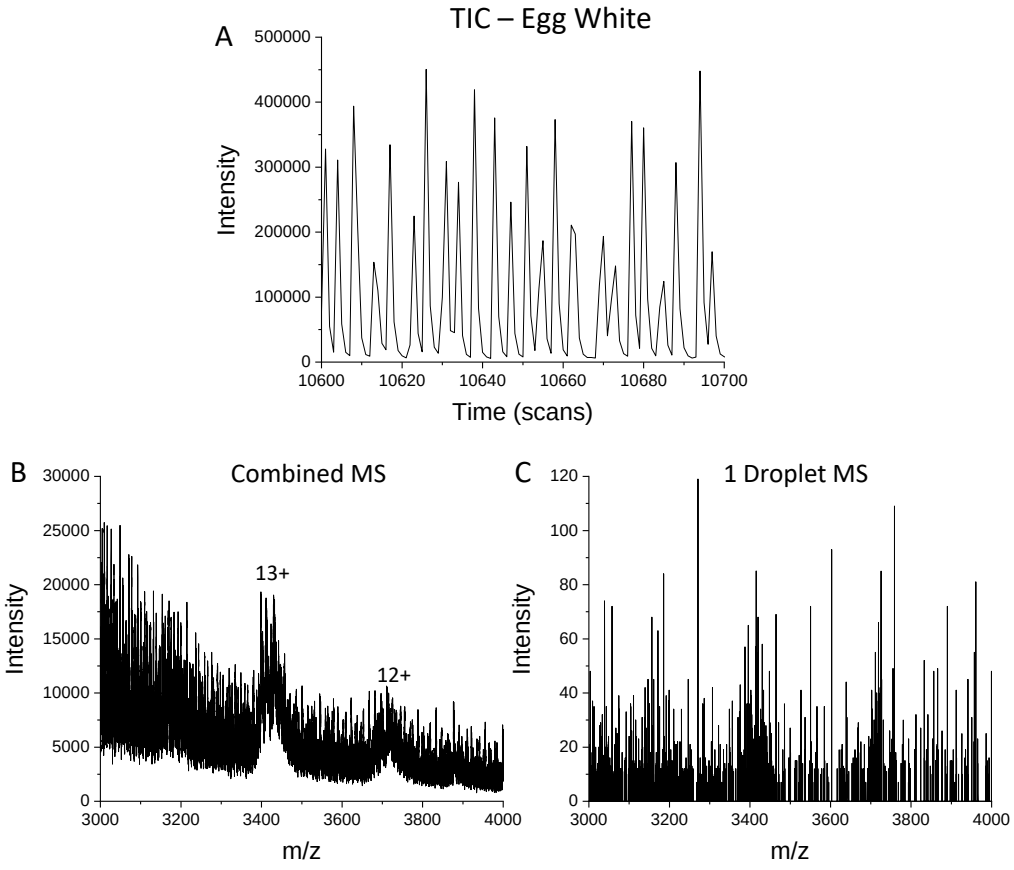


*Figure 3.17: Additional droplet-MS infusion data for the infusion of droplets containing egg white in aqueous ammonium acetate solution (1 M). A) Total ion chromatogram of infused egg white droplets, 100 scans equivalent to ~ 2.6 s are shown (MS total cycle time = 0.026 s/scan). B) Mass spectrum obtained for the infusion of egg white droplets upon combining ~8 minutes of acquisition. Ovalbumin protein (44 kDa) from egg white has been identified in the spectrum with the major charge states of ovalbumin monomer (12+ and 13+) indicated. C) Mass Spectra obtained from 1 egg white droplet.*

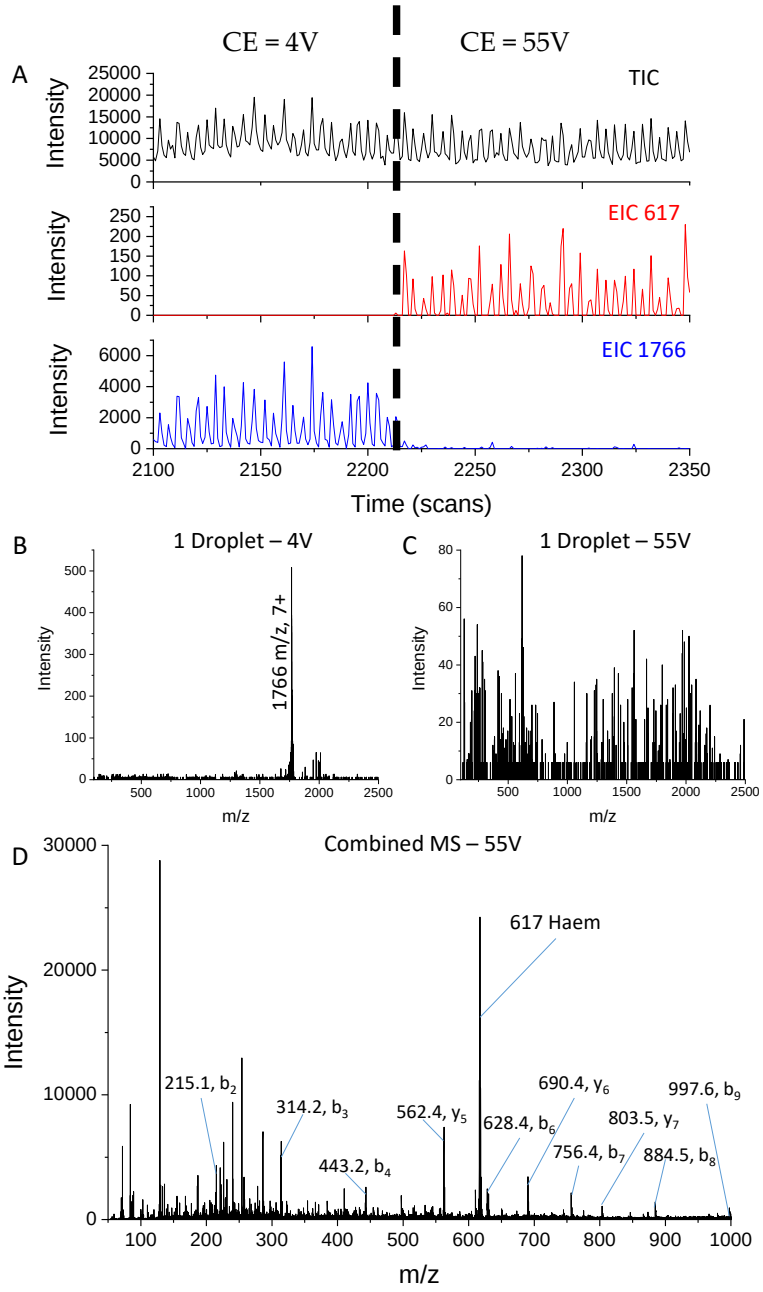


*Figure 3.18: Additional droplet-MS infusion data to indicate the possibility for future MS/MS measurements and top-down fragmentation within droplets. A) Total and extracted ion chromatograms obtained from infusion of cytochrome c droplets. The point at which the collision energy (CE) has been increased from 4V to 55V is indicated by the black dashed line. B) Mass spectrum obtained from 1 droplet when the CE is 4V. Major ion observed is that of [cytochrome c+7]$^{7+}$ due to MS/MS isolation. C) Mass spectrum obtained from 1 droplet when the CE is 55V. A number of ions are observed including Haem (m/z 617) D) Assignment of cytochrome c peptide fragments obtained upon summation of spectra acquired over ~1 minute at CE = 55V.*

# 4

# Assembly of Droplet Reinjection-MS Interfaces: Overcoming Droplet Coalescence for High Throughput Screening Applications

## 4.1 Declaration

This chapter has been written by me as the foundation of a future publication.

Suggested author list:

Emily E. Kempa, Clive A. Smith (CAS), Xin Li (XL), Depanjan Sarkar (DS), Denis Morsa (DM), Reynard Spiess (RS), Anouk M. Rijs (AMR), & Perdita E. Barran (PEB).

For this first author article, I performed the method development, chip fabrication and the majority of experimental procedures. CAS, XL and RS provided technical assistance and guidance. The 3D printed base was designed and fabricated by DS. Supervision was provided by AR and PEB. I drafted and edited the manuscript with input from some of the other authors. A portion of this work was performed in collaboration with the EU ATTRACT Emerging Life (EmLife) project, in which I contributed to the experimental work along with DM under the supervision of AMR. A supporting article detailing the outcomes from the EmLife project can be found at https://attract-eu.com/wp-content/uploads/2019/05/EmLife.pdf

## 4.2 Abstract

Droplet microfluidics coupled with mass spectrometry is evolving for high throughput screening. A commercial solution that can readily interface to existing mass spectrometry instrumentation would be highly desirable and allow the technology to become accessible to those without experience in droplet microfluidics. Here, we demonstrate a droplet reinjection workflow to infuse samples into three common mass spectrometers, each with different electrospray ionisation (ESI) source configurations. The ease of chip-mass spectrometry (MS) coupling is explored and difficulties highlighted. Particular attention has been turned to ESI sources which apply the electrospray voltage directly to the incoming droplet emitter ('push source'), as these were found to cause droplet coalescence within the microfluidic chip reinjection channel. To overcome such a difficulty, we have identified different solutions including a grounded mesh insert as a shielding approach, and minor changes to chips and ESI sources to stabilise incoming droplets. Results obtained allow the mass spectrum of individual reinjected droplets to be determined without hindrance from the electrospray voltage. The problems and solutions identified here, outline the foundations for the development of a commercial droplet reinjection-mass spectrometry interface.

## 4.3 Introduction

### 4.3.1 Label-Free High Throughput Screening and Droplet microfluidics

Screening technologies with the ability to analyse up to tens of thousands of samples per day are highly sought-after throughout the pharmaceutical and biotechnology sectors. [1–3] Current high throughput screening methodologies are highly reliant upon microtiter plates. [4,5] Although, these plates are easily transferable between robotic platforms and analytical techniques, their use can result in unnecessary single-use plastic and reagent waste, in addition to increased storage requirements for assays necessitating numerous plates. Droplet microfluidics provides an alternative to microtiter plates, with each droplet (pL to nL in volume) acting as a self-contained reaction vessel suspended within an immiscible liquid phase, [6,7] eliminating the need for plastic wells. Further to this, miniaturised flow devices or 'microfluidic chips' allow for the manipulation and analysis of these vessels in situ, eradicating transferal (of plates) between equipment.

Label-free analytical techniques such as Mass Spectrometry (MS), NMR, and Raman spectroscopy [8] provide direct analytical measurements reliant on the intrinsic physical properties of a sample. Their ability to produce sample measurements without the incorporation of florescent chromophores or radioactive isotopes is highly advantageous, as the incorporation of such labels can be expensive and requires additional method development to ensure suitability within the sample matrix. Although a number of these label-free techniques have been successfully coupled with microfluidics, [9–11] coupling with droplet microfluidics remains more difficult due to its dual-phase nature. Harnessing this property, however, allows for the exploitation of droplet microfluidics for high throughput screening technologies.

The approach explored here is the use of droplet-reinjection methodologies to design a high throughput MS platform for the analysis of a biotransformation within droplets. Generation of droplets containing biotransformation reagents (and possibly cellular material), followed by reinjection on to the analytical system of choice allows for chemical reactions (and/or cellular incubation) to occur within droplets under a time frame determined by the interval between the two aforementioned steps.

Manipulation of such a time frame can allow reaction kinetics occurring within the droplets to be realised. [12,13] Bio-reactions relying upon the encapsulation of genetic variations within droplets, is also applicable to this approach, as organisms such as bacteria, [14] yeast [15] and fungi [16] have all been shown to proliferate within droplet systems. An example of this is given in Figure 4.1, indicating the growth of *E. coli* bacterial colonies within 450 pL droplets. Subsequent reinjection of such a droplet population onto a suitable analytical system would allow for heterogeneity between colonies to be identified.

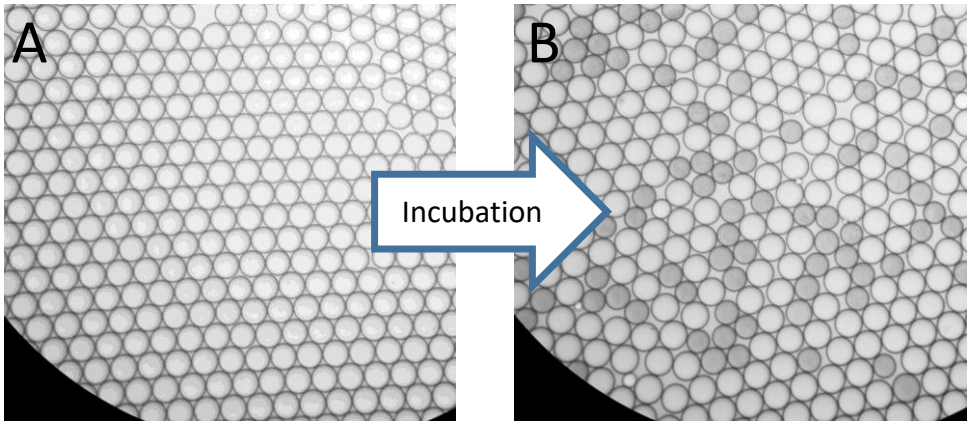


*Figure 4.1: A) Phase contrast microscope image of highly monodisperse droplets (~450 pL) containing bacterial cells before incubation. B) Phase contrast microscope image of the droplet population after incubation (overnight, 30 °C). Grey droplets indicate the growth of a bacterial colony inside the droplet. White droplets indicate a cell-free (empty) droplet, i.e., no encapsulated bacteria to proliferate into a colony during incubation.*

Droplet reinjection-MS has been demonstrated in the literature by several academic groups, [17–19] each utilising a unique microfluidic–mass spectrometry setup. Smith *et al.* demonstrated in 2013 the reinjection of protein-filled droplets, with the protein contents of each droplet identifiable *via* the MS data. [17] Belders' group have furthered this in several publications in which they have reinjected droplets containing different types of actinobacteria, incubated both on [20] and off-chip. [18,21] They have also demonstrated the ability to generate droplets, incubate bacteria, perform a biocatalytic reaction, reinject droplets and couple with MS, all within one device. This device allowed for reaction monitoring of amino acid production inside

the droplets over 8 hours. [20] Although this group has successfully demonstrated an application of droplet reinjection, to date, this has involved the complete redesign of electrospray ionisation (ESI) sources. An equivalent commercial solution coupling droplet microfluidics with MS is yet to become widely available, with only one notable platform, the ESI-Mine™ (Sphere Fluidics Ltd, Cambridge, UK) [22] available on the market. This platform is built upon a Perkin Elmer AxIon II mass spectrometer which has recently been discontinued. Here we explore the reinjection workflow and the hardware implications of such a platform. In particular, we focus upon utilising ESI apparatus most commonly supplied with the purchase of popular (nano)-liquid chromatography (LC)-MS systems.

### 4.3.2 Reinjection Workflow

A droplet reinjection-MS experiment in its simplest form consists of 4 steps: droplet generation, droplet storage, reinjection into the MS, and data visualisation (Figure 4.2 A). Initially, droplets of the required size (500 pL - 1000 pL) and contents are generated using a microfluidic chip with flow focusing, T-junction, or coaxial geometry, [23] before being collected in a suitable vessel (step 1). Subsequently, the droplets are stored (and/or incubated) until the desired analysis time (step 2). The reinjection of droplets can then occur within a microfluidic chip containing a 'Y-shaped' channel configuration. Use of the infusion flow rates determines the length of separation between droplets within the flow channel (assuming plug-like flow is occurring within the channels). These droplets are then introduced into the MS one at a time in rapid succession, *via* an ESI needle emitter incorporated into the reinjection microfluidic chip (step 3). [17] Primary data output consists of a total ion chromatogram (TIC) in which each observed peak consists of one droplet reaching the MS detector. Akin to chromatography, the mass spectrum for each peak can be obtained, thus indicating individual droplet contents (step 4).

Although coupling droplet microfluidics with MS has been described previously by many groups, differences between ESI source types were not explicitly compared until work by Peretzki *et al.* in 2020. [24] In this body of work we have divided the two major ESI source types into those which apply the electrospray voltage

directly to the incoming capillary emitter or solution ('push' type, Figure 4.2 B), and those which maintain the incoming capillary emitter at ground potential with respect to the MS inlet voltage ('pull' type, Figure 4.2 C). Although both types have their advantages and work equally well for LC-MS or direct infusion experiments, their applicability to a droplet microfluidic interface is more complicated due to the dual-phase nature (water-in-oil) of the incoming droplet emulsion. The most notable difficulty is the effect of the 'push' source electrospray voltage located directly on the incoming droplet solution. Although the application of electrical voltages to solutions is a well-exploited approach within digital microfluidics to move and divide droplets, [25] in this case, the electrical potential results in the unwanted disruption of the droplet form. [24] Examples of this phenomenon and viable solutions to control unwanted droplet disruption for reinjection experiments are explored later in this article.

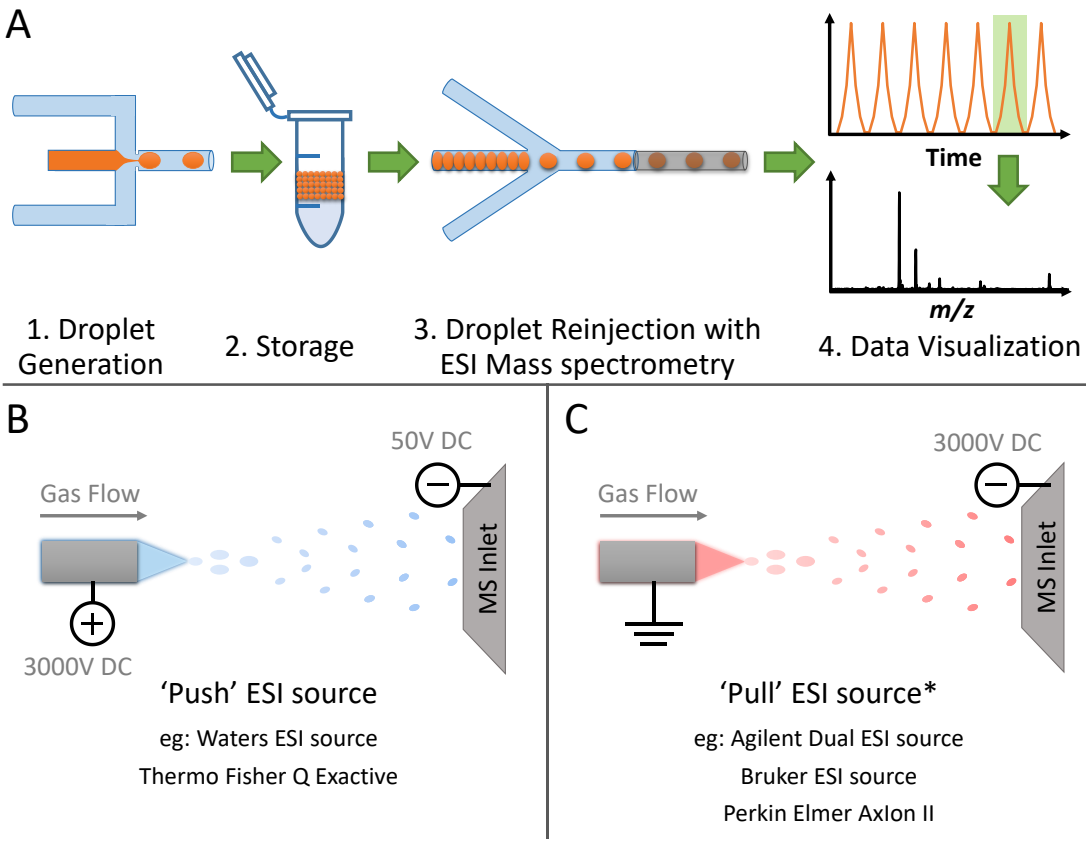


*Figure 4.2: A) Workflow indicating the major steps and results expected in a typical droplet-ESI-MS experiment. Initially, droplets are generated using a microfluidic chip, before storage (and/or incubation) of the droplets in a suitable vessel. After storage, droplets are 'reinjected' into the mass spectrometer via a 'Y-shape' configuration microfluidic chip containing an ESI needle outlet. Typical chromatographic results are shown in which each peak in the chromatogram represents an individual droplet. Mass spectra from each droplet can be obtained. B) Example schematic representation of a 'push' ESI source, in which a voltage is applied to the incoming sample solution before the MS inlet. C) Example schematic representation of a 'pull' ESI source, in which the incoming sample solution is held at ground potential before the MS inlet.*

## 4.4 Experimental Methods, Instrument Assemblies, and Results

### 4.4.1 Methods and Materials

Ammonium acetate was purchased alongside leucine enkephalin, phenylalanine (F) and diphenylalanine (FF) from Sigma-Aldrich (Dorset, UK). Leucine enkephalin was dissolved in a solution of 100 mM ammonium acetate in deionized water (Milli-Q Advantage ultrapure water filtration system, Merck Millipore, Darmstadt, Germany) to produce a ~20 μM solution. Phenylalanine (F)

and diphenylalanine (FF) were dissolved in water to produce solutions of 100 μM and 280 μM respectively.

### 4.4.2 Chip Design and Fabrication

All microfluidic chips used in this work were fabricated from polydimethylsiloxane (PDMS, SYLGARD™ 184 Silicone Elastomer Kit, Dow Chemical Co., MI, USA) using established photolithography and soft lithography techniques as described in the literature. [26,27] Chip designs utilised can be found in the supporting information to this article (Figure 4.11). Two differing types of integrated ESI emitters were used in the experiments. Primarily, stainless steel capillaries (OD: 176 μm, ID: 76 μm, various lengths as stated), (Vita Needle Co., Needham, MA, USA,) were utilised with pull source instrumentation (Figure 4.4), and the initial push source interface (Figure 4.6 A & B). Fused silica capillaries (OD 150 μm, ID 75 μm, Polymicro Technologies, LLC, Phoenix, AZ, USA) were subsequently used as the emitter type for push source solutions (Figure 4.9). These fused silica capillary pieces were cut to 6 cm in length and their outer surfaces sputter coated in Aluminium before insertion into the final microfluidic device. Both emitter types were incorporated into the fluidic outlet channel of the final PDMS devices and secured using ELASTOSIL E43 silicon sealant (Wacker Chemie AG, München, Germany) as described by Wink et al. [18] Copper gauze (60 mesh woven from 0.19 mm diameter wire, Alfa Aesar, Haverhill, MA, USA) utilised as a push source solution was also incorporated into some PDMS devices as stated. A detailed procedure for emitter and copper gauze insertion can be found in the Supporting Information.

### 4.4.3 Droplet Generation and Storage

Droplet generation was achieved using a Picodroplet Single Cell Encapsulation System (Sphere Fluidics Ltd, Cambridge, UK) in which the separative oil phase consisted of Pico-Surf™ 1 (Sphere Fluidics Ltd, Cambridge, UK) diluted to 1% in Novec™ 7500 Engineered Fluid (3M, Maplewood, MN, USA). Droplet collection occurred within a reinjection syringe initially filled with Novec™ 7500 Engineered Fluid as described in Figure 4.3 (steps 1-3) and allowed for the facile

transfer between encapsulation system and mass spectrometer. When not in use, droplet containing reinjection syringes were stored at +4°C (Figure 4.3, step 4).

### 4.4.4 Droplet Reinjection

Droplet reinjection was achieved *via* connection of the reinjection syringe outlet (Figure 4.3, step 5) and spacing oil reservoir to the microfluidic chip using 1.09 mm OD tubing (0.38 mm i.d., Smiths Medical Inc., Minneapolis, MI, USA). Infusion flow rates were controlled using a neMESYS low-pressure syringe pump (CETONI GmbH, Korbußen, Germany) in each case. Droplet infusion was achieved *via* the flow of Novec™ 7500 Engineered Fluid to the base of the reinjection syringe, in which the upward flow of the oil phase displaced the droplet population, subsequently pushing them toward the chip spacing region (Figure 4.3, step 5). Reinjection spacing oil consisted of Novec™ 7500 Engineered Fluid in every experiment. Before coupling the reinjection chip with each MS platform, droplet flow through chips was observed under the microscope to determine suitable droplet reinjection flow rates and frequencies.

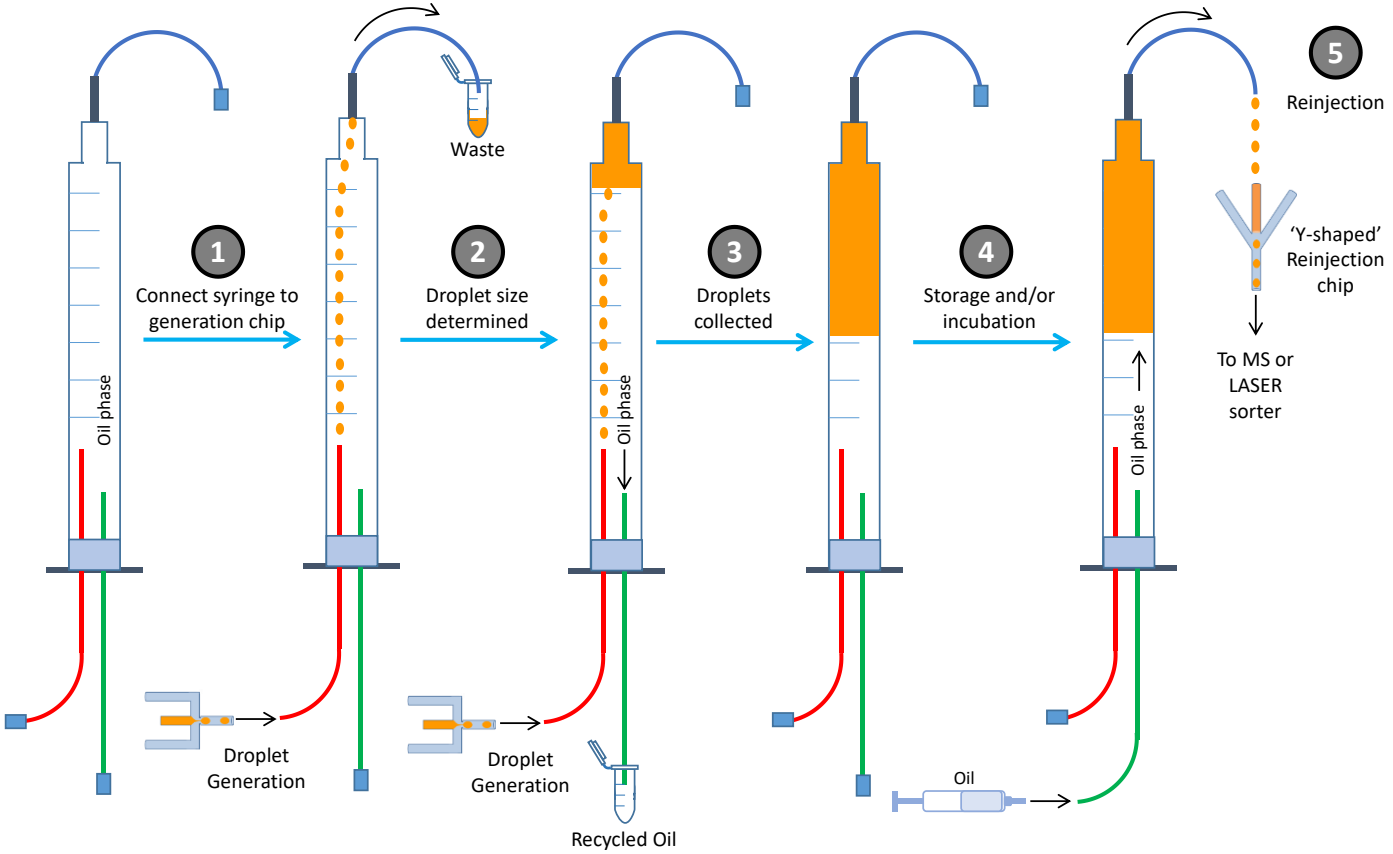


*Figure 4.3: Schematic indicating the major stages of generating, collecting, storing, and reinjecting droplets using a reinjection syringe. 1. Reinjection syringe filled with the chosen oil phase. 2. Syringe inlet connected to the generation chip outlet and droplets allowed to flow up and out of the syringe into waste. 3. Upper outlet capped and lower outlet opened to let oil drain away as incoming droplets rise to the top and are trapped in the syringe. 4. All inlets and outlets capped and syringe containing droplets stored and/or incubated. 5. Syringe inlet connected to spacing oil and droplets pushed out the top of the reinjection syringe and through the 'Y shaped' reinjection chip into the MS.*

### 4.4.5 Pull Source Assembly and Results

Coupling of the droplet reinjection-microfluidic chip with a pull source was achieved on two MS vendors' instrumentation, both utilising ESI sources with considerably similar designs. Both required the incorporation of a stainless-steel emitter of approximately 12 cm in length into the microfluidic chip. Coupling to a 6560 IM-Q-TOF (Agilent Technologies, Santa Clara, CA, USA) with a Dual-ESI source is as described in Figure 4.4. The assembly is based largely upon the standard Dual-ESI setup, but with the ESI-needle supplied by Agilent removed. This removal allows for the steel emitter of the microfluidic chip to be passed through the entirety of the nebuliser block until the emitter protrudes from the original needle outlet. The level of protrusion can be altered *via* movement of the microfluidic chip glass slide along the vertical axis, prior to the supporting glass slide being clamped in place. The fluidic connections can then be carefully added to the microfluidic chip. As described in Figure 4.4 B, the entirety of the nebuliser block is held at ground potential, in a perpendicular arrangement to the MS inlet. A comparable assembly was also achieved with an amaZon SL dual funnel electrospray ionization quadrupole ion trap (ESI-QIT) mass spectrometer (Bruker Daltonics Inc., Billerica, MA, USA) with the schematic for this given in Figure 4.14 A.

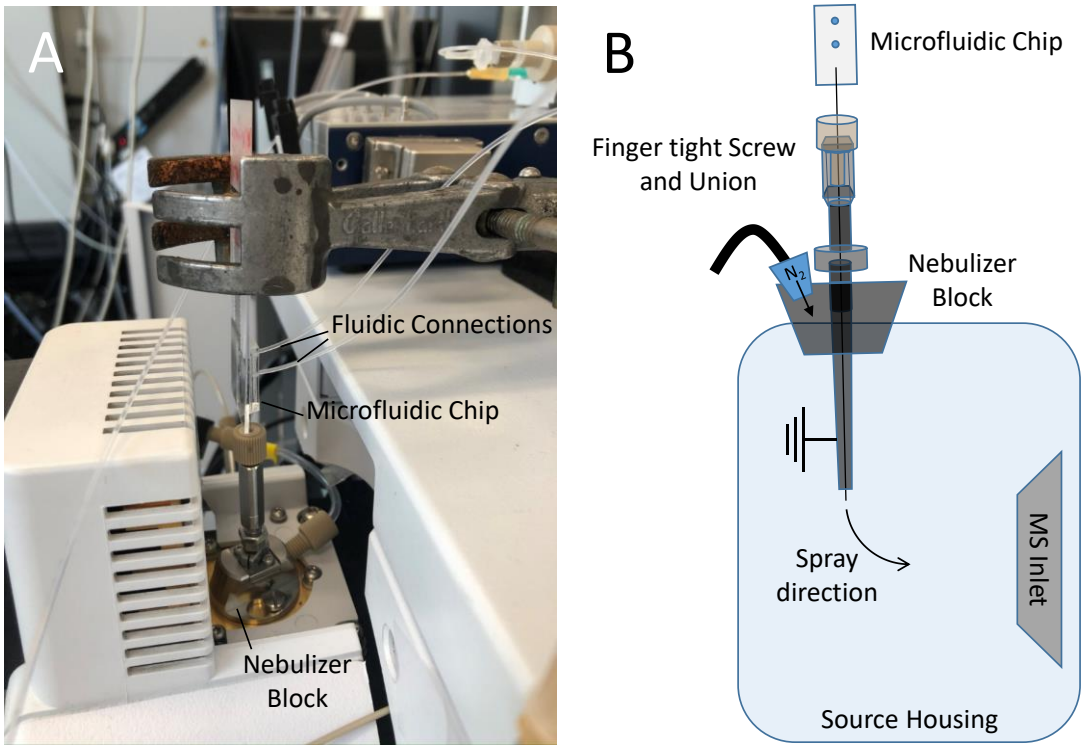


*Figure 4.4: A) Photograph of a microfluidic chip containing a stainless-steel emitter outlet interfaced with an Agilent Dual-ESI source. The emitter outlet has been threaded through the beige finger tight screw and the nebuliser block. The glass slide containing the PDMS microfluidic chip is held in place with a clamp stand. B) Schematic representation (cross-section view) of the chip-Agilent-ESI interface indicating the emitter position threaded through the nebuliser block and held at ground potential wrt to the MS inlet.*

Infusion of ~600 pL droplets containing leucine enkephalin (20 μM solution) *via* the chip-pull source arrangement in Figure 4.4 yielded the expected chromatographic results (Figure 4.5 A). The peaks visualised in the chromatogram each represent one droplet detected by the mass spectrometer, with the spaces between peaks indicating the time between droplets in which the oil is exiting the chip emitter. Note that the oil phase does not ionise readily in positive ionisation mode, and thus is not detected by the mass spectrometer in this mode. Subsequently, the mass spectrum of each droplet can be visualised *via* the extraction and summation of the MS data under the selected peak as shown in Figure 4.5 B, with the protonated species of leucine enkephalin $[M+H]^+$ observed at *m*/*z* 556.3. The frequency of droplet reinjection can also be determined *via* the chromatogram, and in this case, droplet detection is observed at ~8 droplets/s. Alteration of this frequency (for this droplet

volume and others) can be accomplished by changing the flow rates in the droplet infusion and spacing oil channels. Upon increasing the droplet volume (and thus diameter), the droplet reinjection frequency will decrease (when infused under identical flow rates). Data supporting the reinjection of alternative droplet sizes (600 pL, 765 pL and 1075 pL) *via* this apparatus can be found in Figure 4.24.

Data exhibiting the infusion of droplets (1.25 nL) into the analogous ESI-QIT set up can be found in supporting information Figures 4.22 and 4.23. This data supports the pull source apparatus assembly for both droplet generation-MS (as in Kempa *et al.* [28]) and droplet reinjection-MS. [29]

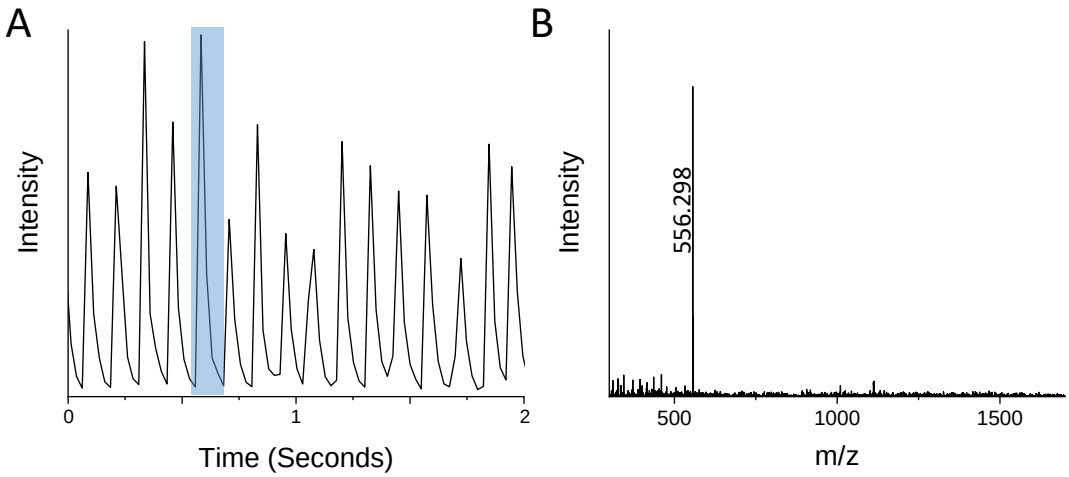


*Figure 4.5: A) Total ion current (TIC) chromatogram obtained from reinjection of ~600 pL droplets via the chip-Agilent-ESI interface into an Agilent 6560 Mass Spectrometer. Each peak indicates detection of an individual droplet, with an approximate infusion frequency of 8 droplets/s. MS scan rate is 40 spectra/s B) Mass spectrum obtained from 1 droplet peak (summation of two scans as indicated in the blue shaded rectangle). The droplet contains μM of Leucine enkephalin peptide, $[M+H]^+$ = 556.298 m/z*

### 4.4.6 Push Source Assembly and Results

Chip coupling to a push source (Synapt G2-Si Q-TOF, Waters Corp., Milford, MA, USA) is as described in our previous publication [28] with a schematic and photograph of this interface given in Figure 4.6 A and B. Briefly, the microfluidic chip with 6 cm stainless-steel emitter is threaded through the sprayer component of a Waters NanoLockSpray ESI source in the place of a picotip emitter or nanospray column. Voltage is applied to the entirety of the sprayer assembly to induce an

electrospray from the emitter outlet, which is then directed into the MS inlet (cone) *via* a voltage gradient and the MS vacuum. As with the pull source arrangement, fluidic inlets can be connected to the microfluidic chip to begin the droplet reinjection experiment. After numerous attempts, and experimentation with differing MS source parameters, it was clear that a steady droplet reinjection trace could not be achieved using this assembly. An example of this is given in Figure 4.6 C, in which peaks that should correspond to stable droplet reinjection are instead differing widely in arrival frequency and peak intensity.

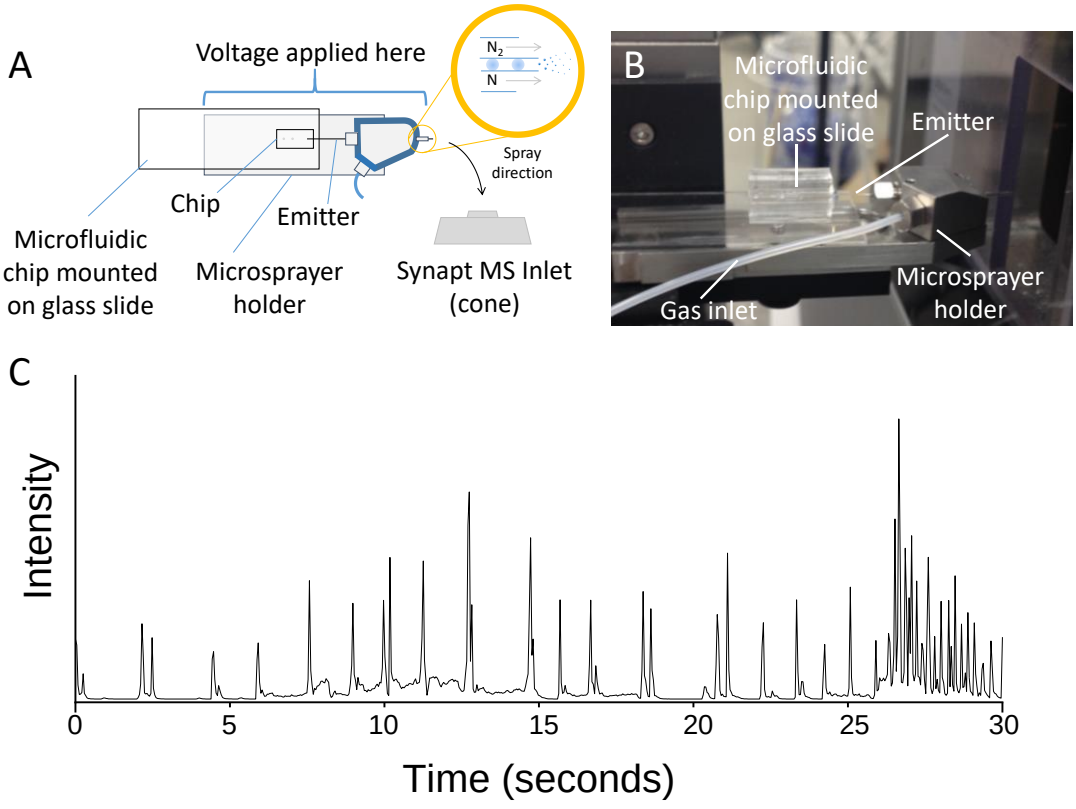


*Figure 4.6: A) Schematic representation of a droplet microfluidic chip interfaced with a Waters sprayer, as mounted on a Waters nanoESI source. The emitter outlet of the chip has been threaded through the sprayer head to which the electrospray voltage is applied. A gas flow (N2) perpendicular to the emitter may be used to aid the electrospray (yellow ringed inset). B) Photograph of the chip-sprayer interface mounted on a Waters nanoESI source. C) Total ion current chromatogram obtained from a droplet reinjection experiment using a Waters Synapt G2-Si mass spectrometer with nanoESI source and chip-sprayer interface. No stable droplet trace is obtained.*

A secondary observation was made inside the tubing leading from the reinjection syringe to the microfluidic chip. Upon initial connection, the droplet emulsion appeared uniform throughout the length of the tubing, however, a short time after application of the electrospray voltage, this uniformity diminished and instead was replaced with interspersed bands of oil and aqueous phase. This observation indicated that the electrical field generated by the applied voltage in the proximity of the microfluidic chip and reinjection syringe was disrupting the droplet population. This confirms the total ion chromatogram obtained in Figure 4.6 C results from disrupted and coalesced droplets entering the mass spectrometer, and thus, in this configuration, the push source is not suited to droplet reinjection.

To further understand and visualise the effect of the voltage upon droplets residing in the chip, the chip, threaded though the sprayer head, was interfaced with the Picodroplet Single Cell Encapsulation System. Using an external HV amplifier (Advance Energy PLC, UK) a +1 kV voltage was placed on the sprayer head, thus applying a voltage to the chip emitter. Images obtained from the microscope high-speed camera (Mikotron-GmbH, Unterschleißheim, Germany) indicated that upon bringing the voltage in proximity, and onto the chip emitter, the coalescence of droplets travelling through the spacing region occurred (Figure 4.7). The frequency of coalescence events was irregular, and the larger droplets generated post-coalescence at the 'Y' shaped junction varied in size. The mechanisms for this phenomenon are explored in more detail in the extended discussion. These coalescence events and consequent mixing of droplet contents confirmed that the droplets initially generated and stored in step 1 and 2 of the reinjection workflow (Figure 4.2 A) are no longer intact. Hence, a droplet reinjection-MS experiment in this push source arrangement is not fit for purpose.

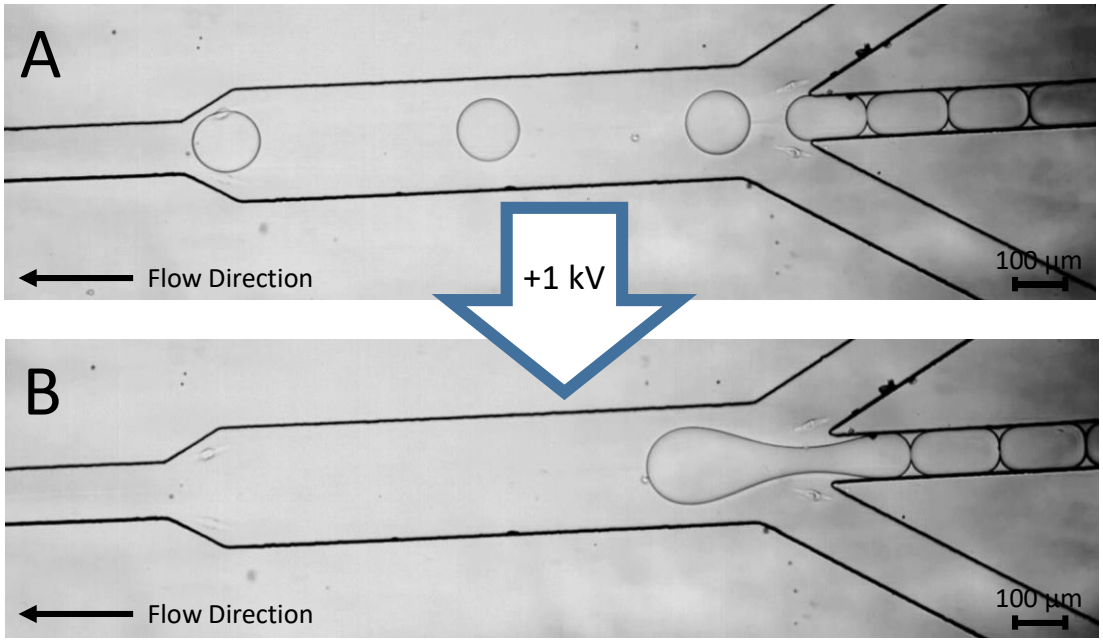


*Figure 4.7: A) Microscope image of stable droplet reinjection using chip design 1 before application of a voltage on the conductive emitter outlet. B) Microscope image indicating coalescence of pre-generated droplets in the droplet spacing region upon application of +1 kV on the conductive emitter outlet.*

### 4.4.7 Push Source Solutions

To find a push source arrangement suitable for droplet reinjection, several modifications to the setup were employed. The most notable alteration being the insertion of copper gauze into the PDMS chip (design 2, Figure 4.11) perpendicular to the channel plane (Figure 4.8 A, Figure 4.13) akin to the method described by Schirmer *et al*. [20] The finished microfluidic device with gauze and stainless steel emitter were interfaced with the Picodroplet Single Cell Encapsulation System as in Figure 4.8 B, with the emitter passed through the sprayer head (supported on a glass slide) as it would be on the MS. The copper gauze was connected to an external grounding plug using a crocodile clip and the fluidic connections inserted into the chip to achieve the desired reinjection flow through the droplet spacing region. The voltage from the HV amplifier was placed on the sprayer head *via* a probe as seen in Figure 4.8 B. As observed in Figure 4.8 D, the copper gauze when connected to the grounding plug shields the reinjection region from the electric field emanating from the voltage placed on the sprayer head and emitter. When disconnected from ground

potential (Figure 4.8 C), the electric field can once again penetrate the droplet reinjection region and droplet coalescence returns.

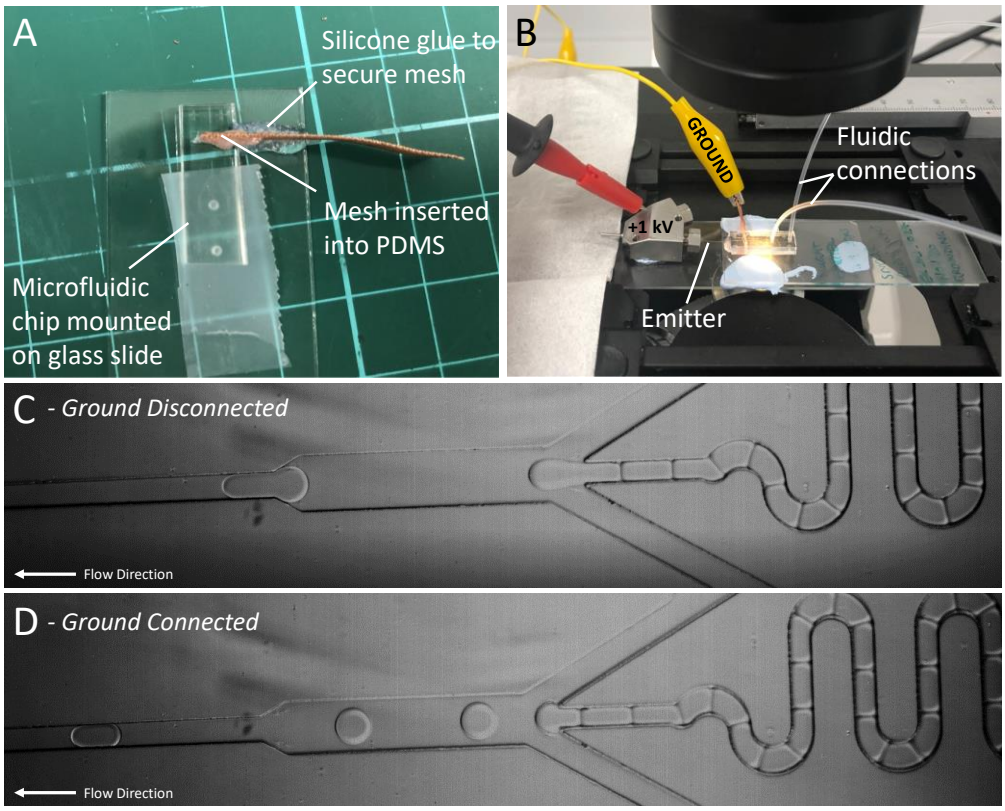


*Figure 4.8: A) Photograph of a microfluidic chip (design 2) with a copper mesh inserted into the PDMS to shield the reinjection region from the electrospray voltage. N.B. Photograph was taken before insertion of the electrospray emitter. B) Photograph of the microscope-chip assembly used to test the shielding properties of the copper grounding mesh on droplet reinjection. The yellow crocodile clip is connected to a grounding plug and the red probe to a HV amplifier. C) Grounding clip disconnected - Microscope image of droplet coalescing in the chip spacing region upon 1 kV application on the emitter and sprayer head. D) Grounding clip connected - Microscope image of stable droplet reinjection in the chip spacing region upon 1 kV application on the emitter and sprayer head.*

Additional observations made from the microscope analysis found the use of stainless steel emitters to disrupt the droplet form at the chip exit (Figure 4.16). The direct application of voltage to the droplet *via* the steel emitter caused unwanted splitting and tailing of the droplet. Hence, the emitter material was changed to fused silica with an outer coating of aluminium. As the emitter inner surface was no longer electrically conductive, droplet splitting at the chip exit ceased (Figure 4.17). The aluminium conductive coating now served as the point of ESI voltage application.

To further negate the effects of the electric field upon the incoming droplets, and to ensure higher voltages could be placed upon the emitter, two other modifications from injection designs were employed. Firstly, an elongation of the chip (designs 3 and 4, Figure 4.11) to further distance incoming droplets from the applied voltage as described by Peretzki *et al*. [24] Secondly, alteration of the NanoLockSpray source to incorporate a 3D printed sprayer base. [30] Both of these modifications are depicted in Figure 4.9 A.

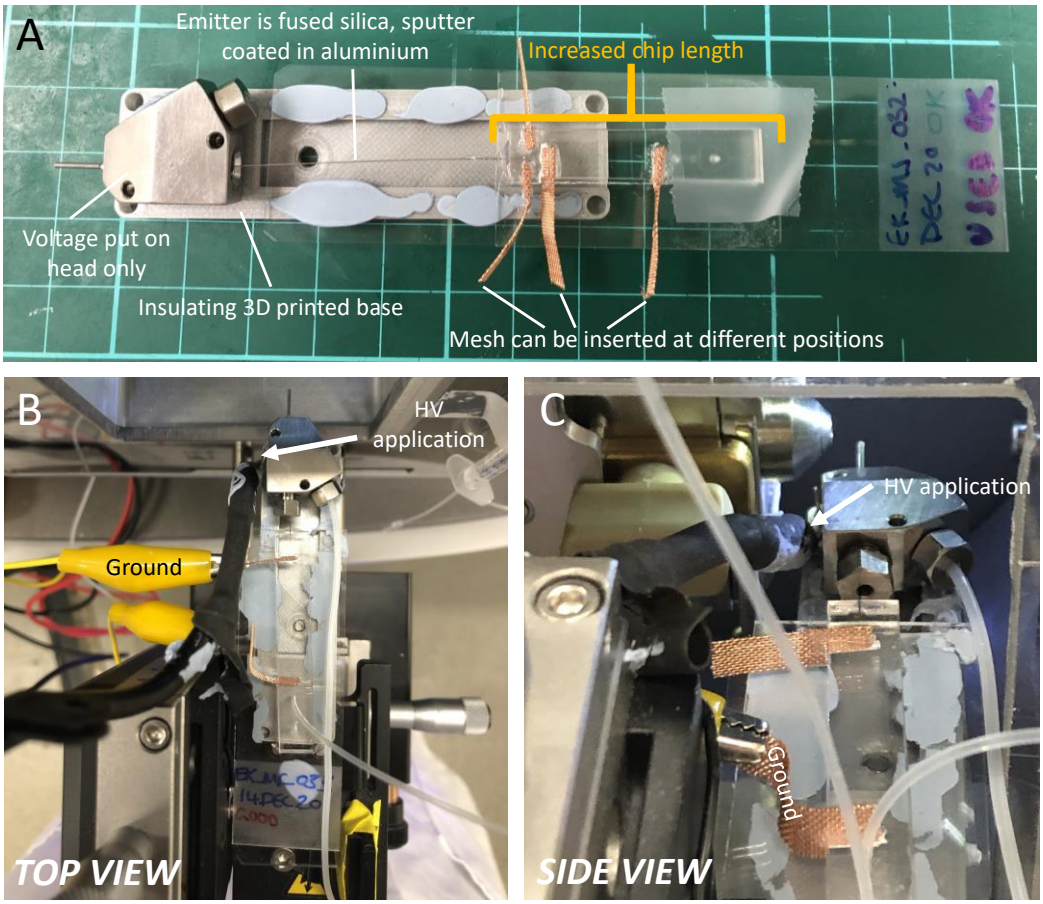


*Figure 4.9: A) Photograph of the sprayer head fixed to a 3D-printed base (silver plastic) on which the microfluidic chip containing grounding mesh sits. The emitter outlet is threaded through the sprayer head and the chip distance from the head is adjusted until the emitter end protrudes from the sprayer head exit. B) Top view photograph of the base, chip, and sprayer head in A interfaced with a Waters NanoLockSpray source. The grounding mesh has been connected to a ground potential using the yellow crocodile clip. The ESI HV cable has been removed from the base of the stage and connected directly to the sprayer head. The stage remains at ground potential. C) Side view photograph of the base, chip, and sprayer head in A interfaced with a Waters NanoLockSpray source, indicating the position of the HV application on the sprayer head and the proximity to the MS inlet (cone).*

Incorporation of the 3D printed base was necessary to insulate the microfluidic chip further from the voltage source. Utilising the standard Waters sprayer component (Figure 4.18 A) fabricated from stainless steel carried the voltage and electric field underneath the PDMS microfluidic chip, thus causing coalescence and rendering the shielding mesh useless. This change in sprayer base material did, however, require movement of the ESI high voltage (HV) cable connection from beneath the sprayer block, too directly onto the sprayer head (Figure 4.9 B and C). This was secured using silver conductive paint (RS Components, Corby, UK). The grounding cable to the stage remained in place and additionally served as the ground connection for the inserted copper gauze (Figure 4.20). Note, some removal of the outer cable heat shrink sleeve was required for the cable to stretch to its new position.

Using the modifications described above to shield droplets from the electrospray voltage, reinjection of single 1 nL leucine enkephalin (20 μM solution) droplets on a push source was successful. This is depicted by the chromatogram obtained in Figure 4.10 A. Regular rises and falls in the TIC indicate the detection of individual droplets as they are infused into the MS at a rate of ~3.5 droplets/s. Mass spectra of individual droplet contents can then be extracted (Figure 4.10 B) indicating the presence of leucine enkephalin *m*/*z*. As to be expected, increasing the droplet channel flow rate results in an increased reinjection frequency (Figure 4.10 C, ~8.5 droplets/s). The spacing oil flow rate remained constant in both cases (200 μL/hr).

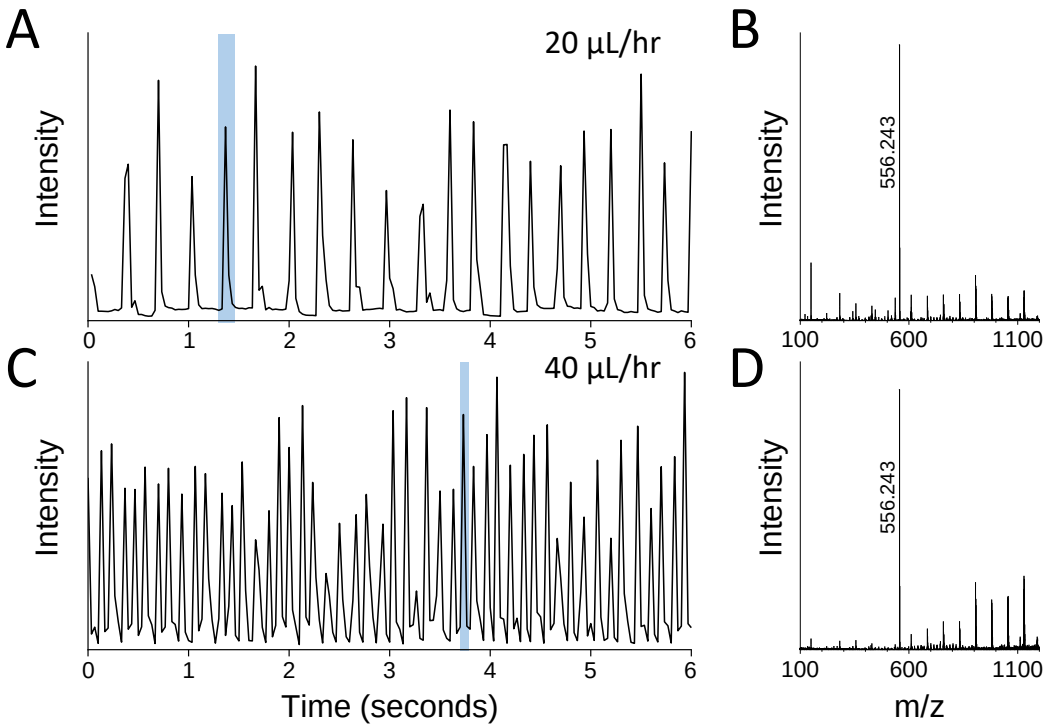


*Figure 4.10: Total ion chromatograms and mass spectra obtained from the reinjection of LeuEnk droplets (~1 nL) into a Waters Synapt G2-Si mass spectrometer using the sprayer-chip interface with insulating base and grounding mesh connected. One peak in a chromatogram corresponds to one droplet detected by the mass spectrometer. The spacing oil flow rate was 200 µL/hr in both cases. A) Droplet infusion flow rate = 20 µL/hr resulting in a droplet reinjection rate equivalent to ~3.5 droplets/s. B) Mass spectrum obtained from one droplet peak in A (peak highlighted in blue). C) Droplet infusion flow rate = 40 µL/hr resulting in a droplet reinjection rate equivalent to ~8.5 droplets/s. D) Mass spectrum obtained from one droplet peak in C (peak highlighted in blue).*

## 4.5 Extended Discussion

### 4.5.1 Droplet Coalescence and Solutions

The fusion of two liquid components can be achieved within Lab-on-a-Chip (LOC) technologies using a variety of methods, including in-flow, [31,32] light-activated, [33] and electro-coalescence. [34,35] The controlled manipulation of droplets using an electric field within droplet microfluidics (and in particular digital microfluidics [25]) is well-established, allowing for the dispensing, movement, splitting, merging [36,37] and sorting of droplets. [38] The unwanted and un-controlled electro-coalescence demonstrated in Figure 4.7 however, posed a major stumbling block to the reinjection of droplets using the push ESI source arrangement. The cause and mechanisms

surrounding this phenomenon have been elegantly described by Zagnoni *et al*. [39] One proposed cause of such 'upstream' coalescence is the effect of the electric field upon the stabilising surfactant molecules at the droplet-oil interface. In the absence of the electric field, the surfactant molecules prevent 'passive' coalescence while droplets are within the flow device. [40] The application of the penetrating electric field causes the polar surfactant molecules to re-orientate due to the electric force exerted over their dipoles. This reorientation generates variations in the surface tension along the droplet surface, with some regions becoming depleted of surfactant molecules. This surfactant interaction, in combination with other field effects described by Zagnoni *et al*., results in the destabilisation of the oil film between two droplets in close proximity and thus, coalescence ensues.

Zagnoni *et al.* demonstrated that at voltages over a certain threshold, droplet coalescence upstream of the electrode region (rather than indirect electrical contact) was possible due to the penetration of the electric field. [39] In this work a larger voltage application (1000 V vs 20 V) has been applied to the droplet microfluidic system, and with this comes electric fields that permeate over an increased distance, such as the entire length of the microfluidic chip and into the reinjection syringe. We hypothesize that a similar mechanism is occurring within the reinjection chip (design 1, Figure 4.11) and the higher voltages applied are penetrating the greater distance towards the reinjection spacing region in comparison to the shorter distances (and lesser voltages) demonstrated by Zagnoni.

To negate the coalescence effects described above, the most discernible solution is the act of distancing the adjoining droplet population from the electric field. This was achieved *via* lengthening the microfluidic chip (designs 3 and 4, Figure 4.11) and reversing the direction of the reinjection junction. This approach has been previously described by Peretzki *et al*. for the stable generation of droplets in glass microfluidic chips when coupling the chip outlet with an electrospray voltage. [24] The authors also consider an approach in which the entirety of the chip is 'floated' at the increased voltage required to generate an electrospray plume. [24] This would allow the droplets to avoid an electric field gradient when travelling towards the electrospray

emitter, and hence retain a stable droplet flow. However with droplet reinjection, care must be taken to also ensure the droplet reservoir and possibly syringe pumps also retain this increased electrical potential. This brings about a number of safety concerns regarding the placement of live voltages onto user accessible equipment and thus was not considered as a viable solution during this work. Peretzki *et al.* also note that the effect upon droplets under an applied electrical field is propagated to a greater extent in glass chips in comparison to those made of PDMS. [24] Thus, for MS coupled applications, any evolution of the microfluidic chip material in the future should be carefully considered.

Although distancing is a valid approach to reducing the electric field effects upon droplets, as the applied electrical voltage increases so does the field and the possibility that further distancing is required. As the chip design lengthens, its capacity to be described as 'miniaturised' decreases and additionally the longer microfluidic channels serve increased back pressure upon the incoming droplets. Hence, there is a limit to such distancing approach and alternative solutions are sought. As shown in Figure 4.8 and 4.9, this was achieved by the insertion of an electrically conducting copper gauze, perpendicular to the channel plane as demonstrated by Schirmer *et al*. [20] This gauze was set to ground potential and successfully circumvented the electrical field generated by the electrospray voltage from penetrating the reinjection region upon application of 1 kV.

Due to the available HV probe utilised in the experiments performed under the microscope (Figure 4.8), the effects of voltages above 1 kV upon the chip with grounded gauze could not be confirmed. Initially, this was considered to be a barrier to the transferal of the apparatus to the MS, particularly as ESI often utilises voltages in the range of 1-5 kV. Upon closer inspection of the NanoLockSpray source HV cable, it was noted that the operator chosen voltage (e.g., 1-5 kV) was not the voltage applied directly to the sprayer block due to a 32 MΩ resistance incorporated into the HV cable (Waters part: 4185077BC1-S, resistor bands shown in Figure 4.21). For example, if +1 kV were applied by the operator software, +260 V would be placed upon the sprayer block and in proximity to the microfluidic chip. This provided a strong indication

that the results obtained in Figure 4.8 D (1000 V applied) would be suitable for transferal to the ESI push source platform up to a chosen ESI operator voltage of 3.8 kV (i.e., ~1000 V on the sprayer head).

As it had been determined that lower voltages were applied directly to the chip emitter than expected, it is possible that one of the two grounding solutions (i.e., distancing or grounding gauze) could be removed. Although this was not explored in these experiments, future iterations of the chip and source design may benefit from returning to shorter chip lengths or less connecting wires to ground. The 3D printed sprayer base is one alteration of the new source setup that should not be removed, particularly if it is to be replaced by a conductive material. Its insulating properties are critical to shielding the microfluidic chip from electric fields propagating from below the supporting glass slide.

### 4.5.2 Instrument Comparisons – push versus pull

The apparatus described in Figures 4.4 and 4.9, although fulfilling the droplet-reinjection-MS workflow, will require further development before becoming a user friendly and marketable solution for high throughput screening. For instance, the clamp stand utilised in the initial pull source setup (Figure 4.4) is not a permanent solution; the fluidic connections to the microfluidic chip are difficult to access. The Bruker pull source arrangement has gone some way to resolve this issue and replaced the clamp stand with a machined steel chip holder (Figure 4.15), which can be screwed directly onto the nebuliser block. This not only gives easier access to the fluidic inlets but also allows for smoother and more facile alteration of the emitter protrusion from the nebuliser outlet. In both pull source arrangements, this protrusion is not fixed and will require optimisation every time a new chip is interfaced. Thus, standardisation of the emitter distance from the end of the chip during chip fabrication would be a worthy undertaking.

Notably, both pull ESI sources from the two vendors apply a fixed position to the nebuliser block with respect to the MS inlet (i.e., no alteration in the X, Y or Z direction). Although this position will be the preferred location for single-phase electrospray, it must be considered whether this fixed position is optimal for droplet

(i.e., dual-phase) electrospray. For example, the push source (Waters NanoLockSpray ESI) allows for such movement in the X, Y and Z directions, as well as alteration of the emitter protrusion. Alteration of these parameters may give rise to a position that is increasingly optimal for dual-phase electrospray. Conversely, fewer alterable parameters will increase the usability of the hardware setup, as trying to find the optimal position for the chip outlet with respect to the MS inlet can become troublesome due to the vast number of possible positions. Upon comparing the two fixed pull source positions (Bruker v Agilent, Figure 4.14), it is clear that there is not only one possible location for the nebuliser to produce a stable electrospray plume. While Agilent's Dual-ESI source features a nebuliser directly perpendicular to the MS inlet, Bruker's ESI adopts a tilted position. It is possible that adopting alternative nebuliser positions results in an increase in ion transmission into the MS inlet and thus, a change in sensitivity between the two pull ESI sources. As sensitivity is also reliant on several other MS factors (for example Q-TOF v QIT) and also droplet factors (e.g., size), several other experiments would be required to test this hypothesis and are beyond the scope of this article.

A major advantage to the push type source design in Figure 4.9 is the accessibility that manufacturers' stage provides to the chip. In this horizontal arrangement, the addition of the fluidic inlets is less cumbersome in comparison to the pull sources' upright or slanted arrangement (Figure 4.14). A secondary advantage to the stage is the possibility to add further fluidic structures beyond the current chip size, and still maintain a platform for the device to rest. Although this may be possible with the pull source, its upright nature is more fragile regards the emitter position and designing and building a scaffold around and above the source would be a more difficult task in comparison to using the currently available push source stage.

Considering the push source and its additional grounding solutions (Figure 4.9, Waters NanoLockSpray), the robustness of the setup requires improvement, and, in particular, the HV cable and 3D printed base attachments to the source stage and sprayer are fragile. Future iterations of the assembly should include several screw

attachments within the 3D base design to more securely hold the sprayer head component as the original stainless-steel base does (Figure 4.18). In addition, an alteration of the base design to better contain the glass slide of the chip would be worthwhile to eliminate the use of reusable blue putty adhesive. The HV attachment to the sprayer head could be more securely fixed *via* a small screw, as used in the original NanoLockSpray assembly, and would require alteration of the manufacturers' sprayer head design. This would be a welcomed addition from a safety perspective as the live HV cable is less likely to become loose during operation reducing the possibility of a shock to the operator.

## 4.6 Conclusion

To conclude, the integration of microfluidic chips with three vendors (nano)-ESI sources have been explored for droplet reinjection-MS workflows. Briefly, these sources have been segmented into those which apply the electrospray voltage directly to the incoming emitter (push type) and those which hold the emitter at ground potential (pull type). Pull type ESI sources fair well during the integration of the microfluidic chip, as only limited modifications to the manufacturer's source are required. The results obtained show clear rises and falls in the TIC corresponding to reinjected droplets. However, in the pull-type examples illustrated in this work, the need to position the chip vertical to the MS inlet may pose a problem for future additions to the apparatus due to inaccessibility around the chip location. Also, the requirement to incorporate an ESI needle of ~12 cm in length will result in increased back pressure within the chip channels. As the chip design evolves to include functionalities such as droplet splitting, this increase in backpressure could give rise to unwanted flow trajectory.

Push type ESI sources require the most modification to successfully couple droplet reinjection-microfluidic chips with MS. We have demonstrated that shielding or distancing of the reinjection region from the ESI voltage is of great importance; and in the case of the Waters SYNAPT G2-Si instrument, the setup also requires a modified base prepared from an insulating material. Implementing these modifications avoids coalescence of droplet populations prior to MS analysis,

allowing for each droplet to be considered as a discrete reaction vessel. Furthermore, the chip emitter interior must not be of conducting material for risk of droplet disruption. For example, the substitution of aluminium coated fused silica in place of the stainless-steel capillaries used previously. This being said, the greater accessibility of the stage employed by the push source exhibits greater potential to expand the chip functionalities beyond merely droplet reinjection.

In the immediate future, the development of these platforms will focus on apparatus robustness, in particular, the construction of a push source stage with components machined to more securely hold the microfluidic chip and sprayer head. Pull source modifications would benefit from the adaptation of the slide holder designed for the Bruker ESI source to more easily adjust the emitter protrusion distance out of the gas nebulising-port assembly. Applying this apparatus to a high throughput application within the biotechnology sector such as a directed evolution or biocatalysis workflow will also be key to raising the profile of this technology as a viable alternative to the traditional well plate methodologies. The current commercial ESI-Mine™ platform and associated microfluidic biochips have incorporated the functions of droplet splitting and MS signal-based sorting to address the destructive nature of MS on a pull type ion source mass spectrometer. The copper gauze shielding approach developed in this paper solved the droplet coalesces issue caused by an adjacent electrical field and allows the selection of ion source go beyond pull type only. This provides great flexibility to droplet microfluidics-MS technology, like ESI-Mine™, to be accommodated on a broader range of mass spectrometers with various ion sources from different vendors.

## 4.7 Acknowledgments

Many thanks go to Dr Andy Currin and SYNBIOCHEM (The University of Manchester) for their cell culture assistance and training, and the use of their picodroplet encapsulation system. The authors would also like to thank the National Graphene Institute (The University of Manchester) for the use of their fabrication facilities and technical assistance. The use of gauze as a grounding solution would not have been possible without Dr Konstantin Wink, Dr Andrea Peretzki and Prof.

Detlev Belder (University of Leipzig) sharing their expertise *via* E-mail, for which the authors are very grateful. In addition, we thank the FELIX Laboratory (Radboud University) for the use of their Bruker Ion Trap MS and Lisa for sample preparation of phenylalanine (F) and diphenylalanine (FF).

## 4.8 References


1 J. P. Hughes, S. S. Rees, S. B. Kalindjian and K. L. Philpott, *Br. J. Pharmacol.*, 2011, **162**, 1239–1249.

2 S. A. Sundberg, *Curr. Opin. Biotechnol.*, 2000, **11**, 47–53.

3 A. A. Hajare, S. S. Salunkhe, S. S. Mali, S. S. Gorde, S. J. Nadaf and S. A. Pishawikar, *Am. J. Pharmtech Res.*, 2014, **4**, 112–129.

4 J. W. Armstrong, *Am. Biotechnol. Lab.*, 1999, **17**, 26–28.

5 P. Jacques, M. Béchet, M. Bigan, D. Caly, G. Chataigné, F. Coutte, C. Flahaut, E. Heuson, V. Leclère, D. Lecouturier, V. Phalip, R. Ravallec, P. Dhulster and R. Froidevaux, *Bioprocess Biosyst. Eng.*, 2017, **40**, 161–180.

6 J. J. Agresti, E. Antipov, A. R. Abate, K. Ahn, A. C. Rowat, J.-C. Baret, M. Marquez, A. M. Klibanov, A. D. Griffiths and D. A. Weitz, *Proc. Natl. Acad. Sci.*, 2010, **107**, 6550–6550.

7 Y.-C. Tan, J. S. Fisher, A. I. Lee, V. Cristini and A. P. Lee, *Lab Chip*, 2004, **4**, 292.

8 Y. Zhu and Q. Fang, *Anal. Chim. Acta*, 2013, **787**, 24–35.

9 G. Perozziello, P. Candeloro, A. De Grazia, F. Esposito, M. Allione, M. L. Coluccio, R. Tallerico, I. Valpapuram, L. Tirinato, G. Das, A. Giugni, B. Torre, P. Veltri, U. Kruhne, G. Della Valle and E. Di Fabrizio, *Opt. Express*, 2015, **24**, A180.

10 A. J. Oosthoek-De Vries, J. Bart, R. M. Tiggelaar, J. W. G. Janssen, P. J. M. Van Bentum, H. J. G. E. Gardeniers and A. P. M. Kentgens, *Anal. Chem.*, 2017, **89**, 2296–2303.

11 P. Hoffmann, U. Häusig, P. Schulze and D. Belder, *Angew. Chemie - Int. Ed.*, 2007, **46**, 4913–4916.

12 E. Fradet, C. Bayer, F. Hollfelder and C. N. Baroud, *Anal. Chem.*, 2015, **87**, 11915–11922.

13 S. Hassan, A. M. Nightingale and X. Niu, *Analyst*, 2016, **141**, 3266–3273.

14 A. M. Kaushik, K. Hsieh, L. Chen, D. J. Shin, J. C. Liao and T. H. Wang, *Biosens. Bioelectron.*, 2017, **97**, 260–266.

15 T. Beneyton, S. Thomas, A. D. Griffiths, J.-M. Nicaud, A. Drevelle and T.

Rossignol, *Microb. Cell Fact.*, 2017, **16**, 18.

16 T. Beneyton, I. P. M. Wijaya, P. Postros, M. Najah, P. Leblond, A. Couvent, E. Mayot, A. D. Griffiths and A. Drevelle, *Sci. Rep.*, 2016, **6**, 27223.

17 C. A. Smith, X. Li, T. H. Mize, T. D. Sharpe, E. I. Graziani, C. Abell and W. T. S. Huck, *Anal. Chem.*, 2013, **85**, 3812–3816.

18 K. Wink, L. Mahler, J. R. Beulig, S. K. Piendl, M. Roth and D. Belder, *Anal. Bioanal. Chem.*, 2018, **410**, 7679–7687.

19 X. W. Diefenbach, I. Farasat, E. D. Guetschow, C. J. Welch, R. T. Kennedy, S. Sun and J. C. Moore, *ACS Omega*, 2018, **3**, 1498–1508.

20 M. Schirmer, K. Wink, S. Ohla, D. Belder, A. Schmid and C. Dusny, *Anal. Chem.*, 2020, **92**, 10700–10708.

21 L. Mahler, K. Wink, R. J. Beulig, K. Scherlach, M. Tovar, E. Zang, K. Martin, C. Hertweck, D. Belder and M. Roth, *Sci. Rep.*, 2018, **8**, 13087.

22 ESI-Mine™: A label-free platform for high-throughput, miniaturised electrospray injection mass spectrometry (ESI-MS), https://spherefluidics.com/products/high-throughput-electrospray-injection-mass-spectrometry/?v=79cba1185463, (accessed 8 February 2021).

23 X. C. I. Solvas and A. deMello, *Chem. Commun.*, 2011, **47**, 1936–1942.

24 A. J. Peretzki, S. Schmidt, E. Flachowsky, A. Das, R. F. Gerhardt and D. Belder, *Lab Chip*, 2020, **20**, 4456–4465.

25 K. Choi, A. H. C. Ng, R. Fobel and A. R. Wheeler, *Annu. Rev. Anal. Chem.*, 2012, **5**, 413–440.

26 J. C. Mcdonald, D. C. Duffy, J. R. Anderson, D. T. Chiu, H. Wu, O. J. Schueller and G. M. Whitesides, *Electrophoresis*, 2000, **21**, 27–40.

27 S. Tang and G. Whitesides, in *Optofluidics: Fundamentals, Devices, and Applications*, 2010, pp. 7–32.

28 E. E. Kempa, C. A. Smith, X. Li, B. Bellina, K. Richardson, S. Pringle, J. L. Galman, N. J. Turner and P. E. Barran, *Anal. Chem.*, 2020, **92**, 12605–12612.

29 D. Morsa, E. Kempa, I. Stroganova, A. Piruska, W. T. S. Huck, P. Nghe, E. Szathmáry, W. Hordijk, J. Commandeur, S. Otto and A. M. Rijs, in *Public*

*deliverable for the ATTRACT Final Conference*, 2020.

30 D. Sarkar, D. Trived, E. Sinclair, S. H. Lim, C. Walton-Doyle, K. Jafri, J. Milne, M. Silverdale and P. E. Barran, , DOI:https://doi.org/10.26434/chemrxiv.12517385.v1.

31 N. Bremond, A. R. Thiam and J. Bibette, *Phys. Rev. Lett.*, 2008, **100**, 1–4.

32 X. Niu, S. Gulati, J. B. Edel and A. J. deMello, *Lab Chip*, 2008, **8**, 1837.

33 C. N. Baroud, M. Robert De Saint Vincent and J. P. Delville, *Lab Chip*, 2007, **7**, 1029–1033.

34 M. Zagnoni, G. Le Lain and J. M. Cooper, *Langmuir*, 2010, **26**, 14443–14449.

35 A. Srivastava, S. Karthick, K. S. Jayaprakash and A. K. Sen, *Langmuir*, 2018, **34**, 1520–1527.

36 S. K. Cho, H. Moon and C. J. Kim, *J. Microelectromechanical Syst.*, 2003, **12**, 70–80.

37 M. G. Pollack, A. D. Shenderov and R. B. Fair, *Lab Chip*, 2002, **2**, 96–101.

38 J.-C. Baret, O. J. Miller, V. Taly, M. Ryckelynck, A. El-Harrak, L. Frenz, C. Rick, M. L. Samuels, J. B. Hutchison, J. J. Agresti, D. R. Link, D. A. Weitz and A. D. Griffiths, *Lab Chip*, 2009, **9**, 1850.

39 M. Zagnoni, C. N. Baroud and J. M. Cooper, *Phys. Rev. E - Stat. Nonlinear, Soft Matter Phys.*, 2009, **80**, 046303.

40 G. Etienne, M. Kessler and E. Amstad, *Macromol. Chem. Phys.*, 2017, **218**, 1600365.

## 4.9 Supporting Information

### 4.9.1 Cell culture in Droplets (Main Paper, Figure 4.1)

25 μL of NEB 5—alpha Competent *E. coli* cells (New England BioLabs Inc., Ipswich, Massachusetts, United States) were added to 1 μL of pBbB11a plasmid (Addgene plasmid # 126114; http://n2t.net/addgene:126114 RRID: Addgene_126114)[S1] and mixed gently. Heat shock at 42 °C was performed for 30 seconds before allowing to rest on ice for 5 minutes. 475 μL of SOC media was added to the Eppendorf before incubation at 37 °C for 1 hr (200 rpm). 40 μL of water and 10 μL of the cell mixture were streaked onto an agar plate with ampicillin (100 μL), before incubation overnight at 37 °C. Cultures were picked and added to 2 mL of LB media containing ampicillin (0.1 %) and incubated for 2 hrs at 37 °C (200 rpm). Absorbance measurements at 600 nm were recorded and samples spun down (3 mins, 3000 rpm). The supernatant was removed from the cell pellet and stored at -80 °C until required.

TB media containing glycerol (0.4%) and ampicillin (0.1%) was filtered through a 0.2 μm syringe filter before reconstitution of the cell pellet to a cell density of ~1 x $10^9$ as per the absorbance measurements recorded before storage. A further 1000-fold dilution was performed, and the resulting solution placed in a 1 mL syringe for droplet generation. A population of highly monodisperse droplets (~450 pL in volume) were generated using the Picodroplet Single Cell Encapsulation System (Sphere Fluidics Ltd., Cambridge, UK). The continuous phase consisted of Novec™ 7500 Engineered Fluid (3M, Maplewood, MN, USA) containing 1 % Pico-Surf™ 1 (Sphere Fluidics Ltd, Cambridge, UK). Droplet populations were collected in Eppendorf's and incubated upright at 30 °C overnight (200 rpm).

10 μL of the incubated droplet population were deposited onto a glass microscope slide and images captured at 10x magnification using an Axio Vert A1 microscope (Carl Zeiss AG, Oberkochen, Germany) equipped with Motion BLITZ EoSens mini camera (Mikrotron GmbH, Unterschleißheim, Germany).

### 4.9.2 Microfluidic Chip Designs and Fabrication

#### 4.9.2.1 Designs

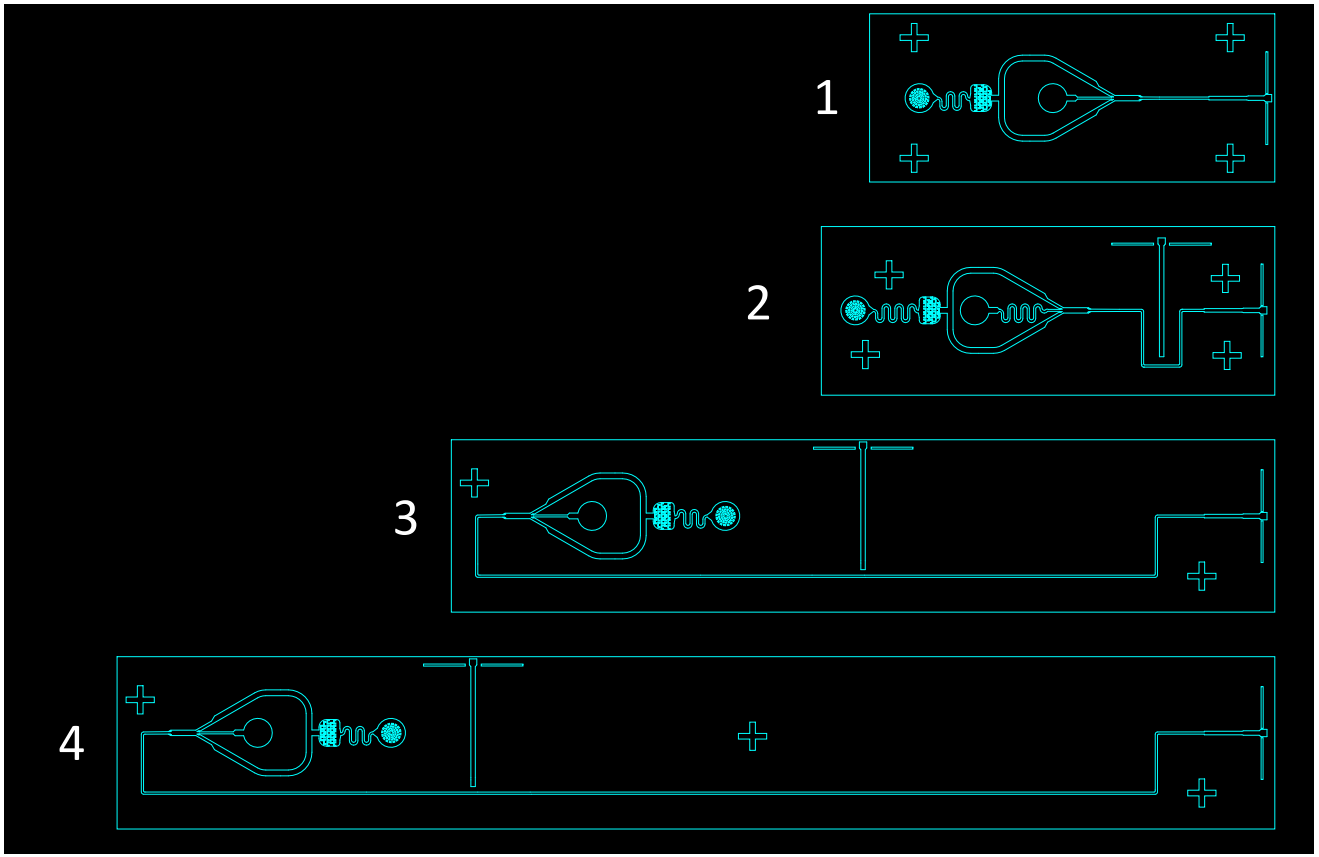


*Figure 4.11: Microfluidic chip designs 1-4 used in this article, arranged in order chip length.*

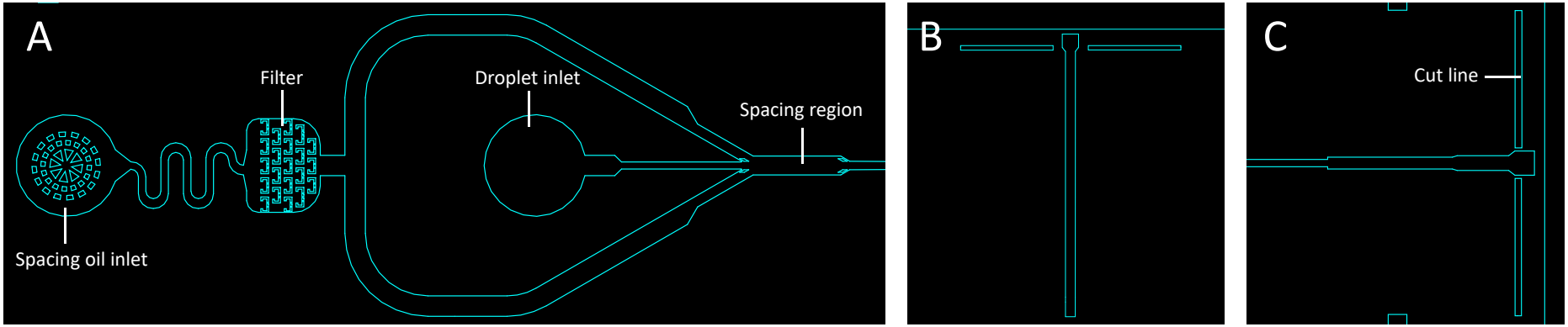


*Figure 4.12: Magnification of important regions in the Microfluidic chip designs. A) Reinjection region highlighting the tubing inlets and rejection spacing region. B) Mesh cut marker. C) Emitter insertion region.*

#### 4.9.2.2 Chip Fabrication including Emitter Insertion

Microfluidic chip designs were drawn using DraftSight software (Dassault Systèmes, Vélizy-Villacoublay, France) before being converted to a film photomask (Micro Lithography Services Ltd, Essex, UK). Device masters were produced by spinning SU-8 2025 epoxy negative photoresist (MicroChem, MA, USA) to a depth of 70 μm upon a silicon wafer. The resulting wafer was baked prior to exposure of the SU-8 2025 using an MJB-4 mask aligner (SUSS MicroTec SE, Garching, Germany), and subsequently, a post-exposure bake was also performed. Designs were developed through the submersion of the exposed wafer in MICRODEPOSIT ™ EC solvent (Dow Chemical Company, MI, USA), rinsed, dried, and baked again to cement the SU-8 design on to the wafer. The master was placed in a petri dish and a mixture of Sylgard 184 silicone elastomer (10:1, base: curing agent, Dow Chemical Company, MI, USA) added to the dish to the required device thickness. The elastomer was then degassed in a vacuum desiccator and baked overnight at 70 °C. Removal of the elastomer from the silicon-SU-8 master was performed using a scalpel to expose the design face, and fluidic connections were added using a 1.00 mm biopsy punch (Kai Medical, Solingen, Germany). Microfluidic chip MS designs consist of both a bottom and a top piece, each containing differing design features. The non-feature containing faces of the bottom piece of each design, along with a glass microscope slide, were exposed to oxygen plasma (Harrick Plasma, NY, USA), and the plasma exposed surfaces bound together. A further round of oxygen plasma activation was then performed upon the feature containing surfaces of both the bottom and the top piece of the PDMS device before these two pieces were bound together employing methanol (~10 μL) as a lubricant to ensure the design on each surface were aligned with one another. The device was then baked overnight at 110 °C, prior to insertion of the stainless-steel capillary (OD 176 μm, ID 76 μm, Vita Needle Company, Needham, MA, US). Insertion of the capillary was performed under a microscope, ensuring the capillary came into contact with the end of the pre-designed channel, and ELASTOSIL E43 silicone sealant (Wacker Chemie AG, München, Germany) added to the PDMS-capillary interface and allowed to solidify.

#### 4.9.2.3 Mesh Insertion

After assembly of the double-layer microfluidic chip (designs 2, 3 and 4, Figure 4.11) a small section of PDMS was cut away using a scalpel (Figure 4.13 A) using the mesh cut marker as a guide to the cut location. The removed section of PDMS spanned the entire depth of the microfluidic chip. A small piece of copper gauze (60 mesh woven from 0.19mm diameter wire, Alfa Aesar, Haverhill, MA, USA) was cut to size (30 mm x 5 mm) and slotted into the cut-out section of the chip. ELASTOSIL E43 silicon sealant (Wacker Chemie AG, München, Germany) was added around the inserted mesh and allowed to dry to ensure the copper mesh did not move during use.

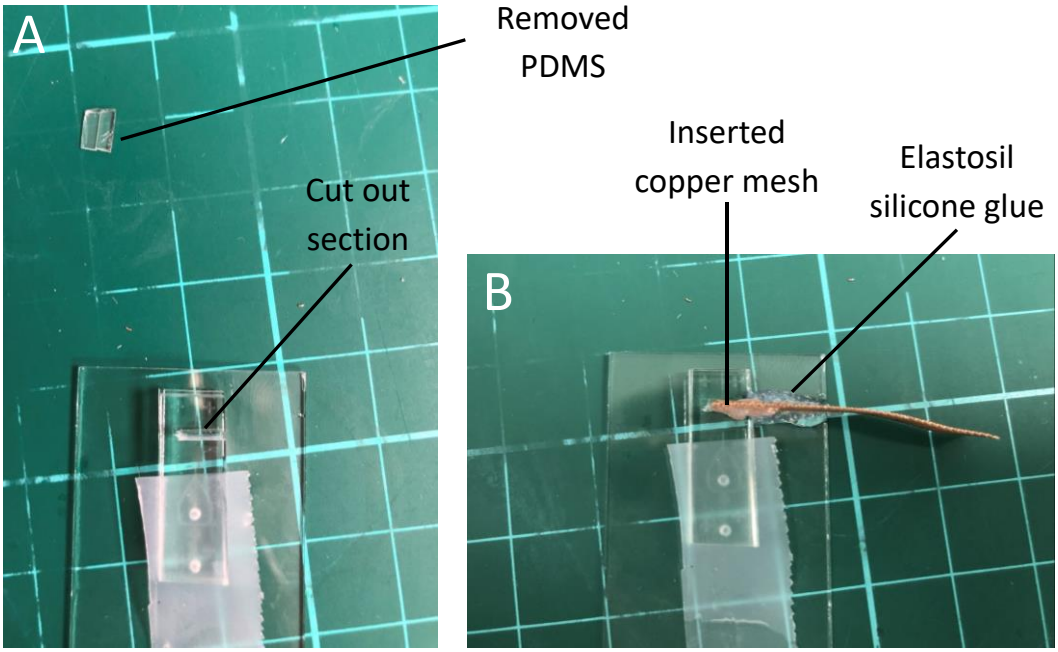


*Figure 4.13: Copper mesh insertion photographs. A) Photograph indicating the location of the cut and the removed PDMS section from the chip. B) Photograph showing the copper gauze inserted in the microfluidic chip and sealed in place with ELASTOSIL glue*

### 4.9.3 Instrument Coupling Photos

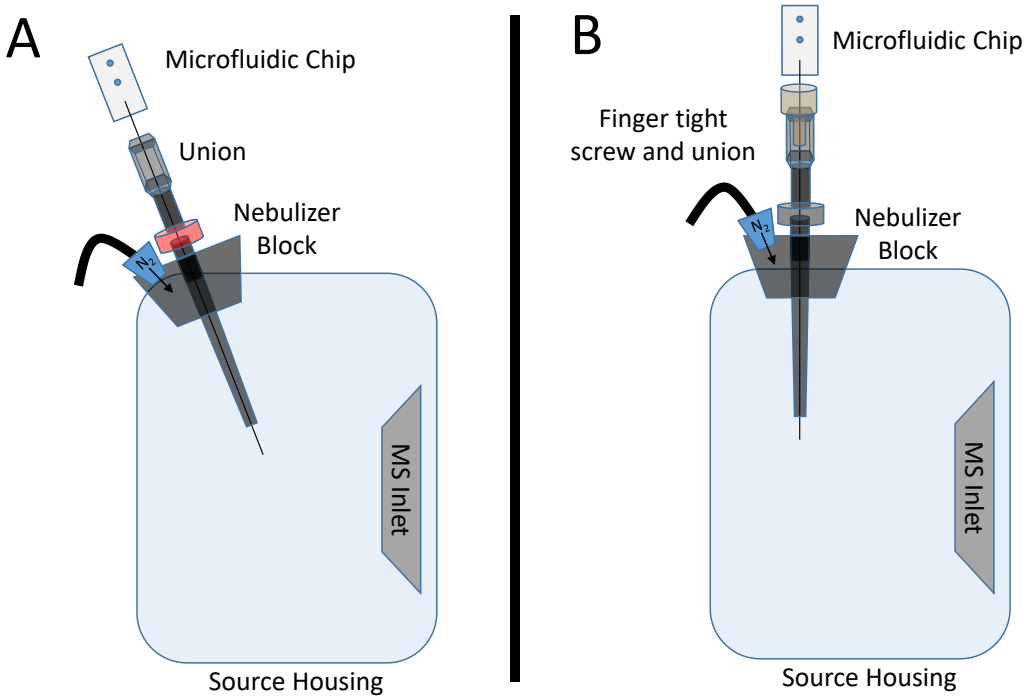


*Figure 4.14: Pull ESI source schematics with integrated microfluidic chip component. A) Bruker ESI source configuration, indicating nebuliser block in an off-axis arrangement. B) Agilent Dual ESI source configuration, nebuliser block is perpendicular to the MS inlet.*

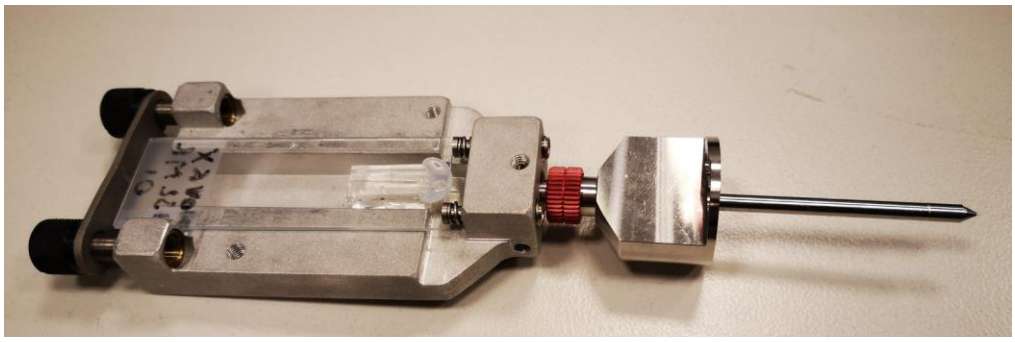

*Figure 4.15: Photograph of the stainless-steel adaption fabricated above the Bruker ESI source nebuliser to hold the microfluidic chip more securely in place and remove the need for the supporting clamp stand.*

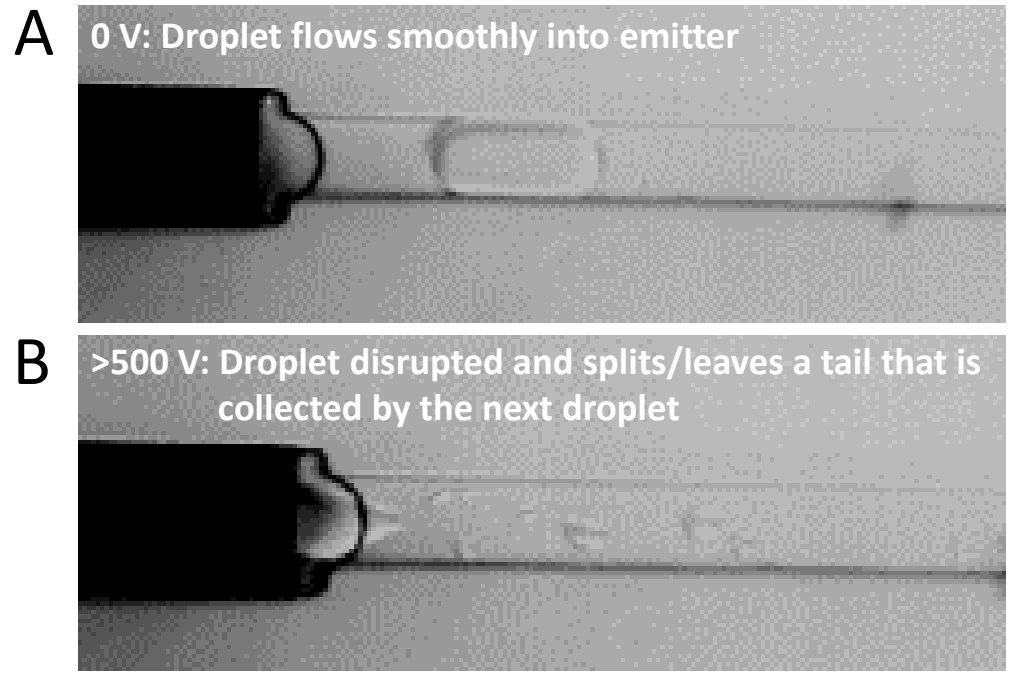


*Figure 4.16: Microscope images of stainless-steel emitters inserted into PDMS chips with droplets flowing into the emitter from the chip channel. A) Uninterrupted droplet form when no voltage applied to the emitter. B) Disrupted droplet flowing into the emitter when the voltage on the emitter is greater than 500 V.*

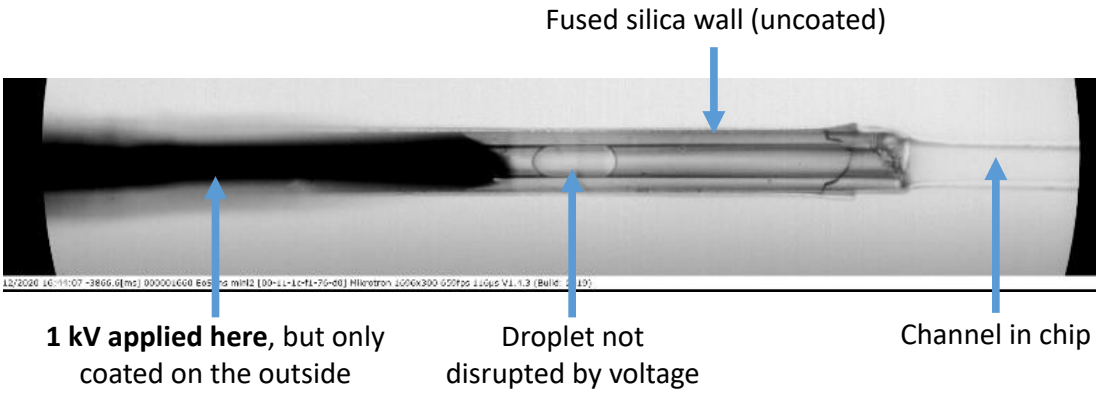


*Figure 4.17: Microscope image of a fused silica emitter with an outer coating of aluminium, inserted into a PDMS chip with a droplet flowing into the emitter from the chip channel. 1 kV has been applied to the aluminium outer coating only and the droplet form has not been disrupted.*

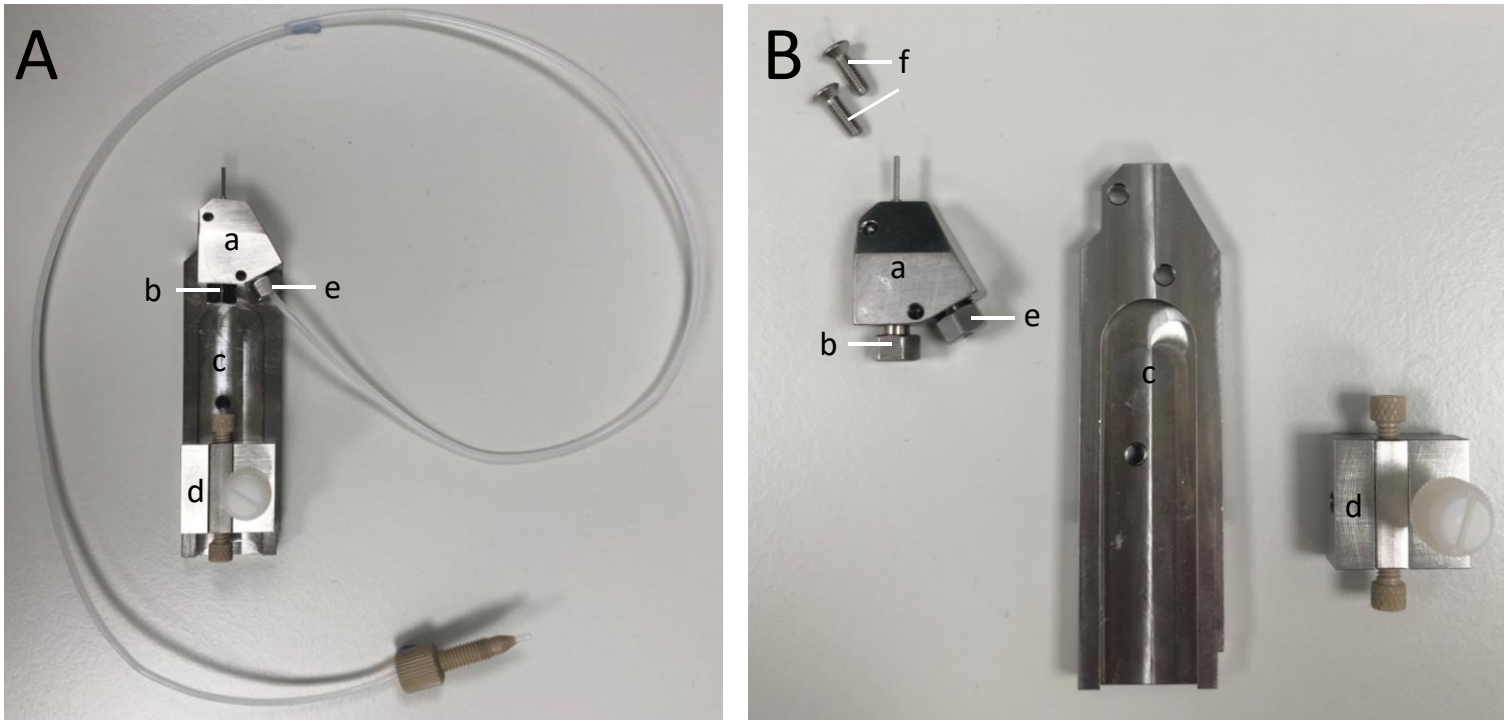


*Figure 4.18: A) Fully assembled Waters universal sprayer probe (P/N: 700003890). B) Waters universal sprayer probe with major components disassembled. Labelled components are as follows in both photographs with some referred to throughout the main text: a) Sprayer head, b) Screw with conductive ferrule inside (chip emitter is threaded through here), c) Sprayer base (stainless steel), d) fused silica connection, (this component is not used in any chip assembly discussed in this work) e) screw with N2 gas line connected, f) small screws (x2) which fix the Sprayer head, a, to the base,*

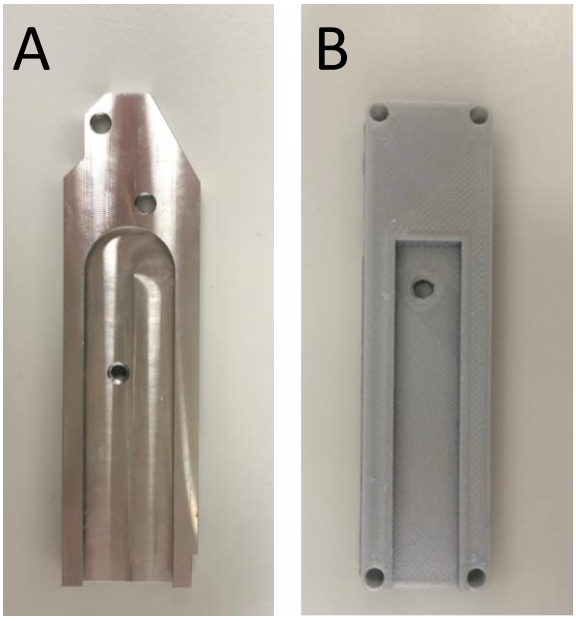


*Figure 4.19: A) Photograph of the stainless-steel base from the Waters universal sprayer probe (P/N: 700003890), with all other connecting components removed. B) Photograph of the 3D printed base used to hold the microfluidic chip in the push source solution assembly. This plastic component (polylactic acid, PLA) replaces the stainless-steel base in A.*

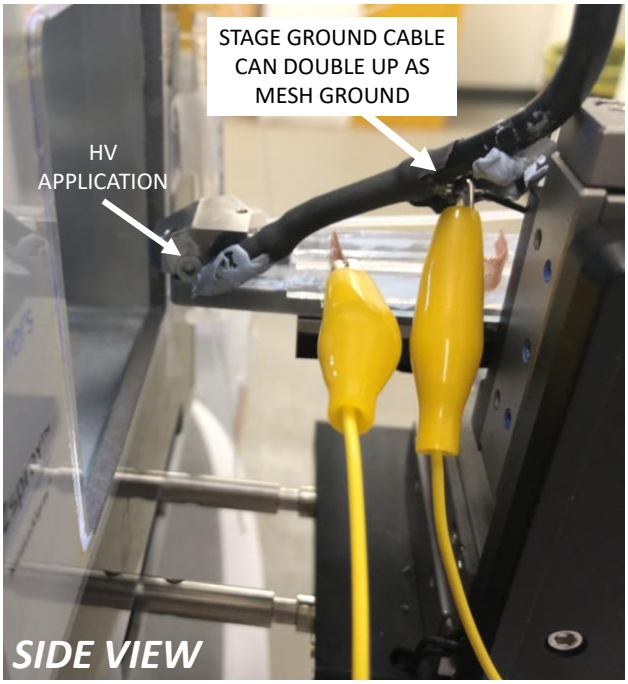


*Figure 4.20: Side view photograph of the base, chip, and sprayer head in Figure 4.9 A (main paper) interfaced with a Waters nanoESI source, indicating the position of the HV application on the sprayer head and the use of the grounding wire inside the HV cable as the ground for the copper mesh (inserted in the chip). The ground wire is connected to the mesh with yellow crocodile clips.*

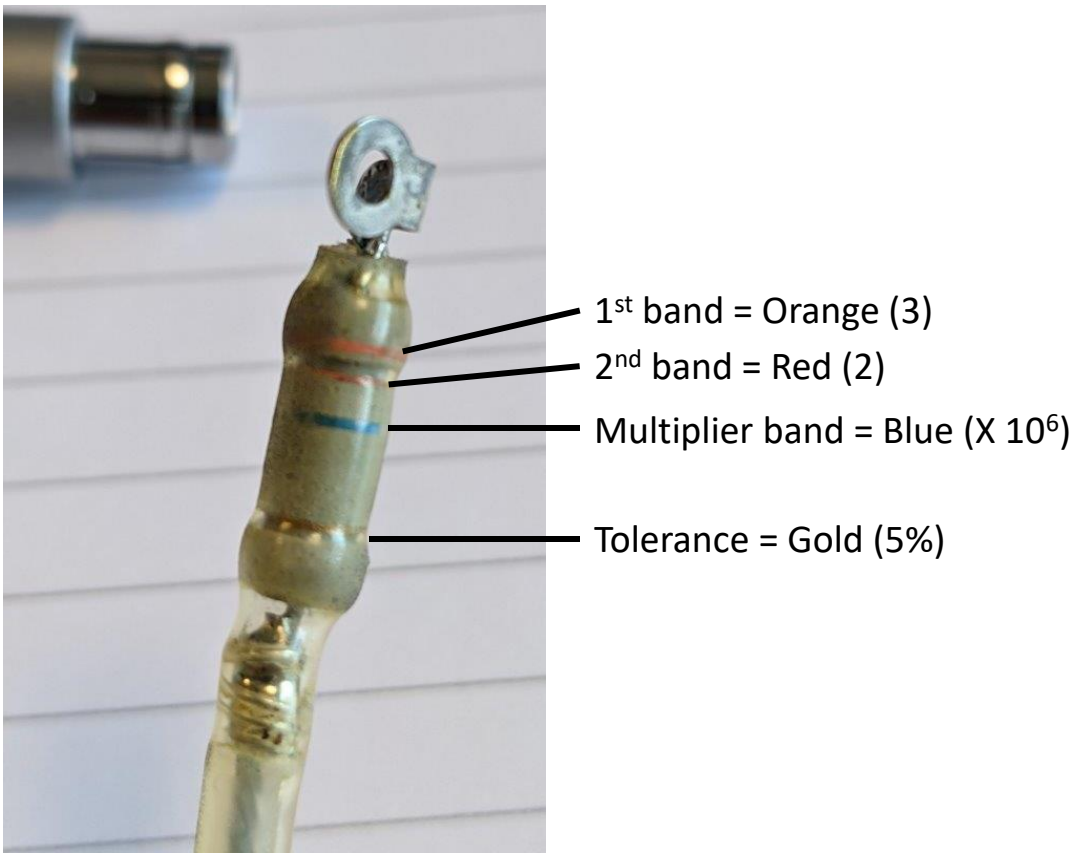


*Figure 4.21: Photograph of resistor inside nESI source HV cable (Waters part: 4185077BC1-S). Resistor band colours are labelled and measured to be 32 x $10^6$ ohms (32 MΩ).*

### 4.9.4 Mass Spectrometry Parameters

*Table 4.1: Agilent 6560 ESI-Q-TOF MS parameters.*

| Parameter | Value |
|---|---|
| **Polarity** | Positive |
| **Gas Temp** | 200 °C |
| **Drying Gas** | 3 L/min |
| **Nebulizer** | 30 PSIG |
| **Sheath Gas Temp** | 200 °C |
| **Sheath Gas Flow** | 10 L/min |
| **VCap** | 2500 V |
| **Nozzle Voltage** | -2000 V |
| **Mass Range** | 300-1700 *m/z* |
| **Scan Rate** | 40 scans/s |

*Table 4.2: Bruker amaZon speed ESI-QIT MS parameters.*

| Parameter | Value |
|---|---|
| **Polarity** | Positive |
| **Gas Temp** | 150 °C |
| **Drying Gas** | 3 L/min |
| **Nebulizer** | 7.2 psi |
| **Capillary** | 4500 V |
| **Offset Voltage** | 500 V |
| **ICC** | On |
| **ICC Target** | 20000 |
| **Max Acquisition Time** | 3.00 ms |
| **Averages** | 1 |
| **Rolling Average** | Off |
| **Mass Range** | 100-700 *m/z* |
| **Scan Rate** | 52000 *m/z* / s (Xtreme) |

*Table 4.3: Waters SYNAPT G2-Si (nanoESI-Q-TOF) MS parameters.*

| Parameter | Value |
|---|---|
| **Polarity** | Positive |
| **Capillary** | 2.5 kV |
| **Sampling Cone** | -70 V |
| **Source Offset** | 0 V |
| **Gas Temp** | 150 °C |
| **Nano Flow Gas** | 0 Bar |
| **Mass Range** | 100-1200 *m/z* |
| **Scan Time** | 0.016 s |
| **ISD (Inter scan delay)** | 0.015 s |
| **Scan Rate** | ~ 32 scans/s |

### 4.9.5 Additional Results

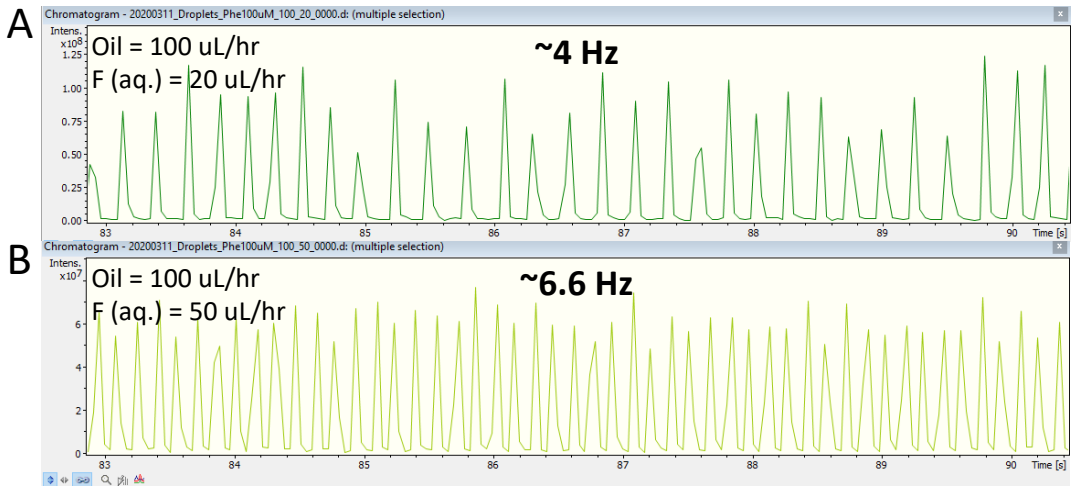


*Figure 4.22: Chromatographic results (~7 seconds) obtained from a droplet generation-MS experiment performed on a Bruker amaZon speed (ESI-QIT) mass spectrometer. In each case, the aqueous phase consisted of a 100 µM solution of phenylalanine (F) in water. The continuous phase (oil) consisted of 1 % Pico-Surf™ 1 in Novec™ 7500 Engineered Fluid. The continuous phase flow rate remained at 100 µL/hr in both cases. A) Aqueous flow rate = 20 µL/hr, with a resulting droplet infusion rate of ~4 droplet/s. B) Aqueous flow rate = 50 µL/hr, with a resulting droplet infusion rate of ~6.6 droplet/s.*

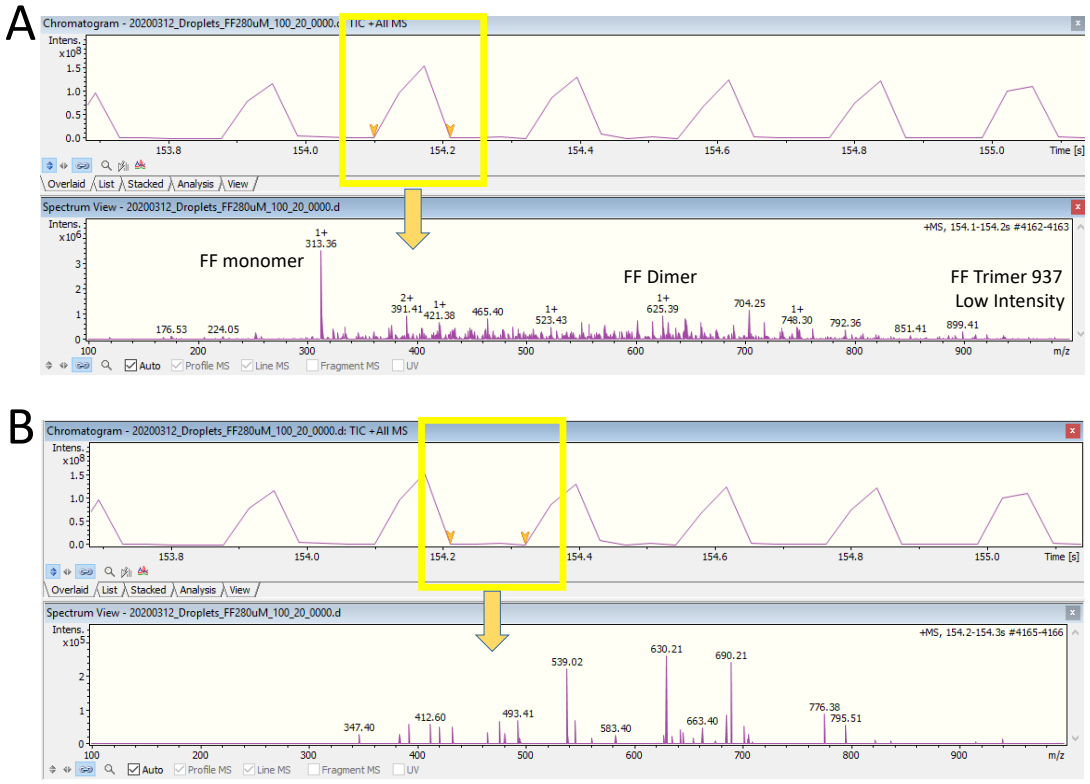


*Figure 4.23: Chromatographic and MS results obtained from a droplet generation-MS experiment performed on a Bruker amaZon speed (ESI-QIT) mass spectrometer. The aqueous phase consisted of a 280 μM solution of diphenylalanine (FF) in water and the continuous phase (oil) consisted of 1 % Pico-Surf™ 1 in Novec™ 7500 Engineered Fluid. Continuous phase flow rate = 100 μL/hr, aqueous (FF) flow rate = 20 μL/hr. A) Mass spectrum extracted from 1 droplet peak (highlighted in the yellow box). Features in the mass spectrum including the FF monomer, dimer and trimer have been highlighted. B) Mass spectrum extracted from between 2 droplet peaks (highlighted in the yellow box). No FF signal is observed.*

Data and methodology concerning reinjection of droplets on the ESI-QIT instrumentation (Bruker amaZon speed) can be found at https://attract-eu.com/wp-content/uploads/2019/05/EmLife.pdf [S2]

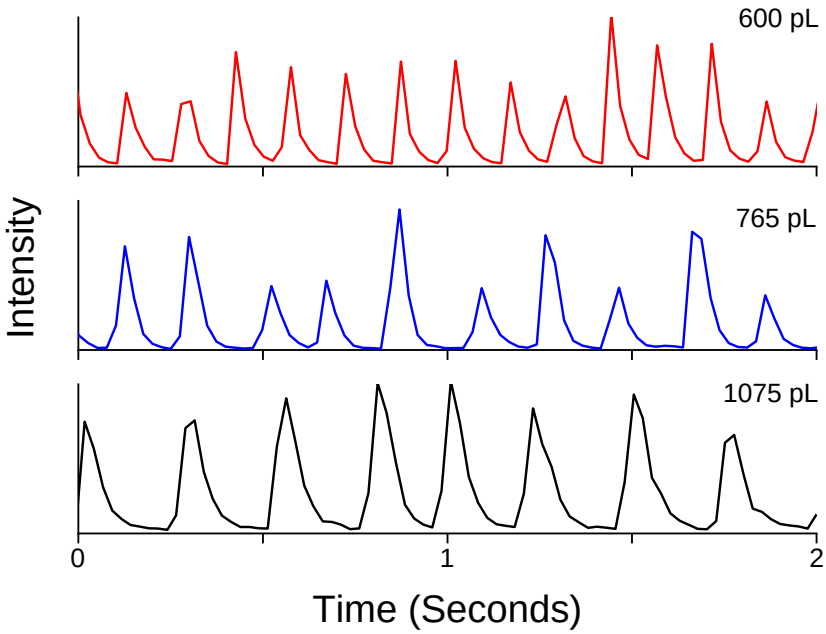


*Figure 4.24: Additional results from a (pull source) droplet reinjection-MS experiment performed on an Agilent 6560 (ESI-Q-TOF) mass spectrometer. The aqueous phase (droplets generated prior to reinjection) in each case consisted of a 20 μM solution of leucine enkephalin in aqueous ammonium acetate solution (100 mM) and the continuous phase (oil) consisted of 1 % Pico-Surf™ 1 in Novec™ 7500 Engineered Fluid. Continuous phase flow rate = 320 μL/hr, aqueous (LeuEnk droplets) flow rate = 20 μL/hr. Three different droplet sizes (600 pL, 765 pL and 1075 pL) were generated and reinjected on to the system and the chromatograms recorded. As the droplet volume increases the reinjection frequency under the same flow rates decreases.*

### 4.9.6 Supporting Information References

[S1] A. J. Jervis, P. Carbonell, S. Taylor, R. Sung, M. S. Dunstan, C. J. Robinson, R. Breitling, E. Takano, and N. S. Scrutton, *ACS Synthetic Biology*, 2019, **8**, 1478-1483.

[S2] D. Morsa, E. Kempa, I. Stroganova, A. Piruska, W. T. S. Huck, P. Nghe, E. Szathmáry, W. Hordijk, J. Commandeur, S. Otto, A M. Rijs, *Public deliverable for the ATTRACT Final Conference*, Emerging Life (EmLife): Technology for the High- Throughput Analysis of the Molecular Composition of Small Volumes, https://attract-eu.com/wp-content/uploads/2019/05/EmLife.pdf.

# 5

# Conclusions and Future Outlook

High throughput screening (HTS) within the biotechnology and pharmaceutical industries is increasingly in demand to accelerate the discovery of new enzymes, therapeutics, chemical entities and biomarkers. HPLC and fluorescence measurements go some way to satisfying the demand in throughput, but both are not without flaws and are limited by their reliance upon incorporated chromophores or fluorophores to enable detection. Thus, the movement towards label-free approaches based on mass spectrometry (MS) is prompting promising developments in both commercial and academic high throughput technologies. MS-coupled platforms such as RapidFire and TriVersa ChipMate offer throughputs as low as 7 seconds/sample with emerging acoustic mist ionisation and droplet microfluidic technologies reaching a sub-second sample infusion rate. The expansion of MS detection towards complex biological samples is also paramount with challenges remaining surrounding contamination, ion suppression and carryover, particularly for samples with high salt content and/or containing cellular material. Sensitivity is also a key issue to address during the infusion of complex samples, as single-cell analysis is gaining traction within academic groups. Investigations into cellular heterogeneity can be realised using several newly described MS-coupled techniques, including nanoPOTS and fluid force microscopy-coupled MALDI-MS. Many, however, do not satisfy high throughput criteria.

Chapter 2 is a collection of the methods used within this thesis, translated into a 'how-to-guide' format. These methods range from newly developed protocols (DESI-MS for biocatalyst screening) to those that are well established in the literature (microfluidic chip fabrication). In both cases, these methods are adapted to the facilities available to The University of Manchester researchers. However, that does not mean that they are not translatable to alternative settings. It is important to note that microfluidic chip fabrication extends far beyond the methodologies used in this thesis, with different chip materials such as glass and silicon requiring equally extensive protocols. For researchers embarking on a microfluidic project of which their chosen chip design is not commercially available, they should be prepared to delve deeply into the field of microfabrication, learning several new skills along the way.

Chapter 3 demonstrates the use of DESI-MS technology for the high throughput screening of biotransformations (termed DiBT-MS). The screening workflow utilises a well plate format that is commonplace within laboratories worldwide. This will not only appeal to researchers due to its familiar nature but will also allow for translatability between other analytical platforms and facile identification of wells (reactions) of interest. This work applies the screening protocol to a range of three differing biotransformations (kinases, IREDs and PALs), alongside illustrating the workflows versatility towards reactions utilising purified enzymes, lysates or whole cells. For kinase reactions, throughputs of 42 s/sample are achieved, indicating a 37-fold increase on the alternative NMR assay. In addition to the increase in throughput, the incorporation of ion mobility technology increases the identification confidence of perceived 'hits' due to the additional drift-time marker obtained alongside the *m*/*z* ratio. Although quantification is not explicitly demonstrated, the obtained MS signal is linear over the range of 5 to 100 μM for two test compounds (phosphorylated sugars). Additional comparisons with quantitative LC-MS and NMR data indicate the possibility for quantitative analysis in the future.

Application of the workflow to a directed evolution experiment was key to identifying new PAL variants with enhanced activity towards electron-rich cinnamic acid derivatives that are significant for lignose biomass degradation. In short, key active site residues were identified using blast sequence alignment and mutated in pairs using selected amino acids. This produced 3 libraries of which 288 possibilities were screened using the DiBT methodology. Identification and subsequent preparative scale reactions for several variants resulted in significantly improved reaction yields in comparison to the wild type enzyme.

Chapter 4 explores droplet microfluidics coupled with MS as an alternative to the DiBT-MS screening employed in Chapter 3. This technology is less well established with little commercial instrumentation of the sort available in comparison to DESI-MS. This chapter focuses primarily on the interfaces between a droplet microfluidic chip and 3 differing mass spectrometers, whilst still utilising the MS manufacturer's supplied ion source. Comparisons between the manufacturers are

made regarding ease of coupling, ease of use and the maximum possible MS scan rates – an important parameter when considering future high throughput screening applications.

Infusion of droplets *via* a stainless steel capillary emitter inserted into the PDMS microfluidic chip was achieved with all three coupled platforms with clear chromatographic outputs visualised from the obtained MS data. Peaks in the chromatogram arise at the rate of droplet infusion, allowing mass spectra of individual droplets to be obtained. Analysis of the peak arrival frequency denotes the sample throughput with rates of 6 Hz achieved on an Orbitrap platform, and up to 33 Hz on a Q-TOF platform using a variant of the SONAR acquisition mode developed by Waters. In addition to focusing upon throughput, expansion of the sample breadth was also demonstrated with small molecules, peptides and proteins that are all detectable by droplet-MS. This was further extended to the analysis of salty protein mixtures, biotransformation supernatant, crude egg white solution with the aspiration to infuse intact bacterial colonies for directed evolution studies in the future.

Chapter 5 extends the work illustrated in Chapter 4 towards a workflow that is more suited to high throughput biotechnology applications. Here, droplet generation-MS (explored in chapter 4) is interchanged with droplet reinjection-MS, allowing for the storage, incubation or manipulation of pre-formulated droplets before analysis. Unfortunately, droplet reinjection-MS comes with its challenges, the most notable of these being droplet coalescence brought about by the application of the electrospray voltage directly onto the chip emitter. Overcoming this challenge required further modification of the chip or MS manufacturer's ion sources to either distance or shield the incoming droplet population from the electrospray voltage. This was achieved *via* the insertion of grounded copper gauze into the body of the PDMS chip, preventing the electric field from penetrating the droplet reinjection region. Further modifications included the use of an insulating 3D-printed base in place of the manufacturer's universal sprayer and alteration of the emitter composition to prevent direct electrical contact with the interior droplet emulsion.

Ultimately, droplet reinjection–MS was attained on three differing mass spectrometers with the intent to transfer the newly identified reinjection solutions towards a refined and user-friendly commercial solution for high throughput screening.

To conclude, the development of two different high throughput, mass spectrometry screening platforms has been achieved for the analysis of complex biological samples. Albeit the slower of the two, the DiBT-MS workflow has successfully been applied to a direct evolution experiment identifying enzyme variants with improved product conversion. Conversely, the droplet microfluidic-MS platform still requires improvement to become a commercial solution and evidence to cement its applicability to screening scenarios. However, there is no doubt that upon the refinement of such a platform, the throughput it affords will see current screening methodologies made redundant.

# 6

# Appendix

## 6.1 Declaration and Preface

This appendix consists of a series of experimental 'How-to-Guides' I have written to accompany Chapters 2, 3 and 4. These guides provide step-by-step instructions for much of the experimental methods undertaken in this thesis, some of which I have developed myself in the laboratory, and others that I have learnt from external collaborators and adapted in Manchester for my research needs using the equipment available.

As the first member of the Perdita Barran Research Group to research the area of droplet microfluidics, many of the experimental methods (in particular microfluidic chip fabrication) were new to the group. As such, these 'How-to-Guides' will remain in the laboratory as a tool for future members of the group continuing with this research. Although the following guides reference specific instrumentation, materials and locations, such methods could be adapted for other laboratories wishing to undertake similar experiments. Laboratory-independent descriptions of the experiments can be found in the appropriate results chapters.

As a guide, the following sections in this chapter can be associated with methods in the subsequent results chapters:

- Section 6.2 for methods used in Chapter 2
- Section 6.3 for methods used in Chapters 3 and 4
- Section 6.4 for methods used in Chapters 3 and 4
- Section 6.5 for methods used in Chapter 4.

## 6.2 DESI Methods

### 6.2.1 DESI-MS Methods Introduction

The following guide provides step-by-step instructions to screen liquid samples from a 96-well plate using DESI-MS as shown in Chapter 3. Well plate samples are deposited in a microarray format for analysis, with the resulting *m/z* heat map output allowing for straightforward identification of wells of interest. Recommended stage speeds and pixels sizes are provided to obtain the optimal sample throughput without compromising the spatial resolution of the heat map output. This guide assumes some prior knowledge about the Waters SYNAPT mass spectrometer with DESI-MS source. If unsure, contact the designated trainer for the instrumentation.

Prior to screening well plate samples for a new compound using DESI-MS, it is advised to prepare and analyse chemical standards for the compounds of interest to optimise MS (polarity, capillary and cone voltage) and DESI parameters (solvent composition and sprayer head positioning).

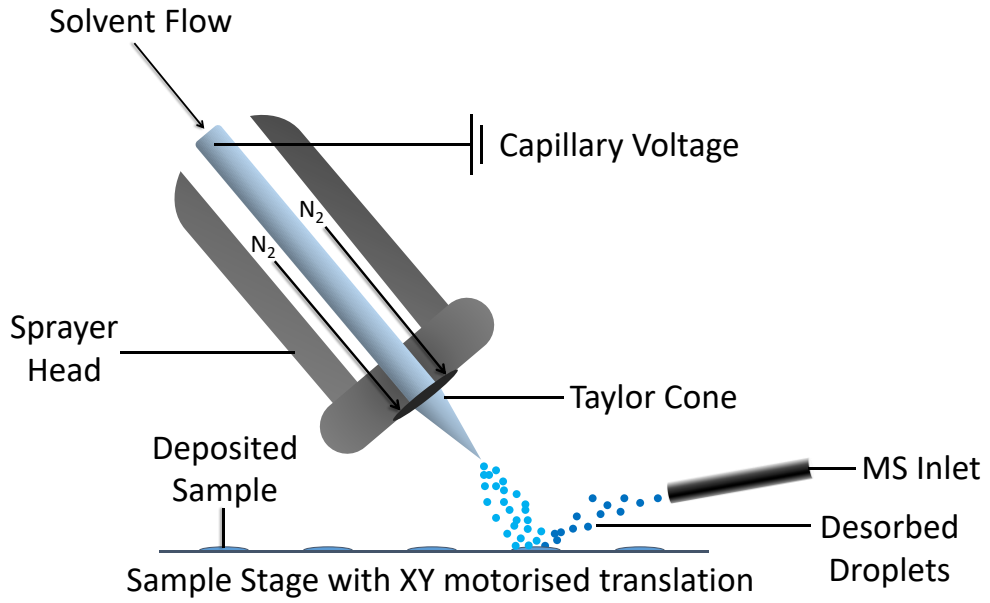


*Figure 6.2.1: DESI-MS schematic illustrating the major components of the DESI source. A capillary voltage and gas pressure (co-axial) are applied to the DESI solvent flow to generate a Taylor cone. Ionised solvent droplets from the Taylor cone impact the stage surface causing surface analytes to be desorbed and transferred to the MS inlet for analysis.*

### 6.2.2 DESI-MS set up

1. Fill a syringe with the required DESI-MS solvent, load into the syringe pump and turn on the flow at a rate of 5 μL/min to flush the DESI solvent line.

2. After 30 minutes decrease the solvent flow to 2.5 μL/min.

3. Switch on the nitrogen tap on the right-hand side of the DESI stage ($N_2$ Pressure is typically set between 2 and 4 bar. This can be altered depending on the experiment).

4. Switch the SYNAPT mass spectrometer to operational and set the desired capillary voltage in the MassLynx tune page.

5. Allow the real-time mass spectrum to stabilise, ensuring MS signal is obtained from the DESI spray at the stage home position.

6. Ensure the DESI device is connected to MassLynx using the 'DESI Control Parameters'. 2D Omnispray software must be closed prior to connection.

7. At this point, it is advised to analyse some test samples (compounds of interest) before screening a 96-well plate. In particular, attention should be given to the ionisation efficiency and sensitivity of the compounds of interest and the location of the home position in the DESI control parameters.

### 6.2.3 96-well plate Preparation

1. Prepare samples or perform an assay in a 96-well plate. Store until required in step 9.

2. Cut a nylon membrane disk (82 mm diameter, Roche, Basel, Switzerland) into a rectangle of size 6 cm by 4 cm (Figure 6.2.2 A).

3. Place 4 rows of 1.5 cm wide double-sided tape into the centre of the DESI screening glass slide (Figure 6.2.2 A).

4. Adhere the nylon membrane to the glass slide using the double-sided tape (Figure 6.2.2 B).

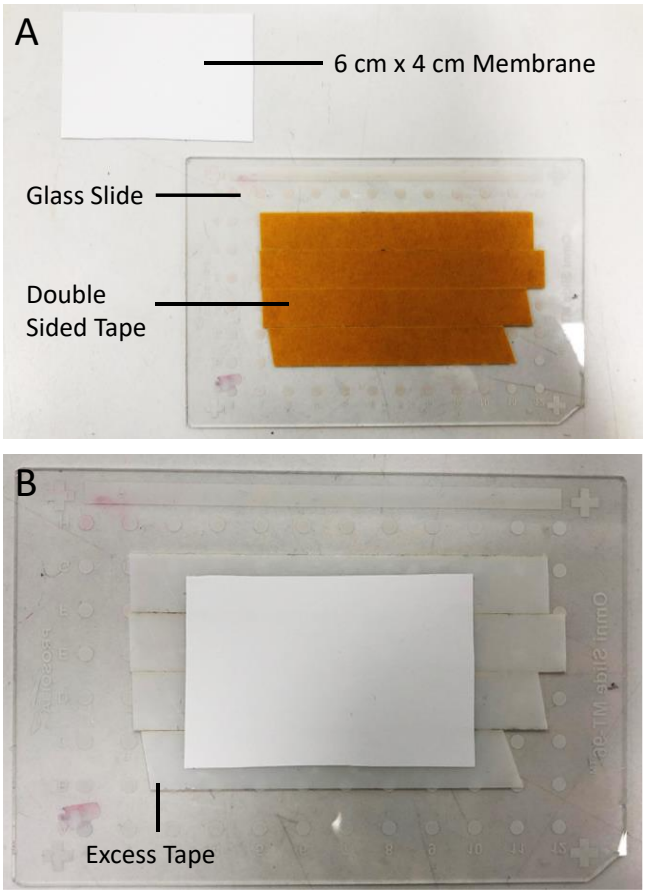


*Figure 6.2.2: A) Photograph of a newly cut 6 cm x 4 cm nylon membrane and DESI-MS full plate glass slide with double-sided tape adhered. B) Photograph of the nylon membrane adhered to the double-sided tape with excess tape around the edge of the membrane indicated.*

5. Remove any excess tape from around the nylon membrane using a scalpel (Figure 6.2.3 A).

6. Using a ruler and a scalpel, mark out a 12 x 8 grid (96 wells) by lightly scoring into the membrane surface. Each nylon membrane 'well' should be 5 mm x 5 mm (Figure 6.2.3 C).

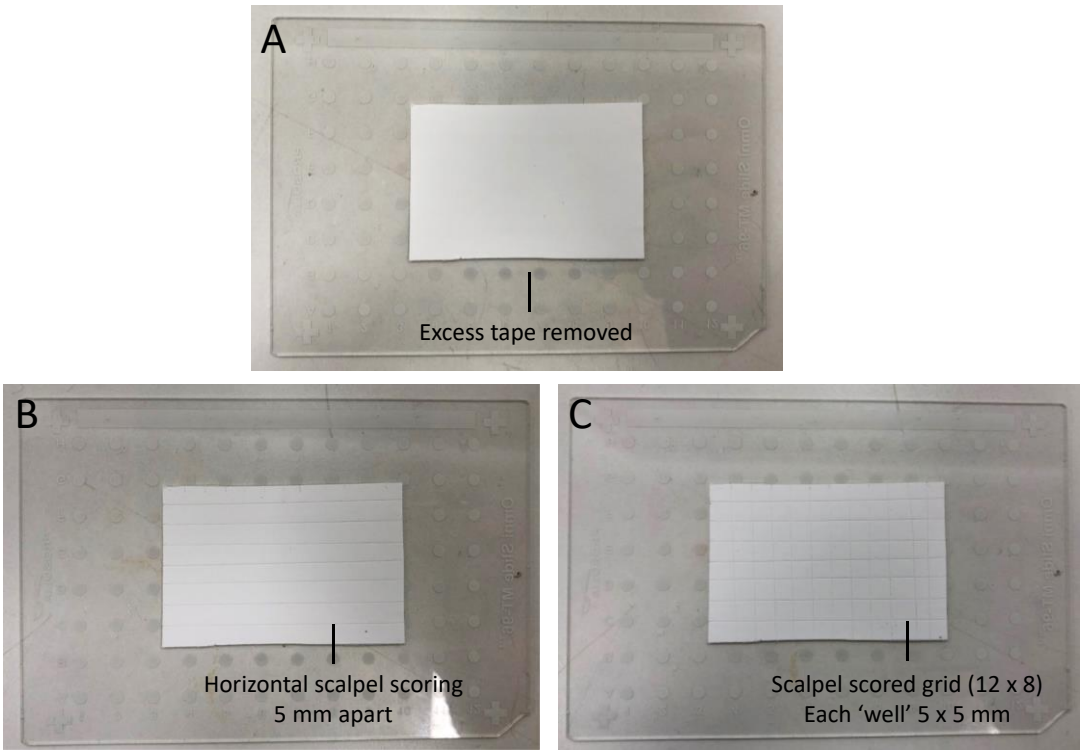


*Figure 6.2.3: A) Photograph of a 6 cm x 4 cm nylon membrane adhered to the DESI-MS full plate with excess tape removed. B) Addition of horizontal scalpel scoring lines 5 mm apart into the membrane surface. C) Vertical scalpel scoring lines (5 mm apart) have been added to form a 12 x 8 grid.*

7. Use a compressed gas line to remove any free nylon dust from the membrane.

8. On the rear of the glass slide, use a marker to highlight the top left-hand corner of the nylon membrane grid, i.e.: well A1.

9. Starting at well A1, transfer 0.5 μL from each well into the appropriate grid location on the nylon membrane (Figure 6.2.4 A).

10. Continue until an aliquot from each well has been deposited onto the membrane and allow to air dry.

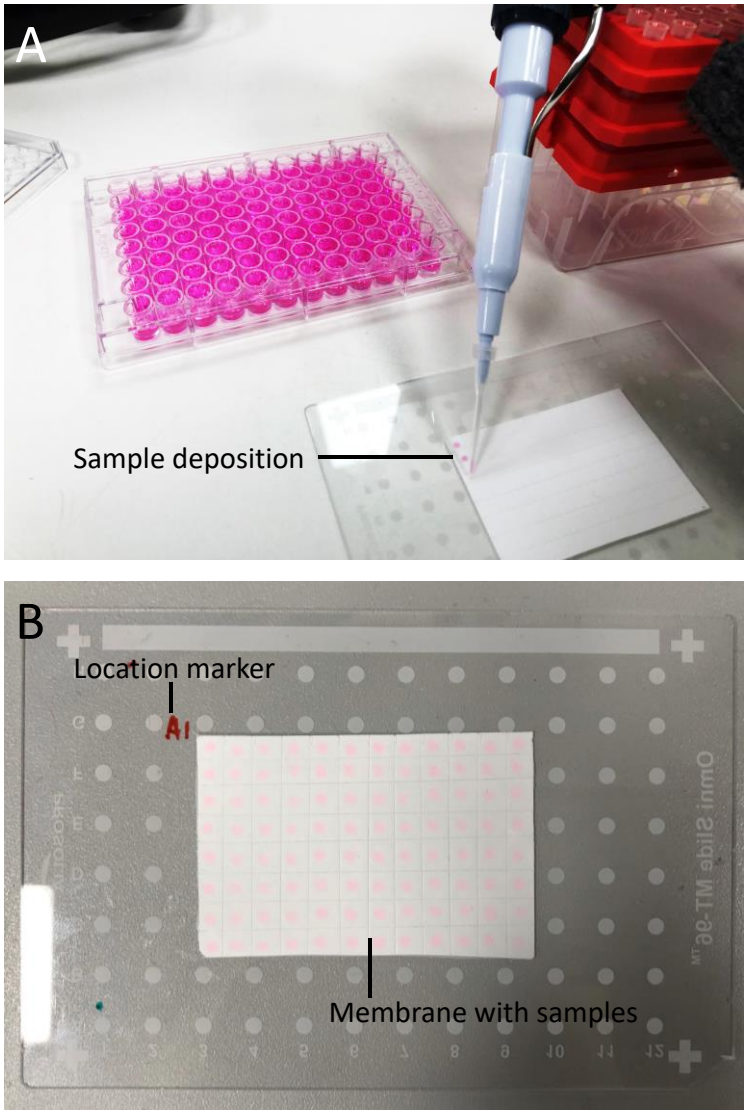


*Figure 6.2.4: A) Photograph of sample deposition (0.5 µL) onto the nylon membrane grid. B) Photograph of a nylon membrane grid after the completion of sample deposition. A location marker (A1, upper left) has been added to the glass slide to indicate the orientation of the 12 x 8 grid in relation to the well plate that samples have been transferred.*

11. Photograph the sample plate and transfer the image to the computer.

12. Place the glass slide onto the DESI stage and adjust the height of the stage as appropriate.

### 6.2.4 Setting up the experiment software

1. Open the HD Imaging software package and create a new plate.

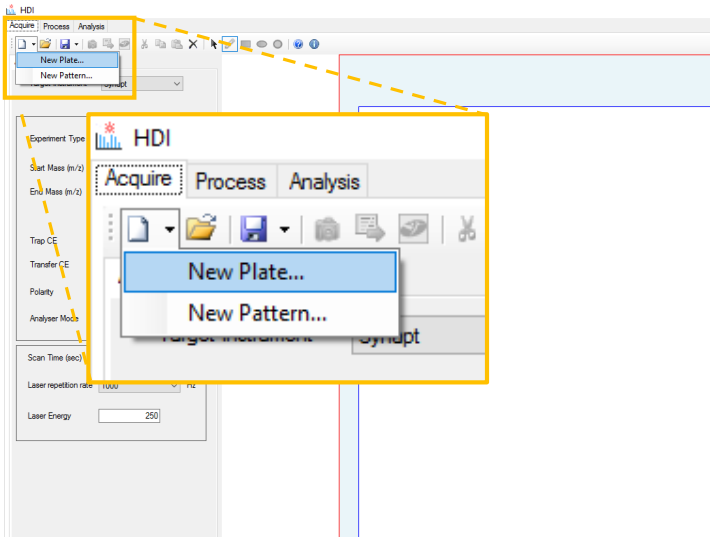


*Figure 6.2.5: Screen capture of HD Imaging software 'Acquire' tab. The location of 'create new plate' icon is indicated in the yellow boxed insert.*

2. A dialog box will open and use the previously taken photograph (Figure 6.2.6 A, yellow rectangle) to define the glass slide area. Select 'DESI full plate' in the drop-down menu (Figure 6.2.6 A, purple rectangle). Use 'Next', to continue to the subsequent dialog window and specify the corners of the DESI full plate slide by clicking on the plate photograph. Yellow crosses will appear in the locations that you have indicated as corners.

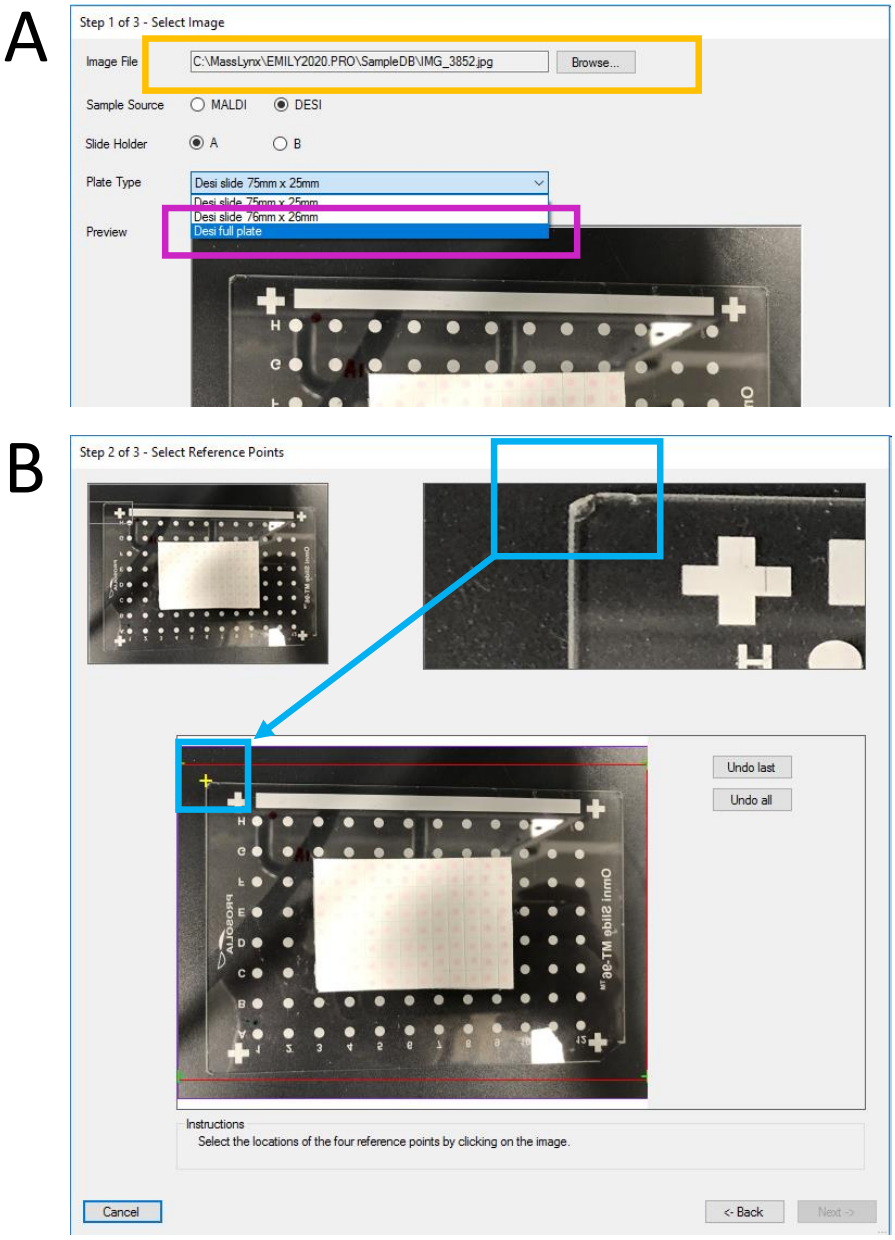


*Figure 6.2.6: A) Screen capture of the 'create new plate' dialog box (step 1). Import a photograph of the DESI plate to be analysed (yellow box). Selection of 'DESI full plate' (plate type) is indicated in the purple box. B) Screen capture of the 'create new plate' dialog box (step 2). Using the mouse and photograph, the corner of the slide has been indicated and a yellow cross added in the appropriate location.*

3. When satisfied with your full slide area use finish to close the dialog box. Use the 'Acquire' tab to define the experimental parameters (Figure 6.2.7 A) e.g.: mass range and ionisation mode). Note: all DESI experiments should be undertaken in 'Sensitivity mode'.

4. In the 'Pattern' tab use the rectangle drawing tool to define the area inside the full plate that you wish the DESI-MS to sample from (Figure 6.2.7 C). In this case, draw a rectangle over the entirety of the membrane area on your photograph.

5. Set the pixel size and stage speed as appropriate for your experiment (Figure 6.2.7 B). As a guide, a 96-well plate analysed using a pixel size of 500 μm x 500 μm, at a speed of 2000 μm, will give a total well plate analysis time of 62 minutes (equivalent to ~39 s/well). Tip: always ensure you have enough solvent in the DESI syringe for the entirety of your experiment.

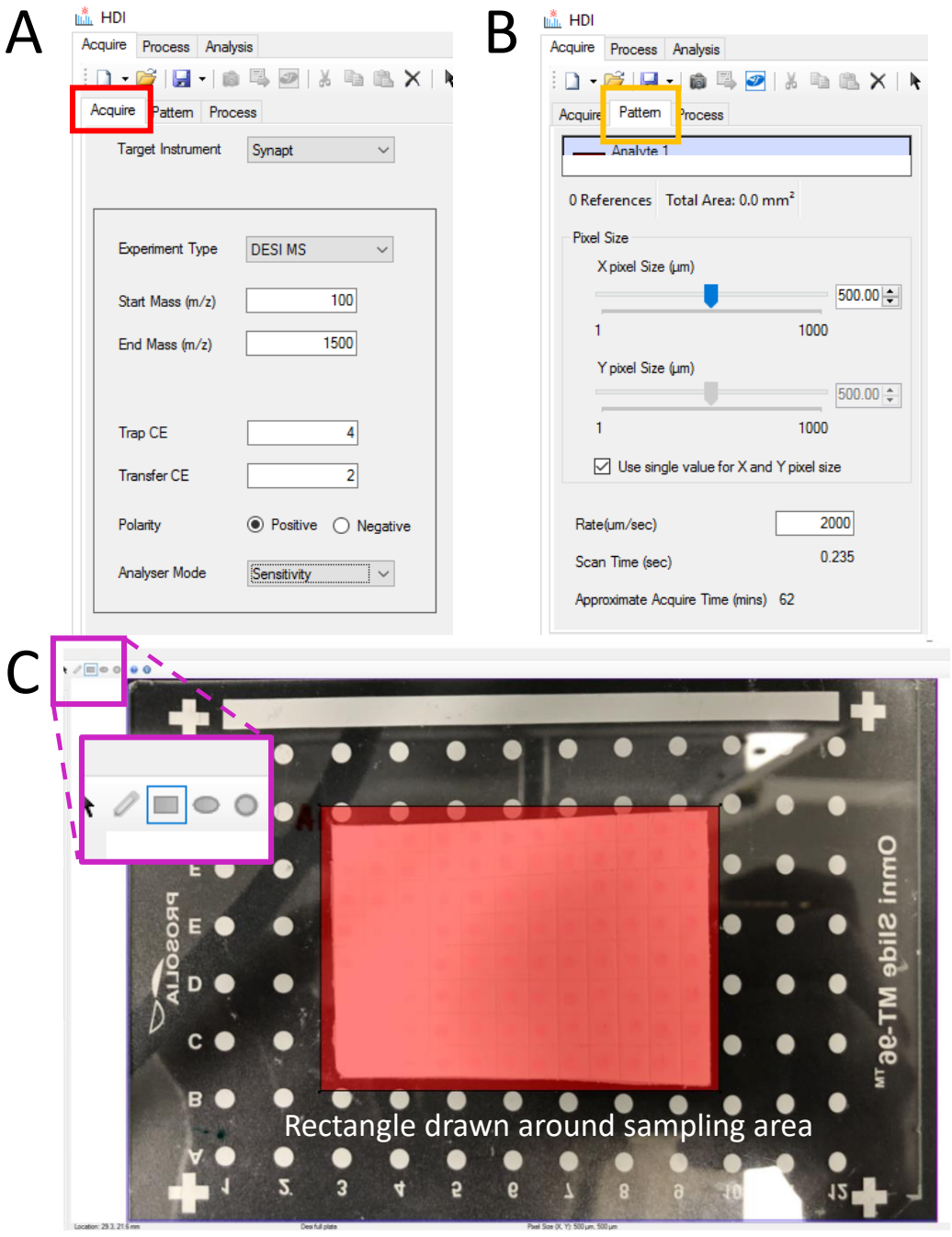


*Figure 6.2.7: A) Screen capture of the 'Acquire' tab. Here, the mass spectrometry parameters (experiment type, mass range, collision energies, polarity and analyser mode (sensitivity)) are selected. B) Screen capture of the 'Pattern' tab. Here, the DESI experimental parameters (pixel size and stage speed) are selected. C) Screen capture highlighting the 'draw rectangle' tool (purple boxed insert), and an example of a rectangular pattern drawn around the nylon membrane area.*

6. Save your pattern file.

7. Export the pattern file to MassLynx (Figure 6.2.8).

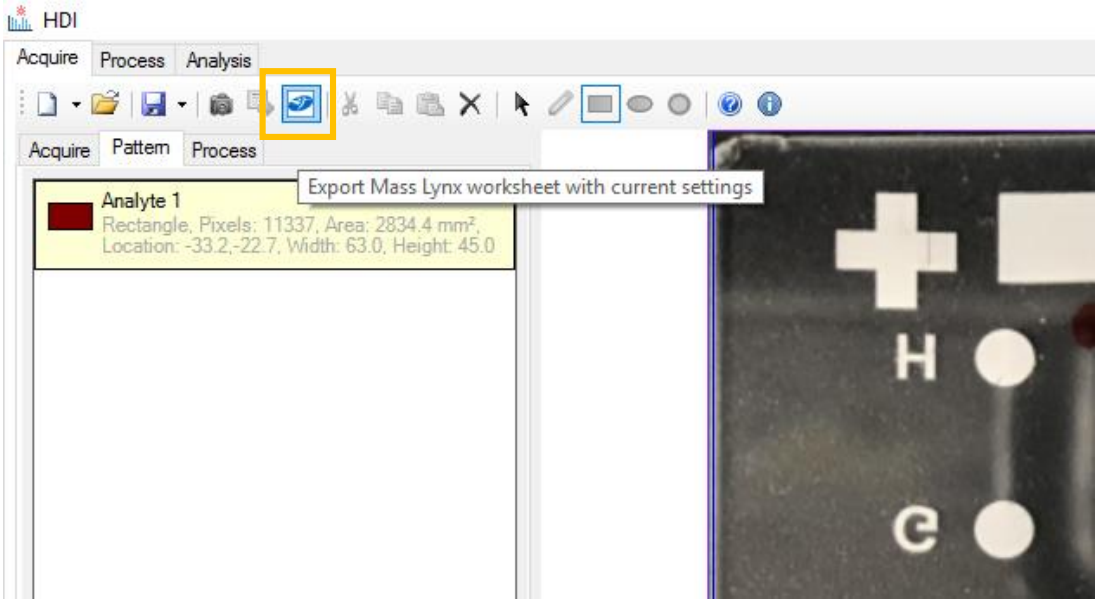


*Figure 6.2.8: Screen capture indicating the 'Export to MassLynx' icon (yellow box).*

8. Open MassLynx Software. Use 'File -> import worklist' to import the pattern file from step 7 into the MassLynx sample list (Figure 6.2.9).

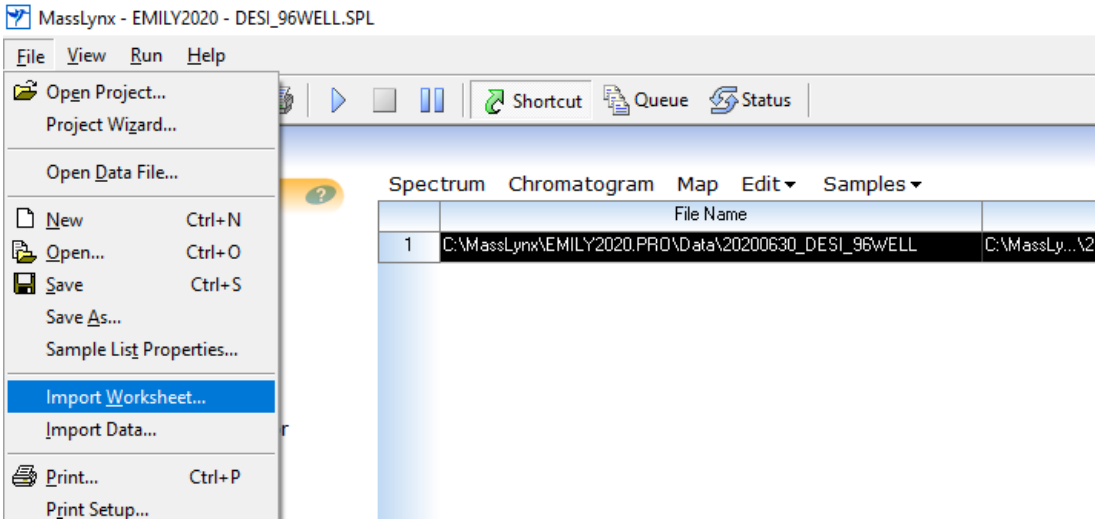


*Figure 6.2.9: Screen capture of MassLynx software indicating the location of the 'Import Worksheet' instruction in the file menu.*

9. Give the sample an appropriate file name and ensure the correct experimental file is present. This should have been filled in automatically when importing the worksheet.

10. In the 'Parameter file' column ensure the corresponding '.ini' file to your pattern file is selected. This should have been filled in automatically when importing the worksheet.

11. Save your sample list.

12. Run your sample list using the green triangle, selecting 'analysis' only in the dialog box.

13. The sample stage should now move to the pattern start position (roughly well A1) and begin the analysis. Wait for the DESI stage to return to the home position (top left-hand corner of the full slide). MS acquisition is now complete.

### 6.2.5 Data Processing and Analysis

1. Using the 'Process' tab in HD Imaging, convert your MS data into heat map data. Import the appropriate '.raw' file using the green '+' icon and input the mass ranges and resolution required. Use the green triangle icon to run the processing script (Figure 6.2.10).

2. Allow the script to complete (*'Maldichrom.exe completed'*) before moving to the 'Analysis' tab.

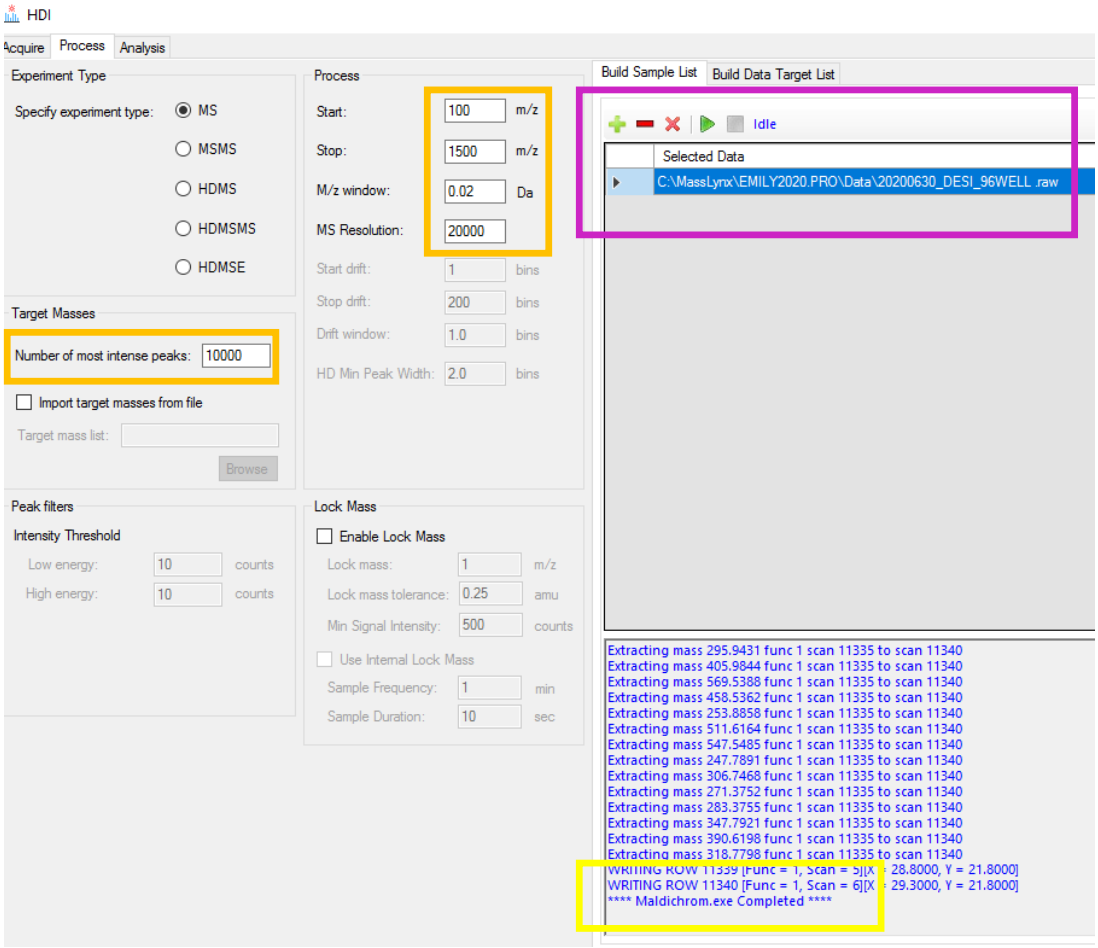


*Figure 6.2.10: Screen capture of the HD Imaging 'Process' tab. Importing a data file (purple box), processing parameters (orange boxes) and script completion (yellow box) have been indicated.*

3. In the 'Analysis' tab, open the appropriate imaging '.raw' file and allow to load. For large imaging files with small pixels, this can take some time (Figure 6.2.11).

4. Using the table or mass spectrum, select the *m/z* value of interest. Use the 'home' button to show the corresponding heat map to that *m/z* value.

5. Complete your analysis by examining all *m/z* values of interest and the corresponding heat maps to identify well plate positions of interest.

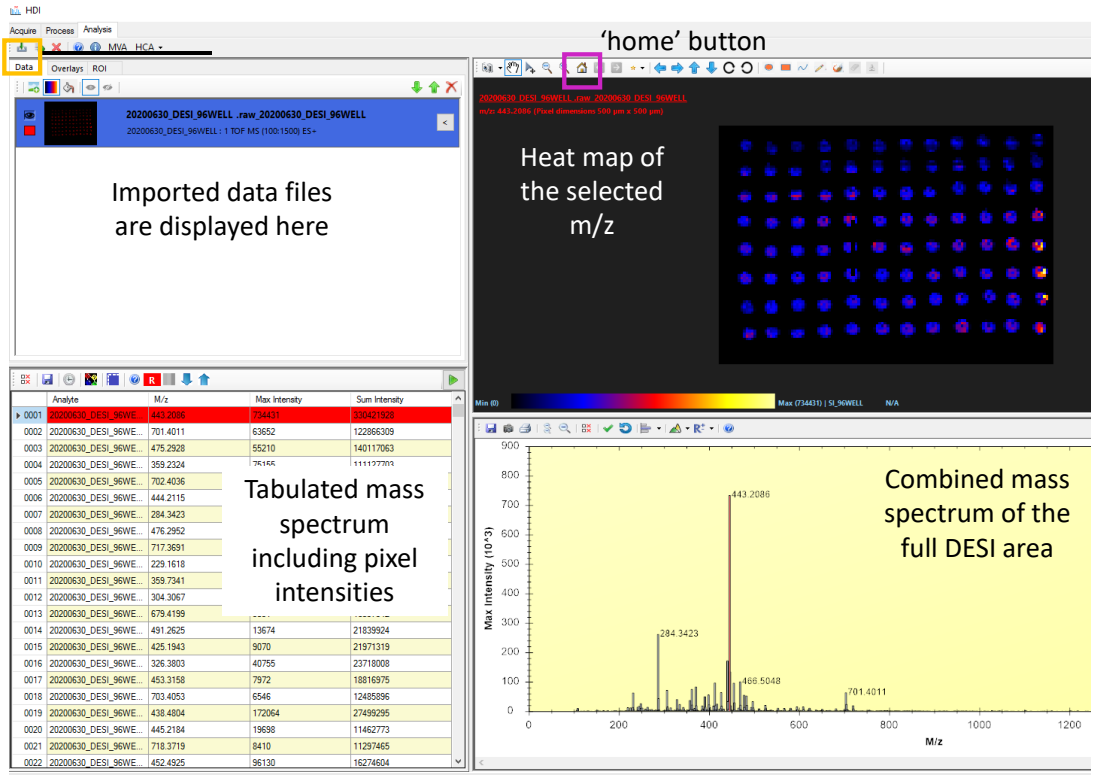


*Figure 6.2.11: Screen capture of the HD Imaging 'Analysis' tab in which MS data, (bottom left and right), and the corresponding heat maps (top right) generated from the DESI-MS acquisition can be viewed.*

6. The 'Visualisation' tab can be used to alter the colours and intensity of the heat map data. Reducing the 'max' value will make the pixels appear at the more intense end of the colour scale (Figure 6.2.12 A and B).

7. Images can be moved to the gallery by using the keyboard short cut: 'Ctrl+G'. Use the 'save as' icon to export the images into an appropriate picture file format (Figure 6.2.12 C).

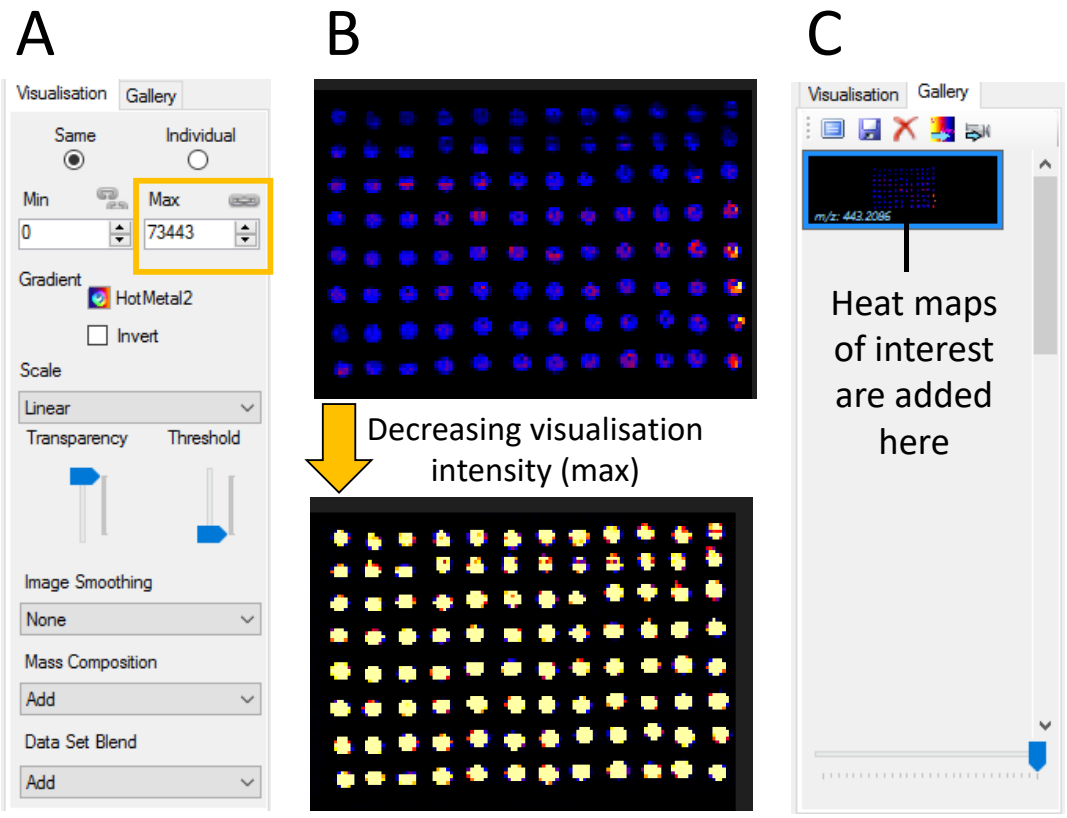


*Figure 6.2.12: A) Screen capture of the 'Visualisation' tab. Here, heat map colours and intensities can be altered. The 'max' value for altering the heat map intensity is indicated in the orange box. B) Effect of decreasing the visualisation intensity upon the heat map. Top heat map, max = 734431. Bottom heat map, max = 73443. C) Screen capture of the 'Gallery' tab. Here, heat maps of interest can be saved and exported as images.*

## 6.3 How to Fabricate a PDMS Microfluidic Chip

This guide provides step-by-step photolithography and soft lithography instructions to fabricate PDMS microfluidic chips in the Centre for Mesoscience and Nanofabrication (CMN) and the Manchester Institute of Biotechnology (MIB). Figure 6.3.1 below roughly outlines the fabrication process in its entirety. Before fabrication, a computational approach to microfluidic chip design is required and brief instructions for this are provided in Section 6.3.1.

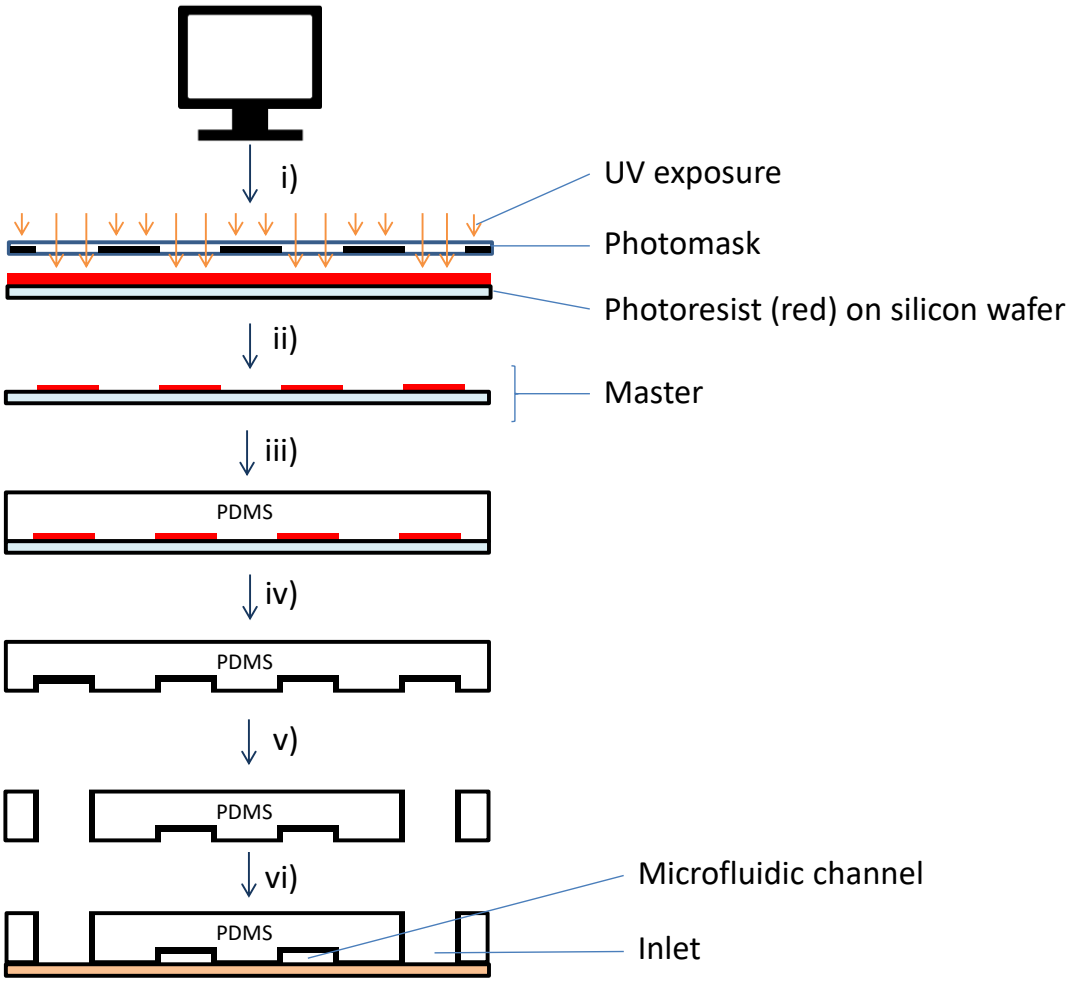


*Figure 6.3.1: Schematic illustrating the design, photolithography and soft lithography steps required to fabricate a PDMS microfluidic chip. i) CAD production of a photomask. ii) Generation of the master by photolithography. iii) Addition of liquid PDMS and curing agent into master. iv) Removal of PDMS from the master. v) Introduction of ports by punching. vi) Binding of PDMS to a glass slide (orange) to create channels.*

### 6.3.1 Designing a Microfluidic Chip using DraftSight

The following instructions provide a brief guide to drawing a microfluidic channel design in DraftSight software (Dassault Systèmes, Vélizy-Villacoublay, France). This design will be printed onto a photolithography mask that will be subsequently used for fabrication of the microfluidic device. More detailed instructions for using DraftSight, including tips and tricks can be found in the software help menu.

1. Open DraftSight software and load the file entitled MASKS_TEMPLATE.dwg. This template outlines a drawing area equivalent in size to an A4 page, and inside this area is 6 circles into which different channel designs can be drawn. These circles are approximately equivalent in size to a 3" silicon wafer (Figure 6.3.2).

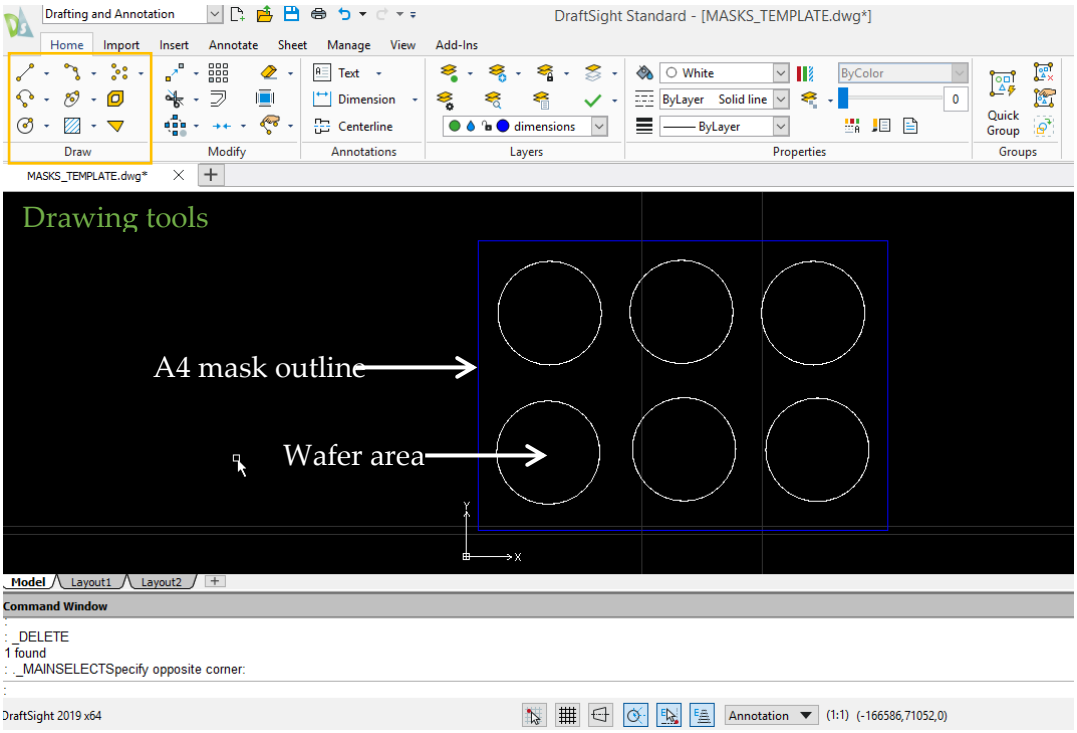


*Figure 6.3.2: Screen capture of DraftSight software illustrating the MASKS_TEMPLATE.dwg file within the drawing region. The A4 mask outline (blue rectangle), 6 wafers (white circles) and the drawing tools (orange box) are indicated.*

2. Use 'Save as' to rename and save your design file.

3. Use the drawing tools (i.e. lines, arcs and polygons) to draw your channel design into one of the 6 wafer templates. Shapes and lines with specific measurements can be drawn using the command window. The channel design should be surrounded by two concentric rectangles or squares (i.e. the sides of the chip, Figure 6.3.3).

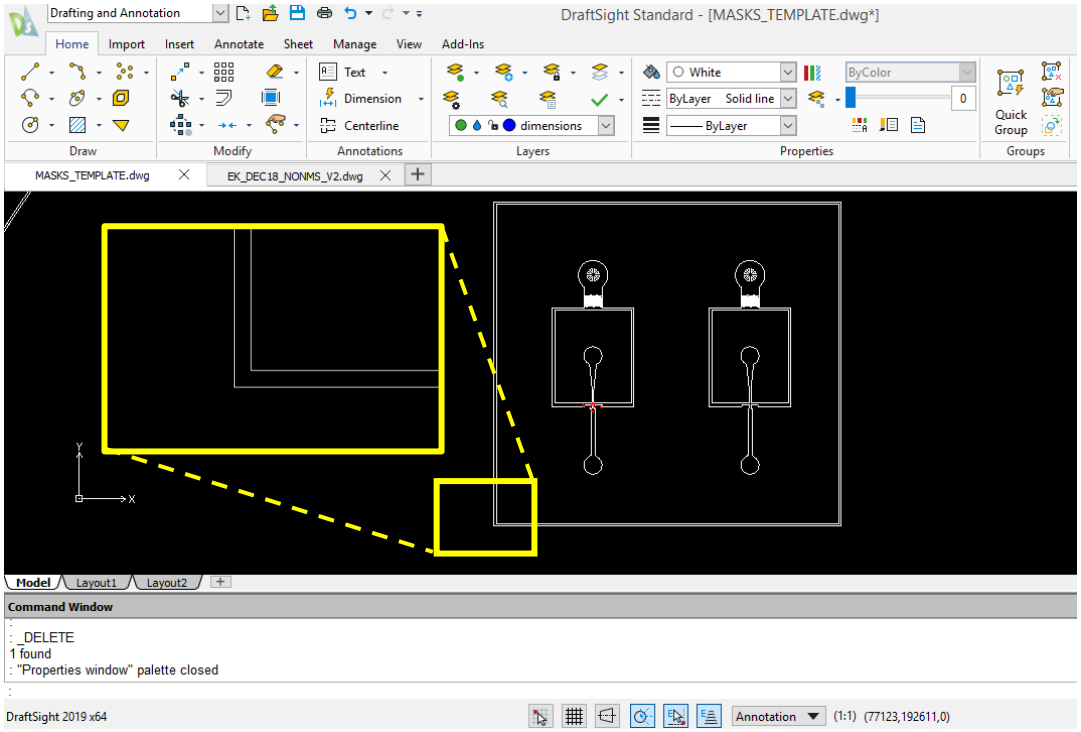


*Figure 6.3.3: Screen capture of an example microfluidic channel design drawn within DraftSight software. The concentric rectangles which will become the walls of the microfluidic chip and enclose the channel designs have been enlarged in the yellow inset.*

4. The linear dimension tool can be used to find channel dimensions. Select the tool and draw a line between the two points of interest to return a measurement in microns (μm) (Figure 6.3.4).

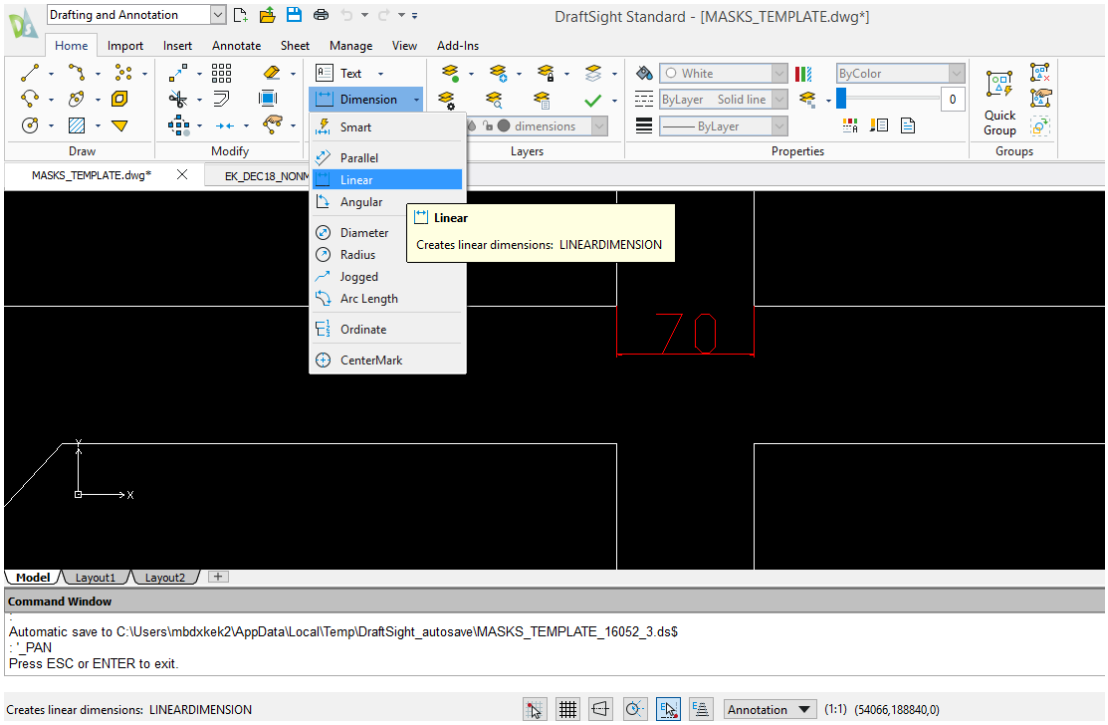


*Figure 6.3.4: Screen capture of DraftSight software indicating the location of the linear dimension tool used for measuring channel sizes. A channel measurement in µm (red text and lines) has been added as an example.*

5. Upon completion of your chip design, you must ensure that all lines and shapes are connected at intersections and there are no open gaps. Select the entirety of the design using the cursor and then use the 'Hatch/Fill' tool to deduce if your chip is sufficiently enclosed. Use the boundary setting 'specify entities' to fill your channels (Figure 6.3.5) and if you are happy that there are no gaps in your design use 'cancel' to remove the hatched pattern. Should the 'Hatch/Fill' tool suggest that there are open regions in your design (Figure 6.3.6) or the design has not filled as you expected, use cancel to close the 'Hatch/Fill' dialog box and correct the detached shapes.

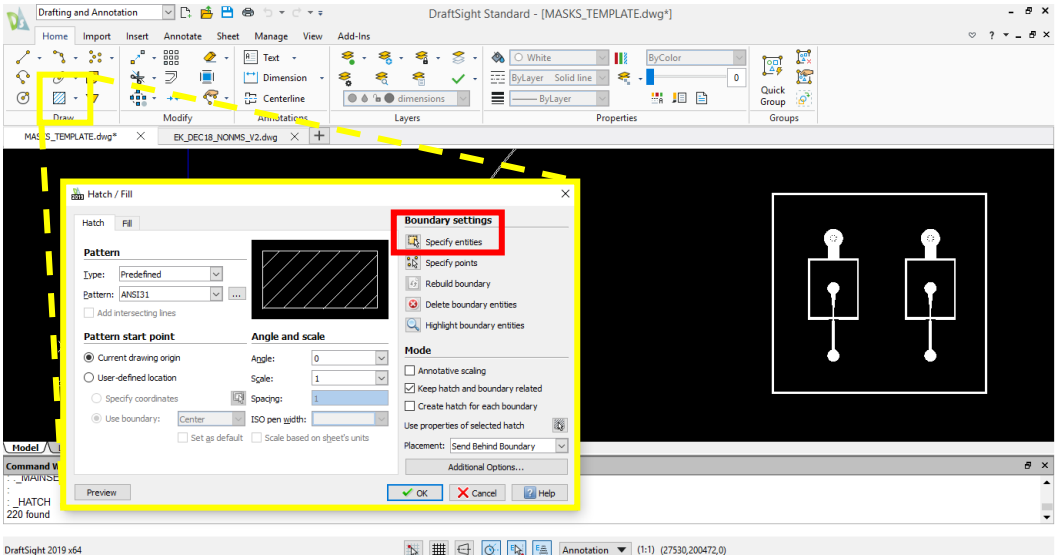


*Figure 6.3.5: Screen capture of DraftSight software indicating the location and dialog box (yellow boxed inset) of the 'Hatch/Fill' tool. The location of the 'specify entities' setting has also been highlighted in the red box. To the right of the 'Hatch/Fill' dialog box, the microfluidic chip design drawn previously has been successfully filled.*

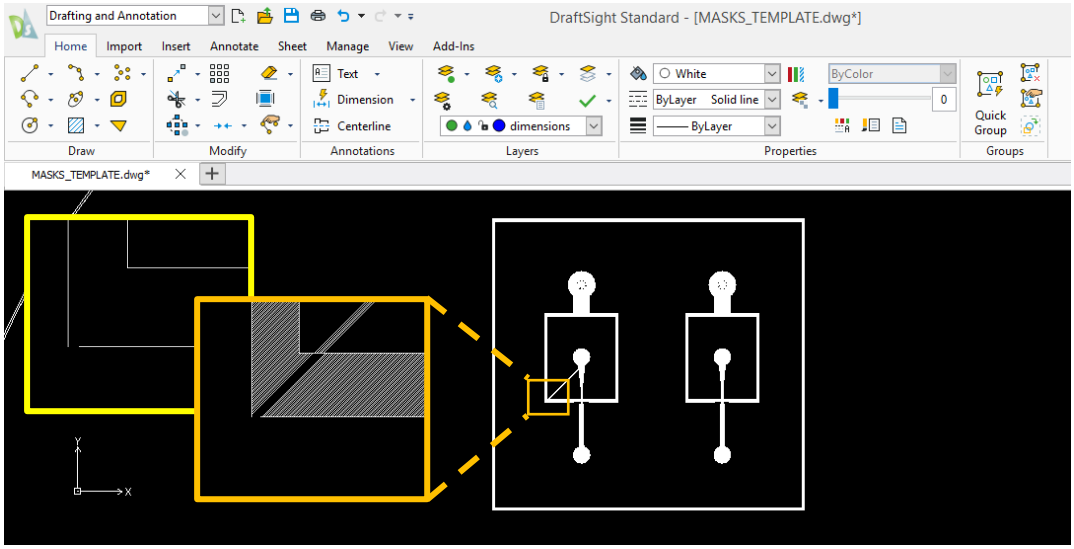


*Figure 6.3.6: Screen capture of DraftSight software demonstrating a microfluidic chip design in which the 'Hatch/Fill' tool has indicated presence of an open shape. The orange and yellow boxed insets show the open shape (unconnected line) that has caused this 'Hatch/Fill' error more clearly.*

6. When your 6 wafer designs are complete (no remaining 'Hatch/Fill'), save your design as a .dxf file type (R2018 ASCII Drawing). This is the file that will be sent to Micro Lithography Services Ltd. (Essex, UK).

7. Email the design file(s) to '*info@microlitho.co.uk*' and ask for the printing of A4 film mask(s) at their highest resolution. Don't forget to include the postal address.

8. When Micro Lithography Services Ltd. have returned a quote for printing of the mask(s), raise a 'non-catalogue request' using the university procurement system. Once the request has been processed by finance, ensure you include the purchase order number and the invoice address in your reply to Micro Lithography Services Ltd.

9. Upon the arrival of the mask, do not remove the A4 film from the inner wrapping of the packaging until inside the cleanroom. Once inside the cleanroom, the A4 film mask can be cut into 6 square mask designs (Figure 6.3.7) ready for use with the MJB4 mask aligner.

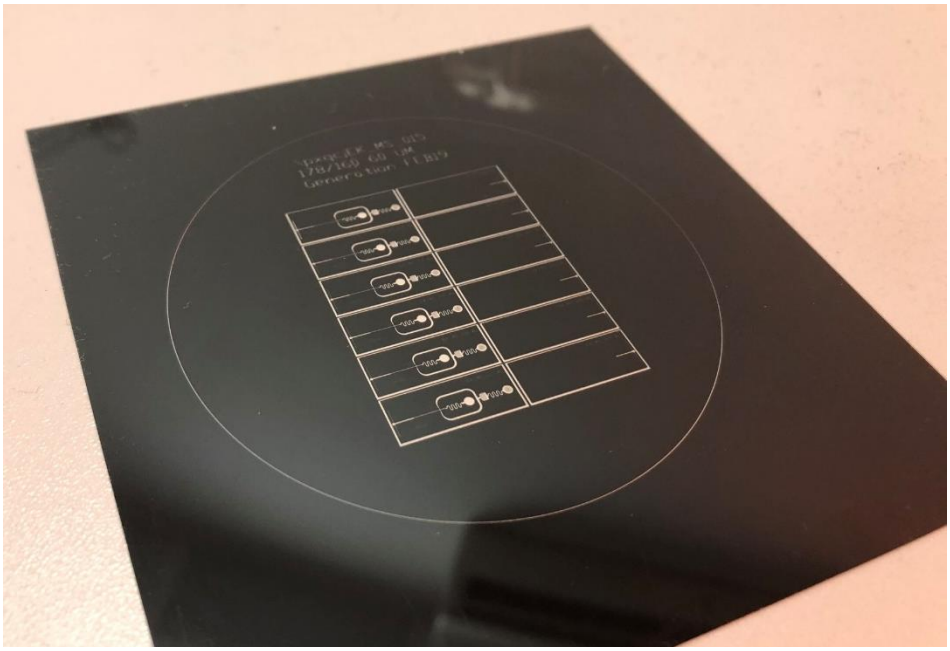

*Figure 6.3.7: Photograph of a photolithography film mask received from Micro Lithography Services Ltd and cut to size (~10 cm by 10 cm) for use in subsequent fabrication steps.*

### 6.3.2 Production of a Master using Photolithography in the CMN

1. Prepare a 4" silicon wafer by rinsing thoroughly with Acetone and Isopropyl alcohol. Dry using the Nitrogen gun. Dehydrate on a hot plate for 15-20 minutes at 130 °C.

2. Use the Oxford Reactive Ion Etcher (Oxford Instruments Plasma Technology, Yatton, Bristol, UK) to plasma clean the wafer according to the following recipe:

*Table 6.3.1: Oxford instruments reactive ion etcher conditions for plasma cleaning 4" silicon wafers before deposition of SU-8 2025.*

| Plasma Cleaning Conditions | |
|---|---|
| RF Forward Power | 50 W |
| ICP Forward Power | 150 W |
| Pressure | 50 mTorr |
| $O_2$ Flow | 45 sccm |

3. Pour a large amount of SU-8 2025 photoresist (Kayaku Advanced Materials, Westborough, MA, USA) onto the centre of the wafer (Figure 6.3.8 A). Place on the spin coater and spin according to the thickness of SU-8 required. Example programs for 3 common SU-8 2025 thicknesses can be found in Table 6.3.2.

   Tip: do not use SU-8 2025 directly from the fridge. Allow the bottle to come to room temperature before pouring onto your wafer. Centre your wafer on the spin coater if possible and don't forget the clean the spin coater after use. Acetone will remove SU-8 residue.

*Table 6.3.2: Example spin coater programs for SU-8 2025 photoresist.*

| **Thickness required (μm)** | Acceleration (rpm/s) | Step 1 | Step 2 | **Step 3** |
|---|---|---|---|---|
| **70** | 300 | 100 rpm for 10 s | 500 rpm for 5 s | **1000 rpm for 60 s** |
| **50** | 300 | 100 rpm for 10 s | 500 rpm for 5 s | **1650 rpm for 60 s** |
| **35** | 300 | 100 rpm for 10 s | 500 rpm for 5 s | **3000 rpm for 60 s** |

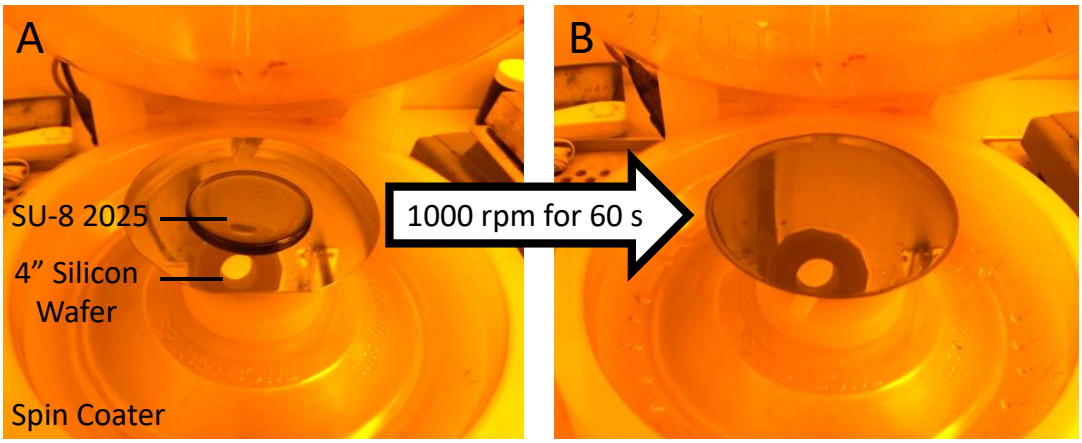


*Figure 6.3.8: Photograph of a 4" silicon wafer containing an SU-8 2025 deposit on a spin coater A) Before spin coating steps. B) After spin coating (Step 3: 1000 rpm for 60s).*

4. Soft bake conditions vary with thickness and the process requires two hot plates (65 °C and 95 °C). After spin-coating, place the SU-8 coated wafer on the first hotplate (65°C) and allow to bake for the allotted time (step 1). Move the wafer between the hot plates using wafer tweezers until the soft bake steps are complete. As a guide, soft bake conditions for 70 um SU-8 thicknesses are given in Table 6.3.4 below.

*Table 6.3.4: Soft bake conditions for 70 µm thick SU-8 2025 photoresist.*

| Soft Bake Step | Hot Plate Temperature (°C) | Time (minutes) |
|---|---|---|
| 1 | 65 | 3 |
| 2 | 95 | 9 |
| 3 | 65 | 3 |

5. Once the wafer has cooled after the final soft bake step, use the MJB4 mask aligner and a film mask to expose the SU-8 covered wafer. The exposure time required is dependent on SU-8 2025 thickness and as a result exposure testing will be required for different thicknesses. As a guide a 70 um SU-8 film is exposed for 5 s, under hard contact (10 s), reflected light conditions, ensuring the mask is as close as possible to the substrate.

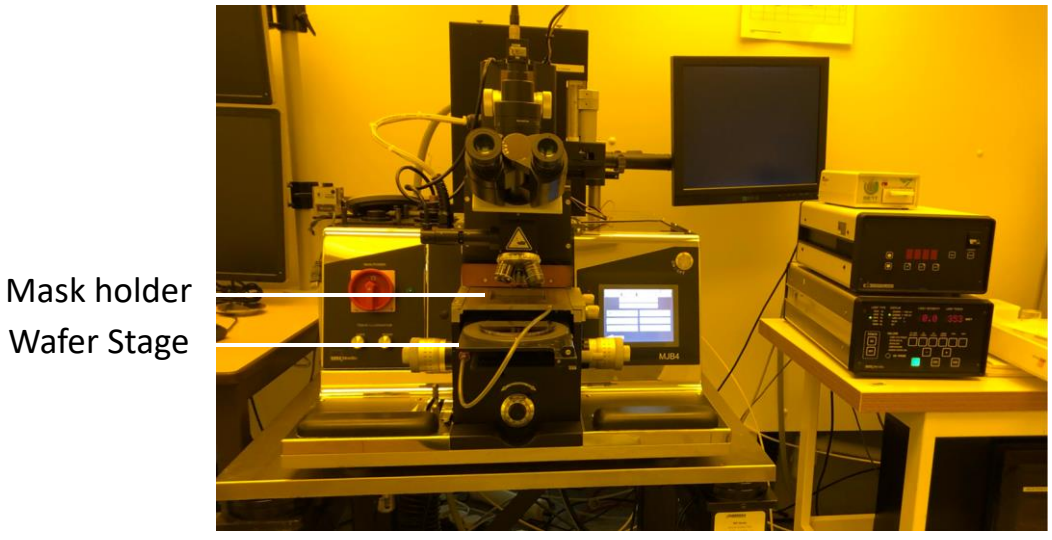


*Figure 6.3.9: Photograph of the MBJ4 mask aligner. The wafer stage and mask holder have been indicated as shown.*

6. Repeat step 4 using the hot plates for the post-exposure bake (PEB). PEB conditions vary with thickness, as a guide match the PEB conditions with the soft bake conditions (e.g. Table 6.3.4). Upon placing the newly exposed wafer on the 95 °C hot plate, a latent image of your mask design should be visible within approximately 1 minute.

7. Develop the exposed SU-8 features using MICROPOSIT EC solvent (or propylene glycol monomethyl ether acetate) by submerging the whole wafer in a large crystallising dish. When most of the un-exposed SU-8 has dissolved from around the features (approximately 4 minutes submerge time for 70 μm thickness), gently pour the solvent away and replace with fresh solvent. Using wafer tweezers remove the wafer from the dish and use the spray development airbrush (filled with MICROPOSIT EC solvent) to remove the remaining SU-8 from around the edge of the wafer and from between the features (Figure 6.3.10).

   Tip: Concentrate the airbrush stream between tight features to ensure all remaining un-exposed SU-8 is removed and a clear image of your design remains, however, be careful not to overdevelop the features by exposing them to the solvent for excessive amounts of time. Overdevelopment will cause the features to be removed from the wafer.

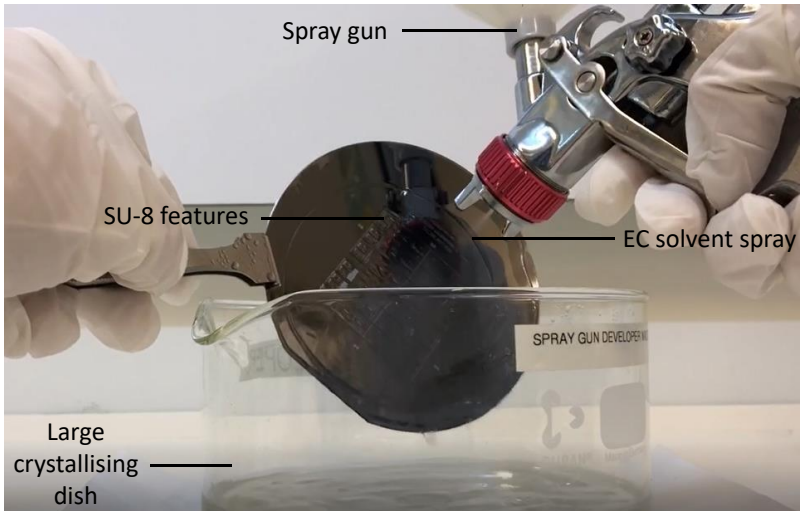


*Figure 6.3.10: Photograph of wafer development using a spray gun. A jet stream of EC solvent is directed at the wafer to dissolve and remove un-cross-linked SU-8 as shown.*

8. Rinse the wafer with isopropyl alcohol. If a white 'film' appears during this rinse, return to step 7 as more development solvent is required to remove any remaining unexposed SU-8. When the isopropyl alcohol runs clear, dry the wafer with a Nitrogen gun.

9. Bake the wafer for 5 minutes at 150 °C to give the features added mechanical stability (hard bake). This also aids the annealing of surface cracks in the SU-8 features (Figure 6.3.11).

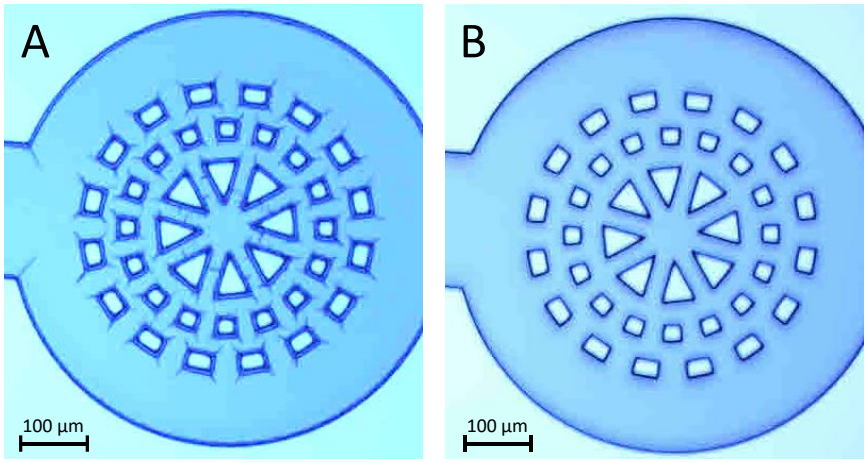


*Figure 6.3.11: Two microscope images (5x magnification) of a SU-8 microfluidic channel inlet illustrating the effect of the hard bake step upon SU-8 surface features. A) Image before hard bake. Surface cracks are visible. B) Image after hard bake (150 °C for 5 minutes). Surface cracks have annealed.*

10. Observe wafer features for quality under the microscope. Pay particular attention to any overexposure or under development that may have occurred and amend your wafer processing times (e.g. exposure, baking and development) accordingly during future fabrication procedures.

### 6.3.3 Soft lithography in the CMN

1. Mix the PDMS elastomer with cross-linker in a 10:1 w/w ratio in a plastic beaker and stir thoroughly.

2. Place the SU-8 patterned wafer in a Petri dish and pour over the PDMS mixture to the desired thickness/weight (Figure 6.3.12).

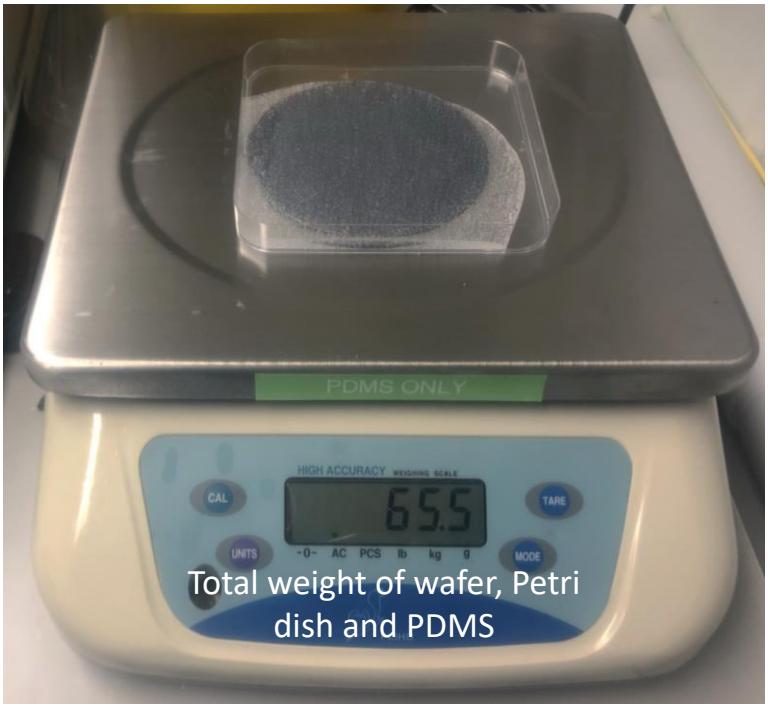


*Figure 6.3.12: Photograph of a Petri dish containing a silicon wafer with SU-8 features. Mixed PDMS elastomer (10:1 base: cross-linker) has been poured over the SU-8 features until a total weight is reached.*

3. De-gas the Petri dish in a vacuum desiccator until all bubbles have been removed.

4. Place the Petri dish in an oven at 65°C overnight. Make sure the oven shelf is level or the PDMS will cure aslant. Alternatively, cure on the bench for 24 hours (25 °C).

5. Remove from the oven, and once cool use a scalpel to cut around the patterned PDMS and gently peel it away from the silicon wafer to reveal the microfluidic channels. The resulting PDMS piece containing channels can then be transported to the MIB for microfluidic chip assembly.

6. Fresh PDMS mixture can then be poured, degassed and cured again into the same Petri dish to produce more chips of the same design.

   Tip: To ensure a consistent thickness of PDMS between batches of chips, when pouring new PDMS onto the features, ensure the total weight of the petri dish, wafer and PDMS equals that of the previous weight achieved.

### 6.3.4 Microfluidic chip assembly in the MIB (single-layer)

Note: The following assembly instructions apply to microfluidic chip designs which have 1 PDMS 'feature side' only (e.g. droplet generation chips used in Chapter 5). For designs that encompass two feature sides (e.g. mass spectrometry or droplet sorting chips) follow the instructions given in Section 6.3.5.

1. Place the PDMS piece feature side up on a cutting mat.

2. Use a 1 mm biopsy punch to add the tubing inlets and outlets in the appropriate places in the design (Figure 6.3.13 A). Use a Nitrogen gun to blow away any PDMS excess.

3. Using a blade, cut around the edges of each microfluidic chip following the design pattern (Figure 6.3.13 B).

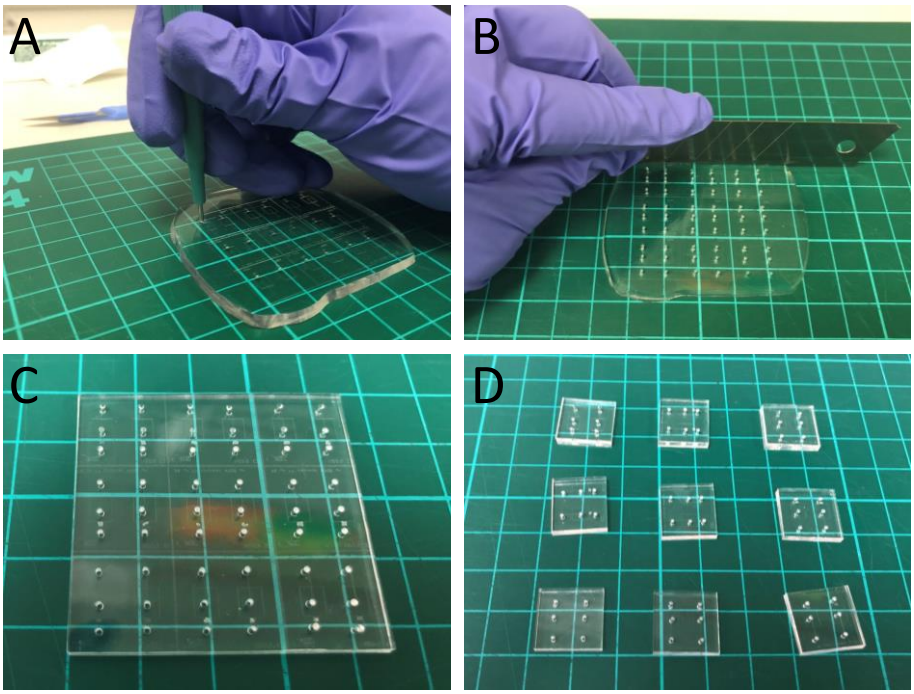


*Figure 6.3.13: A) Use of a biopsy punch to introduce fluidic inlets and outlets to the microfluidic chip PDMS pieces. B) Use of a stainless steel blade to cut the PDMS to size according to the design. C) PDMS piece containing 9 chip designs. D) 9 individual microfluidic chip pieces that have been cut to size using a blade. Scale: In all photos green squares are equivalent to 1 cm x 1 cm.*

4. Use scotch tape to clean all sides of the microfluidic chip by repeatedly pressing and removing fresh strips of tape on to the PDMS surface. This removes dust from the PDMS surface. Cover the piece of PDMS in scotch tape to keep it dust-free until required in step 13.

5. Mix the PDMS elastomer with cross-linker in a 10:1 w/w ratio in a plastic beaker and stir thoroughly.

6. Pour the PDMS mixture into a new plastic 5 cm Petri dish to the required thickness. This will be the base of the microfluidic chip and form the underside wall of the channel.

7. De-gas the Petri dish in a vacuum desiccator until all bubbles have been removed.

8. Place the Petri dish in an oven at 65°C overnight. May sure the oven shelf is level or the PDMS will cure aslant. Alternatively, cure on the bench for 24 hours (25 °C).

9. Once cured, allow to cool before using a scalpel to cut around the edge of the PDMS in the 5 cm Petri dish. Carefully remove the PDMS from the Petri dish and use a blade to cut into a square shape (approx. 3 cm x 3 cm). Use scotch tape to remove any dust from the PDMS square and cover in scotch tape until required in step 13.

10. Using scotch tape, clean a glass microscope slide by repeatedly pressing and removing fresh strips of tape on to the glass surface to remove dust. Cover in the slide in scotch tape until required in step 20.

11. Switch on the PlasmaFlo and plasma cleaner units (Harrick Plasma, Ithaca, NY, USA) and the attached vacuum pump (Figure 6.3.14). Open the oxygen

cylinder (1 Bar), and close the plasma cleaner chamber door and wait until a stable chamber pressure is reached as indicated on the digital display. The pressure in the chamber (and consequently the flow of $O_2$) can be adjusted by gently turning the needle valve in front of the chamber door. As a guide set the pressure to 600 mTorr with an $O_2$ flow of approximately 15 sccm (flow meter 1). Allow the plasma cleaner to pump at this pressure for approximately 5 minutes to ensure $O_2$ is reaching the chamber.

12. Switch off the vacuum pump and gently turn the Swagelok valve to release the vacuum from the chamber until the door opens.

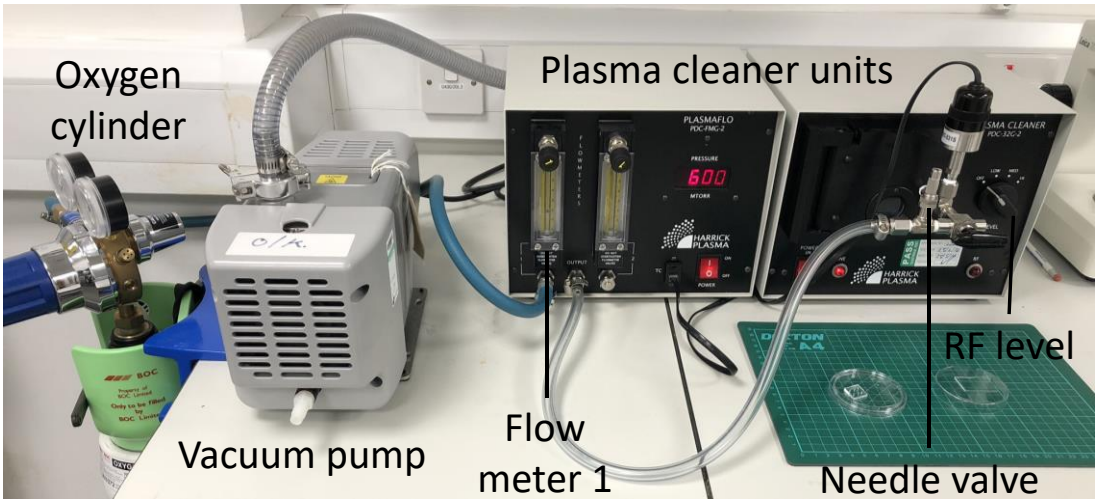


*Figure 6.3.14: Photograph of a Harrick Plasma plasma cleaner system. The major components of the instrumentation have been indicated.*

13. Remove the scotch tape from the PDMS piece from step 4, and place the PDMS feature side **up** on a Petri dish lid. Place both this piece and the PDMS square from step 9 into the plasma cleaner chamber and close the door (Figure 6.3.15 A).

14. Switch the vacuum pump on and allow the chamber to reach the desired pressure as set in step 11. Once stabilised, allow the chamber to remain at this pressure for 2 minutes to allow $O_2$ to flow in.

15. Using the dial, turn the RF level to the high position to generate $O_2$ plasma in the chamber. The chamber should glow lilac-purple and this indicates the presence of $O_2$ plasma. Keep the RF level high for 25 seconds before switching the RF dial back to the off position.

16. Switch off the vacuum pump and gently turn the Swagelok valve to release the vacuum from the chamber until the door opens.

17. Remove the PDMS piece and Petri dish from the chamber and promptly place the PDMS piece feature side **down** onto the PDMS base in the Petri dish (Figure 6.3.15 B). Press down on the PDMS pieces to bind them. Place the resulting Petri dish containing the double layer of PDMS in an oven at 65 °C for 1-2 hours.

18. Remove from the oven and once cool, use a blade to cut around the microfluidic chip to remove the excess PDMS from the base layer (Figure 6.3.15 C).

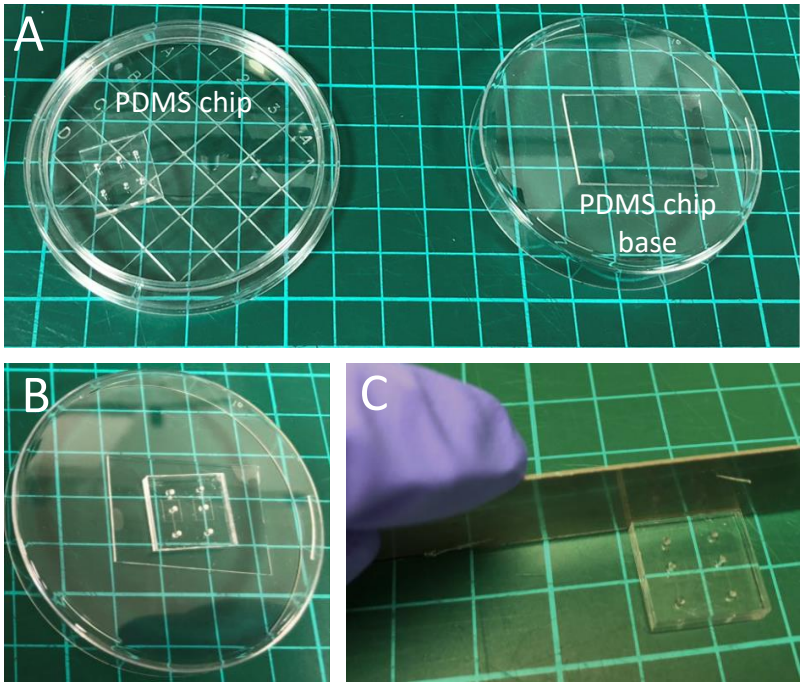


*Figure 6.3.15: A) Photograph of the two PDMS pieces that make up a single-layer microfluidic chip before insertion into the plasma cleaner unit. B) Photograph of the placement of the 'channel containing' PDMS piece on top of the PDMS base piece after exposure to oxygen plasma. C) Use of a stainless steel blade to cut excess PDMS from the base piece of the microfluidic chip. Scale: In all photos, green squares are equivalent to 1 cm x 1 cm.*

19. Use scotch tape to clean all sides of the microfluidic chip by repeatedly pressing and removing fresh strips of tape on to the PDMS surface. Cover the resulting PDMS chip in scotch tape to keep it clean until required in step 20.

20. Remove the tape from the glass microscope slide (from step 10) and the PDMS chip from step 19. Place the PDMS chip inlet side **down** on a Petri dish lid and place this and the glass slide into the plasma cleaner chamber and close the door. (Note: Two PDMS generation chips can be adhered onto a standard size microscope slide if required, see Figure 6.3.16).

21. Switch the vacuum pump on and allow the chamber to reach the desired pressure as set in step 11. Once stabilised allow the chamber to remain at this pressure for 2 minutes to allow $O_2$ to flow in.

22. Using the dial, turn the RF level to high to generate $O_2$ plasma in the chamber. The chamber should glow lilac-purple and this indicates the presence of $O_2$ plasma. Keep the RF level high for 25 seconds before switching the RF dial to the off position.

23. Switch off the vacuum pump and gently turn the Swagelok valve to release the vacuum from the chamber until the door opens.

24. Remove the glass slide and microfluidic chip from the chamber and promptly place the chip(s) base side down onto the glass slide. Press down on the PDMS chip to bind it to the glass. Place the resulting slide in an oven at 110 °C for 1-2 hours.

25. Ensure the plasma cleaner units are switched off and the oxygen cylinder is closed after use.

26. Remove the slide containing the PDMS chip (step 24) from the oven, allow to cool and protect the chip inlets from dust by covering them with scotch tape. Your microfluidic chip is now complete and ready for use (Figure 6.3.16).

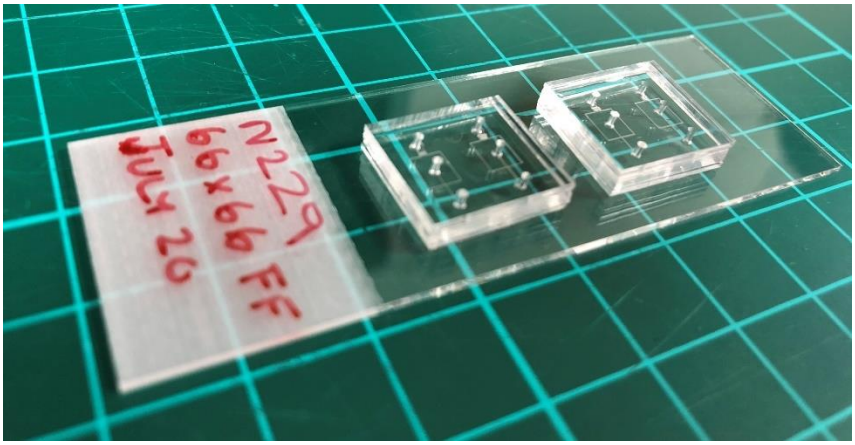


*Figure 6.3.16: Photograph of a completed microfluidic chip containing two generation chips. Scale: Green squares are equivalent to 1 cm x 1 cm.*

### 6.3.5 Microfluidic chip assembly in the MIB (double-layer)

Note: The following assembly instructions apply to microfluidic chip designs which have 2 PDMS feature sides and require alignment of the 2 designs during assembly (e.g. mass spectrometry chips used in Chapters 4 and 5 or sorting chips). For designs that use only 1 feature side (e.g. droplet generation and droplet splitting chips) follow the instructions given in Section 6.3.4.

1. Place the PDMS piece(s) feature side up on a cutting mat.

2. Use the 1 mm biopsy punch to add the tubing inlets and outlets into the appropriate places in the design. Use a Nitrogen gun to blow away any PDMS excess.

3. Using a blade, cut around the edges of each chip following the design pattern. Depending on the design other features may also require cutting away (e.g. mass spectrometry chip emitter outlets).

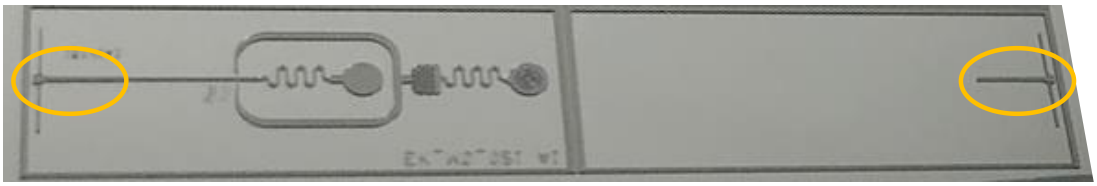


*Figure 6.3.17: Example of a double layer mass spectrometry chip design. The pieces that will form the top and bottom of the PDMS chip are as indicated. The areas highlighted with the orange rings require alignment during the assembly of the top and bottom PDMS pieces.*

4. Use scotch tape to clean all sides of the two PDMS pieces by repeatedly pressing and removing fresh strips of tape on to the PDMS surface. This removes dust from the PDMS surface. Cover both pieces of PDMS in scotch

tape to keep them clean until required in steps 6 (bottom layer) and 12 (top layer).

5. Using scotch tape, clean a glass microscope slide by repeatedly pressing and removing fresh strips of tape on to the glass surface to remove dust. Cover the slide in scotch tape until required.

6. Remove the tape from the bottom piece of the microfluidic chip from step 4. Place the PDMS feature side **down** on a Petri dish lid and place this and the glass slide into the plasma cleaner chamber and close the door.

7. Switch on the PlasmaFlo and plasma cleaner units (Harrick Plasma, Ithaca, NY, USA) and the attached vacuum pump. Open the oxygen cylinder (1 Bar), and wait until a stable chamber pressure is reached as indicated on the digital display. As a guide set the pressure to 600 mTorr with an $O_2$ flow of approximately 15 sccm (flow meter 1). Allow the plasma cleaner to pump at this pressure for approximately 2 minutes to ensure $O_2$ is reaching the chamber.

8. Using the dial, turn the RF level up to high to generate $O_2$ plasma in the chamber. The chamber should glow lilac-purple and this indicates the presence of $O_2$ plasma. Keep the RF level high for 25 seconds before switching the RF dial to the off position.

9. Switch off the vacuum pump and gently turn the Swagelok valve to release the vacuum from the chamber until the door opens.

10. Remove the PDMS piece and the glass slide from the chamber and promptly place the chip piece feature side **up** onto the glass slide near the non-frosted end of the slide (Figure 6.3.18 B). (Note: the emitter channel outlet should face

away from the frosted glass). Press down on the PDMS piece to bind it to the glass slide. Place the resulting glass slide in an oven at 110 °C for 1-2 hours.

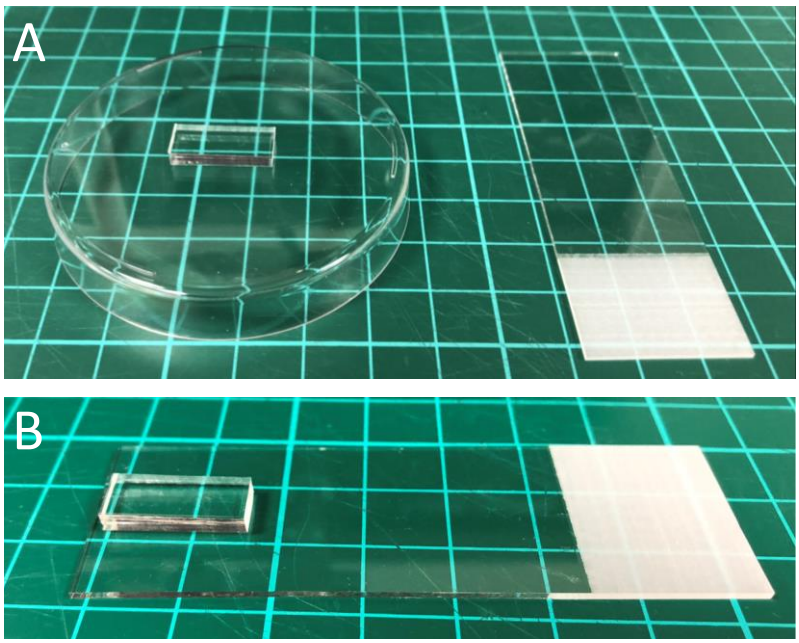


*Figure 6.3.18: A) Photograph of a PDMS bottom piece and glass slide that make up the lower part of a double-layer microfluidic chip before insertion into the plasma cleaner unit. B) Photograph of the placement of the PDMS bottom piece on to the glass slide after exposure to oxygen plasma. Scale: In all photos, green squares are equivalent to 1 cm x 1 cm.*

11. Remove the glass slide from the oven and allow to cool. Clean the attached PDMS with scotch tape to remove any dust which may have settled on the PDMS whilst in the oven.

12. Remove the tape from the top part of the microfluidic chip from step 4. Place the PDMS feature side **up** on a Petri dish lid and place this and the glass slide containing PDMS bottom layer into the plasma cleaner chamber and close the door.

13. Switch the vacuum pump on and allow the chamber to reach the desired pressure. Once stabilised allow the chamber to remain at this pressure for 2 minutes to allow $O_2$ to flow in.

14. Using the dial, turn the RF level up to high to generate $O_2$ plasma in the chamber. The chamber should glow lilac-purple and this indicates the presence of $O_2$ plasma. Keep the RF level high for 25 seconds before switching the RF dial to the off position.

15. Switch off the vacuum pump and gently turn the Swagelok valve to release the vacuum from the chamber until the door opens.

16. Remove the glass slide and PDMS from the chamber and promptly place the glass slide under the microscope and focus on the feature area which requires alignment with the top piece.

17. Without touching the PDMS with the pipette tip, place 10 µL of filtered methanol on to the PDMS bottom piece ensuring the whole of the PDMS surface is covered (Figure 6.3.19).

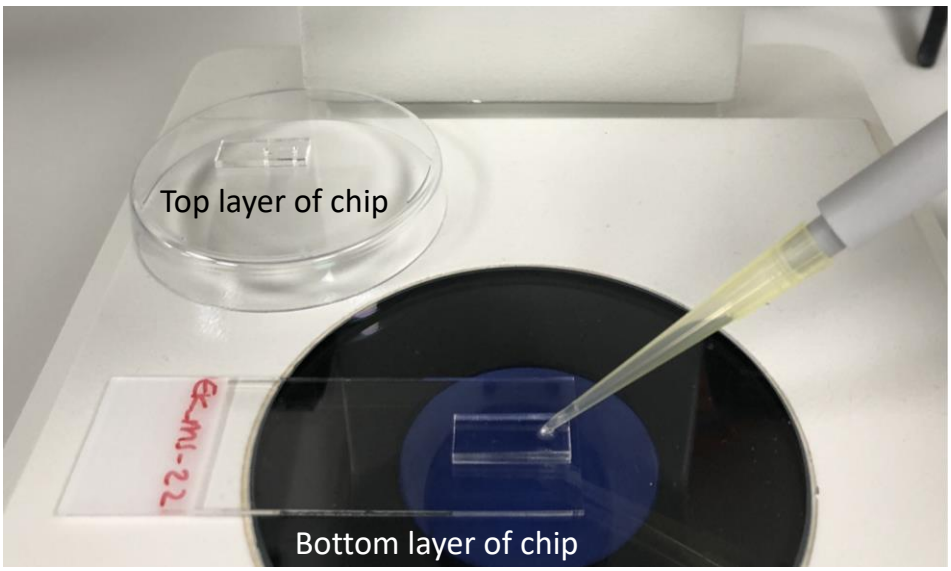


*Figure 6.3.19: Addition of methanol to the bottom layer of the PDMS chip after exposure to oxygen plasma and before the placement and alignment of the top PDMS layer.*

18. Place the PDMS top piece feature side **down** onto the bottom piece, roughly aligning the top and bottom designs by eye.

19. Whilst looking under the microscope, move the top piece of the PDMS over the methanol coated bottom piece to align the top and bottom designs more accurately (Figure 6.3.20).

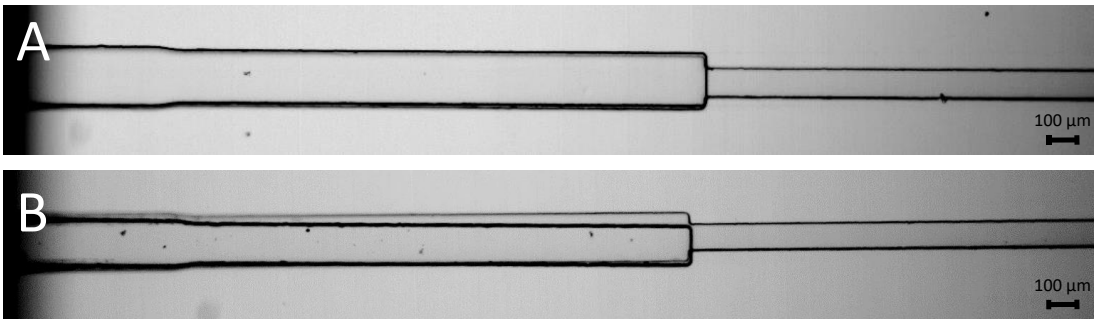


*Figure 6.3.20: Placement of the two PDMS pieces to achieve alignment of the top and bottom designs. A) Good Alignment. B) Misalignment.*

20. When satisfied with the alignment, place the resulting slide in an oven at 110 °C for 1-2 hours.

21. Ensure the plasma cleaner units are switched off and the oxygen cylinder is closed.

22. Remove the slide containing the PDMS chip (step 20) from the oven (Figure 6.3.21), allow to cool and protect the chip inlets from dust by covering them with scotch tape. Your microfluidic chip is now ready for use or further fabrication steps (e.g. the addition of emitters or electrodes).

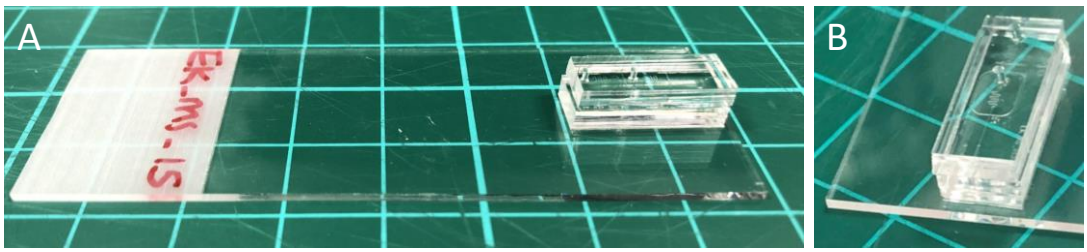


*Figure 6.3.21: A) Fully assembled double-layer PDMS chip including glass slide. B) Close up photograph of the PDMS double-layer chip. Scale: In both photos, green squares are equivalent to 1 cm x 1 cm.*

### 6.3.6 Insertion of emitters into Mass Spectrometry microfluidic chips

The following instructions assume pre-assembly of a double-layer PDMS mass spectrometry chip as described in Section 6.3.5.

1. Cut the mass spectrometry emitter (fused silica or stainless steel capillary) to the desired length using a ceramic tile cutter.

2. Position the double-layer microfluidic chip underneath the microscope so the emitter entrance is visible (Figure 6.3.22 A).

3. Using tweezers or fingers align the emitter cut in step 1 with the emitter entrance at the side of the chip and carefully insert the emitter into the open channel (Figure 6.3.22 B).

4. Gently push the emitter down the PDMS opening until the emitter reaches the microfluidic channel (Figure 6.3.22 C, this is also where the features in the bottom layer of the chip end).

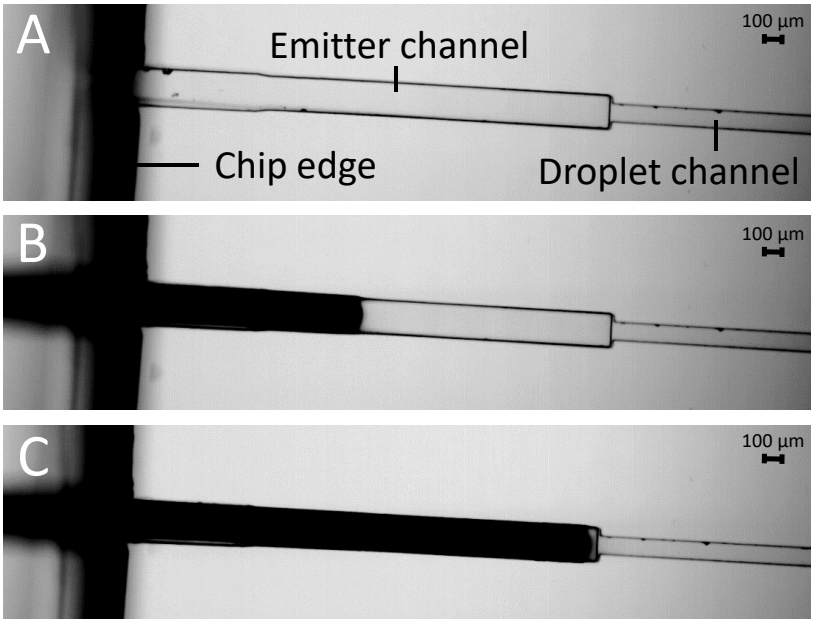


*Figure 6.3.22: A) Microscope image (5x) of the microfluidic emitter channel into which the emitter will be placed. The microfluidic channel and edge of the chip have been indicated. B) Microscope image (5x) showing partial insertion of a stainless steel capillary into a double-layered MS chip. C) Microscope image (5x) showing full insertion (i.e. up to the microfluidic channel) of a stainless steel capillary into a double-layered MS chip.*

5. Apply a small amount ELASTOSIL® E43 silicone rubber (Wacker Chemie, Munich, Germany) around the emitter entrance to hold the emitter in place (Figure 6.3.23).

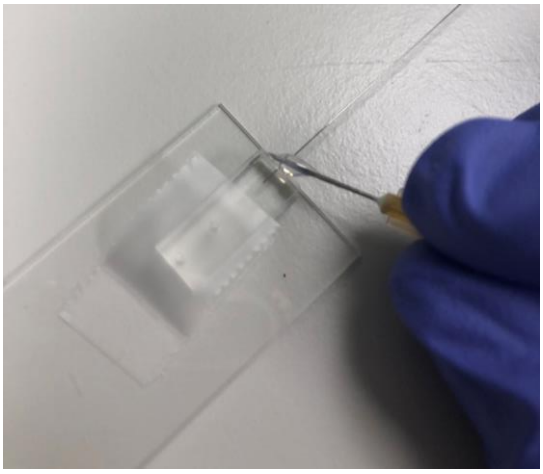

*Figure 6.3.23: Addition of ELASTOSIL® E43 silicone rubber to seal the emitter entrance and hold the stainless steel emitter in place within the microfluidic chip.*

6. Allow ELASTOSIL® E43 silicone rubber to dry overnight before using the chip.

## 6.4 Microfluidic Chip Use - Droplet Generation

### 6.4.1 Droplet Generation Introduction

This guide provides step-by-step instructions on how to generate and collect a population of mono-disperse droplets using the Sphere Fluidics Ltd Single-Cell Encapsulation System. The system utilises a microscope, high-speed camera and syringe pumps, alongside a droplet generation microfluidic chip containing a flow-focusing (FF) junction at which droplet generation takes place. Furthermore, this system in conjunction with a spreadsheet template allows for droplet generation frequencies and droplet sizes to be determined during collection.

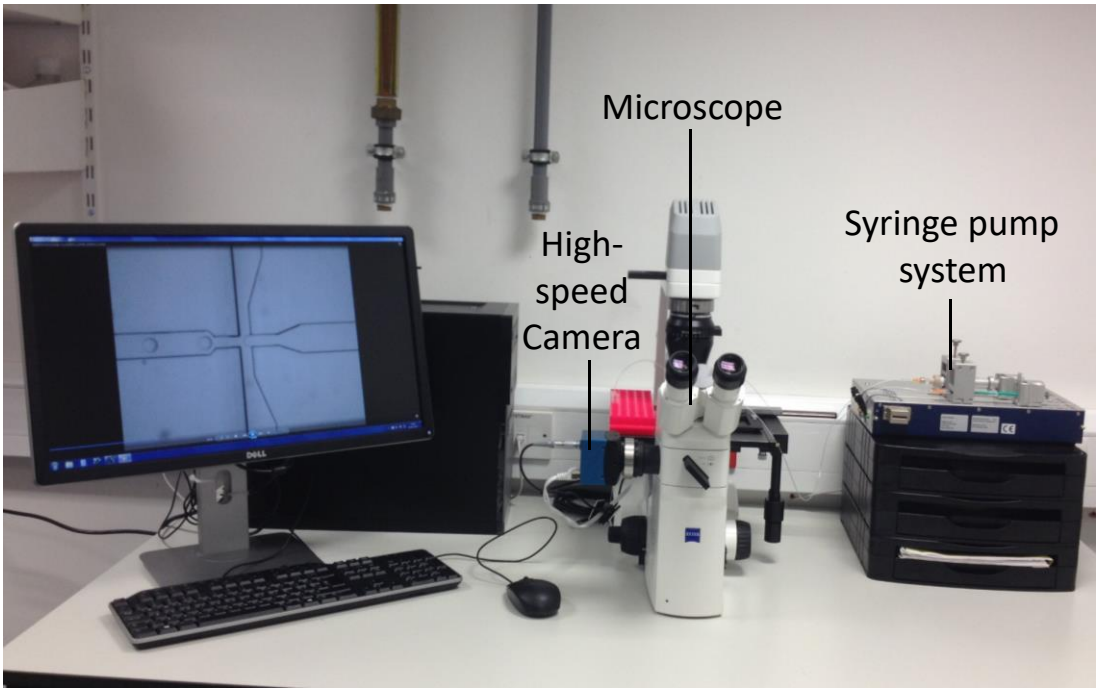


*Figure 6.4.1: Photograph of the Sphere Fluidics Ltd Single-Cell Encapsulation System situated within the Manchester Institute of Biotechnology.*

Note on droplet sizes: Along with the chosen flow rates and liquid viscosities, the dimensions of the FF junction employed will affect the size of the droplets generated. See Table 6.4.1 for a guide to FF dimensions and their corresponding droplet ranges.

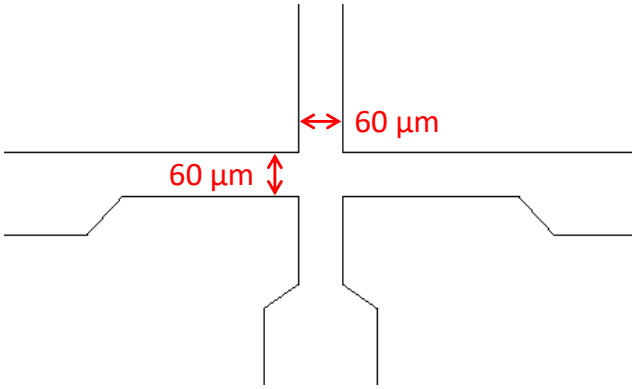


*Figure 6.4.2: Flow-focusing junction design indicating the dimensions of the junction that have the greatest effect on the droplet size generated. Drawn to scale (x100).*

*Table 6.4.1: A guide to microfluidic chip flow-focusing (FF) junction dimensions and the corresponding range of droplet sizes they produce with high mono-dispersity. Data in this table relates to droplet generation chips manufactured by Sphere Fluidics Ltd (Pico-Gen™) and has been adapted from their Pico-Gen™ user guide (https://spherefluidics.com/wp-content/uploads/2018/10/Pico-Gen-User-Guide-2016-12-02-V1.pdf?v=79cba1185463).*

| FF junction size | Droplet Diameter (µm) | Droplet Volume (pL) |
|---|---|---|
| 40 x 40 | 40 – 75 | 35 – 220 |
| 60 x 60 | 65 – 100 | 150 – 550 |
| 80 x 80 | 95 – 125 | 500 – 1,000 |

#### 6.4.1.1 Notes on Droplet Generation with Mass Spectrometry emitter

The following instructions may also be applied to droplet generation chips which feature a mass spectrometry (MS) emitter in place of the outlet tubing (Figure 6.4.3). This emitter allows for droplets generated at the FF junction to flow directly into the MS with the added advantage that the smaller internal diameter of the inserted emitter causes the droplets to form 'plugs' of the aqueous phase, thus keeping the spacing between droplets equal (Figure 6.4.4).

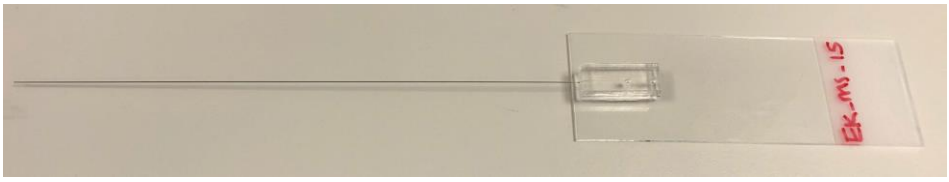

*Figure 6.4.3: Droplet generation microfluidic chip with mass spectrometry emitter outlet.*

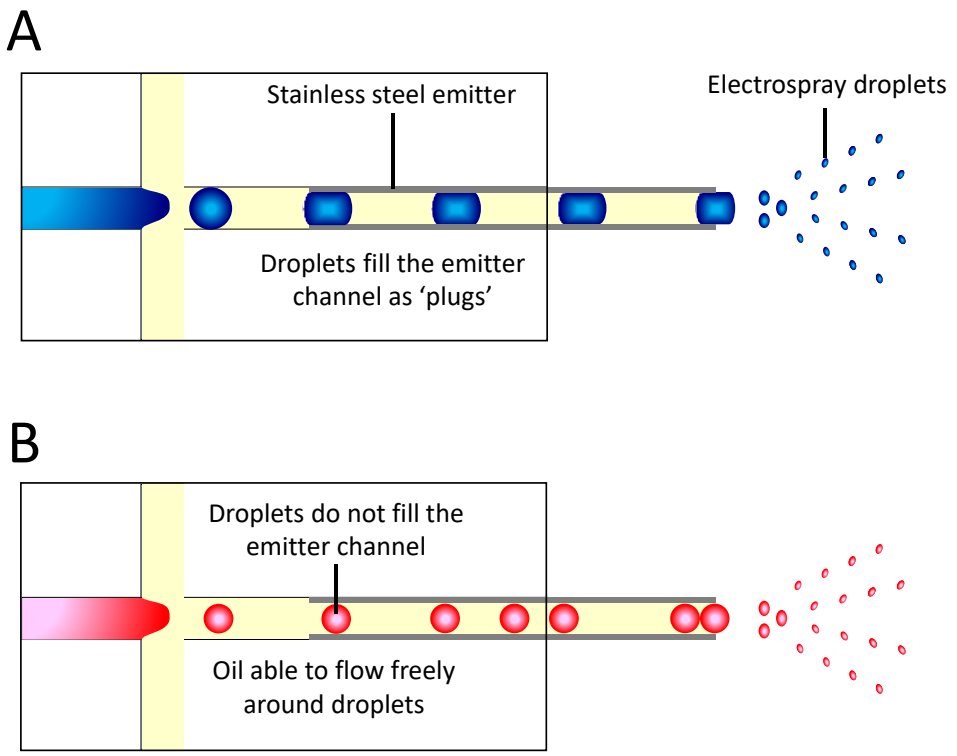


*Figure 6.4.4: A) Diagram illustrating 'plug-like flow' of droplets within a stainless steel mass spectrometry emitter. Droplet diameter is larger than that of the internal diameter of the emitter, and thus even spacing remains between droplets. B) Diagram illustrating 'non-plug-like flow' of droplets within a stainless steel mass spectrometry emitter. Droplet diameter is smaller than that of the internal diameter of the emitter, resulting in oil being able to flow freely around droplets, thus droplets exit the emitter with uneven spacing.*

Before coupling with an MS instrument, it is advised to examine the performance of a new MS microfluidic chip design under a microscope. This not only aids in the selection of appropriate flow rates but also allows for the droplet generation frequency (and consequently the droplet size) to be determined. Please note that the droplet ranges given in Table 6.4.1 may not apply to MS chip designs. This is due to the lower flow rates utilised when undertaking microfluidics - mass spectrometry experiments, and also as a result of the increased backpressure experienced upon the fluidic system as a consequence of the inserted capillary emitter.

### 6.4.2 Preparation of liquid phases and microfluidic chip

1. Turn on the syringe pumps, microscope lamp, and computer, and connect the high-speed camera to the power supply cable.

2. Remove the protective tape from the droplet generation chip and mount the slide securely onto the microscope stage.

3. Open the high-speed camera software (MotionBLITZDirector2, Mikrotron GmbH, version 1.4.3 (Build: 2419)) and link the camera by selecting 'EoSens mini' in the upper left-hand menu and press 'connect' (Figure 6.4.5).

4. In the lower horizontal bar select 'live' to see the microscope image and use the coarse and fine focus of the microscope along with the XY moveable stage to find and focus upon the flow-focusing junction of the droplet generation chip. This can be achieved in 5x, 10x or 20x optical zoom.

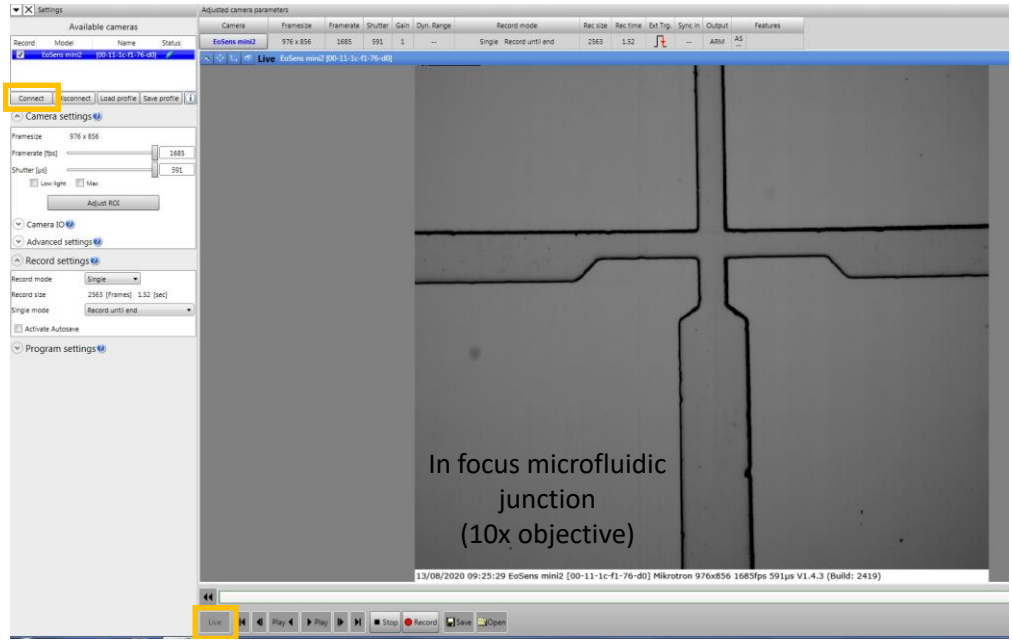


*Figure 6.4.5: Screen capture of the high-speed microscope camera user interface (MotionBLITZDirector2, Mikrotron GmbH, version 1.4.3 (Build: 2419)). The 'Connect' and 'Live' icons have been highlighted within orange boxes.*

5. Open the syringe pump software (neMESYS UserInterface, Cetoni GmbH, version 2016.6.14.1), select 'scan devices' and use the orange triangle icons ('refill syringe') to drive both the oil and aqueous syringes to their highest position (Figure 6.4.6).

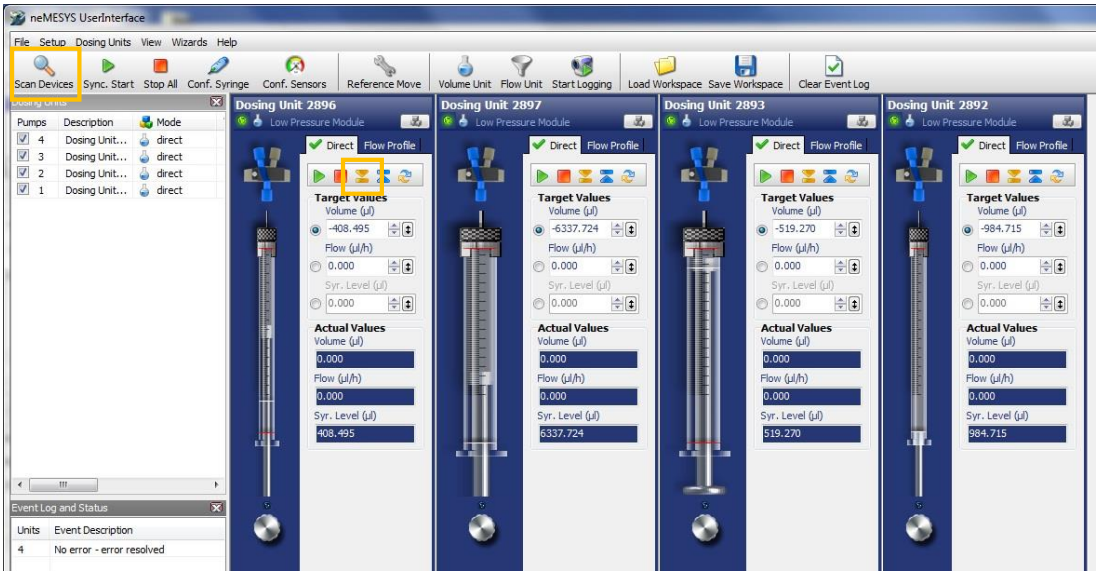


*Figure 6.4.6: Screen capture of the syringe pump user interface (neMESYS UserInterface, Cetoni GmbH, version 2016.6.14.1). The 'Scan Devices' and 'Refill Syringe' icons have been highlighted within orange boxes.*

6. Fill a gas-tight syringe with the desired immiscible (oil) phase (e.g. 1% Pico-surf™ surfactant (Sphere Fluidics Ltd, Cambridge, UK) diluted in filtered Novec 7500 Engineered fluid (3M, Maplewood, MN, USA)).

7. Using tweezers, carefully thread fine bore tubing (0.38 mm ID, 1.09 mm OD, Smiths Medical International Limited, Kent, UK) over a 25G (5/8") needle and connect the needle to the gas-tight syringe outlet (Figure 6.4.7).

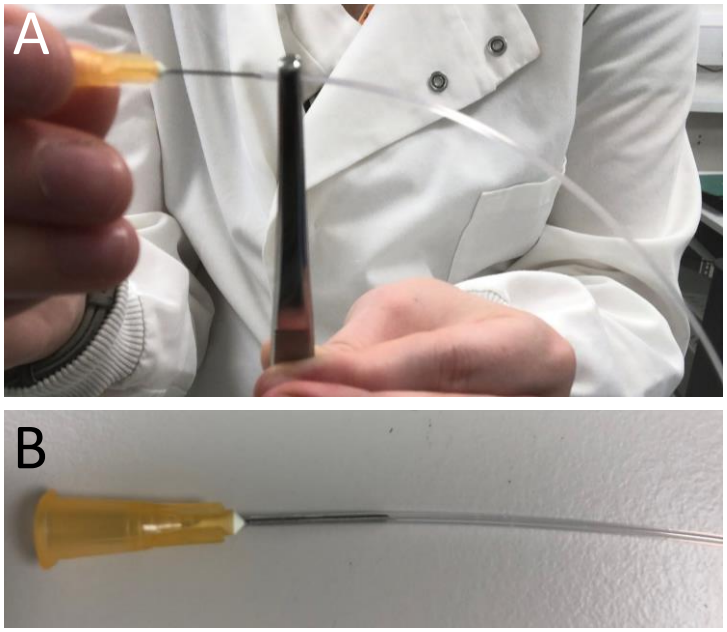


*Figure 6.4.7: A) Photograph indicating correct procedure to thread fine bore tubing over a 25G needle. Tubing should be held with tweezers to avoid needle stick injury to fingers. B) Photograph of fine bore tubing with a 25G needle fully inserted before connection to a syringe.*

8. Mount the gas-tight syringe into the oil pump, and fit the cap and holder by using the screws.

9. Run the oil syringe pump at a rate of 2000 μL/hr to purge the line, and observe oil running from the fine bore tubing. Ensure that no air bubbles remain in the tubing line or syringe. Stop the pump.

10. Using tweezers connect the fine bore tubing containing the oil phase to the oil inlet on the microfluidic chip (Figure 6.4.8) by pushing the tubing into the 1 mm punched oil port. (This port has a filter adjacent to the inlet).

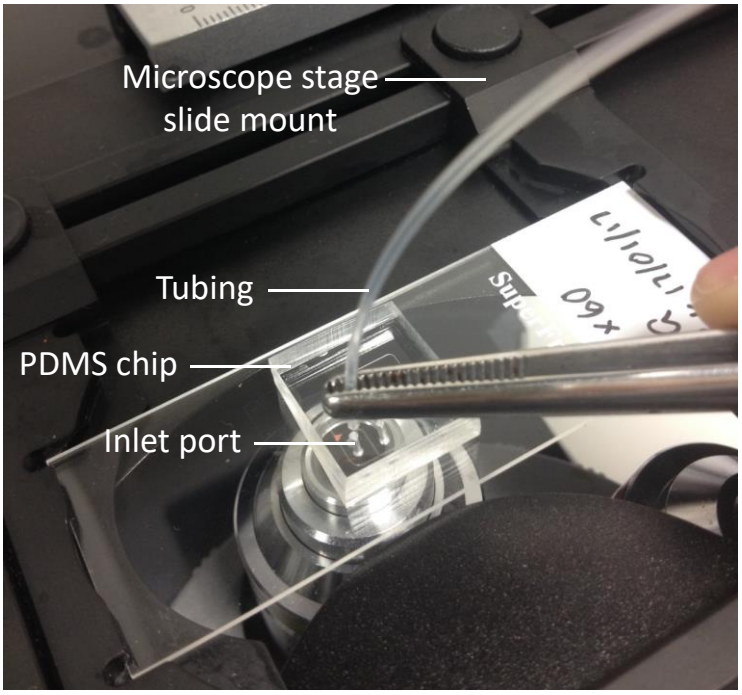


*Figure 6.4.8: Photograph showing a droplet generation microfluidic chip mounted on the microscope stage. Tweezers hold the fine bore tubing as it is being inserted into the inlet port.*

11. Cut a length of fine bore tubing to be used as the waste outlet line (ensure sufficient length), and push one end into the 1 mm outlet port on the chip. The open end should be directed into a waste Eppendorf or falcon tube. Note: if using a droplet generation mass spectrometry chip, this waste tubing is not needed, and the droplets will instead flow out of the capillary emitter.

12. Fill a 1 mL Norm-Ject syringe with the aqueous sample. If the aqueous sample does not contain cells it is advisable to filter the solution before introduction into the 1mL syringe.

13. Using tweezers, thread fine bore tubing over a 5/8" needle and connect the needle to the Norm-Ject syringe outlet.

14. Mount the 1 mL syringe onto the aqueous syringe pump, and fit the cap and holder by using the screws.

15. Run the aqueous syringe pump at a rate of 2000 μL/hr to purge the line, and observe a small amount of aqueous sample running from the fine bore tubing. Ensure that no air bubbles remain in the tubing line or syringe. Stop the pump.

16. Using tweezers, connect the fine bore tubing containing the aqueous phase to the aqueous inlet on the microfluidic chip by pushing the tubing into the 1 mm port. (This port has no filter adjacent to the inlet).

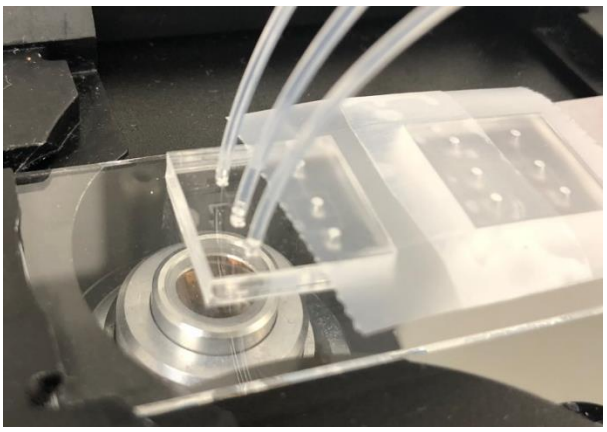

*Figure 6.4.9: Close up photograph of a droplet generation microfluidic chip with 3 tubing connections inserted into the ports. (2x inlet ports, 1x outlet port).*

### 6.4.3 Droplet Generation

1. Select 'flow' for the aqueous pump and set the value to your desired flow rate in μL/hr (Figure 6.4.10). Press enter.

2. Select 'flow' for the oil pump and set the value to your desired flow rate in μL/hr (Figure 6.4.10). Press enter.

3. At the top of the window select 'start all' and use the checkboxes to select the pumps in use followed by 'OK' to start running the pumps at the rates set in steps 1 and 2 (Figure 6.4.10).

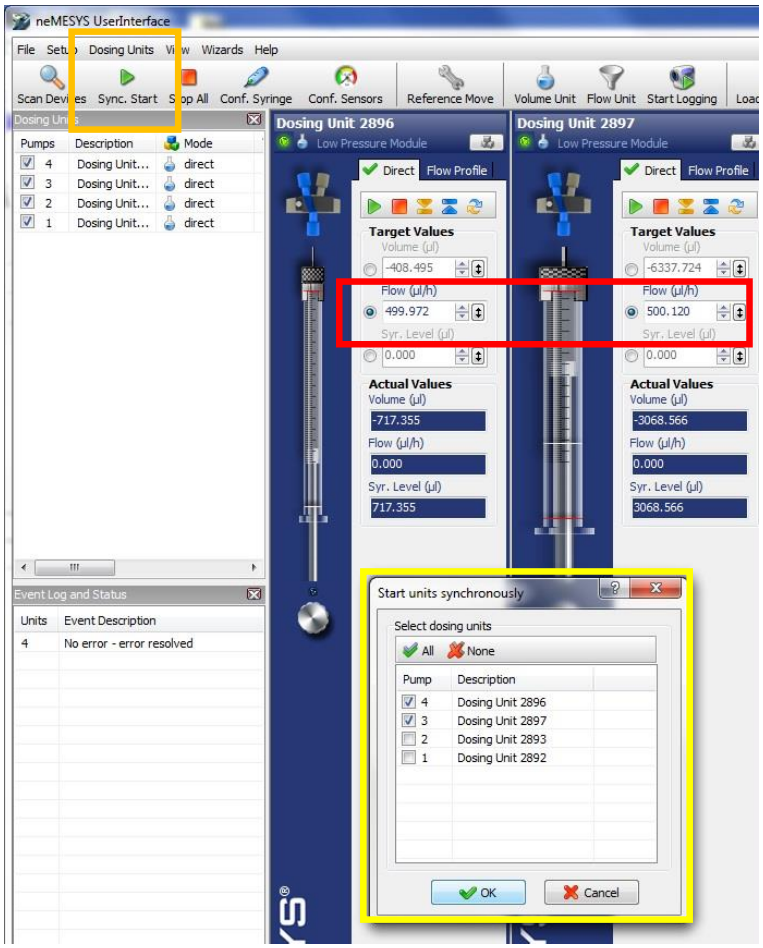


*Figure 6.4.10: Screen capture of syringe pump software (neMESYS UserInterface, Cetoni GmbH, version 2016.6.14.1) highlighting the flow rate input for the two syringes in use (red box), 'Sync. Start' icon (orange box) and the subsequent dialog box (yellow boxed inset). The two syringe pump units to be started simultaneously have been selected in the dialog.*

4. Observe the oil and aqueous flows beginning to flow through the flow-focusing junction on the chip using the camera software.

5. Droplets will begin to be created at the junction, however, allow for the generation to flow for a few minutes before droplet collection to ensure the syringe pumps and droplet size have stabilised. Droplets with a dark black ring around them are droplets of air dispersed in the oil phase and not droplets of the aqueous phase (Figure 6.4.11 A).

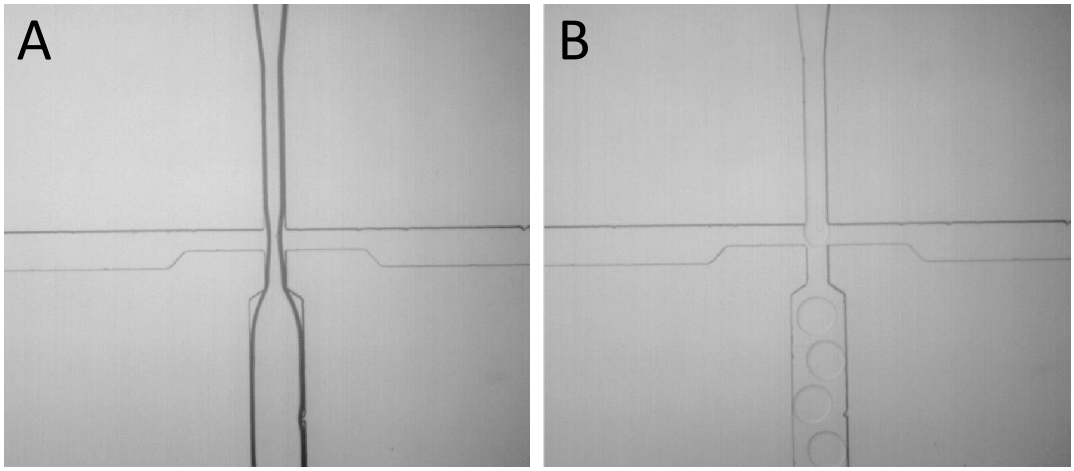


*Figure 6.4.11: A) Microscope image (10x objective) demonstrating air flowing through the aqueous channel of the flow-focusing junction. Flowing or trapped air bubbles are typically observed with a thick black outline within the channels. B) Microscope image (10x objective) of aqueous droplet generation occurring within the flow-focusing junction.*

6. Open the droplet calculator excel spreadsheet (Figure 6.4.12). Add the required details and flow rates before using 'saving as' to rename your spreadsheet.

| | A | B | C | D | E | F | G | H | I | J | K | L | M | N |
|---|---|---|---|---|---|---|---|---|---|---|---|---|---|---|
| 1 | Date: | 13/08/2020 | | | | | | | | | | | | |
| 2 | Operator: | EK | | | | | | | | | | | | |
| 3 | Oil pump: | 2897 | | | | | | | | | | | | |
| 4 | Aqueous pump: | 2896 | | | | | | | | | | | | |
| 5 | Oil: | ~1% PS-1 in Novec7500 | | | | | | | | | | | | |
| 6 | Aqueous: | LEU ENK in 100mM AmAc | | | | | | | | | | | | |
| 7 | Chip used | 70 x 70 N229 | | | | | | | | | | | | |
| 8 | | | | | | | | | | | | | | |
| 9 | | | | | | | | | | | | | | |
| 10 | | | | | | | | | | | | | | |
| 11 | | | | | | | | | | | | | | |
| 12 | Note: | | Aque. uL/hr | Fluo. uL/hr | F/A Ratio | Time ms | Start ms | End ms | Drop No | Freq. Hz | Aque. pL/s | Volume pL | Cubic Rad. um^3 | Diameter um |
| 13 | 1 | | | | #DIV/0! | 0 | | | 20 | #DIV/0! | 0 | #DIV/0! | #DIV/0! | #DIV/0! |
| 14 | 2 | | | | #DIV/0! | 0 | | | 20 | #DIV/0! | 0 | #DIV/0! | #DIV/0! | #DIV/0! |
| 15 | 3 | | | | #DIV/0! | 0 | | | 20 | #DIV/0! | 0 | #DIV/0! | #DIV/0! | #DIV/0! |
| 16 | 4 | | | | #DIV/0! | 0 | | | 20 | #DIV/0! | 0 | #DIV/0! | #DIV/0! | #DIV/0! |
| 17 | 5 | | | | #DIV/0! | 0 | | | 20 | #DIV/0! | 0 | #DIV/0! | #DIV/0! | #DIV/0! |
| 18 | 6 | | | | #DIV/0! | 0 | | | 20 | #DIV/0! | 0 | #DIV/0! | #DIV/0! | #DIV/0! |
| 19 | | | | | | | | | | | Average | #DIV/0! | | #DIV/0! |

*Figure 6.4.12: Screen capture of the 'droplet calculator spreadsheet' before use (i.e. without input values).*

7. Set the fast camera software to record a high number of frames per second (fps). The number of fps available is dependent upon the size of the region of interest (ROI) area, (i.e. larger ROI, fewer fps available). You may also need to

adjust the shutter speed and microscope lamp (bright field) intensity to obtain the optimal image of your junction.

8. Click ‘record’ to record a video of droplet generation at the junction. This video is comprised of a large number of still images from which the individual images or the combined video can be saved and exported if required.

9. To calculate the droplet generation frequency and size, select a frame, or time point, at which one droplet has just been generated at the junction (Figure 6.4.13). This is droplet number 1. Note the time of this frame in milliseconds (ms), and add it to the ‘start time’ column of the excel spreadsheet.

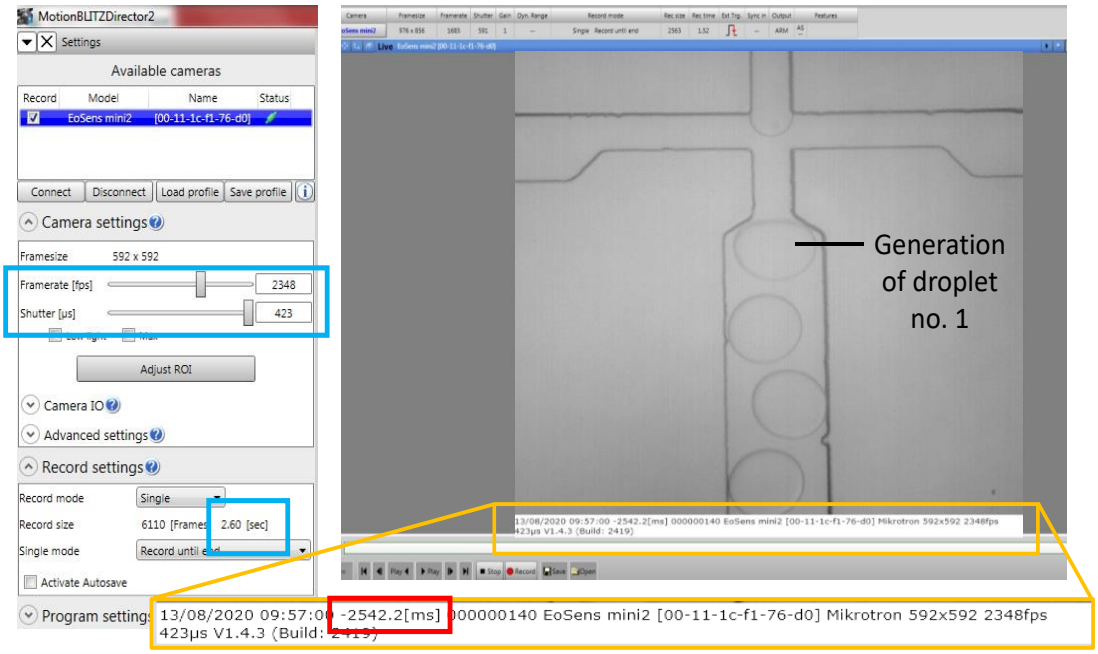


*Figure 6.4.13: Screen capture of high-speed camera software (MotionBLITZDirector2, Mikrotron GmbH, version 1.4.3 (Build: 2419)) highlighting the camera settings used (blue boxes) and the frame time used (red box) for input into the droplet calculator spreadsheet as the ‘start time’.*

10. Observe and count the generation of 20 droplets in the recording using the keyboards right arrow. Note the time in milliseconds of the frame where the

20th droplet was generated. Add this time to the 'end time' column in the spreadsheet.

11. Ensure the 'Drop No.' cell within the row is set to 20. The spreadsheet formulae will then calculate the droplet generation frequency, droplet volume (pL) and droplet diameter (μm) based upon the time it took for 20 droplets to flow through the FF junction and the corresponding aqueous flow rate (Figure 6.4.14).

| | A | B | C | D | E | F | G | H | I | J | K | L | M | N |
|---|---|---|---|---|---|---|---|---|---|---|---|---|---|---|
| 1 | Date: | 13/08/2020 | | | | | | | | | | | | |
| 2 | Operator: | EK | | | | | | | | | | | | |
| 3 | Oil pump: | 2897 | | | | | | | | | | | | |
| 4 | Aqueous pump: | 2896 | | | | | | | | | | | | |
| 5 | Oil: | ~1% PS-1 in Novec7500 | | | | | | | | | | | | |
| 6 | Aqueous: | LEU ENK in 100mM AmAc | | | | | | | | | | | | |
| 7 | Chip used | 70 x 70 N229 | | | | | | | | | | | | |
| 8 | | | | | | | | | | | | | | |
| 9 | | | | | | | | | | | | | | |
| 10 | | | | | | | | | | | | | | |
| 11 | | | | | | | | | | | | | | |
| 12 | Note: | | Aque. uL/hr | Fluo. uL/hr | F/A Ratio | Time ms | Start ms | End ms | Drop No | Freq. Hz | Aque. pL/s | Volume pL | Cubic Rad. um^3 | Diameter um |
| 13 | 1 | | 200 | 300 | 1.5 | 120.5 | 2542.2 | 2421.7 | 20 | 166 | 55556 | 335 | 80 | 86 |
| 14 | 2 | | 200 | 300 | 1.5 | 123.5 | 2576.3 | 2452.8 | 20 | 162 | 55556 | 343 | 82 | 87 |
| 15 | 3 | | 200 | 300 | 1.5 | 122.7 | 2586.5 | 2463.8 | 20 | 163 | 55556 | 341 | 81 | 87 |
| 16 | 4 | | 200 | 300 | 1.5 | 120.9 | 2529.4 | 2408.5 | 20 | 165 | 55556 | 336 | 80 | 86 |
| 17 | 5 | | 200 | 300 | 1.5 | 121 | 2569.5 | 2448.5 | 20 | 165 | 55556 | 336 | 80 | 86 |
| 18 | 6 | | 200 | 300 | 1.5 | 120.1 | 2520.5 | 2400.4 | 20 | 167 | 55556 | 334 | 80 | 86 |
| 19 | | | | | | | | | | | Average | 337 | | 86 |

*Figure 6.4.14: Screen capture of the 'droplet calculator spreadsheet' upon completion of a droplet generation experiment. The aqueous and oil flow rates have been added to the appropriate cells in the spreadsheet along with the droplet start and end times as indicated by the camera software. Six repetitions of the droplet recording and counting procedure have been executed to calculate an average droplet volume and diameter (as indicated in the yellow cells). Spreadsheet formulae can be found in Figure 6.4.16.*

12. If satisfied with the size of the droplets generated, the outlet tube can be removed from the waste Eppendorf/falcon tube and inserted into the collection Eppendorf/falcon tube to collect your droplets. Note: it is best to rest the outlet tube on the side of the collection vessel, rather than directly in the liquid or letting the droplets drip into the tube.

13. It is advised to continue monitoring droplet size throughout collection using the spreadsheet to ensure that the droplet size does not drift from the desired size.

14. If the droplet size is not as desired, adjust the aqueous and oil flow rates before repeating steps 8 through 11 until the appropriate droplet size is reached.

### 6.4.4 Discontinuation of Droplet Generation

1. When the desired volume of droplets has been generated, the outlet tubing can be moved back into the waste Eppendorf/falcon tube. Seal the droplet containing vessel and keep upright until required.

2. Use 'stop all' in the syringe pump software to stop the pumps.

3. Remove the oil and aqueous inlet tubing from the generation chip and discard the chip into a glass or sharps bin.

4. Seal the oil tubing outlet using a lighter and tweezers. This allows for any oil remaining in the syringe to be used in a future experiment. Undo the holding screws and remove the syringe from the pump for storage.

5. Remove the aqueous syringe from the pump and discard the sample, syringe and tubing as appropriate.

6. Close the syringe pump software and switch off the syringe pump unit.

### 6.4.5 Droplet Mono-dispersity check

1. Mount a new glass microscope slide onto the XY stage.

2. Pipette ~10 μL of previously prepared droplets (including a small amount of the oil phase) onto the glass slide, and use the XY stage and microscope focus to locate the droplet monolayer.

3. Observe the level of mono-dispersity throughout the population of droplets in the high-speed camera software (Figure 6.4.15 B and C). Record and save the images as required. This can be achieved using 5x, 10x, or 20x objective.

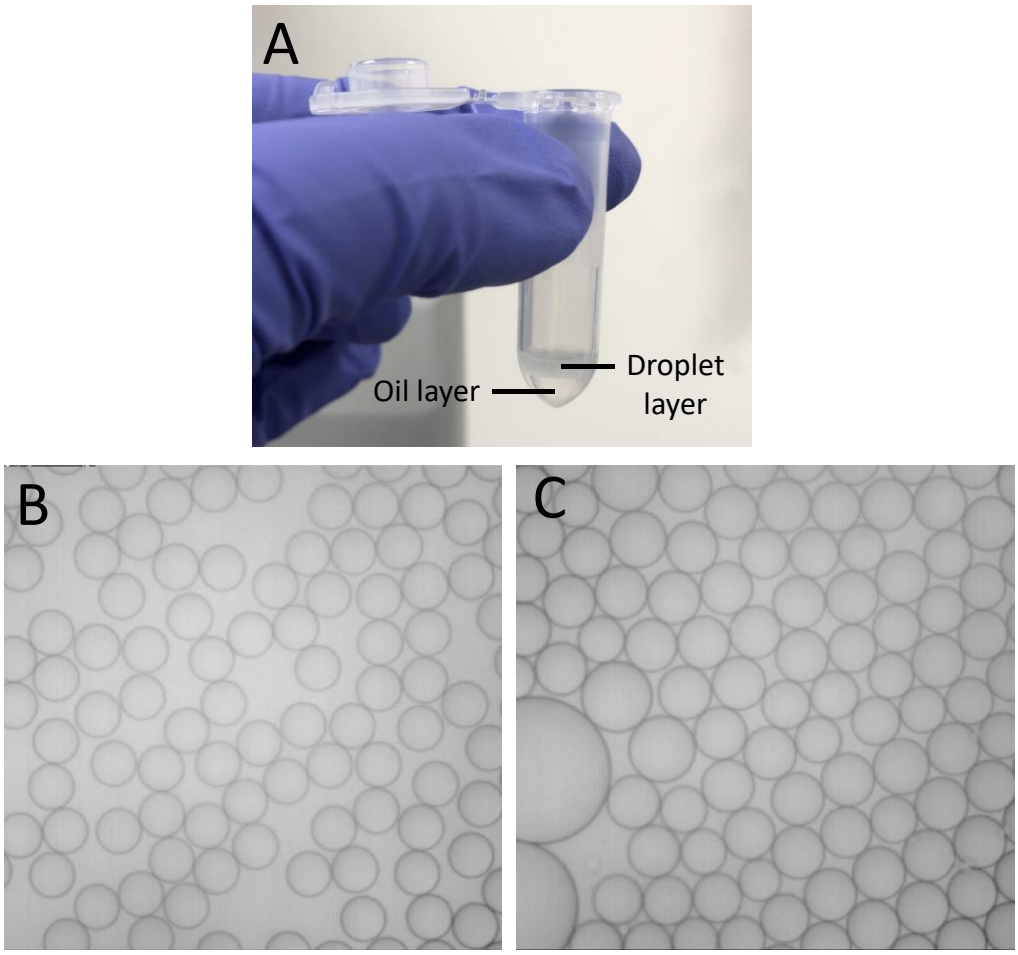


*Figure 6.4.15: A) Photograph of an Eppendorf containing collected droplets. The droplet layer and oil layer have been indicated on the photograph. B) Microscope image (10x objective) of droplets collected with high mono-dispersity (~340 pL). C) Microscope image (10x objective) of droplets collected with lower mono-dispersity - i.e. droplets occur in a mixture of sizes.*

4. Once imaged, discard the glass slide in the sharps or glass bin.

5. Close the camera software, disconnect the camera power cable and turn off the microscope lamp.

6. Shut down the computer and ensure the area is tidy and all samples have been removed or discarded as appropriate. Waste oil and surfactant should be discarded in a halogenated waste drum.

7. The remaining droplets are then ready for use in further experimental work or disposal *via* an appropriate waste vessel.

### 6.4.6 Spreadsheet Formulae

| | A | B | C | D | E | F | G | H | I | J | K | L | M | N |
|---|---|---|---|---|---|---|---|---|---|---|---|---|---|---|
| 1 | Date: | 13/08/2020 | | | | | | | | | | | | |
| 2 | Operator: | EK | | | | | | | | | | | | |
| 3 | Oil pump: | 2897 | | | | | | | | | | | | |
| 4 | Aqueous pump: | 2896 | | | | | | | | | | | | |
| 5 | Oil: | ~1% PS-1 in Novec7500 | | | | | | | | | | | | |
| 6 | Aqueous: | LEU ENK in 100mM AmAc | | | | | | | | | | | | |
| 7 | Chip used | 70 x 70 N229 | | | | | | | | | | | | |
| 8 | | | | | | | | | | | | | | |
| 9 | | | | | | | | | | | | | | |
| 10 | | | | | | | | | | | | | | |
| 11 | | | | | | | | | | | | | | |
| 12 | Note: | | Aque. uL/hr | Fluo. uL/hr | F/A Ratio | Time ms | Start ms | End ms | Drop No | Freq. Hz | Aque. pL/s | Volume pL | Cubic Rad. um^3 | Diameter um |
| 13 | 1 | | | | =D13/C13 | =G13-H13 | | | 20 | =I13/F13*1000 | =C13*1000000/3600 | =K13/J13 | =L13*3/4/3.14159265 | =10*2*POWER(M13, 1/3) |
| 14 | 2 | | | | =D14/C14 | =G14-H14 | | | 20 | =I14/F14*1000 | =C14*1000000/3600 | =K14/J14 | =L14*3/4/3.14159265 | =10*2*POWER(M14, 1/3) |
| 15 | 3 | | | | =D15/C15 | =G15-H15 | | | 20 | =I15/F15*1000 | =C15*1000000/3600 | =K15/J15 | =L15*3/4/3.14159265 | =10*2*POWER(M15, 1/3) |
| 16 | 4 | | | | =D16/C16 | =G16-H16 | | | 20 | =I16/F16*1000 | =C16*1000000/3600 | =K16/J16 | =L16*3/4/3.14159265 | =10*2*POWER(M16, 1/3) |
| 17 | 5 | | | | =D17/C17 | =G17-H17 | | | 20 | =I17/F17*1000 | =C17*1000000/3600 | =K17/J17 | =L17*3/4/3.14159265 | =10*2*POWER(M17, 1/3) |
| 18 | 6 | | | | =D18/C18 | =G18-H18 | | | 20 | =I18/F18*1000 | =C18*1000000/3600 | =K18/J18 | =L18*3/4/3.14159265 | =10*2*POWER(M18, 1/3) |
| 19 | | | | | | | | | | | Average | =AVERAGE(L13:L18) | | =AVERAGE(N13:N18) |

*Figure 6.4.16: Screen capture of the 'droplet calculator spreadsheet' formulae.*

## 6.5 Microfluidic Chip Use - Droplet Reinjection

### 6.5.1 Droplet Reinjection Introduction

This guide provides step-by-step instructions on how to reinject a population of mono-disperse droplets using the Sphere Fluidics Ltd Single-Cell Encapsulation System for either mass spectrometry or sorting applications. This method is used extensively in Chapter 5. The system utilises a microscope, high-speed camera and syringe pumps, alongside a droplet reinjection microfluidic chip containing a Y-shaped junction at which the spacing of pre-formulated droplets takes place. Furthermore, this system in conjunction with a spreadsheet template allows for droplet reinjection frequencies to be determined for comparison with mass spectrometry infusion rates. Prior knowledge of the droplet generation 'how-to-guide' featured in Section 6.4 is required to undertake these experiments.

#### 6.5.1.1 Notes on Droplet Reinjection with Mass Spectrometry emitter

The following instructions can be applied to droplet reinjection chips which feature a mass spectrometry (MS) emitter in place of the outlet tubing. This emitter allows for droplets to flow directly into the MS after spacing the droplets from one another in the reinjection region.

Before coupling with an MS instrument, it is advised to examine the performance of a new MS microfluidic chip design under a microscope. This not only aids in the selection of appropriate flow rates but also allows for the droplet reinjection frequency to be determined. Frequencies appropriate for MS are typically in the range of 2 – 10 Hz.

### 6.5.2 Fabrication of a Reinjection Syringe

1. Collect the required materials and equipment.
   You will need: PDMS elastomer mix, needles (21G, 4¾ "), oven, 1 mL Norm-Ject syringes, needles (25G, 5/8 "), tubing (1.09 mm OD, 0.38 mm ID), tubing (0.80 mm ID), scalpel, 2 x 1 mm biopsy punch, tweezers, lighter, scissors, 1 mL pipette, Novec 7500 Engineer fluid (or alternative oil phase).

2. Mix the PDMS elastomer with cross-linker in a 10:1 w/w ratio in a plastic beaker and stir thoroughly.

3. Remove the 21G (4¾ ") needle from the sleeve and discard the needle appropriately. Plug one end of the sleeve with previously cured PDMS or equivalent.

4. Using a 1 mL syringe, dispense the freshly mixed PDMS into the sleeve to about half way up (8 cm). This will make approximately 15 rejection syringes.

5. Place the sleeve in the oven (65 °C) and allow the PDMS to cure (approx. 4 hrs). Note: for this application, the PDMS does not need to be degassed.

6. Once cured, remove the needle sleeve containing cured PDMS from the oven and allow to cool.

7. Use a scalpel to cut off a 5 mm section of the sleeve containing PDMS (Figure 6.5.1 A).

8. Using the 1 mm biopsy punch, punch two holes into the PDMS inside the sleeve (Figure 6.5.1 C and D).

9. Using the scalpel, carefully cut away the sleeve from around the PDMS (Figure 6.5.1 E and F).

10. Cut 3 lengths of 1.09 mm OD tubing, 2 x 15 cm, 1 x 25 cm.

11. Stretch one end of each piece of 15 mm tubing lengths from step 10, and push them through the punched holes (Figure 6.5.1 G). Cut off the stretched regions using scissors (Figure 6.5.1 H). These are the lower inlet and lower outlet of the reinjection syringe.

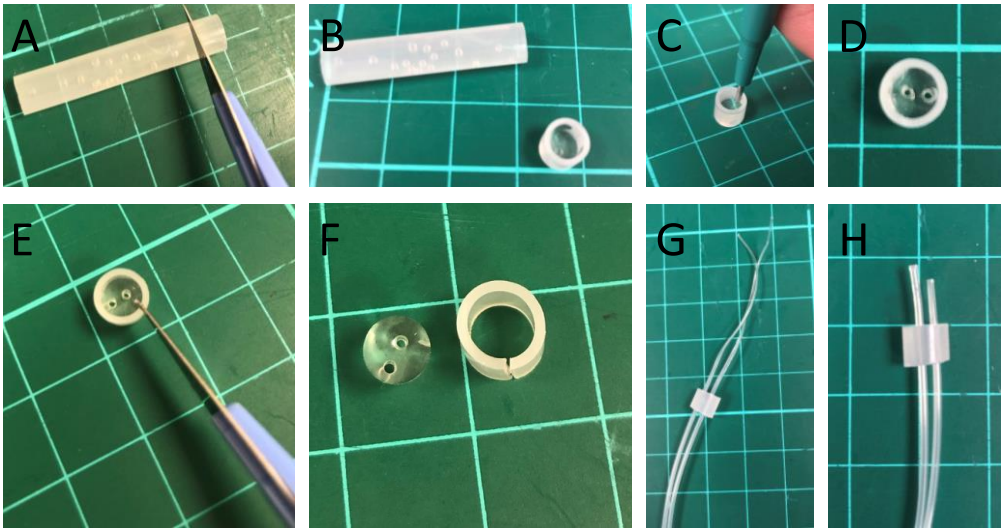


*Figure 6.5.1: Photographs illustrating steps required during the fabrication of a reinjection syringe. A) Cutting of the cured PDMS inside the syringe casing using a scalpel. B) Cut PDMS ready to be punched. C) Punching holes into PDMS using 1 mm biopsy punch. D) Two punched holes in PDMS piece. E) Removal of syringe casing from around the PDMS using a scalpel. F) Syringe casing fully removed from the PDMS. G) Tubing passed through PDMS holes with stretched ends. H) Tubing passed through PDMS holes with stretched ends removed.*

12. Remove the plunger from a 1 mm Norm-Ject syringe and discard the plunger.

13. Push the PDMS piece containing the 2 tubing pieces into the base of the Norm-Ject syringe (Figure 6.5.2 B, i.e. where the plunger would usually go).

14. Prepare the upper outlet by removing the sleeve from the 25G needle, and pass the 25 cm tubing prepared in step 10 over the needle. Use the instructions in step 7 in Section 6.4.2 to do this (Figure 6.4.7). Do not discard the sleeve.

15. Use the second biopsy punch to punch a hole in the top of the needle sleeve (Figure 6.5.2 C). Thread the punched sleeve over the 25 cm tubing and back onto the 25G needle (Figure 6.5.2 D).

16. Cut 3 x 5 mm sections of 0.80 mm ID tubing, and 3 x 15 mm sections of 1.09 mm OD tubing.

17. Melt the ends of the three, 1.09 mm tubing pieces with the lighter and seal each piece using tweezers. Push one 1.09 mm OD tubing pieces into each of the 0.80 mm ID tubing pieces. These are to be used as the reinjection syringe tubing stoppers (Figure 6.5.2 E).

18. Put one stopper onto each of the lower tubing pieces in the Norm-Ject syringe, and one onto the upper outlet tubing connected to the 25G needle.

19. Using a pipette, fill the Norm-Ject syringe (with tubing stoppers) with the desired oil phase.

20. Place the 25G needle from step 15 (with sleeve and stopper) onto the syringe.

21. The reinjection syringe is now ready to use (Figure 6.5.2 F).

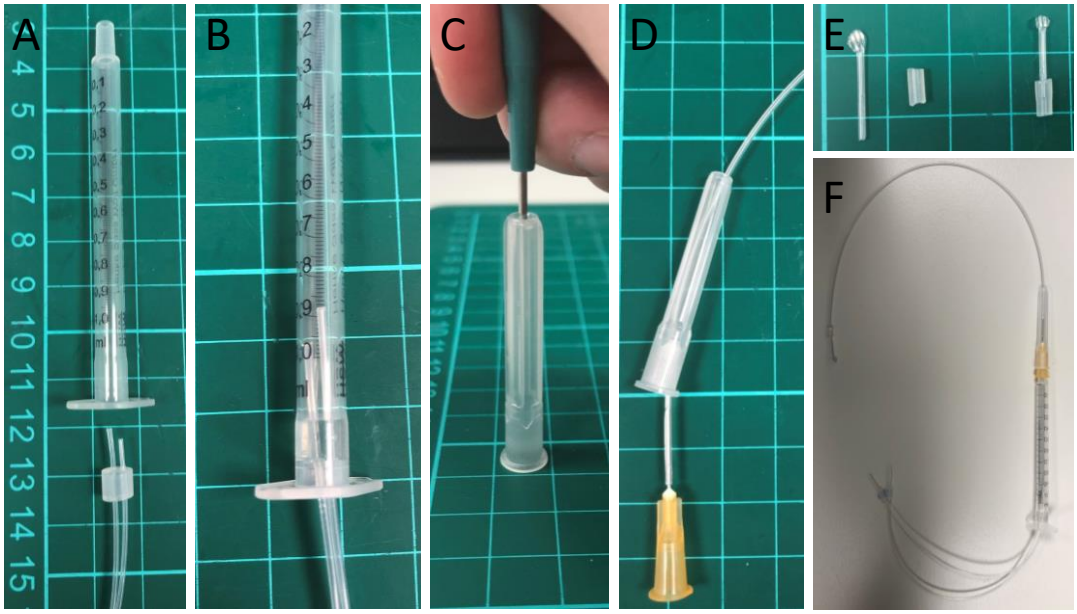


*Figure 6.5.2: Photographs illustrating steps required during the fabrication of a reinjection syringe. A) Syringe piece and PDMS tubing piece before pushing the PDMS into the syringe. B) PDMS piece has been inserted into the syringe base. C) Using a biopsy punch to make a hole in the tip of a needle sleeve. D) Passing the upper outlet tubing (connected to a needle) through the newly punched needle sleeve. E) Stopper pieces. F) Completed reinjection syringe.*

### 6.5.3 Preparation of liquid phases and microfluidic chip

1. To prepare the liquid phases and droplet generation microfluidic chip, follow steps 1 through 16 in Section 6.4.2.

### 6.5.4 Droplet Generation

1. Begin droplet generation by following steps 1 through 5 in Section 6.4.3.

2. Allow stable droplet generation to occur and droplets to flow out of the outlet tubing into waste.

3. Connect the outlet tubing from the generation chip, to the lower inlet tubing of the reinjection syringe (Figure 6.5.3 A). Ensure the upper outlet of the reinjection syringe is open and flowing to waste.

4. Keep generating droplets, allowing the droplets to flow out of the reinjection syringe *via* the upper outlet. Check the generation frequency and droplet size is as desired using the droplet generation spreadsheet described in steps 6 to 11 in Section 6.4.3.

5. When satisfied with the droplet size and flow, use a stopper to cap the upper outlet and open the lower outlet tubing, allowing oil to drain into to a waste reservoir as it is displaced by incoming droplets (Figure 6.5.3 B).

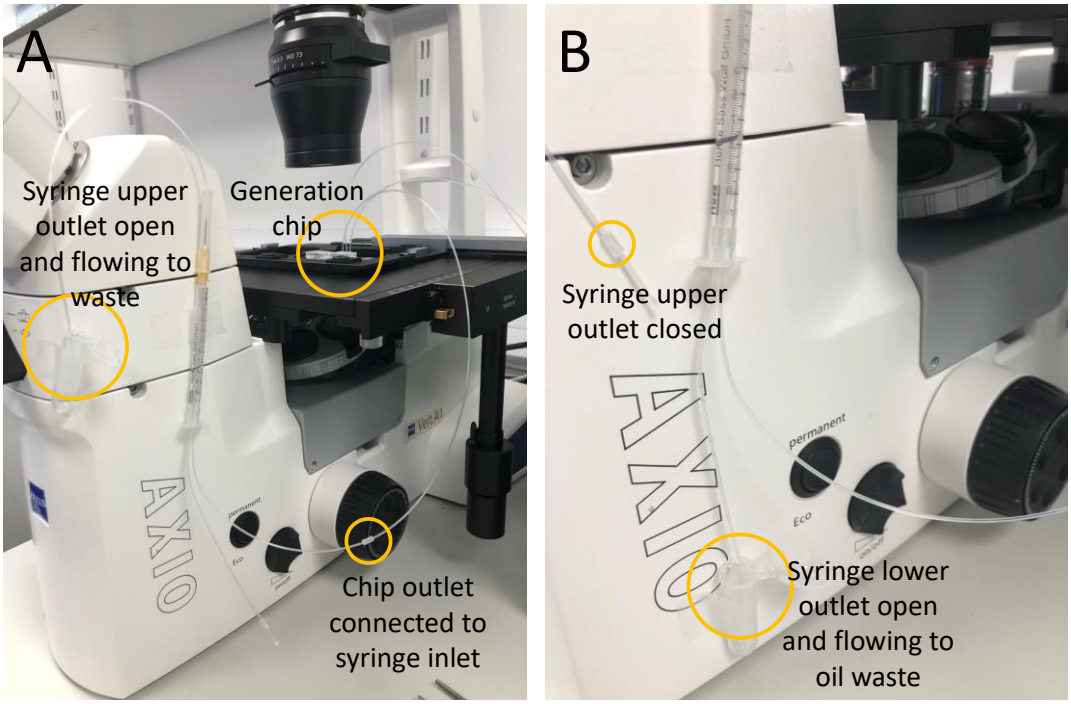


*Figure 6.5.3: Assembly of a droplet generation experiment in which droplets are collected within a reinjection syringe. A) Generation of droplets with droplet flowing up and through the reinjection syringe into waste. B) Incoming droplets are trapped in the reinjection syringe due to upper outlet closure. The displaced oil phase flows downwards out of the lower syringe outlet into oil waste.*

6. Incoming droplets will float to the top of the reinjection syringe and become trapped (collected).

7. Continue droplet generation until the desired volume of droplets within the syringe has been collected.

### 6.5.5 Discontinuation of Droplet Generation

1. Reconnect the stopper to the lower oil drain tubing

2. Disconnect the incoming droplets from the reinjection syringe, and replace the stopper onto the tubing end to seal the reinjection syringe

3. To stop the liquid phases and droplet generation microfluidic chip, follow steps 1 through 6 in Section 6.4.4.

### 6.5.6 Reinjection syringe storage or incubation

1. Store or incubate the reinjection syringe according to the experimental parameters. It is advised to store upright at all times if possible.

   Tip: If using a shaking incubator, shake upright (not lying flat) or risk droplet disruption.

### 6.5.7 Droplet Reinjection

1. Remove the syringe containing droplets from storage and secure upright in the proximity of the Sphere Fluidics Ltd Picodroplet Sing-Cell Encapsulation System.

2. Connect the lower inlet tubing to a 1 mL Norm-Ject syringe containing the oil phase of the same type as the filled reinjection syringe. Place the 1 mL syringe in the neMESYS syringe pump system.

3. Remove the stopper from the upper outlet and start the flow of oil phase into the reinjection syringe (100 μL/hr). This will begin to push the droplets out of the upper outlet. Allow the droplets to flow into waste for a few minutes.

4. Meanwhile, prepare the droplet reinjection chip. Place the slide with chip onto the microscope stage and use the focusing rings to observe the reinjection spacing region in the chip.

5. Fill a gas-tight syringe with the desired spacing oil composition and place into the syringe pump system.

6. Connect the spacing oil tubing to the chip oil inlet and start the flow (100 μL/hr).

7. Connect the upper outlet of the reinjection syringe to the reinjection chip droplet inlet. (Figure 6.5.4)

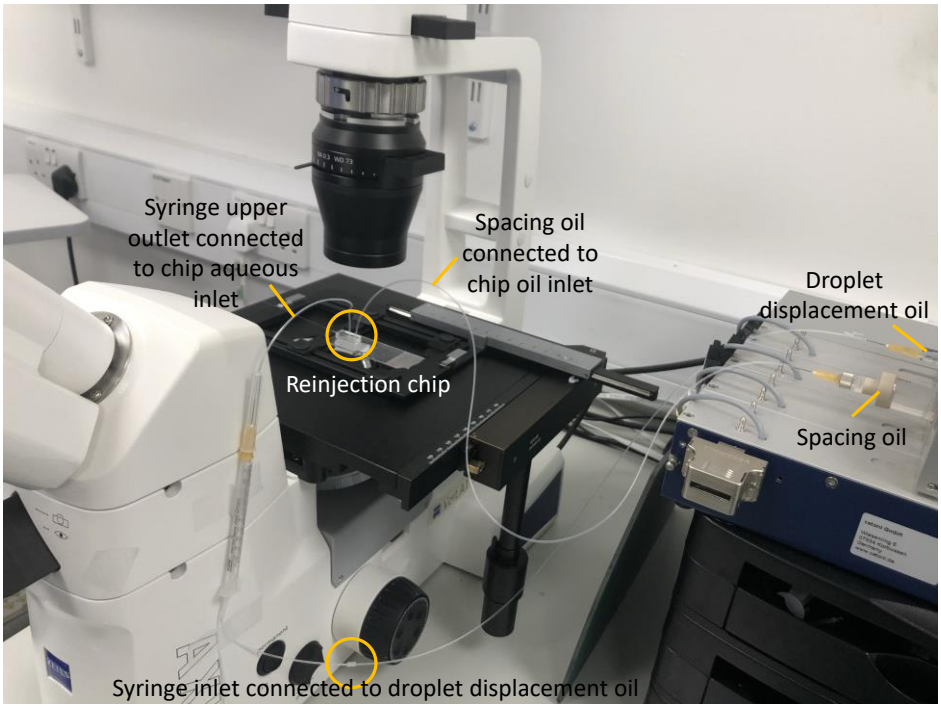


*Figure 6.5.4: Assembly of a reinjection experiment highlighting the positions of the major components and connections, including the reinjection syringe, reinjection chip and oil phases used.*

8. Begin the droplet infusion flow rate (50 μL/hr).

9. Alter both flow rates to achieve steady flow and droplet spacing through the spacing region (Figure 6.5.5). (Droplets will flow out of the chip *via* the outlet tubing or mass spectrometry emitter depending on the type of chip being used).

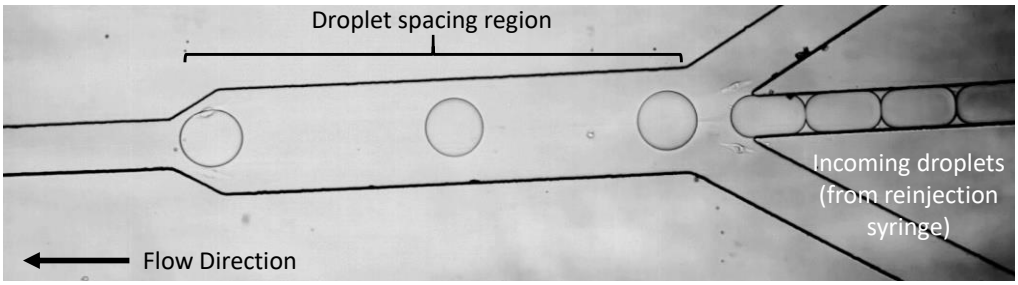


*Figure 6.5.5: Example of droplet reinjection, as observed under the microscope.*

10. Reinjection frequency can be determined using a spreadsheet similar to that used in Section 6.4.3.

11. To calculate the droplet reinjection frequency, first record a video of reinjection at an appropriate frame rate. Identify the first droplet to exit the reinjection spacing region and note the frame time as the start time in the spreadsheet (Figure 6.5.6).

12. Count 10 droplets passing through the spacing region exit. Note the frame time of the 10th droplet and record it in the spreadsheet as the end time (Figure 6.5.6).

13. The spreadsheet will calculate the droplet reinjection frequency automatically.

14. Repeat steps 10 through 12 on a minimum of 3 video recordings to find a reinjection frequency average (Figure 6.5.6, highlighted yellow).

| | A | B | C | D | E | F | G | H | I | J |
|---|---|---|---|---|---|---|---|---|---|---|
| 2 | Droplet Size: | | Aque. uL/hr | Fluo. uL/hr | F/A Ratio | Time ms | Start ms | End ms | Drop No | Freq. Hz |
| 3 | 1 | | 50 | 100 | 2.0 | 1327.4 | 1328.6 | 1.2 | 10 | 7.5 |
| 4 | 2 | | 50 | 100 | 2.0 | 1175.9 | 1497.3 | 321.4 | 10 | 8.5 |
| 5 | 3 | | 50 | 100 | 2.0 | 1313.8 | 1394.1 | 80.3 | 10 | 7.6 |
| 6 | | | | | | | | | Average: | 7.9 |

*Figure 6.5.6: Screen capture of the 'droplet calculator spreadsheet' upon completion of a droplet reinjection experiment. The aqueous and oil flow rates have been added to the appropriate cells in the spreadsheet. The time calculated from the start and end times (as indicated by the camera software) is the time taken for 10 droplets to pass through the spacing region. Three repetitions of the droplet recording and counting procedure have been executed to calculate an average droplet reinjection frequency (as indicated in the yellow cell). Spreadsheet formulae can be found in Figure 6.5.7.*

### 6.5.8 Spreadsheet Formulae

| | A | B | C | D | E | F | G | H | I | J |
|---|---|---|---|---|---|---|---|---|---|---|
| 2 | Droplet Size: | | Aque. uL/hr | Fluo. uL/hr | F/A Ratio | Time ms | Start ms | End ms | Drop No | Freq. Hz |
| 3 | 1 | | 50 | 100 | =D3/C3 | =G3-H3 | | | 10 | =I3/F3*1000 |
| 4 | 2 | | 50 | 100 | =D4/C4 | =G4-H4 | | | 10 | =I4/F4*1000 |
| 5 | 3 | | 50 | 100 | =D5/C5 | =G5-H5 | | | 10 | =I5/F5*1000 |
| 6 | | | | | | | | | Average: | =AVERAGE(J3:J5) |

*Figure 6.5.7: Screen capture of the 'droplet calculator spreadsheet' formulae for reinjection experiments.*